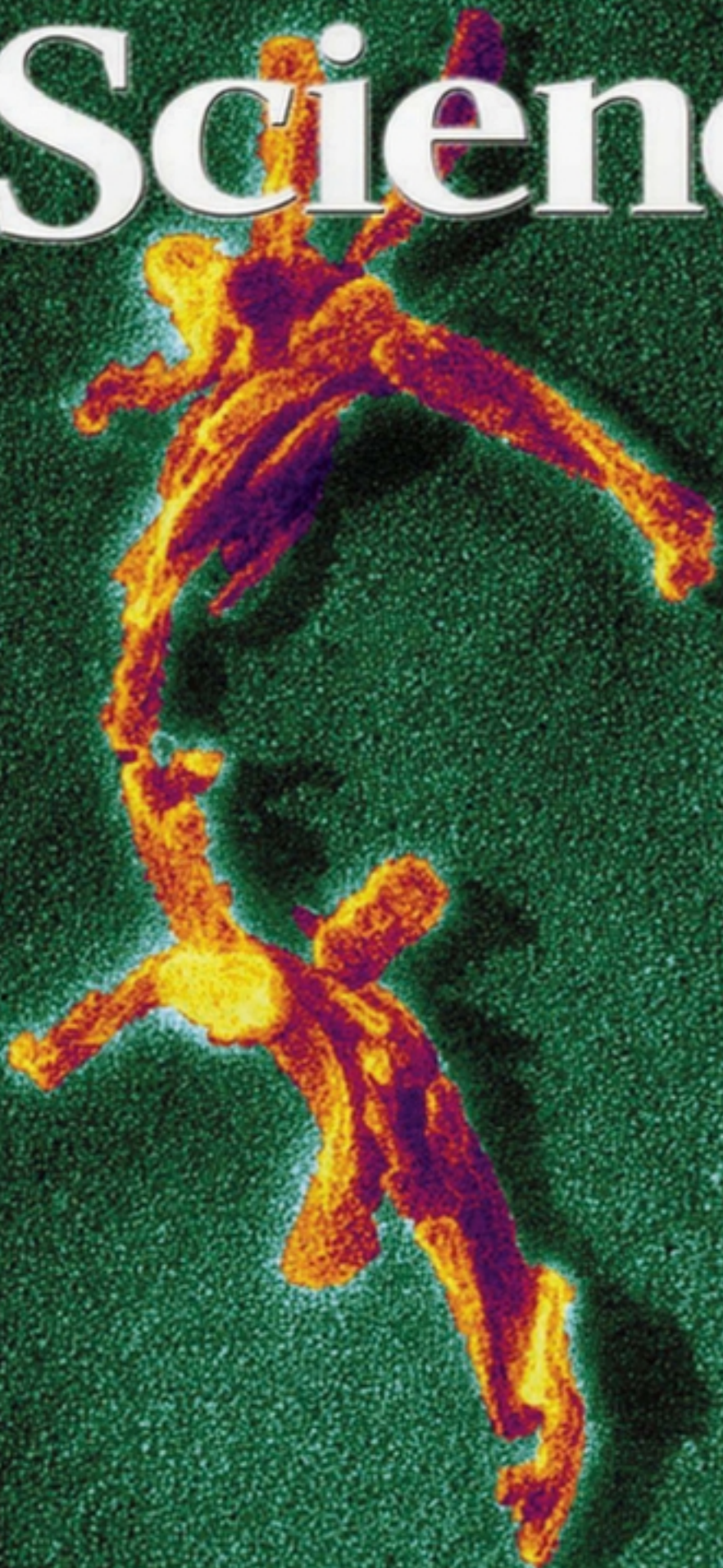
27 January 2012 | $10

Science



AAAS

EDITORIAL

380 Teaching Real Science
Bruce Alberts
>> Essay p. 418

NEWS OF THE WEEK

384 A roundup of the week's top stories

NEWS & ANALYSIS

387 Flu Controversy Spurs Research Moratorium
Ron Fouchier: In the Eye of the Storm
>> Letter by R. A. M. Fouchier et al., p. 400

390 An Explosive Return of the 'Great Pox'

391 Worldwide Telescope Aims to Look Into Milky Way Galaxy's Black Heart

392 DOE Funding Crunch Threatens Future of Only U.S. Collider Still Running

NEWS FOCUS

394 What It'll Take to Go Exascale
>> Science *Podcast*

397 Ferreting Out the Hidden Cracks in the Heart of a Continent

398 Modernizing an Academic Monastery

LETTERS

400 Pause on Avian Flu Transmission Research
R. A. M. Fouchier et al.
>> News story p. 387

Recognizing Existing Models
W. J. Rosenberg

Portugal's Age of Enlightenment
N. C. Santos

401 CORRECTIONS AND CLARIFICATIONS

401 TECHNICAL COMMENT ABSTRACTS

BOOKS *ET AL.*

403 The Statues That Walked
T. Hunt and C. Lipo, reviewed by R. Torrence

404 Understanding Autism
C. Silverman, reviewed by B. A. Malow

POLICY FORUM

405 Mixed Messages on Prices and Food Security
J. Swinnen and P. Squicciarini

PERSPECTIVES

408 Antigen Feast or Famine
M. L. Dustin and M. Meyer-Hermann
>> Report p. 475

409 A Clearer View from Fuzzy Images
M. E. Herberstein and D. J. Kemp
>> Report p. 469

410 The Role of Coevolution
J. N. Thompson
>> Research Article p. 428

411 The Risk of Prion Zoonoses
J. Collinge
>> Report p. 472

413 Creating New Types of Carbon-Based Membranes
D. R. Paul
>> Reports pp. 442 and 444

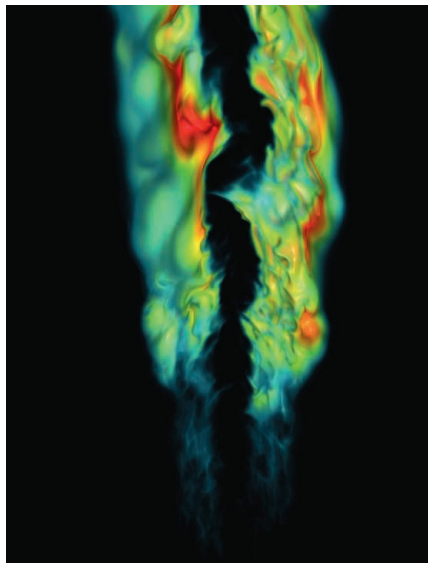
415 Another Remembered Present
K. Meyer

416 The Inner Workings of a Dynamic Duo
H. Poulsen and P. Nissen
>> Research Articles pp. 432 and 436

SCIENCE PRIZE ESSAY

418 An Inquiry-Based Curriculum for Nonmajors
D. P. Jackson et al.
>> Editorial p. 380

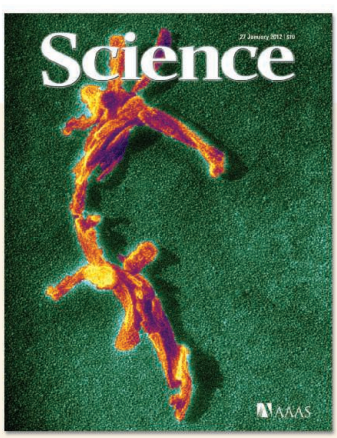
CONTENTS continued >>



page 394



pages 409 & 469



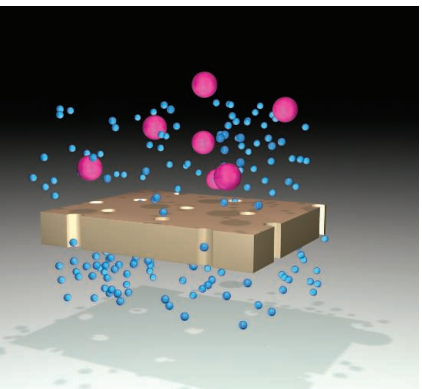
COVER

False-colored transmission electron micrograph of a prion [average dimensions: ~150 nanometers (nm) long, 10 nm thick], the infectious protein responsible for deadly brain diseases in animals and humans. Although cross-species prion transmission may show no detectable sign of disease in the brain, lymphoid tissue is much more susceptible to infection. This discovery may be relevant when assessing the public health risks of exposure to animal prions and silent carriers of prion disease. See page 472.

Image: Eye of Science/Photo Researchers, Inc.

DEPARTMENTS

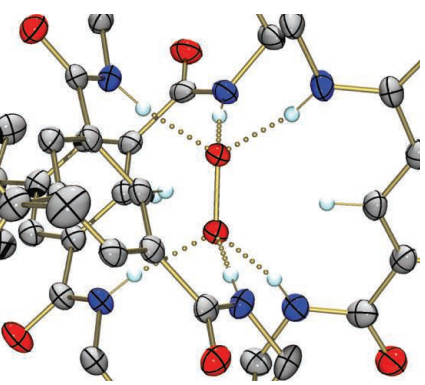
377 This Week in *Science*
381 Editors' Choice
383 *Science* Staff
420 AAAS News & Notes
481 New Products
482 *Science* Careers



pages 413, 442, & 444



page 415



page 450

REVIEW

422 The Centrosome in Cells and Organisms
M. Bornens

BREVIA

427 Broadband Light Bending with Plasmonic Nanoantennas
X. Ni et al.
A plasmonic antenna array is used to control the propagation of a light beam across an interface.

RESEARCH ARTICLES

428 Repeatability and Contingency in the Evolution of a Key Innovation in Phage Lambda
J. R. Meyer et al.
A receptor shift required four mutations that accumulated by natural selection and with the host's coevolution.
>> *Perspective p. 410*; Science *Podcast*

432 Crystal Structure of the Human Two–Pore Domain Potassium Channel K2P1
A. N. Miller and S. B. Long

436 Crystal Structure of the Human K2P TRAAK, a Lipid- and Mechano-Sensitive K^+ Ion Channel
S. G. Brohawn et al.
Structural features provide a basis for understanding gating and ion conduction of these channels.
>> *Perspective p. 416*

REPORTS

442 Unimpeded Permeation of Water Through Helium-Leak–Tight Graphene-Based Membranes
R. R. Nair et al.
Graphite oxide membranes are impermeable to many liquids, vapors, and gases, including He, but allow evaporation of water.

444 Ultrafast Viscous Permeation of Organic Solvents Through Diamond-Like Carbon Nanosheets
S. Karan et al.
Membranes made from diamond-like carbon are used to rapidly separate organic compounds.
>> *Perspective p. 413*

447 An All-Silicon Passive Optical Diode
L. Fan et al.
A silicon-based device is developed that allows the asymmetric propagation of light.

450 Reversible Reduction of Oxygen to Peroxide Facilitated by Molecular Recognition
N. Lopez et al.
The highly reactive peroxide dianion (O_2^{2-}) can be captured and stabilized by hydrogen bonding in a molecular box.

453 A Long-Lived Lunar Core Dynamo
E. K. Shea et al.
Analysis of a lunar basalt sample suggests that a lunar core dynamo existed between 4.2 and 3.7 billion years ago.

457 The Molecular Diversity of Adaptive Convergence
O. Tenaillon et al.
Replicate *Escherichia coli* lines show multiple convergent adaptations via different mutations in response to high temperature.

461 Centrosome Loss in the Evolution of Planarians
J. Azimzadeh et al.
Analysis of centriole assembly in planaria gives insight into the evolution and function of the centrosome in animal cells.

464 Global Correlations in Tropical Tree Species Richness and Abundance Reject Neutrality
R. E. Ricklefs and S. S. Renner
Comparison of species numbers between forests shows that patterns of diversity are dominated by deterministic processes.

467 Heavy Livestock Grazing Promotes Locust Outbreaks by Lowering Plant Nitrogen Content
A. J. Cease et al.
High-protein plants inhibit locust swarming, which explains why grazed systems are more prone to outbreaks.
>> Science *Podcast*

469 Depth Perception from Image Defocus in a Jumping Spider
T. Nagata et al.
To jump exact distances to capture prey, spiders, like computers, use defocus as a major cue for depth perception.
>> *Perspective p. 409*

472 Facilitated Cross-Species Transmission of Prions in Extraneural Tissue
V. Béringue et al.
Lymphoid tissue is more permissive than the brain to foreign prions.
>> *Perspective p. 411*

475 Asymmetric Segregation of Polarized Antigen on B Cell Division Shapes Presentation Capacity
O. Thaunat et al.
Antigen distribution across activated B cells influences B-T lymphocyte interactions.
>> *Perspective p. 408*

Published by AAAS

SCIENCEONLINE

SCIENCEXPRESS

www.sciencexpress.org

Lithium Isotope History of Cenozoic Seawater: Changes in Silicate Weathering and Reverse Weathering
S. Misra and P. N. Froelich
Historical changes in the lithium isotope ratio in seawater imply episodes of tectonic uplift and carbon dioxide drawdown.
10.1126/science.1214697

Mountains, Weathering, and Climate
A. Paytan
10.1126/science.1218342

Epithelial Nitration by a Peroxidase/NOX5 System Mediates Mosquito Antiplasmodial Immunity
G. de Almeida Oliveira et al.
Expression of nitric oxide synthase followed by peroxidase activity makes *Plasmodium* visible to the insect's complement system.
10.1126/science.1209678

Unique Processing During a Period of High Excitation/Inhibition Balance in Adult-Born Neurons
A. Marín-Burgin et al.
A specific set of functional properties can be attributed to immature granule cells developing in the hippocampus.
10.1126/science.1214956

Evolutionarily Assembled cis-Regulatory Module at a Human Ciliopathy Locus
J. H. Lee et al.
Mutation in either of a pair of neighboring, coordinately expressed genes causes indistinguishable human disease.
10.1126/science.1213506

Unraveling the Spin Polarization of the $\nu = 5/2$ Fractional Quantum Hall State
L. Tiemann et al.
Nuclear magnetic resonance shows that an exotic state of matter may have the properties necessary for error-free quantum computing.
10.1126/science.1216697

TECHNICALCOMMENTS

Comment on "Dynamics of Dpp Signaling and Proliferation Control"
G. Schwank et al.
Full text at www.sciencemag.org/cgi/content/full/335/6067/401-b

Response to Comment on "Dynamics of Dpp Signaling and Proliferation Control"
O. Wartlick et al.
Full text at www.sciencemag.org/cgi/content/full/335/6067/401-c

SCIENCENOW

www.sciencenow.org
Highlights From Our Daily News Coverage

Embryonic Stem Cells Appear Safe, May Help Eye Disease
The first published results for a clinical trial using stem cells give this field a boost.
http://scim.ag/Eye-Disease

Mapping the Psychedelic Brain
The active ingredient in magic mushrooms disrupts communication between brain regions.
http://scim.ag/Psychedelic-Brain

Stem Cells Build a Better Rat Penis
A new approach could help men with injuries or deformities.
http://scim.ag/Stem-Cells

SCIENCESIGNALING

www.sciencesignaling.org
The Signal Transduction Knowledge Environment
24 January issue: http://scim.ag/ss012412

RESEARCH ARTICLE: A Phosphorylated Pseudokinase Complex Controls Cell Wall Synthesis in Mycobacteria
C. L. Gee et al.

PERSPECTIVE: A Pseudokinase Debut at the Mycobacterial Cell Wall
D. F. Warner and V. Mizrahi
A serine-threonine kinase targets a pseudokinase to control the synthesis of the cell wall of the bacterium that causes tuberculosis.

RESEARCH ARTICLE: Extracellular Ca^{2+} Acts as a Mediator of Communication from Neurons to Glia
A. Torres et al.

PERSPECTIVE: Depletion of Extracellular Ca^{2+} Prompts Astroglia to Moderate Synaptic Network Activity
D. A. Rusakov
Local decreases in extracellular calcium trigger signaling events in astrocytes that activate inhibitory neurotransmission.

SCIENCETRANSLATIONAL MEDICINE

www.sciencetranslationalmedicine.org
Integrating Medicine and Science
25 January issue: http://scim.ag/stm012512

COMMENTARY: Triggers for Research Ethics Consultation
M. Havard et al.
Research ethics consultation services can help scientists to address ethical and societal issues that go beyond the purview of existing regulatory frameworks.

COMMENTARY: A Virtual National Laboratory for Reengineering Clinical Translational Science
D. M. Dilts et al.
The CTSA Consortium has developed a national testbed that can be used for evaluating approaches aimed at reducing wasted efforts and speeding clinical trial completion.

RESEARCH ARTICLE: Molecular Diagnosis of Infantile Mitochondrial Disease with Targeted Next-Generation Sequencing
S. E. Calvo et al.
Applying next-generation sequencing to 42 infants with mitochondrial disease highlights both the potential and the challenge of using this technology in clinical diagnosis.

RESEARCH ARTICLE: Surgical Stress Resistance Induced by Single Amino Acid Deprivation Requires *Gcn2* in Mice
W. Peng et al.
A protein-free diet or one missing certain amino acids can protect against kidney and liver damage due to ischemia in mice.

RESEARCH ARTICLE: Teplizumab Induces Human Gut-Tropic Regulatory Cells in Humanized Mice and Patients
F. Waldron-Lynch et al.
Humanized mice can be successfully used as a preclinical testing platform to identify the mechanism of action of immunotherapies in humans.

SCIENCECAREERS

www.sciencecareers.org/career_magazine
Free Career Resources for Scientists

Your Voice: Your Passport to Authority
S. Louët
An authoritative voice can be a definite asset in a scientific career.
http://scim.ag/VoiceCoach

HHMI's International Early-Career Scientists
E. Pain
Three awardees discuss how HHMI support will help them pursue their careers in China, Spain, and Portugal.
http://scim.ag/HHMI_International

Experimental Error: The Top 10 Worst Things About Working in a Lab
A. Ruben
Lab work left you feeling dissatisfied? Our Experimental Error columnist feels your pain.
http://scim.ag/EE_WorstThings

SCIENCEPODCAST

www.sciencemag.org/multimedia/podcast
Free Weekly Show

On the 27 January *Science* Podcast: repeatability in natural selection, livestock grazing and locust outbreaks, new frontiers in supercomputing, and more.

SCIENCE (ISSN 0036-8075) is published weekly on Friday, except the last week in December, by the American Association for the Advancement of Science, 1200 New York Avenue, NW, Washington, DC 20005. Periodicals Mail postage (publication No. 484460) paid at Washington, DC, and additional mailing offices. Copyright © 2012 by the American Association for the Advancement of Science. The title SCIENCE is a registered trademark of the AAAS. Domestic individual membership and subscription (51 issues): $149 ($74 allocated to subscription). Domestic institutional subscription (51 issues): $990; Foreign postage extra: Mexico, Caribbean (surface mail) $55; other countries (air assist delivery) $85. First class, airmail, student, and emeritus rates on request. Canadian rates with GST available upon request, GST #1254 88122. Publications Mail Agreement Number 1069624. **Printed in the U.S.A.**

Change of address: Allow 4 weeks, giving old and new addresses and 8-digit account number. **Postmaster:** Send change of address to AAAS, P.O. Box 96178, Washington, DC 20090–6178. **Single-copy sales:** $10.00 current issue, $15.00 back issue prepaid includes surface postage; bulk rates on request. **Authorization to photocopy** material for internal or personal use under circumstances not falling within the fair use provisions of the Copyright Act is granted by AAAS to libraries and other users registered with the Copyright Clearance Center (CCC) Transactional Reporting Service, provided that $30.00 per article is paid directly to CCC, 222 Rosewood Drive, Danvers, MA 01923. The identification code for *Science* is 0036-8075. *Science* is indexed in the *Reader's Guide to Periodical Literature* and in several specialized indexes.

AAAS
ADVANCING SCIENCE, SERVING SOCIETY



Locust Heaven

Locust outbreaks have severe consequences for agriculture, but the conditions that promote an outbreak are unknown. Cease *et al.* (p. 467) investigated aspects of the locust diet and found that increased nitrogen content of cereal grasses reduced the size and viability of a herbivorous locust species. This locust prefers low N plants, which result from heavy grazing by livestock and erosion.

Natural Selection Caught in the Act

Understanding how new functions evolve has been of long-standing interest. However, the number of mutations needed to evolve a key innovation is rarely known, or whether other sets of mutations would also suffice, whether the intermediate steps are driven by natural selection, or how contingent the outcome is on steps along the way. **Meyer *et al.*** (p. 428; see the Perspective by **Thompson**) answer these questions for a case in which phage lambda evolved the ability to infect its host *Escherichia coli* through a novel receptor. This shift required four mutations, which accumulated under natural selection in concert with coevolution of the host. However, when **Tenaillon *et al.*** (p. 457) exposed 115 lines of *E. coli* to high temperature and sequenced them, adaptation occurred through many different genetic paths, showing parallelism at the level of genes and interacting protein complexes, but only rarely at the nucleotide level. Thus, epistasis—nonadditive genetic interaction—is likely to play an important part in the process of adaptation to this environment.

Potassium Permeation

Two–pore domain potassium (K2P) channels conduct K^+ ions across the plasma membrane of eukaryotic cells. They help to maintain the cellular resting potential and their modulation can tune cellular excitability (see the Perspective by **Poulsen and Nissen**). **Miller and Long** (p. 432) describe a high-resolution crystal structure of the human K2P channel K2P1 (TWIK-1) and **Brohawn *et al.*** (p. 436) present a high-resolution structure of the lipid and mechanosensitive human channel TRAAK. In both structures an extracellular domain constricts the channel entrance so that K^+ ions reach the selectivity filter through side portals. Openings in the transmembrane region expose the central cavity to the lipid bilayer and a helix is kinked so that its C-terminal part lies in the cytosol-membrane interface. The structural features explain K2P conductance and gating and give insight into how the channels are regulated by diverse stimuli.

Porous Membranes

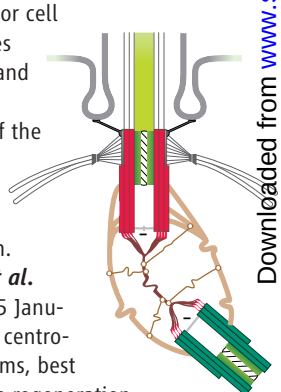
Thin semi-permeable membranes are commonly used as chemical barriers or for filtration purposes. While the size of the pores will influence which molecules are able to pass, other factors—including the surface chemistry of the pore walls, electrostatic interactions, and differences in solubility—can also affect the diffusion rates. There is also a trade-off between the thickness of the membrane regarding strength and permeation rates (see the Perspective by **Paul**). **Karan *et al.*** (p. 444) fabricated membranes from amorphous carbon, which showed excellent strength and could be used for filtrations involving organic solvents. **Nair *et al.*** (p. 442) observed unusual behavior in graphene-based membranes which were able to prevent the diffusion of many small-molecule gases, including helium, but showed almost barrier-free movement of water.

Boxing in Peroxide

Hydrogen peroxide (H_2O_2) is a powerful oxidant, and its reactivity is exploited in numerous biological, as well as synthetic, contexts. **Lopez *et al.*** (p. 450) have now managed to capture its dianion (O_2^{2-}) in a cryptand—essentially a molecular box assembled from benzamide derivatives—keeping the dianion stable in organic solution for days through a net of well-placed internal hydrogen-bond donors. The encapsulated dianion exhibited clean oxidative reactivity back to O_2 either by chemical or by electrochemical means.

Centrosome Center Stage?

The centrosome is a major organizer of the cytoskeleton in animal cells. The precise duplication of this organelle at each cell cycle ensures proper organization of the mitotic apparatus and chromosome segregation. However, centrosomes are dispensable for cell division during some stages of development in mouse and *Drosophila*. **Bornens** (p. 422) reviews the role of the centrosome in a variety of organisms and discusses how and why they can be dispensed with on occasion. In this vein, **Azimzadeh *et al.*** (p. 461, published online 5 January) now demonstrate that centrosomes in Planarian flatworms, best known for their remarkable regeneration abilities, are completely dispensable for both cell division and development.



Magnetic Moon

It has long been suspected that the Moon once had a core-dynamo magnetic field. **Shea *et al.*** (p. 453) describe a lunar basalt brought back by Apollo 11 that records evidence for a strong dynamo on the Moon 3.7 billion years ago. This study, together with a previous study of different lunar rock, implies that a lunar core dynamo existed between 4.2 and 3.7 billion years ago, which extends the known lifetime of the lunar dynamo by 500 million years.

Continued on page 379

CREDITS (TOP TO BOTTOM): ARIANNE CEASE; BORNENS *ET AL.*

Downloaded from www.sciencemag.org on January 27, 2012

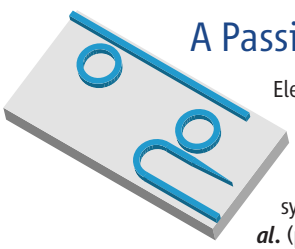
Continued from page 377

Forest Diversification

The relative role of neutral and deterministic processes in generating species richness in ecological communities (particularly tropical trees) has dominated recent discussions about patterns of diversity and abundance of species. **Ricklefs and Renner** (p. 464) present a test of random diversification and population change by comparing the numbers of individuals and species in plant families between forest plots on different continents that have diversified independently for millions of years. Stochastic theory, based on random events, predicts that there should be no correlation between the regions; however, the data reveal strong, statistically significant correlations. Thus, patterns of diversity appear to be dominated by deterministic processes.

A Good Judge of Distance

Jumping spiders actively pursue their prey, often jumping relatively long distances in order to catch them. Such feats require accurate depth perception. **Nagata *et al.*** (p. 469; see the Perspective by **Herberstein and Kemp**) show that jumping spiders use a process called image defocus, which allows depth perception to be obtained through the comparison of a nonfocused image to a focused image within the same eye. A single layer within the spider's eye that could not focus green light nevertheless contained a green sensitive pigment. Thus, this layer always receives an unfocused image, while other layers receive images in focus. Confirming this eye arrangement's role in depth perception, spiders unlucky enough to be bathed in green light nearly always jumped short of their target.



A Passive Optical Diode

Electrical diodes are at the core of microelectronics. The optical equivalent, however, has been difficult to realize owing to the time-reversal symmetry of Maxwell's equations that describe electromagnetic propagation. Usually, a control input in the form of a magnetic field is required that breaks that symmetry. Such inputs are not practical for optical integrated circuits. **Fan *et al.*** (p. 447, published online 22 December) developed a silicon-based microresonator device that could control the asymmetric transmission of light through it. The passive optical diode was compatible with current complementary metal-oxide semiconductor processing technology and thus should be readily integrated into optoelectronic circuitry.

Prion Problem

Prion disease, like "mad cow disease," has shown a frightening ability to cross the species transmission barrier, but, mercifully, with low efficiency. However, the role of different tissues in prion cross-species transmission is unclear. **Béringue *et al.*** (p. 472; see the cover; see the Perspective by **Collinge**) compared the ability of brain and lymphoid tissues from "ovinized" (sheeplike) and "humanized" transgenic mouse models to replicate prion transmission across a robust transmission barrier. Lymphoid tissue of these mice was consistently more permissive than brain tissue to prions such as those causing chronic wasting disease and bovine spongiform encephalopathy. Because previous measures of the transmission barrier have focused on the brain, this heightened susceptibility of lymphoid tissues could strongly impact estimates of the number of silent carriers of prion disease.

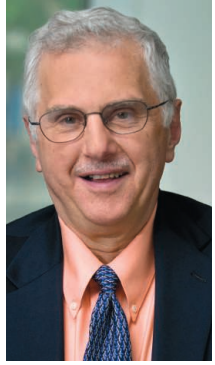
Antigen Polarity in B Cell Differentiation

Communication received through cell contact is critical for the differentiation of specialized effector cell populations during the immune response. For example, B lymphocytes acquire antigen that they present to helper T lymphocytes. T lymphocytes, in turn, provide key differentiation signals to B lymphocytes. In order to learn more about this process, **Thaunat *et al.*** (p. 475; see the Perspective by **Dustin and Meyer-Hermann**) used multiphoton microscopy and imaging flow cytometry to visualize the localization of antigen in B lymphocytes during an immune response. Antigen acquired by B lymphocytes exhibited a polarized distribution that was sustained over several rounds of cell division. This produced a population of activated B lymphocytes that contained very low levels of antigen. Daughter cells that received more antigen were better able to stimulate T cells. Because cues received through T lymphocyte interactions are likely to influence B lymphocyte fate decisions, unequal distribution of antigen in dividing B lymphocytes may influence their differentiation.

CREDIT: FAN *ET AL.*

Downloaded from www.sciencemag.org on January 27, 2012

Published by AAAS



Bruce Alberts is Editor-in-Chief of *Science*.

Teaching Real Science

IN THIS ISSUE OF *SCIENCE*, WE ARE PUBLISHING THE FIRST OF 15 WINNING ENTRIES FOR the 2011 *Science* Prize for Inquiry-Based Instruction (p. 418), a laboratory module entitled Light, Sight, and Rainbows. Created for introductory college science courses, each module can be readily used in many different settings and schools. The winning modules were selected by a jury of more than 70 scientists and science teachers, and the subjects include physics, math, chemistry, geology, molecular biology, plant science, and evolution. Throughout 2012, each will be published as a two-page printed synopsis supplemented by online material that contains the details needed to teach it.

Our goal is to make it much easier for teachers everywhere to provide their students with laboratory experiences that mirror the open-ended explorations of scientists, instead of the traditional "cookbook" labs where students follow instructions to a predetermined result. To this end, we are announcing a second year of the contest, now broadened to include engineering in addition to science, as well as courses at the advanced high-school level (see www.scim.ag/inquiryprize). We hope that these contests will help support a rethinking of science education that is consistent with the new *Framework for K-12 Science Education* (precollege) from the U.S. National Academies, as well as with one of the central goals in the international Programme for International Student Assessment (PISA) Science Competencies: "Understands the characteristic features of science as a form of human knowledge and enquiry."*



Although our 2011 contest focused on college science teaching, the same goals can be applied even to early years of schooling. Consider, for example, an article published by the U.S. National Science Teachers Association, *Growing Seeds and Scientists*, which describes a science lesson for kindergarten students (age 5).† The students are presented with seeds of very different sizes and shapes—an avocado seed, a corn kernel, a marigold seed, and so on—mixed with objects such as pebbles and shells. For three times a week over the course of 6 weeks, the students explore the question, "How do we know if something is a seed?", forming a "scientists' conference" to share ideas respectfully and learn from each other as real scientists might in a laboratory. Thus, after the students discover that they disagree about what makes an object a seed, the class is asked to come up with ways in which they might test their ideas, again modeling the behavior of scientists. Through experiments that they suggest and perform on their own, the class discovers which objects are seeds. Finally, the students dissect some of the seeds and examine them with a magnifying glass, finding the tiny embryo inside and its source of food. Compare this exercise with a more traditional approach, which would at best give the students a seed and step-by-step instructions on how to grow it, bypassing the scientific process of facing a question, proposing solutions, and testing one's theories.

Last week, I described how current school science often resembles a game in which the participants are challenged to recall boring, incomprehensible facts.‡ How might the world recover from this destructive form of science education? We should begin by teaching science to young children with a curriculum like that described in *Growing Seeds and Scientists*, which might require a total of only 20 hours of the school year. And we should aim for an education system in which every child is exposed to at least this many hours of high-quality science inquiry in each year of elementary and middle school, supported by carefully prepared science specialists. In this way, "science education" would be redefined, with a laser-sharp focus on gaining the scientific habits of mind that will be needed by everyone to successfully negotiate his or her way through our increasingly complex, crowded, and confusing societies. **– Bruce Alberts**

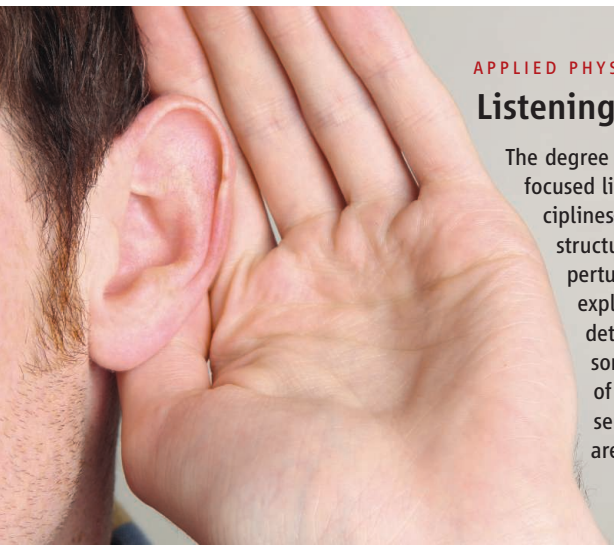
10.1126/science.1219216

*For *Framework*, see www.nap.edu/catalog.php?record_id=13165; for PISA, see www.oecd.org/dataoecd/15/13/39725224.pdf. †D. C. Smith, J. L. Cowan, A. M. Culp, *Science & Children* **47**, 48 (2009); www.nsta.org/pdfs/ScienceAndChildren_200909_48-51.pdf. ‡B. Alberts, *Science* **335**, 263 (2012).

Downloaded from www.sciencemag.org on January 27, 2012

CREDITS: (TOP) TOM KOCHEL; (LEFT) ISTOCKPHOTO.COM

Published by AAAS



APPLIED PHYSICS

Listening In by Nanoparticle

The degree of control with which particles can be trapped, rotated, pulled apart, and manipulated by focused light beams has made optical tweezers an extremely useful laboratory tool across many disciplines—from probing the mechanical properties of cells and DNA to building three-dimensional structures and cooling gases to their quantum ground state. It might be expected that external perturbation or excitement would produce a wobble of a light-trapped particle. Ohlinger *et al.* exploit this effect to show that a trapped gold nanoparticle can be used as an ultrasensitive detector of sound waves. A typical empty room has a sound level of 20 decibels. By comparison, the trapped gold nanoparticle can detect sounds down to –60 decibels—over six orders of magnitude more sensitive than the human ear. The authors suggest that such enhanced sensitivity could be used to probe live bacteria and cells that produce acoustic vibrations but are not easily seen with optical microscopes. — ISO

Phys. Rev. Lett. **108**, 18101 (2012).

STRUCTURAL BIOLOGY

A Fuzzy Fit

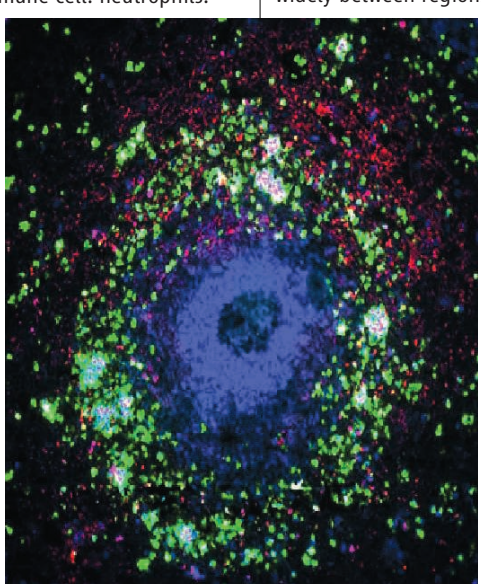
Careful tuning of gene regulation is crucial for proper cell function. Temporal or spatial changes in gene expression or changes in gene expression level can compromise cell activity or even viability. Transcriptional activators interact with coactivators, which in turn communicate with the general transcription machinery or chromatin remodeling factors to effect changes in gene expression. Using NMR, Brzovic *et al*. have examined the structural basis for the binding of the transcriptional activator Gcn4 to the coactivator Mediator subunit Gall11/Med15 (Gal11) in yeast. Activation domains, which are generally rich in acidic residues, often bind diverse coactivators through multiple low-affinity interactions. In this study, the activation domain shows a disordered structure that morphs to a more stable alpha-helical structure upon binding to Gal11. The protein-protein interface is rather simple and consists of only hydrophobic interactions, which allows the activator and coactivator to bind in multiple orientations, forming a so-called "fuzzy" complex. Gcn4 can also interact with other unrelated coactivators using the same residues through a similar mechanism, suggesting that this mechanism may enable transcriptional activators to interact with multiple targets. — BAP

Mol. Cell **44**, 942 (2011).

IMMUNOLOGY

Neutrophils Lend a Hand

Diverse antibody production by B cells, which is critical for protection against a variety of infections, often requires the help of T cells. Marginal zone (MZ) B cells in the spleen, which are situated at the interface of the circulation and the immune system, are unusual in that they are able to provide a rapid, first line of antibody defense that is independent of T cells. Puga *et al*. now show that despite being independent of T cells, MZ B cells in humans do get help from another immune cell: neutrophils. These so-called "B cell–helper neutrophils" were located in close proximity to MZ B cells in the spleens of humans, nonhuman primates, and mice. Their localization to the spleen coincided with postnatal colonization by microbes. Through the production of the cytokines APRIL, BAFF, and interleukin-21, B cell–helper neutrophils promoted the expression of activation-induced cytidine deaminase (AID), antibody isotype class switching, and somatic hypermutation by MZ B cells, events that help to diversify the antibody response but are typically associated with T cell help. Reduced MZ B cell numbers and altered MZ B cell antibody responses in patients deficient in neutrophils revealed the importance of B cell–helper neutrophils in vivo. — KLM



Nat. Immunol. 10.1038/ni.2194 (2011).

CLIMATE SCIENCE

Whence the Little Ice Age?

In the second half of the past millennium, glaciers advanced and temperatures fell in many regions around the world, although the timings and durations of the cold spells differed widely between regions. Numerous causes for this Little Ice Age have been proposed, including cyclical reductions in solar irradiance, changes in ocean circulation, and increases in volcanic activity, but the direct radiative effects of these processes are either weak or short-lived and require substantial feedbacks within the climate system. Miller *et al.* now exploit the fact that small ice caps in Arctic Canada are retreating, exposing vegetation that was entombed when the ice caps were advancing. By radiocarbon-dating these plants, the authors can accurately determine the time of glacial advance. They identify abrupt summer temperature decreases in the late 13th century and between 1430 and 1455 CE; subsequently, most ice caps remained in an expanded state until the 20th century. Comparison with varved sediments recording ice-cap growth from

Continued on page 382

CREDITS (TOP TO BOTTOM): ISTOCKPHOTO.COM; PUGA *ET AL., NAT. IMMUNOL.* 10.1038/NI.2194 (2011)

Downloaded from www.sciencemag.org on January 27, 2012

Call for Papers

Science Translational Medicine

Integrating Medicine and Science

The new journal from the publisher of *Science* stands at the forefront of the unprecedented and vital collaboration between basic scientists and clinical researchers.

- Cardiovascular Disease
- Neuroscience/Neurology/ Psychiatry
- Infectious Diseases
- Cancer
- Health Policy
- Bioengineering
- Chemical Genomics/ Drug Discovery
- Other Interdisciplinary Approaches to Medicine

Submit your research at www.submit2scitranslmed.org



Chief Scientific Adviser
Elias A. Zerhouni, M.D.
Former Director,
National Institutes of Health

Science Translational Medicine
AAAS

ScienceTranslationalMedicine.org

Continued from page 381

Iceland provides support for these dates, which coincide with periods of enhanced volcanic activity. Climate model results suggest that short-lived volcanic eruptions, reinforced by weak solar irradiance changes, can cause a sea-ice/ocean feedback that yields a centuries-long reduction in summer air temperature across the Arctic. — JFU

Geophys. Res. Lett. 10.1029/2011GL050168 (2012).

PSYCHOLOGY

Us vs. Them in Context

Us versus Them is both an enduring view of the world and a malleable one. It is enduring in the sense that groups form naturally even where there are no preexisting differences and malleable in the sense that the group that one identifies with can change over time or between situations. Theoretical and empirical evidence justifies the generalization that members of a majority group tend to favor the assimilation of immigrants into the native culture, whereas immigrants are more likely to vote for pluralistic policies that acknowledge the distinctiveness of minority cultures. Hehman *et al.* have examined students' cultural assimilation and pluralism preferences at both a national and university campus level. As one would predict on the basis of their histories in the United States, white American undergraduates were more likely than their black classmates to vote for the establishment of English as the sole official language of the country. Similarly, when surveyed about funds to support multicultural activities on campus, white students were much less keen than their black classmates—when the context was a majority-white university. This preference disappeared, however, when white students at a majority-black institution were quizzed, revealing an association between minority status and pluralistic attitudes, regardless of individual identity. — GJC

Psychol. Sci. **23**, 46 (2012).

MICROBIOLOGY

Full Sequence Ahead

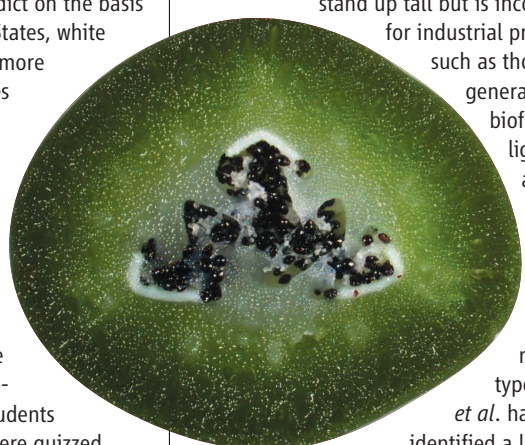
Some of the most abundant microorganisms in surface ocean communities are resistant to cultivation in the laboratory. Metagenome sequencing can reveal insights into the metabolism and physiology of such microbes, but the other ~200 fully sequenced marine microbial genomes to date remain poor references for useful comparisons. To provide a better genomic context for uncultivated microbes, Dupont *et al*. used metagenomic reconstructions of Global Ocean Survey samples to generate two nearly complete genomes of SAR86 bacteria, a clade of ubiquitous nonphotosynthetic γ–proteobacteria. The authors also sequenced two partial genomes of single cells within the SAR86 lineage collected off the coast of San Diego, USA. The reconstructed genomes and single-cell genomes all suggest that SAR86 bacteria have streamlined metabolisms: They cannot synthesize all of their required vitamins or amino acids and rely on specialized carbon sources. All four genomes also contain at least one gene encoding green light–tuned proteorhodopsin, which suggests that the organisms generate ATP via light-sensitive enzymes. The genomes vary significantly according to biogeography (i.e., sample locations and water temperatures), implying physiological differences. This broader genomic context may aid in future cultivation efforts. — NW

ISME J. 10.1038/ismej.2011.189 (2011).

PLANT SCIENCES

A Cactus by Any Other Name

Lignin polymers toughen up plant cell walls, which may be good for the plant that needs to stand up tall but is inconvenient for industrial processes such as those that generate pulp or biofuels. Most lignins are assembled from a small handful of common monomer types. Chen *et al*. have now identified a lignin that is constructed from an unusual subunit, the catechyl (C) monolignol caffeyl alcohol. The lignins in the black coats of seeds within the vanilla bean are entirely composed of these catechyl subunits. Other portions of the vanilla plant—the seed pod, stem, and leaves—instead contain the more standard sort of lignin, without the C subunit. A similarly high content of C-lignin was also found in seed coats of several cactus species, seeds that, like the vanilla seeds, carried black coats. Thus, there is greater natural diversity in these sturdy polymers than previously appreciated. — PJH



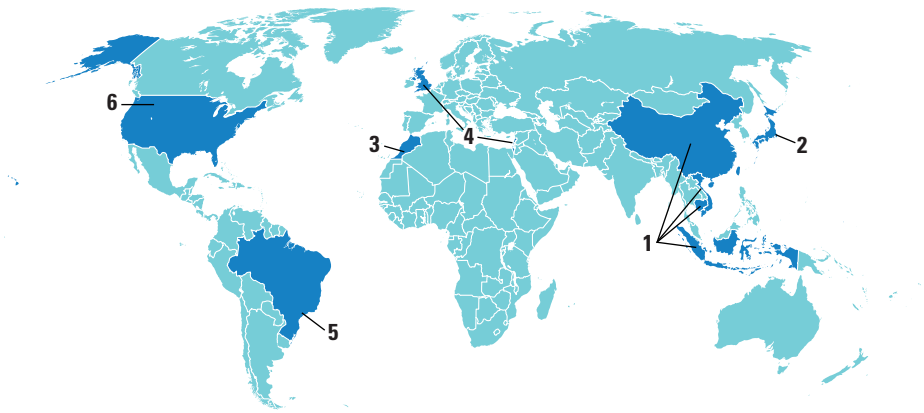
CREDIT: CHEN *ET AL.*, *PROC. NATL. ACAD. SCI. U.S.A.* **109**, 10.1073/PNAS.1120992109 (2012)

Proc. Natl. Acad. Sci. U.S.A. **109**, 10.1073/pnas.1120992109 (2012).

Downloaded from www.sciencemag.org on January 27, 2012

Published by AAAS

AROUND THE WORLD



Cambodia, China, Indonesia, and Vietnam **1**

H5N1 Continues to Kill

Even as controversy over a lab-created strain of the H5N1 bird flu virus rages, outbreaks of the natural strain continue in poultry in much of south and southeast Asia—and the human death toll is mounting. Since the beginning of the year, the virus has killed individuals in Cambodia, China, Indonesia, and Vietnam, and there has been a case of human infection in Egypt, according to the World Health Organization (WHO) and local press accounts. WHO reports that most of the recent human cases can be traced to contact with sick birds.

Since 2003, avian influenza has proved fatal in 343 of the 582 humans infected with H5N1. That high death rate portends a devastating pandemic if the virus evolves the ability to pass easily between humans. Earlier this year, two labs created a strain of H5N1 that might do just that, spreading from ferret to ferret with ease (*Science*, 6 January, p. 20). The teams have responded to the international uproar over the dangers of the studies by agreeing to halt related research for 60 days to allow for an "international discussion" (see p. 387).



Bird-borne. H5N1 deaths are linked to sick birds.

Tokyo **2**

University Considers Shifting Academic Year

Worried about being left behind in the globalization of higher education, the University of Tokyo is laying plans to shift the start of its school year from April to autumn—in 5 years or so.

Japan's April-to-March academic year is out of sync with the majority of universities around the world and is "one big reason" the country lags in both attracting international students and in sending its own youth abroad, said Takao Shimizu, a university biochemist who heads a committee recommending the switch.

The panel's preliminary report, released 20 January, notes that last year a mere 1.9% of undergrads at Todai, as the university is called in Japan, were international students. This compares with 10% at Harvard University and 7% at Stanford University.

Shimizu's committee will gather comment from within and beyond the university before finalizing its recommendations by the end of March. Todai doesn't want to go it alone, however. Officials there intend to launch discussions with 11 other top Japanese universities interested in the idea.
http://scim.ag/TodaiYear

Tissint, Morocco **3**

Mars Scientists Ecstatic Over 'Fresh' Mars Rocks

With samples hand-carried from Mars still decades away, researchers are rushing to look for signs of life in the latest arrivals from the Red Planet, the Tissint meteorites seen blazing through the atmosphere over Morocco last July. "I'm throwing everything I have at" the meteorites, says microbiologist Andrew Steele of the Geophysical Laboratory of the Carnegie Institution for Science in Washington, D.C.

Just last week, a committee of meteorite experts associated with the Meteoritical Society tentatively confirmed a martian origin for the meteorites. Meteorite dealers, who retrieved 7 kilograms of meteorites from the Moroccan desert in December, immediately shared samples with scientists in order to verify the meteorites' origin. Now that they've been verified as martian, slivers of these rocks are selling at tens of thousands of dollars an ounce.



New arrival. Freshly-fallen Mars meteorites are enticing scientists.

Since the excitement in the late 1990s over purported signs of ancient life in Mars meteorite ALH84001, Steele had reported finding remnants of microorganisms in that famous rock. But he also showed that those were contamined from the rock's 10,000 years on Earth. With only 6 months spent in the desert, Moroccan Mars meteorites look far more promising.

United Kingdom and Israel **4**

Partnership With Israeli Firm Stirs U.K. Museum Protest

The Natural History Museum in London is under fire for its scientific cooperation with an Israeli cosmetics company, Ahava/Dead Sea Laboratories, which conducts research in the occupied West Bank. On 17 January, *The Independent* newspaper published a letter from 21 prominent intellectuals, including scientists, musicians, authors, and film directors, calling on the museum to end its E.U.-funded collaboration with the firm on a nanoparticle research study.

Though officially headquarted south of Tel Aviv, Ahava's laboratories and factory are located in Mitzpe Shalem, a Jewish settlement on the banks of the Dead Sea, about 10 kilometers north of the recognized border between Israel and the Palestinian Territories. The United Nations and the International Court of Justice have said that Israel's settlements in the occupied West Bank are illegal. Israel, however, has dis-

CREDITS (TOP TO BOTTOM): LAURENCE GARVIE/ARIZONA STATE UNIVERSITY; REUTERS/NEWSCOM

Downloaded from www.sciencemag.org on January 27, 2012

Published by AAAS



Moon mappers. Ebb and Flow will map the moon's gravity.



puted that characterization.

Although the project will end in November, the letter writers say it's an issue still worth raising as the European Union reconsiders its criteria for future funding. "The main reason for doing it was to warn other people" who might be considering working with the company, says Patrick Bateson, president of the Zoological Society of London, who signed the letter.

http://scim.ag/AhavaDSL

São Paulo, Brazil **5**

Space Chief Appointed New Science Minister

Marco Antônio Raupp, currently president of the Brazilian Space Agency, will become his nation's new minister of science, technology, and innovation on 24 January. Raupp, 73, has more than 40 years of experience in research, a sharp contrast from his predecessor Aloizio Mercadante, an economist and leading figure in the governing Worker's Party who never received wide support from Brazil's scientific community.

A native of the relatively developed south of the country, Raupp graduated in physics from the Federal University of Rio Grande do Sul and got his Ph.D. in mathematics from the University of Chicago. He has taught at universities in Brazil's three most important cities: São Paulo, Rio de Janeiro, and Brasília.

Raupp said he was honored by his selection by Brazil's president and called it "a crucial moment" in the ministry's development. He said in a statement: "I am totally aware of the unprecedented demands being made on science, technology and innovation to contribute as an essential part of Brazil's social and economic development."

http://scim.ag/MARaupp

Bozeman, Montana **6**

Moon Orbiters Dubbed 'Ebb' and 'Flow'

Smash a (retroactive) champagne bottle on them. On 17 January, NASA's twin spacecraft—formerly dubbed Gravity Recovery and Interior Laboratory, or GRAIL A and B—were officially christened Ebb and Flow.

The monikers come thanks to Nina DiMauro's fourth-grade class at Emily Dickinson Elementary School in Bozeman, Montana, which wrote the winning essay in a contest to name the orbiters. If Ebb and Flow bring to mind the lunar pull on the tides, that's the point: DiMauro's pupils noted that they wanted to evoke the moon's most noticeable effect on Earth. "GRAIL-A and GRAIL-B are on a journey just like the moon is on a journey around the Earth," they wrote.

The Bozeman students beat out nearly 900 other classrooms across the country to name the probes, which launched last September and will begin their scientific mission in March. Ebb and Flow will keep an eye on the moon's gravity, mapping subtle changes across ridges and valleys.

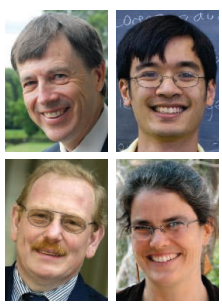
Lost and Found After 165 Years



A collection of "lost" fossils, some collected by Charles Darwin during his famous voyage on the HMS *Beagle*, went on display online at the British Geological Survey 17 January. Last year, Howard Falcon-Lang, a researcher at Royal Holloway, University of London, stumbled on the collection of 314 glass slides gathering dust bunnies in a wooden cabinet in the corner of the Geological Survey. Botanist Joseph Hooker, a close friend of Darwin's, originally assembled the collection in 1846 for the British Geological Survey. However, by the time the survey instituted a formal specimen register in 1848, Hooker had left to explore the Himalayas and was unavailable to help catalog his work. The slides contain micrometer-thin slices of fossilized wood and plants, early examples of thin sections that reveal the internal structures of monkey-puzzle tree cones (shown), petrified wood, and giant club mosses.

NEWSMAKERS

Crafoord Prizes Announced



Clockwise from top left: Bourgain, Tao, Ghez, and Genzel.

The Royal Swedish Academy of Sciences announced 19 January the four winners of the 2012 Crafoord Prize in the fields of mathematics and astronomy.

The two awardees in mathematics were **Terence Tao** of the University of California, Los Angeles (UCLA) and **Jean Bourgain** of the Institute for Advanced Study (IAS) in Princeton. **Reinhard Genzel** of the Max Planck Institute for Extraterrestrial Physics in Garching, Germany, and **Andrea Ghez** of UCLA will claim the prize for astronomy.

In 2004, Tao posited the Green-Tao theorem, which states that it's possible to create sequences of prime numbers of any length by adding any integer progressively to a starting number. For instance, in the sequence 5, 17, 29, 41, each prime is equally spaced by 12. Bourgain has proved several groundbreaking results on "well-posedness" of nonlinear differential equations, such as the Schrödinger equation of quantum mechanics and the Korteweg–de Vries equation of wave propagation.

Genzel and Ghez, are arguably the Coke and Pepsi of researchers studying supermassive black holes. Their groups independently produced compelling evidence that such a feature, 4 million times more massive than the sun, sits at the center of the Milky Way.

http://scim.ag/Crafoord

CREDITS (TOP TO BOTTOM): NASA/JPL-CALTECH; NASA/JPL-CALTECH/LMSS; CLIFF MOORE; REED HUTCHINSON/UCLA; MAX PLANCK INSTITUTE FOR EXTRATERRESTRIAL PHYSICS; ANDREA GHEZ; IPR/145-66CT BRITISH GEOLOGICAL SURVEY © NERC. ALL RIGHTS RESERVED

Downloaded from www.sciencemag.org on January 27, 2012

Published by AAAS

Random Sample

A New Way for Journals To Peer Review Papers?



Carsten Rahbek, editor-in-chief of *Ecography*, has a problem facing many journal editors. "Due to an explosion in the number of submitted papers, we have major problems finding people to review, and the quality has gone down as well," he says.

So Rahbek's journal, published by Wiley, has joined Peerage of Science, an online social network that aims to provide journals with already-peer-reviewed manuscripts. Recently founded by three Finnish ecologists, the Web site accepts paper submissions—and matches them with potential reviewers: Scientists with a potentially publishable paper can upload it to the Web site, while other members with relevant expertise, alerted by keywords in the papers, can provide reviews that scientific journals can use to decide whether to offer to publish the work.

Janne-Tuomas Seppänen, a postdoc at University of Jyväskylä, came up with the idea for Peerage of Science in 2010. Scientists receive one credit for every review they finish, whereas uploading a manuscript costs two credits divided by the number of authors. The author who uploads the paper must have a positive balance. "This formalises an unwritten rule: He who wants his manuscripts reviewed, reviews other manuscripts in return," says Seppänen. Since November, four manuscripts have received reviews.

Peerage of Science is currently free for journals, but its founders plan to charge fees that they say will be below what it costs a journal to handle its own peer review. Rahbek has so far encountered one article of interest to Ecography—which he decided not to publish. "But," he says, "I liked the procedure and the quality of the reviews." **http://scim.ag/peerofsci**

>>NEWSMAKERS

Smithsonian Director to Take Over Wildlife Conservation Society


Samper

Cristián Samper, director of the Smithsonian National Museum of Natural History, is shifting gears in August to become the president and CEO of the Wildlife Conservation Society (WCS), a $200 million conservation organization that runs the Bronx Zoo, other New York City zoos, and wildlife programs in 65 countries.

Samper started his career in conservation and says he is eager to get back to that focus. The natural history museum director since 2003, Samper helped transform the museum, bringing in 25 new curators, starting an endowed fellowship program, and redoing two-thirds of the exhibits, including the mammals, ocean, and human origins halls. In 2007, he took over temporarily for Smithsonian Institution Secretary Lawrence Small, who resigned amidst controversy. Samper again became the natural history museum's director after Wayne Clough was hired as the institution's secretary 15 months later.

Samper leaves the museum with a "major legacy," says Clough. "It's a great gain for WCS," says Jonathan Coddington, the museum's associate director for research and collections.

FINDINGS

Signature of Senescence

Last year, researchers retracted a *Science* paper that aimed to predict one's chance of living to 100 after critics discovered errors that invalidated the results. Now, the original group has revamped and republished their results, this time in *PLoS ONE*. Boston University biostatistician Paola Sebastiani, geriatrics specialist Thomas Perls, and their colleagues report a new "genetic signature" of 281 gene variants that has some overlap with the one they described in *Science* in July 2010, though it's less predictive, except in very old people.

The flap began 18 months ago, after the Boston team proposed a gene signature that they said could predict with 77% accuracy one's chance of becoming a centenarian. The work was criticized by geneticists who said it inflated the importance of a number of gene variants. Last July, the authors retracted the paper.

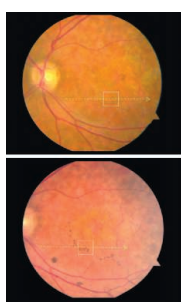
In the new work, almost no gene variants were very significant on their own at predicting life span, but in extremely elderly people, the overall signature was more likely to accurately predict their old age than in younger ones—evidence, says Perls, that "the heritability of longevity" increases the older we get. **http://scim.ag/_oldage**

BY THE NUMBERS

18% Percentage of reviewed research grant proposals that were funded by the National Institutes of Health in 2011, a record low.

5.7 million to 6.7 million Number of bats that have died from white nose syndrome since the disease was first documented in 2006, according to a new estimate by U.S. Fish and Wildlife Service biologists.

Embryonic Stem Cells for Eye Disease Appear Safe


Eye test. A Stargardt patient's eye before (*top*) and after receiving RPE cells.

In the first published report from a clinical trial using human embryonic stem cells, two legally blind patients who received hESC-derived cells in one eye have experienced no harmful side effects and appear to have slightly better vision. Although preliminary, the results are an important milestone for the hESC field.

Advanced Cell Technology (ACT) of Marlborough, Massachusetts, used hESCs to derive retinal pigment epithelium (RPE) cells, which nourish the retina's light-sensing cells. Collaborators at the University of California, Los Angeles, then injected 50,000 of these RPE cells under the retinas of a woman with Stargardt's macular dystrophy and another woman with dry age-related macular degeneration. Four months later, the patients have not developed tumors from the hESC-derived cells or shown signs of rejection, the team reported online this week in *The Lancet*. Both women showed some improvement on vision tests.

Other hESC researchers welcomed the report, but cautioned that the study was very small and designed only to test the safety of the procedure. ACT plans to test a total of 12 patients in each trial. **http://scim.ag/_eyes**

CREDITS (TOP TO BOTTOM): PEERAGE OF SCIENCE; S. D. SCHWARTZ *ET AL.*, *THE LANCET* (PUBLISHED ONLINE 23 JANUARY 2012); DONALD E. HURLBERT/NATIONAL MUSEUM OF NATURAL HISTORY, SMITHSONIAN INSTITUTION

Downloaded from www.sciencemag.org on January 27, 2012

Published by AAAS



Taking a break. Leading flu researchers will halt controversial studies involving H5N1 viruses (blue) for 2 months.

Flu Controversy Spurs Research Moratorium

Stung by a growing global controversy over the potential dangers of experiments involving the H5N1 avian influenza virus—and worried about possible government regulation—a group of leading influenza researchers last week agreed to a 60-day moratorium on some sensitive flu studies "to provide time" for international discussions.

"We recognize that we and the rest of the scientific community need to clearly explain the benefits of this important research and the measures taken to minimize its possible risks," the 39 researchers wrote in a statement published by *Science* and *Nature* (see p. 400). During the "voluntary pause," the scientists—who represent the world's major H5N1 research centers—have agreed to halt several types of studies, including experiments that could create H5N1 viruses that move more easily between mammals.

Flu experts are also helping to organize a summit on the issue, to be hosted by the World Health Organization (WHO) in Geneva on 16–17 February, which is expected to involve about 50 experts. But "it's not going to be a simple one-meeting process," says Keiji Fukuda, WHO's assistant director-general for health security and environment. "We don't want it to take forever, but [we] can't address all the issues at the same time."

"Governments and organizations need time to react," says virologist Ron Fouchier of Erasmus MC in Rotterdam, the Netherlands, who helped craft the agreement and is involved in the research that triggered the global debate (*Science*, 6 January, p. 20). Investigators on all sides of the controversy, meanwhile, welcomed the move, saying it will help ease tensions and clarify potential risks. But some question whether 2 months is enough time to resolve thorny conflicts between science and security or to institute national or international oversight. Biosecurity expert John Steinbruner of the University of Maryland, College Park, for instance, wonders whether governments can "do anything meaningful within the 60-day period. … What happens if they do not?" And one skeptic calls the moratorium "an empty gesture" designed to fend off stringent U.S. controls on research.

The announcement capped months of rising tension over two studies, in press at *Science* and *Nature*, which describe how researchers made the H5N1 virus more transmissible between ferrets, the animal model that most closely resembles humans in flu studies. The researchers say the work offers benefits for preventing flu pandemics, but others are worried that the studies could provide a blueprint for the creation of a bioweapon or lead to an accidental release of the virus. (Although H5N1 viruses readily kill entire chicken flocks and occasionally infect humans, they have not until now transmitted efficiently between mammals.)

In late December 2011, the U.S. National Science Advisory Board for Biosecurity (NSABB) announced that it had taken the unprecedented step of asking Fouchier, the lead author of the *Science* paper, and *Nature* lead author Yoshihiro Kawaoka of the University of Wisconsin, Madison, and the University of Tokyo to omit key details. The researchers and the journals reluctantly agreed, provided that the U.S. government, which funded the studies, came up with a way of sharing the details with "responsible" scientists and public health experts.

The deal sparked extensive criticism—with some scientists saying that redaction went too far, and others arguing that researchers should not have conducted the studies in the first place. It also set off shock waves in policymaking circles. In Washington, U.S. officials rapidly restarted a long-stalled process aimed at tightening oversight of so-called dual-use biological research. WHO, meanwhile, warned that the redactions could imperil a nascent global agreement to share flu viruses and the benefits of research on them. On 8 January, *The New York Times* weighed in with an editorial headlined "An Engineered Doomsday" that questioned the studies and called on scientists to destroy the new H5N1 variants in the name of safety.

Such high-profile attention prompted senior scientists at the U.S. National Institutes of Health (NIH) and elsewhere to warn flu researchers that the controversy could prompt government officials and lawmakers to impose onerous new rules on research. Others argued that the episode exposed the need to address troubling gaps in U.S. and global efforts to oversee research that could be used for good and evil. To give such issues a full hearing, a number of key players in the debate, including NSABB Chair Paul Keim, a microbiologist at Northern Arizona University in Flagstaff, floated the idea of a moratorium. But Keim advocated a stop only on publishing the results; flu scientists have gone much further by halting research. The pause is modeled in part on a landmark 1975 pact reached by scientists in the then-new field of recombinant DNA, who were also facing questions about safety. That moratorium led to a meeting in Asilomar, California, where scientists proposed safety guidelines for genetic engineering.

"I thought it would be a good idea for the investigators themselves to call for a time-

Online
sciencemag.org
More H5N1 coverage is at http://scim.ag/_H5N1.

CREDIT: GETTY IMAGES/PHOTO RESEARCHERS

Downloaded from www.sciencemag.org on January 27, 2012

Published by AAAS

Ron Fouchier: In the Eye of the Storm

In a statement posted on the Web sites of *Nature* and *Science* last week and published on page 400 of this issue, a group of leading influenza researchers announced a 2-month moratorium on studies that make the avian influenza strain H5N1 more transmissible between mammals. The moratorium is intended to allow time for an international debate about this type of research, which some people say has the potential to help bioterrorists.

Science talked to Ron Fouchier of Erasmus MC in Rotterdam, the Netherlands, who carried out one of the two studies that triggered the international debate. (His paper is under review at *Science*.) Fouchier's answers have been translated from Dutch and edited for clarity and brevity. An extended transcript of the interview is posted online at http://scim.ag/RFouchier.

–MARTIN ENSERINK

Q: Who took the initiative for this announcement?
R.F.: The initiative came from Adolfo Sastre-García [an influenza researcher at Mount Sinai Medical Center in New York City who has a grant from the National Institute of Allergy and Infectious Diseases that funded Fouchier's study], Yoshihiro Kawaoka [whose H5N1 study, in press at *Nature*, has also been reviewed by the U.S. National Science Advisory Board for Biosecurity (NSABB)], and myself. We discussed it with a group of about 10 scientists who are doing similar studies themselves; then we asked another 30 or so influenza researchers who are not working on these studies but who could do them, if they wanted to sign. They all agreed wholeheartedly. So it's not a Fouchier show. It's an initiative that is supported very broadly.

Q: Why did you take this step now?
R.F.: We were advised by various organizations, and of course we've followed the press coverage and the political debates. We had the impression, based partly on advice from third parties, that it would be sensible to announce a moratorium.

Q: Which third parties?
R.F.: The organizations that fund our research, but also governments that we are talking to. So much is happening at the moment that it makes sense to take a break, to give the infectious diseases field time to think this over and talk about how to handle this kind of research in the future.

Q: Are you doing this because if you don't, governments might move to halt the research?
R.F.: The debate is so controversial that we can't rule that out. We'd rather have everybody take a breather to reflect carefully on how to handle this.

Q: How do you feel about the moratorium yourself?
R.F.: It's a pity that it has to come to this. I would have preferred if this hadn't caused so much controversy, but it has happened and we can't change that. So I think it's the right step to make. It's comparable to what happened in 1975 at the Asilomar conference. But I think that was driven more by the scientists themselves; this time it's mostly the public controversies that drive it.

Q: Has the scale of the controversy surprised you? Had you expected this when you first discussed the study at a meeting in Malta in September?
R.F.: When we presented this, of course we expected that there would be some commotion, and that we would have to explain to the public and the press why we're doing this and how you can do it safely.

out," says Anthony Fauci, head of the National Institute of Allergy and Infectious Diseases (NIAID) in Bethesda, Maryland, who discussed the idea at length with Fouchier. "I have concerns that people [who are] understandably concerned about security may put restrictions on important research that might go a little bit too far. We have to be extremely sensitive to safety and security, … but what I would not want to see is an overreaction."

The announcement has drawn mostly positive reviews. "Anything that moves us toward a thoughtful and comprehensive discussion is really helpful," says flu expert Michael Osterholm, a member of the NSABB and director of the Center for Infectious Disease Research and Policy at the University of Minnesota, Twin Cities.

That view is also shared by an outspoken critic of NSABB's redaction request, virologist Vincent Racaniello of Columbia University. "A dialogue to identify the crucial issues and develop plans to address them, while continuing this important line of research, is certainly welcome," he says. Indeed, 2 days before the moratorium announcement, Racaniello was one of 18 researchers who signed a letter to Osterholm and other NSABB members, asking them to reconsider its recommendation that the papers be redacted. Such a request "warrants pause and a rational discussion of the scientific facts." The signers also included Eckard Wimmer of Stony Brook University in New York, the author of a controversial 2002 study that demonstrated how to assemble a synthetic poliovirus (*Science*, 9 August 2002, p. 1016), and NSABB critics Peter Palese and Adolfo García-Sastre of the Mount Sinai School of Medicine in New York City. (Both also signed the moratorium letter, and García-Sastre leads an NIAID-funded center that subcontracted for Fouchier's work.)



Fact checker. WHO's Fukuda says a flu summit will help clarify issues.

CREDIT: COURTESY OF WHO

On the other side of the debate, smallpox expert Donald Henderson of the Center for Biosecurity at the University of Pittsburgh in Pennsylvania, who has backed NSABB's decision and criticized the studies, calls the moratorium "wise. … This has to be a societal decision," and the pause will "provide an interval for [people] other than the laboratory scientists to weigh in," including political and religious leaders.

Another vocal critic of the flu studies, however, is not impressed, calling the moratorium "pure PR." It's telling, says Richard Ebright, a biologist at Rutgers University in Piscataway, New Jersey, and the Howard Hughes Medical Institute, that the researchers' statement emphasizes the safety and benefits of H5N1 research but "rejects, out of hand, the need for enhanced biosafety, biosecurity, and dual-use oversight." If the researchers had proposed a moratorium that lasted until those issues were addressed, "it could be taken seriously," he says. Without that, the letter "is strictly symbolic. An empty gesture."

Ebright would like to see all research on H5N1 strains engineered to be transmissible among mammals halted until the WHO dis-

Downloaded from www.sciencemag.org on January 27, 2012

Published by AAAS

I think we have done that very well in the Netherlands. We were very proactive; before we submitted the paper for publication, we informed all the relevant authorities so they knew what was happening and had the time to prepare, and when the story started making the rounds in the U.S. media, we spent 3 days talking to [Dutch] newspapers, TV, and radio. And that nipped the debate [in the Netherlands] in the bud. In the U.S., this hasn't happened. And the people who are the most vocal in the press are the biosecurity experts. It's a pity that so few people from the flu field have jumped in front of the cameras, especially in the U.S.

Q: Did the NSABB recommendations take you by surprise?

R.F.: Absolutely. This was something that was unprecedented, and something I wasn't counting on at all.

NSABB has said that the risks outweigh the benefits, and now many people are saying, "In that case, you shouldn't do this research at all." That's a very logical response. But the infectious-disease community doesn't agree with NSABB on this. What NSABB should explain better is what the risks are exactly. How much bioterrorism have we seen in the past? What are the chances that bioterrorists will recreate these viruses? And is it really true that publication of this research would give bioterrorists or rogue nations an advantage? That's what I would like to hear from the NSABB.



"It's a pity that it has come to this."

—RON FOUCHIER, ERASMUS MC

Q: You think it doesn't give them an advantage?

R.F.: No. Because bioterrorists can't make this virus; it's too complex, you need a lot of expertise. And rogue nations that do have the capacity to do this don't need our information. … Meanwhile, NSABB gives very little credit to the public health benefits, while the entire influenza community is crying just how important that is. For them the balance between risk and benefit is very different than for NSABB.

Q: In a policy forum you co-authored and which was published last week on *Science*'s Web site, you suggest that you cannot promise to always keep the key details from your paper secret. Under what circumstances would you decide to reveal them?

R.F.: Well, *Science* and we have said that we're going to try to adhere to NSABB's recommendations. The U.S. government is now searching for a mechanism to share the key details with people who have a legitimate need to see them, but this is far from easy; there are all kinds of legal issues. So what that mechanism will look like and whom that information can be shared with is very unclear. Meanwhile, the World Health Organization has said: This research is super-important, but it's just as important that the data are shared, or it could mean the end of the *Pandemic Influenza Preparedness Framework*. … Also, as researchers, we work very closely with people in Indonesia. It would be very unwise for us not to share our results with our close collaborators.

Downloaded from www.sciencemag.org on January 27, 2012

cussions produce stringent global controls, including limiting the total number of labs working with the strains to just two. He also supports the creation of a global oversight panel—similar to the WHO panel that oversees smallpox research—to review studies and ensure that experiments occur only under the most stringent safety conditions.

WHO's Fukuda, however, notes that "we are not a regulatory agency. We know we are not going to put out any regulatory framework." Instead, he says a first step will be simply getting the facts. NSABB members haven't briefed WHO on their reasoning, he notes, and "my overall sense is that most people are pretty confused about what are all the issues. Most people are standing back to see if they should feel one way or another. … One country or research group doesn't reflect the concerns of others."

Then, he says, he hopes the group will first tackle the most urgent issues, such as deciding how best to deal with potentially sensitive information in the papers. The journals have said that they will not publish the papers until that is resolved, and the U.S. government has reportedly asked to have until at least late February to figure it out. "The first thing I would tell everyone," Fukuda says, is "convince me that [redacting the papers is] the only option out there. Let's talk about what's the nature of the sensitivity. … What are the concerns, what do we hope for in getting the information out, and then what are the options? We want to go in not prejudging any of the issues."

One big concern will be how any information-sharing system might affect WHO's new Pandemic Influenza Preparedness (PIP) Framework, agreed to earlier this year after 4 years of often-acrimonious debate. The PIP, which stipulates that countries that provide virus samples should also receive at least some benefits of influenza research, such as vaccines, "is in a vulnerable period," Fukuda says. "As we work through this quite complicated set of questions, we want to make sure … that the whole global system of providing viruses and sharing benefits doesn't take a pause." The issue is especially sensitive, other researchers note, because WHO's global lab network provided the H5N1 isolates used by Fouchier and Kawaoka.

Fukuda says other questions may have to wait a bit longer for answers, such as: "How do we make sure we continue research but do it in a way that doesn't cause people and countries undue anxiety?" In the end, however, he is optimistic the group can reach consensus, noting that "at WHO we often deal with tough issues. … We can start the discussions and see how far we get. Starting with 60 days doesn't mean you can't do something afterwards that keeps the pressure down."

Whether the moratorium and summit will reduce growing pressure for tighter research oversight in the United States, however, remains unclear. A multiagency group has restarted work on formalizing 2007 recommendations from NSABB on procedures for reviewing dual-use research, with a draft statement due sometime this spring. NIH has briefed staff members for several key lawmakers—including senators Joe Lieberman (I–CT) and Susan Collins (R–ME), the top members of the U.S. Senate Committee on Homeland Security and Governmental Affairs. So far, however, Congress has been notably silent on the controversy.

–DAVID MALAKOFF

With reporting by Martin Enserink, Gretchen Vogel, and Jon Cohen.

CREDIT: DIRK-JAN VISSER

Published by AAAS

CHINA

An Explosive Return of the 'Great Pox'

NANJING, CHINA—Examining a patient one day in the 1980s, newly minted doctor Chen Xiangsheng saw a pinkish rash covering the man's chest. He never imagined it could be syphilis, which was eliminated by an aggressive 1950s campaign that shut down brothels, screened sex workers, and administered penicillin. By the time Chen entered medical school in 1979, students were no longer trained to spot the disease. He thought his patient had *pityriasis rosea,* a skin rash. Chen's supervisor corrected the diagnosis.

Chen has since become all too familiar with the telltale symptoms of a sexually transmitted disease (STD) once known as "the great pox." As breakneck economic development ushered in widespread migration, rising inequality, and evolving sexual mores, syphilis transmission spiked in China. It now holds the dubious title of the nation with the largest increase in reported cases in the penicillin era. (For half a century, the antibiotic has been the main defense against *Treponema pallidum*, the bacterium that causes the disease.) In response, China's health ministry has just embarked on a 10-year plan to combat what Chen, now vice director of the National Center for STD Control here, calls "a scourge lurking in the shadows."

China's troubles date to social and economic changes unleashed in the 1980s, when millions of farmers flocked to the cities. At the same time, restrictions on cohabitation and marriage were loosened or ignored. "Ideas and concepts came in from outside, and more people wanted sexual freedom," Chen explains. Prostitution grew along with inequality, and a swelling disadvantaged class had poor access to health care, says Francis Ndowa, lead specialist for controlling STD infections at the World Health Organization.

By the late 1990s, China's reported syphilis cases were rising by about 30% per year. The annual increase has since slowed but remains high, at 8.4% in 2010, and reported cases more than doubled between 2005 and 2009, to 11.7 cases per 100,000 people—compared with 4.6 cases per 100,000 people that year in the United States. In 2008, Guangdong Province reported more syphilis cases than the entire European Union.

Scientists say those figures should be treated with caution. Underreporting may be common in poorer provinces, some warn. Others dispute the extent to which syphilis is spreading. They point out that cases spiked after China switched to a Web-based reporting system in 2004. But everyone agrees that syphilis is rampant, especially in coastal cities with large migrant populations. In several major cities in China, it is now the leading reported infectious disease.

Some researchers suspect that China's elimination of syphilis in 1964, through limiting herd immunity, left the population unusually susceptible to *T. pallidum* infection. More critical may be the behavior of members of key risk groups. About 10% of urban Chinese men age 18 to 49 say they have hired a prostitute. Condom use is low, and demand for commercial sex is fueled by a gender imbalance brought on by sex-selective abortion, which has left tens of millions of men with poor marriage prospects. Another sizable risk group is men who have sex with men, of whom roughly a third are married, meaning their wives may be at risk too.Says Chen: "Many developed countries have a syphilis epidemic among men who have sex with men. Many developing countries have an epidemic among female sex workers. China has it in both groups."



According to figures from China reported in 2010, an estimated 8.4% of men who have sex with men, and 2.9% of sex workers, were seropositive for syphilis—compared with 1.1% and 1.6%, respectively, among the same groups in Vietnam in 2009. Also under surveillance are pregnant women, who can pass the disease to their babies. A 2007 study of half a million expectant mothers in Shenzhen found that one in 200 had syphilis. The trend is doubly worrisome, as syphilis increases the risk of HIV acquisition and transmission.

The health ministry's new initiative aims to halt the rise in adult syphilis cases and reduce congenital syphilis from the current reported rate of 66.5 cases per 100,000 live births to under 15 per 100,000 by 2020. The central government has tagged $3.2 million for syphilis prevention and control this year, a fraction of the budget for HIV control, but public health experts hope a separate $140 million pool of funding for preventing mother-to-child transmission of STDs through screening and treatment will help tamp down congenital syphilis cases. "China has an advantage in its unique ability to act so definitively in public health," says Myron Cohen, an AIDS researcher at the University of North Carolina, Chapel Hill.

But much has changed since the war on syphilis a half-century ago. Cultural stigma keeps many patients away from the clinic: Sex workers and gay men have been singled out for persecution and remain wary of testing and treatment efforts. That's one reason the health ministry is warming to nongovernmental organizations, which have been viewed with suspicion in the past. "Civil society groups are quite well connected with the target group, and the community may be more receptive to them,"says Loretta Wong, director of AIDS Concern, a Hong Kong–based group that does syphilis outreach with gay men and sex workers.



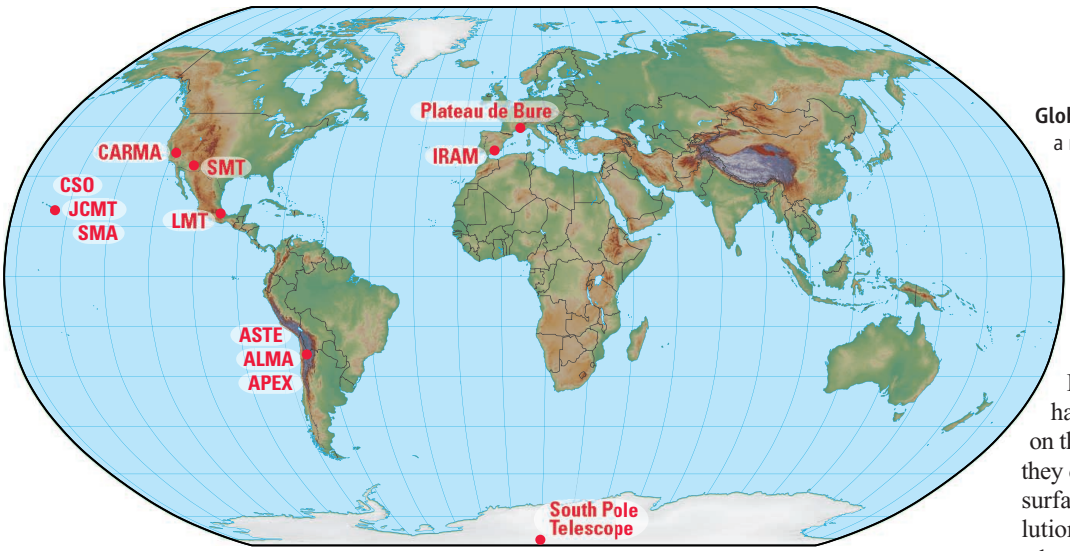
Ancient scourge. National Center for STD Control vice director Chen Xiangsheng (*right*) worries about the rapid spread of syphilis in China.

One source of hope is rapid tests that can be performed outside the clinic. Yin Yueping, a lab director at the national STD center, spreads a selection of test kits on a table. The tests cost less than $1 each, require only a finger prick, and, as with over-the-counter pregnancy tests, results are fast and easy to read. Yin is working to get the kits into rural health centers. That won't be easy. But like it or not, these days Chinese doctors know their enemy when they see it. **–MARA HVISTENDAHL**

GRAPH SOURCE: CHEN XIANG-SHENG; PHOTO CREDIT: MARA HVISTENDAHL

Downloaded from www.sciencemag.org on January 27, 2012

Published by AAAS



Global coverage. Radio telescopes that could play a role in the Event Horizon Telescope.

ASTRONOMY

Worldwide Telescope Aims to Look Into Milky Way Galaxy's Black Heart

The center of our galaxy—surrounded by a maelstrom of stars, gas, and dust, and separated from us by 26,000 light-years of space filled with all the detritus of the galactic plane—is one of the most challenging things for astronomers to observe. Last week, astronomers gathered in Tucson, Arizona, to work out a plan to combine data from radio telescopes worldwide and create, in effect, a dish the size of Earth. With such a virtual instrument, they say, they'll be able to peer into our galaxy's heart and see the supermassive black hole that resides there.

"It would be an amazing thing. It's never been done before, getting an image of a black hole," says one of the project's organizers, astronomer Daniel Marrone of the University of Arizona's Steward Observatory. Heino Falcke of Radboud University in Nijmegen, the Netherlands, agrees. "This is a very, very important thing to do," he says. Despite such enthusiasm, however, it's not yet clear how a worldwide collaboration would be organized or funded. "Most of the relevant telescopes had someone present [in Tucson], and all wanted to make it work. But there was no real consensus on how to do it," says Falcke, who, along with two colleagues, first suggested in 2000 that such observations might be possible (*Science*, 7 January 2000, p. 65).

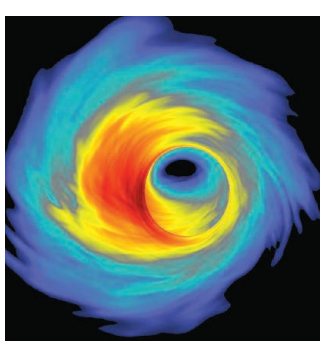
The organizational details are "still in flux," says Shep Doeleman, an astronomer at the Massachusetts Institute of Technology's Haystack Observatory in Westford and principal investigator of the project, known as the Event Horizon Telescope (EHT). But with such a tantalizing scientific goal and an estimated cost of a few million dollars to upgrade instruments at some telescopes, "I don't see problems getting the resources," Doeleman says.

Black holes are extremely difficult to see directly because they emit no light, except possibly the proposed very faint Hawking radiation. Astronomers have inferred the presence of black holes by observing nearby gas or orbiting stars. Being able to observe one directly would be a huge advance for astrophysicists. "Black holes may be part of our everyday lives, but they haven't been proven. No one has seen an event horizon," Falcke says. As well as obtaining proof, direct observation would allow astronomers to study how black holes swallow up nearby material, a process known as accretion, and how the jets of material often seen coming out of them form. They could also conduct precise tests of general relativity, something never done in such a strong gravitational field.

Our galaxy's central black hole, known as Sagittarius A* (Sgr A*), is thought to be 4 million times as massive as the sun but only 30 times as wide, smaller than Mercury's orbit. Proponents of EHT believe they can image it—or rather, see its "shadow" against a bright background of hot gas—using a technique known as very long baseline interferometry (VLBI). It takes data from widely spaced dishes and combines them as if they were two small patches of a large dish. A VLBI array lacks the light-collecting power of a full dish its size, but with enough small patches it can build up a high-resolution image of distant objects.

In a sense, EHT has begun observing already. For several years, Doeleman, Marrone, and colleagues have been observing Sgr A* using dishes in Hawaii, Arizona, and California. They have seen features of the galactic center on the same scale as the black hole, although they don't yet have the resolution to image its surface, the event horizon. To improve resolution they need to use shorter wavelengths, a longer baseline, or both. The shorter wavelengths are on the way: The team hopes soon to switch its observations from light with a wavelength of 1.3 millimeters to 0.83 millimeters—fortuitously, a wavelength in which the material of the galactic plane is relatively transparent. But they are "pushing up to near the limit of the radio window in the atmosphere," Marrone says.

To extend the baseline will require more telescopes. About a dozen around the world either are equipped to work at such short wavelengths or can be adapted relatively cheaply. In addition, EHT needs to incorporate the Atacama Large Millimeter/Submillimeter Array (ALMA) in Chile (*Science*, 30 September 2011, p. 1820). ALMA's 66 dishes high in the Andes will match the collecting power of a 90-meter-wide dish. "ALMA is key because of its enormous collecting power and sensitivity," says theorist Dimitrios Psaltis of the Steward Observatory. It is also far from other observatories, creating a long baseline.



Eye of the storm. Simulation of hot gas around a black hole.

EHT researchers at Haystack have won $4 million from the U.S. National Science Foundation to equip ALMA for VLBI. ALMA, which is not yet complete, should be ready to play a part in EHT by 2015. To get an even longer baseline, the project would also like to enlist the South Pole Telescope (*Science*, 16 March 2007, p. 1523), but it will require upgrading to make it suitable.

EHT's enthusiastic reception at Tucson has set the ball rolling, and researchers have set up a committee to work out the details of an international collaboration. "We're aiming for an MOU [memorandum of understanding] this summer, though tests and work will go on under the current, less formal, arrangements," Marrone says. **–DANIEL CLERY**

CREDIT: SCOTT NOBLE/RIT

Downloaded from www.sciencemag.org on January 27, 2012

Published by AAAS



Double-barreled. The Relativistic Heavy Ion Collider uses two independent accelerators in a tunnel.

NUCLEAR PHYSICS

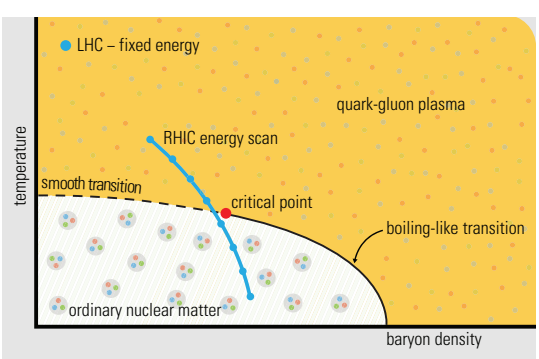
DOE Funding Crunch Threatens Future Of Only U.S. Collider Still Running

UPTON, NEW YORK—Here beneath the hushed pine barrens of Long Island, scientists first recreated the conditions of the big bang. Using an atom smasher called the Relativistic Heavy Ion Collider (RHIC) at Brookhaven National Laboratory, physicists melted atomic nuclei to produce a soup of particles called a quark-gluon plasma, the same stuff that filled space a microsecond after the cosmos's birth. Over the past decade those experiments have given researchers a new perspective on the strong nuclear force that binds 99.95% of ordinary matter. "RHIC has been enormously productive and has established leadership in pioneering a new field of nuclear physics," says Steven Vigdor, Brookhaven's associate director for nuclear and particle physics.

Brookhaven physicists plan to press their advantage. As they continually upgrade the $1.1 billion collider and the two big particle detectors it feeds, known as STAR and PHENIX, they hope to map out the relationship between ordinary nuclear matter made of protons and neutrons and the quark-gluon plasma, which may be analogous to the relationship between liquid water and steam. They are also planning a $500 million upgrade for early next decade that would enable the collider to answer a key puzzle about the proton itself—if RHIC lasts that long.

With Congress slashing spending, the Department of Energy (DOE), which owns Brookhaven, faces intense pressure on its science budget. On 1 December 2011, Timothy Hallman, head of the $550 million nuclear physics program in DOE's Office of Science, told the nuclear science advisory committee that the department's 2013 budget request, to be unveiled next month, probably won't support all the projects the committee specified in its 2007 long-range plan. So DOE officials may soon have to toss overboard one of three major projects (see table, p. 393).

In particular, observers say, DOE may have to choose between running RHIC or building a $615 million accelerator, known as the Facility for Rare Isotope Beams (FRIB), at Michigan State University in East Lansing. "I would hate to see it come down to a shootout like that, but it's kind of looking that way," says Thomas Ludlam, chair of Brookhaven's physics department.



Mapping mission. By probing nuclear matter at different temperatures and densities, RHIC hopes to fill out the "phase diagram" describing the universe's primordial matter.

RHIC scientists say their machine still has plenty of fertile ground to till, as the 4-trillion-degree plasma that it has blasted into existence has proved stranger than expected. To create the plasma, physicists must melt the building blocks of the atomic nucleus: protons and neutrons. A proton or a neutron consists of three quarks with gluons zinging among them to convey the strong force. That force is so strong that an isolated quark or gluon cannot exist. Knock a quark out of a proton, and it will pull quarks and antiquarks out of the vacuum to create more particles that contain either three quarks or a quark and an antiquark.

Still, physicists predicted that they could liberate quarks and gluons to a certain degree if they collided nuclei with enough energy to melt the protons and neutrons. They did just that by colliding gold ions within RHIC, which comprises two countercirculating accelerators in a 3.8-kilometer tunnel.

Theorists had predicted that the resulting quark-gluon plasma would act like a gas, in which the particles barely interact. Instead, as researchers reported in 2005, the quarks and gluons feel one another's presence strongly, so that an oblong puff of plasma flows like a liquid before condensing into thousands of particles. "We don't really understand what we've created," says Brookhaven's Edward O'Brien, who works on RHIC's PHENIX detector. "There were all these predictions that turned out to be wrong."

In the past 2 years, experimenters have begun to map out the relationship between the quark-gluon plasma and ordinary nuclei. A "phase diagram" for water shows the temperatures and pressures at which it is a liquid or a vapor. A line traces the boiling transition between the two phases and ends at a "critical point," beyond which transition is seamless. A similar diagram may describe nuclear matter, with the role of pressure played by "baryon density," the number of protons and neutrons crammed into a volume.

RHIC researchers have searched for the transition line and critical point by going down in energy to reduce temperature and increase baryon density. In coming years, they will perform more such variations and will characterize the plasma more quantitatively, Ludlam says.

Even as some physicists at RHIC have reconstructed the primordial plasma, others have probed the proton itself. In reality, a proton is more than just three quarks. Within it, countless

CREDITS (TOP TO BOTTOM): COURTESY OF BROOKHAVEN NATIONAL LABORATORY; GARVIN GRULLÓN

Downloaded from www.sciencemag.org on January 27, 2012

Published by AAAS

gluons whiz about, and quark-antiquark pairs flit in and out of existence to form a "sea" surrounding the three "valence" quarks. How the proton's properties emerge from that mess remains murky.

For example, physicists have long known that the proton's electrical charge is just the sum of the charges of the three valence quarks. But the proton also possesses an unquenchable half-quantum of angular moment or spin. Most physicists had assumed that the sum of the valence quarks' spins would account for the proton's spin. But in the 1980s, researchers at CERN, Europe's particle physics laboratory in Switzerland, fired electrons into protons and found that the alignment of valence quarks accounted for a small fraction of the total spin.

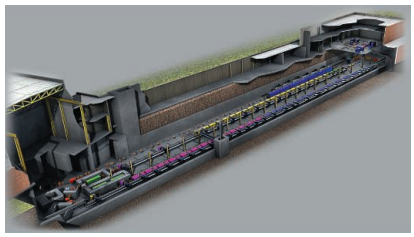
Physicists responded to that "spin crisis" by hypothesizing that the proton's spin must emerge from the alignment spins of the gluons. RHIC was uniquely suited to test that assumption, as it is the only collider in the world that can create beams of protons "polarized" so that most of them spin in the same direction. But in 2006, RHIC researchers showed that the gluons—at least the more energetic ones—provide very little spin. "All the predictions that the spin is in the gluons are ruled out," says Brookhaven's Elke Aschenauer.

The mystery isn't unsolvable. The spin could originate in the polarization of low-energy gluons or the "orbital" motion of the valence quarks around each other. In fact, RHIC's long-term future lies in sorting the matter out. Physicists propose to add an electron accelerator to collide electrons and polarized protons, giving them the tool they need. "I don't see anywhere else where this puzzle can be solved," says Abhay Deshpande of Stony Brook University in New York.

When it comes to making quark-gluon plasma, RHIC is not the only game in town. The Large Hadron Collider (LHC) at CERN, which turned on in 2010, makes the stuff by smashing lead ions. Last year, it put the only U.S. collider besides RHIC out of business. Particle physicists at Fermi National Accelerator Laboratory in Batavia, Illinois, had been using the lab's Tevatron to blast protons into antiprotons and search for a prized particle called the Higgs boson. But with the LHC coming on strong, DOE shuttered the 26-year-old Tevatron in September.

At first blush, the LHC might appear to render RHIC obsolete, too. "When I talk to particle physicists, they say, 'Well, the LHC is at higher energy [than RHIC], so why don't you just give up?' " says Brookhaven's Vigdor. However, even physicists who work at the LHC say the machines are complementary. "To say 'Oh, we have the LHC, so just shut RHIC down,' that would be a scientific disaster," says Alexander Milov of the Weizmann Institute of Science in Rehovot, Israel, who studies quark-gluon plasma with a massive particle detector called ATLAS at the LHC.

RHIC is more flexible than the LHC, says Paolo Giubellino of Italy's National Institute of Nuclear Physics in Turin, spokesperson for the team working with ALICE, a particle detector at the LHC that is dedicated to quark-gluon plasma studies. For example, RHIC can go down in energy and can collide dissimilar ions such as copper and uranium. Still, with its higher energy, the LHC can probe the plasma in ways RHIC can't, Giubellino says, for example, by producing heavier types of particles within it.



Fountainhead. The Facility for Rare Isotope Beams would produce myriad exotic nuclei.

CREDIT: COURTESY OF FRIB

On a Collision Course?

Facility	Location	Mission	Status
RHIC Relativistic Heavy Ion Collider	Brookhaven National Laboratory, Upton, NY	Reproduce quark-gluon plasma that filled early universe	$1.1 billion collider running since 2000
CEBAF Continuous Electron Beam Accelerator Facility	Thomas Jefferson National Accelerator Facility, Newport News, VA	Probe the inner workings of protons and neutrons	$310 million upgrade halfway completed
FRIB Facility for Rare Isotope Beams	Michigan State University, East Lansing	Produce exotic short-lived nuclei for myriad experiments	$615 million accelerator not yet approved for construction

Time on task also favors RHIC. The LHC smashes heavy nuclei for at most a few weeks a year, notes Boleslaw Wyslouch of the Massachusetts Institute of Technology in Cambridge, who studies quark-gluon plasma with the CMS detector at the LHC. "At the LHC, you do one thing for 4 weeks and that's it," he says. "The next chance is in 1 or 2 or 3 years." RHIC can study quark-gluon plasmas for extended periods.

Such considerations may not ensure RHIC's continuation, however. DOE may have chose among its three major nuclear physics projects. DOE also funds the Continuous Electron Beam Accelerator Facility (CEBAF) at Thomas Jefferson National Accelerator Facility in Newport News, Virginia, which uses electrons largely to probe the innards of protons and neutrons. And in December 2008, DOE picked the National Superconducting Cyclotron Laboratory (NSCL) at Michigan State as the site for FRIB, which would produce exotic nuclei for myriad experiments.

DOE is halfway through a $310 million upgrade to CEBAF and, thus, probably won't pull the plug on it, observers say. The choice could then come down to continuing to run RHIC or building FRIB.

The United States needs FRIB to maintain its lead in the broadest part of nuclear physics, the study of actual nuclei, says Konrad Gelbke, director of NSCL, which is now funded by the National Science Foundation. FRIB would generate highly unstable exotic nuclei at rates thousands of times higher than NSCL's current accelerators can. Data from FRIB could pin down where in stellar explosions half the nuclei heavier than iron come from, Gelbke says.

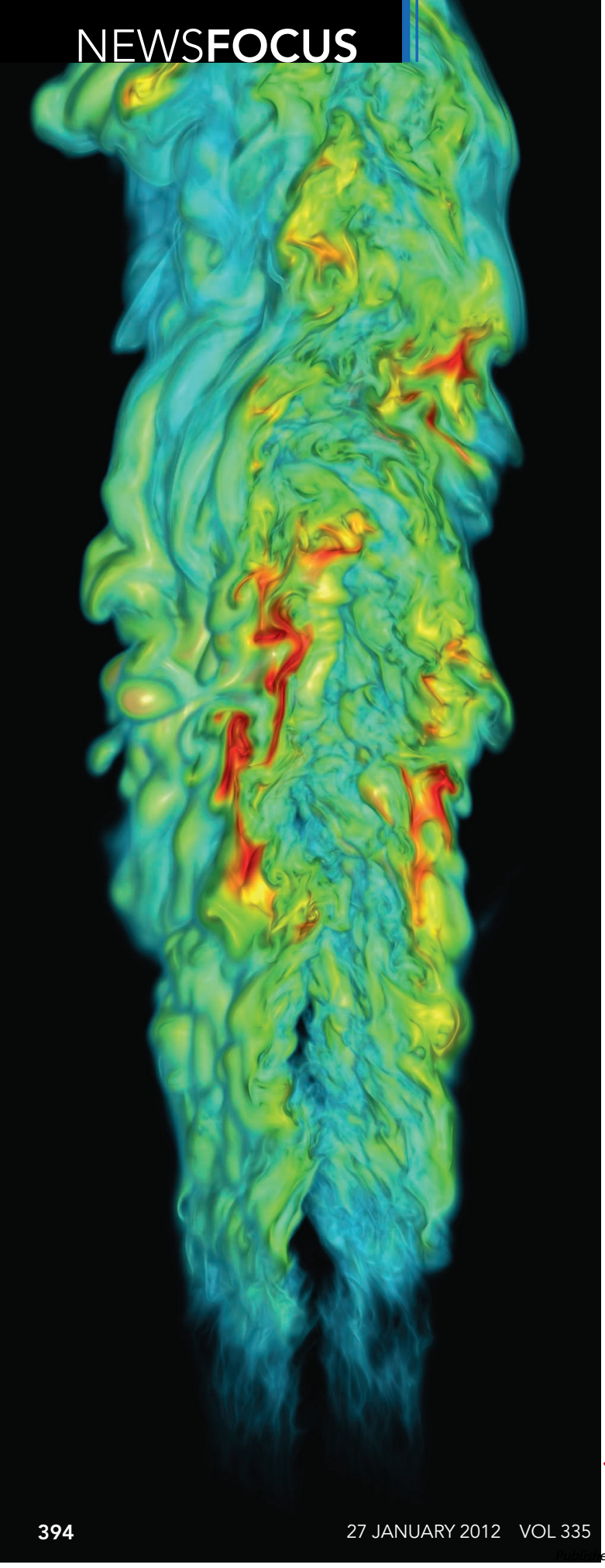
Researchers hope for the go-ahead on civil construction this spring. Michigan State has pledged $94 million to the project and has already built a $25 million office building for it. "We're leaning way out the window here," Gelbke says.

Brookhaven officials say they don't fear that DOE will suddenly abandon RHIC but worry that the agency will further curb its operating time. RHIC can run for 30 weeks a year but has reached that capacity in only 3 of 11 years. This year it's scheduled to run for 20 weeks, at a cost of $500,000 a week in electricity. "I don't think RHIC is in imminent danger of being stopped," says Brookhaven Director Samuel Aronson. "But we could go onto a path that could force its early termination."

William Brinkman, director of the Office of Science, which oversees DOE's 10 science laboratories, declined to discuss how the various projects fare in the 2013 budget request. "We certainly think that all three of these projects are important to us, and we'll have to figure out what to do," he says. The results of that soul-searching will likely inform the 2014 budget, Brinkman says. For nuclear physicists, crunch time is near. **–ADRIAN CHO**

Downloaded from www.sciencemag.org on January 27, 2012

Published by AAAS



What It'll Take To Go Exascale

Scientists hope the next generation of supercomputers will carry out a million trillion operations per second. But first they must change the way the machines are built and run

USING REAL CLIMATE DATA, SCIENTISTS AT LAWRENCE BERKELEY National Laboratory (LBNL) in California recently ran a simulation on one of the world's most powerful supercomputers that replicated the number of tropical storms and hurricanes that had occurred over the past 30 years. Its accuracy was a landmark for computer modeling of global climate. But Michael Wehner and his LBNL colleagues have their eyes on a much bigger prize: understanding whether an increase in cloud cover from rising temperatures would retard climate change by reflecting more light back into space, or accelerate it by trapping additional heat close to Earth.

To succeed, Wehner must be able to model individual cloud systems on a global scale. To do that, he will need supercomputers more powerful than any yet designed. These so-called exascale computers would be capable of carrying out 10^{18} floating point operations per second, or an exaflop. That's nearly 100 times more powerful than today's biggest supercomputer, Japan's "K Computer," which achieves 11.3 petaflops (10^{15} flops) (see graph), and 1000 times faster than the Hopper supercomputer used by Wehner and his colleagues. The United States now appears poised to reach for the exascale, as do China, Japan, Russia, India, and the European Union.

Online
sciencemag.org
Podcast by author Robert F. Service.

It won't be easy. Advances in supercomputers have come at a steady pace over the past 20 years, enabled by the continual improvement in computer chip manufacturing. But this evolutionary approach won't cut it in getting to the exascale. Instead, computer scientists must first figure out ways to make future machines far more energy efficient and tolerant of errors, and find novel ways to program them.

"The step we are about to take to exascale computing will be very, very difficult," says Robert Rosner, a physicist at the University of Chicago in Illinois, who chaired a recent Department of Energy (DOE) committee charged with exploring whether exascale computers would be achievable. Charles Shank, a former director of LBNL who recently headed a separate panel collecting widespread views on what it would take to build an exascale machine, agrees. "Nobody said it would be impossible," Shank says. "But there are significant unknowns."

Gaining support

The next generation of powerful supercomputers will be used to design high-efficiency engines tailored to burn biofuels, reveal the causes of supernova explosions, track the atomic workings of catalysts in real time, and study how persistent radiation damage might affect the metal casing surrounding nuclear weapons. "It's a tech-

On fire. More powerful supercomputers now in the design stage should make modeling turbulent gas flames more accurate and revolutionize engine designs.

CREDIT: J. CHEN/CENTER FOR EXASCALE SIMULATION OF COMBUSTION IN TURBULENCE, SANDIA NATIONAL LABORATORIES

Downloaded from www.sciencemag.org on January 27, 2012

Published by AAAS

nology that has become critically important for many scientific disciplines," says Horst Simon, LBNL's deputy director.

That versatility has made supercomputing an easy sell to politicians. The massive 2012 spending bill approved last month by Congress contained $1.06 billion for DOE's program in advanced computing, which includes a down payment to bring online the world's first exascale computer. Congress didn't specify exactly how much money should be spent on the exascale initiative, for which DOE had requested $126 million. But it asked for a detailed plan, due next month, with multiyear budget breakdowns listing who is expected to do what, when. Those familiar with the ways of Washington say that the request reflects an unusual bipartisan consensus on the importance of the initiative.

"In today's political atmosphere, this is very unusual," says Jack Dongarra, a computer scientist at the University of Tennessee, Knoxville, who closely follows national and international high-performance computing trends. "It shows how critical it really is and the threat perceived of the U.S. losing its dominance in the field." The threat is real: Japan and China have built and operate the three most powerful supercomputers in the world.

The rest of the world also hopes that their efforts will make them less dependent on U.S. technology. Of today's top 500 supercomputers, the vast majority were built using processors from Intel, Advanced Micro Devices (AMD), and NVIDIA, all U.S.-based companies. But that's beginning to change, at least at the top. Japan's K machine is built using specially designed processors from Fujitsu, a Japanese company. China, which had no supercomputers in the Top500 List in 2000, now has five petascale machines and is building another with processors made by a Chinese company. And an E.U. research effort plans to use ARM processing chips made by a U.K. company.

Getting over the bumps

Although bigger and faster, supercomputers aren't fundamentally different from our desktops and laptops, all of which rely on the same sorts of specialized components. Computer processors serve as the brains that carry out logical functions, such as adding two numbers together or sending a bit of data to a location where it is needed. Memory chips, by contrast, hold data for safekeeping for later use. A network of wires connects processors and memory and allows data to flow where and when they are needed.

For decades, the primary way of improving computers was creating chips with ever smaller and faster circuitry. This increased the processor's frequency, allowing it to churn through tasks at a faster clip. Through the 1990s, chipmakers steadily boosted the frequency of chips. But the improvements came at a price: The power demanded by a processor is proportional to its frequency cubed. So doubling a processor's frequency requires an eightfold increase in power.

With the rise of mobile computing, chipmakers couldn't raise power demands beyond what batteries could store. So about 10 years ago, chip manufacturers began placing multiple processing "cores" side by side on single chips. This arrangement meant that only twice the power was needed to double a chip's performance.

This trend swept through the world of supercomputers. Those with single souped-up processors gave way to today's "parallel" machines that couple vast numbers of off-the-shelf commercial processors together. This move to parallel computing "was a huge, disruptive change," says Robert Lucas, an electrical engineer at the University of Southern California's Information Sciences Institute in Los Angeles.

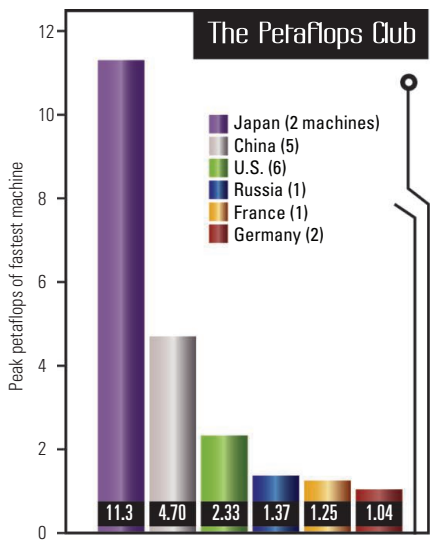
Hardware makers and software designers had to learn how to split problems apart, send individual pieces to different processors, synchronize the results, and synthesize the final ensemble. Today's top machine—Japan's "K Computer"—has 705,000 cores. If the trend continues, an exascale computer would have between 100 million and 1 billion processors.

But simply scaling up today's models won't work. "Business as usual will not get us to the exascale," Simon says. "These computers are becoming so complicated that a number of issues have come up that were not there before," Rosner agrees.

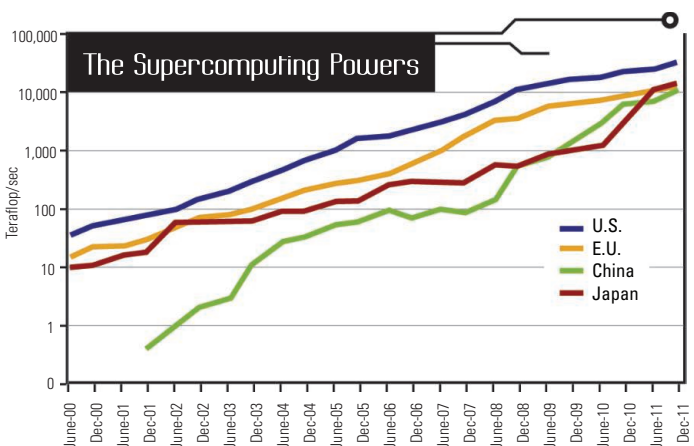
The biggest issue relates to a supercomputer's overall power use. The largest supercomputers today use about 10 megawatts (MW) of power, enough to power 10,000 homes. If the current trend of power use continues, an exascale supercomputer would require 200 MW. "It would take a nuclear power reactor to run it," Shank says.

Even if that much power were available, the cost would be prohibitive. At $1 million per megawatt per year, the electricity to run an exascale machine would cost $200 million annually. "That's a nonstarter," Shank says. So the current target is a machine that draws 20 MW at most. Even that goal will require a 300-fold improvement in flops per watt over today's technology.

Ideas for getting to these low-power chips are already circulating. One would make use of different types of specialized cores. Today's top-of-the-line supercomputers already combine conventional processor chips, known as CPUs, with an alternative version called graphical processing units (GPUs), which are very fast at certain types of calculations. Chip manufacturers are now looking at going from "multicore" chips



New king. Japan has the fastest machine (bar), although the United States still has the most petascale computers (number in parentheses).



On the rise. The gap in available supercomputing capacity between the United States and the rest of the world has narrowed, with China gaining the most ground.

CREDITS (TOP TO BOTTOM): ADAPTED FROM JACK DONGARRA/TOP 500 LIST/UNIVERSITY OF TENNESSEE

Downloaded from www.sciencemag.org on January 27, 2012

Published by AAAS

with four or eight cores to "many-core" chips, each containing potentially hundreds of CPU and GPU cores, allowing them to assign different calculations to specialized processors. That change is expected to make the overall chips more energy efficient. Intel, AMD, and other chip manufacturers have already announced plans to make hybrid many-core chips.

Another stumbling block is memory. As the number of processors in a supercomputer skyrockets, so, too, does the need to add memory to feed bits of data to the processors. Yet, over the next few years, memory manufacturers are not projected to increase the storage density of their chips fast enough to keep up with the performance gains of processors. Supercomputer makers can get around this by adding additional memory modules. But that's threatening to drive costs too high, Simon says.

Even if researchers could afford to add more memory modules, that still won't solve matters. Moving ever-growing streams of data back and forth to processors is already creating a backup for processors that can dramatically slow a computer's performance. Today's supercomputers use 70% of their power to move bits of data around from one place to another.

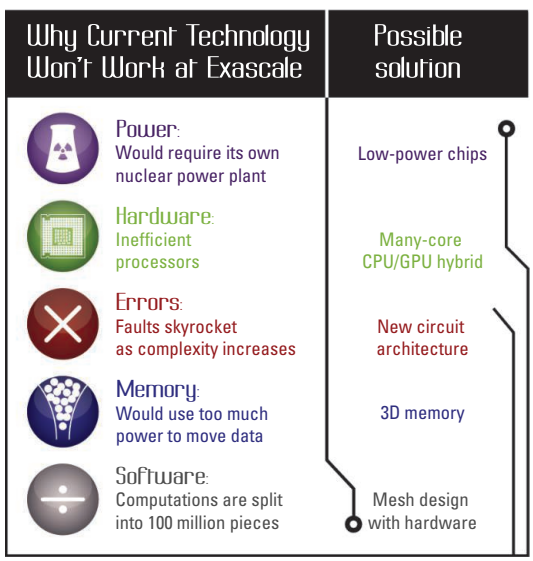
One potential solution would stack memory chips on top of one another and run communication and power lines vertically through the stack. This more-compact architecture would require fewer steps to route data. Another approach would stack memory chips atop processors to minimize the distance bits need to travel.

A third issue is errors. Modern processors compute with stunning accuracy, but they aren't perfect. The average processor will produce one error per year, as a thermal fluctuation or a random electrical spike flips a bit of data from one value to another.

Such errors are relatively easy to ferret out when the number of processors is low. But it gets much harder when 100 million to 1 billion processors are involved. And increasing complexity produces additional software errors as well. One possible solution is to have the supercomputer crunch different problems multiple times and "vote" for the most common solution. But that creates a new problem. "How can I do this without wasting double or triple the resources?" Lucas asks. "Solving this problem will probably require new circuit designs and algorithms."

Finally, there is the challenge of redesigning the software applications themselves, such as a novel climate model or a simulation of a chemical reaction. "Even if we can produce a machine with 1 billion processors, it's not clear that we can write software to use it efficiently," Lucas says. Current parallel computing machines use a strategy, known as message passing interface, that divides computational problems and parses out the pieces to individual processors, then collects the results. But coordinating all this traffic for millions of processors is becoming a programming nightmare. "There's a huge concern that the programming paradigm will have to change," Rosner says.

DOE has already begun laying the groundwork to tackle these and other challenges. Last year it began funding three "co-design" centers, multi-institution cooperatives led by researchers at Los Alamos, Argonne, and Sandia national laboratories. The centers bring together scientific users who write the software code and hardware makers to design complex software and computer architectures that work in the fastest and most energy-efficient manner. It poses a potential clash between scientists who favor openness and hardware companies that normally keep their activities secret for proprietary reasons. "But it's a worthy goal," agrees Wilfred Pinfold, Intel's director of extreme-scale programming in Hillsboro, Oregon.



Not so fast. Researchers have some ideas on how to overcome barriers to building exascale machines.

Coming up with the cash

Solving these challenges will take money, and lots of it. Two years ago, Simon says, DOE officials estimated that creating an exascale computer would cost $3 billion to $4 billion over 10 years. That amount would pay for one exascale computer for classified defense work, one for nonclassified work, and two 100-petaflops machines to work out some of the technology along the way.

Those projections assumed that Congress would deliver a promised 10-year doubling of the budget of DOE's Office of Science. But those assumptions are "out of the window," Simon says, replaced by the more likely scenario of budget cuts as Congress tries to reduce overall federal spending.

Given that bleak fiscal picture, DOE officials must decide how aggressively they want to pursue an exascale computer. "What's the right balance of being aggressive to maintain a leadership position and having the plan sent back to the drawing board by [the Office of Management and Budget]?" Simon asks. "I'm curious to see." DOE's strategic plan, due out next month, should provide some answers.

The rest of the world faces a similar juggling act. China, Japan, the European Union, Russia, and India all have given indications that they hope to build an exascale computer within the next decade. Although none has released detailed plans, each will need to find the necessary resources despite these tight fiscal times.

The victor will reap more than scientific glory. Companies use 57% of the computing time on the machines on the Top500 List, looking to speed product design and gain other competitive advantages, Dongarra says. So government officials see exascale computing as giving their industries a leg up. That's particularly true for chip companies that plan to use exascale designs to improve future commodity electronics. "It will have dividends all the way down to the laptop," says Peter Beckman, who directs the Exascale Technology and Computing Initiative at Argonne National Laboratory in Illinois.

The race to provide the hardware needed for exascale computing "will be extremely competitive," Beckman predicts, and developing software and networking technology will be equally important, according to Dongarra. Even so, many observers think that the U.S. track record and the current alignment of its political and scientific forces makes it America's race to lose.

Whatever happens, U.S. scientists are unlikely to be blindsided. The task of building the world's first exascale computer is so complex, Simon says, that it will be nearly impossible for a potential winner to hide in the shadows and come out of nowhere to claim the prize. **–ROBERT F. SERVICE**

Downloaded from www.sciencemag.org on January 27, 2012

Published by AAAS

GEOSCIENCE

Ferreting Out the Hidden Cracks In the Heart of a Continent

Deep beneath the central United States, researchers find signs of buried faults that have triggered earthquakes in the past—and may still be kicking

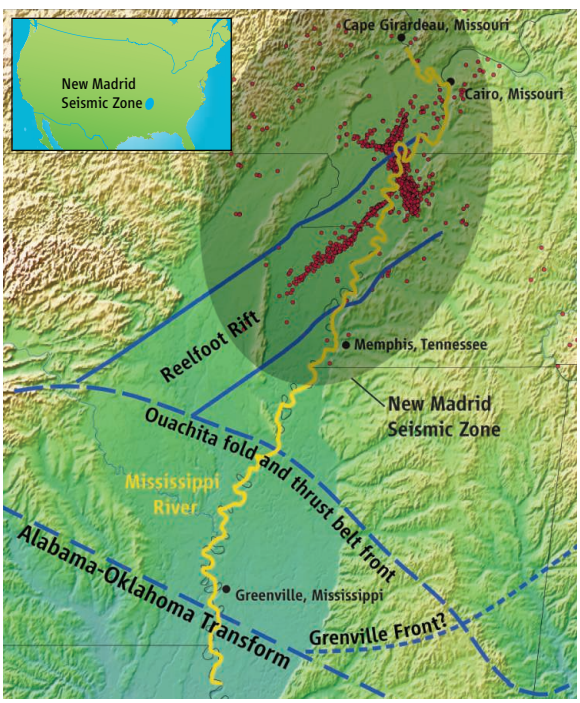
Two hundred years ago, large earthquakes shook the central United States, near what was then the tiny town of New Madrid, Missouri. The shaking on 16 December 1811 was felt all the way to the East Coast. Two more earthquakes followed in January and February. Magnitude estimates for the largest quake have ranged from 6.8 to as high as 8.

Today, the so-called New Madrid seismic zone continues to crackle with tiny earthquakes. But now, 4 million people live in the region, heightening the importance of answering the question of what could have triggered the recorded quakes—and whether and where big ones are likely to strike again. Looking beyond the faults thought to be responsible for the 1811–12 events, seismologists and geologists are discovering evidence for faults outside the active zone that may be less predictable than anyone suspected.

A network of ancient faults could be influencing the shaking in the central United States, says M. Beatrice Magnani, a geophysicist at the Center for Earthquake Research and Information (CERI) at the University of Memphis in Tennessee. Last month at the American Geophysical Union meeting in San Francisco, Magnani reported new data showing how buried faults both inside and outside the New Madrid Seismic Zone have warped the continental crust there over millions of years. That means "the seismogenic zone might be larger than illuminated by modern seismicity," she says—and that unrecorded earthquakes may have rocked now-quiet regions in the interior.

The hidden faults formed hundreds of millions of years ago, when the tectonic plate under the then–Atlantic Ocean slid beneath eastern North America—much as plates are doing today in Japan, Chile, Haiti, and elsewhere. The plate reversed direction, leaving parts of Europe and Africa stuck to North America and raising the mountains whose eroded stumps are now Appalachia. Today the ancient faults of the "failed rift" remain, buried tens of kilometers beneath the American Midwest and Eastern Seaboard. Nobody knows exactly where those faults are or how they connect and interact.

To image the faults in the region around New Madrid, Magnani and her colleagues have taken ocean-observing techniques to the Mississippi River—"seismology à la Mark Twain," she calls it. In research cruises in 2008, 2010, and 2011, the team sent sonic waves through the Mississippi River and the kilometer-deep lens of sediments it has deposited. The sound waves reflected off different layers to create seismic profiles that reveal where the layers have been warped or squished by earthquakes and other tectonic forces.



Connect the dots. Buried faults in the U.S. interior extend far outside the New Madrid Seismic Zone (oval patch at top).

The team found faults with "indistinguishable" profiles both within and outside the New Madrid Seismic Zone, Magnani says. In some places, the warping increases in the older rocks, which are millions of years old. Some faults also deform the young sediments above—evidence of more recent earthquakes and fault movements in the past 10,000 years or so. Higher resolution profiles, only tens of meters deep, show gently folded layers on one fault, hundreds of kilometers south of New Madrid. The folds, Magnani said at the meeting, most likely formed when sediment particles shook like liquid—a phenomenon called liquefaction—during an estimated magnitude-7.6 quake of unknown date.

These profiles suggest that a 500-million-year-old plate boundary south of New Madrid remains active, Magnani says. Other evidence—gathered by Martitia Tuttle, an independent consulting geologist, and others who have dated liquefaction features—suggests that another fault of the same age, which crosses from Alabama into Oklahoma, has had at least three major seismically active periods in the past 10,000 years. But Magnani says her team's new data show that the nearby Ouachita fault remained quiet for reasons still unclear.

In the New Madrid Seismic Zone, geoscientist Seth Stein of Northwestern University in Evanston, Illinois, and colleagues have argued that faults in inner continental settings can turn off and on as built-up stress shifts from one fault to another, lowering the risk of earthquakes in one place but raising it in another. As a result, Stein thinks, the risk of more big quakes in the New Madrid region is much lower than researchers have assumed. Magnani says her team's findings confirm some of Stein's ideas. "But that doesn't necessarily mean we should lower the seismic hazard in the central United States—actually, quite the opposite," Magnani says: The discovery of unseen faults outside of New Madrid's obvious seismic zone may mean more danger, not less.

Elsewhere in the central and eastern continent, modern earthquakes have revealed seismic hot spots in places such as Charleston, South Carolina; central Indiana; and Virginia, where a magnitude-5.8 quake struck in August 2011. But in quiet areas in between, ancient faults may still lurk undiscovered. The earthquake catalog is incomplete, says Susan Hough, a seismologist at the U.S. Geological Survey in Pasadena, California, who has estimated magnitudes of the historic New Madrid cycle using shaking-intensity reports.

At the meeting, Hough said findings by Magnani's team make sense if stress released along old faults caused deformation or earthquakes in previously unexpected places. "Let others pop off elsewhere, and it all begins to hang together," Hough says.

–NAOMI LUBICK

Naomi Lubick is a freelance writer based in Stockholm.

CREDIT: ADAPTED FROM M. BEATRICE MAGNANI

Downloaded from www.sciencemag.org on January 27, 2012

Published by AAAS





BEHAVIORAL SCIENCES

Modernizing an Academic Monastery

A venerable institution tries to reinvent itself by applying behavioral science to 21st century problems

Thomas Kuhn wrote much of his landmark 1962 book, *The Structure of Scientific Revolutions*, at a secluded retreat in the foothills above Palo Alto, California. In the 1970s, future Nobelist Daniel Kahneman spent time here in the formative days of the field that came to be known as behavioral economics. For decades after the Ford Foundation started it in 1954, behavioral and social scientists coveted an invitation to the exclusive Center for Advanced Study in the Behavioral Sciences. The center's yearlong fellowships offered leading scholars freedom from teaching and other academic obligations, as well as a quiet place to reflect and write. Those who came produced seminal works in fields as diverse as political science and primatology.

But in recent years, the center seems to many observers to have lost some of its luster, attracting fewer big-name scholars and producing fewer high-impact works. In part because of financial issues, nearby Stanford University took over the once-independent center in 2008. "The decision the trustees faced is do they just want to let it limp along, dissolve it, or try something new," says Stephen Kosslyn, the center's current director.

They opted for something new and recruited Kosslyn to shake things up. A distinguished psychologist, he left his post as dean of social sciences at Harvard University to become the director of the center in January 2011. "The culture here was that of a monastery," Kosslyn says. He wants to open the center up more to the outside world and emphasize real-world problem solving over heady academic ruminations. He has proposed, among other things, setting up networks of researchers to examine specific issues, from how to make technology more accessible to elderly people to documenting psychological obstacles to peace in the Middle East. "We want to make behavioral science relevant," he says.

Food for thought

Kosslyn is soft-spoken and unassuming, and he looks every bit the professor in round wire-rimmed glasses and a tweed jacket. At the same time, he's proud to say he saw the Grateful Dead perform on campus when he was a Stanford undergraduate in the 1970s, and he keeps an electric bass in his office. He plays whenever he can find a group of musicians with similar skills and tastes (mainly classic rock). He and his wife chose to live in San Francisco, more than 50 kilometers away from the center, because they were turned off by what Kosslyn describes as the materialism and anti-intellectualism of Silicon Valley, whose office parks and suburbs sprawl out below the center's hillside perch. "I don't like the culture," he says.

Several of his colleagues say Kosslyn is well-suited to revive the center. "He's a person of tremendous energy," says Jonathan Cole, a sociologist at Columbia University and chair of the center's board of directors. "He's willing to take risks and experiment," Cole says. Harvard psychologist Steven Pinker credits Kosslyn, his former graduate adviser, with breathing new life into another venerable institution. "The Harvard University psychology department had been a backwater, coasting on its reputation, before Steve reinvigorated it in the 1990s with an aggressive program of hiring young mid-career scientists, which vaulted the department into the front ranks," says Pinker, who joined the department in 2003. Pinker also cites Kosslyn's leadership through the financial crisis as evidence that he's the right person to turn around the Stanford center: "I'd be surprised if Steve didn't make the center financially viable and intellectually vibrant within a few years."

The world was a different place when the center was founded, at the midpoint of a century that had brought two world wars, the Holocaust, and the Great Depression. And then there was the Cold War. A *San Francisco Chronicle* article about the center's launch raised the specter of mind-control methods presumably under development in the Soviet Union. "This could be a weapon of great power in Communist hands, unless comparable advances in the West produce effective countermeasures," the article reads, apparently quoting from a statement from a group of social scientists convened by then–Vice President Richard Nixon.

The center's founders realized that solutions to societal problems could come from the social and behavioral sciences, but they also realized how poorly developed these disciplines were, says Robert Scott, a former

CREDITS: G. MILLER/*SCIENCE*

Downloaded from www.sciencemag.org on January 27, 2012

Published by AAAS





Intellectual haven. The Center for Advanced Study in the Behavioral Sciences at Stanford has provided a quiet environment for scholars to think and write since 1954. The center's library (*center*) houses hundreds of books written by past fellows. Stephen Kosslyn, the center's new director, wants the center to engage more with real-world problems.

CREDIT: G. MILLER/*SCIENCE*

deputy director of the center and its de facto historian. One early adviser, the Austrian-born sociologist Paul Lazarsfeld, proposed that the center be based on the European model, in which promising young students learn at the feet of the masters, Scott says. That model didn't last long. "It was very un-American," Scott says with a chuckle.

Instead, a more egalitarian culture quickly emerged. Despite its somewhat isolated setting, the center was designed to foster informal exchanges among its 50 or so resident fellows, Cole says. Cozy, low-slung buildings house private offices for each fellow, but their arrangement around several courtyards forces a certain amount of walking between buildings, increasing the likelihood of chance encounters. Lunch is not left to chance, however: Fellows were, and still are, expected to attend lunch each day, catered by the center's private chef. "Where you eat you tend to talk, and where you talk you get ideas," Cole says.

The center has no permanent faculty or students and no laboratories. In the early days, candidates were nominated by past fellows and other academics and ultimately selected by the center's board. For the chosen ones, an invitation would suddenly arrive out of the blue. "It was considered a huge honor," Cole says. Alumni include 22 Nobel Prize winners, 10 Pulitzer Prize winners, 44 MacArthur Fellows, and 128 current members of the National Academy of Sciences. "The simplest way to describe what the center then offered was what most people who went into academia thought they were getting into and never found—that is, a genuine community of intensely interacting, smart, interesting people from diverse fields," Scott says.

Paradigm shift

"The center was a phenomenal place in its time for a select group of people who had a rare kind of experience that couldn't be gotten anywhere else," Cole says. "But that's not the world we live in today." In one nod to modernity, the old-boys' network (literally, for the most part) that hand-selected fellows was replaced years ago by a competitive application process. Nearly half of the members of this year's class are women. But other changes have reduced the center's magnetic pull, Cole says. The Internet has made far-flung collaborations easier, for example, and more researchers today have spouses with professional careers, making it difficult for some prospective fellows to move to Palo Alto for a year. (Fellows typically visit the center on sabbatical from their home institutions, which continue to pay at least part of their salaries.)

Then came the financial crisis. By 2008, the returns on the center's endowment were barely keeping up with its growing operating costs, and the board agreed to let Stanford take over the center's finances and administration. The center's endowment was folded into Stanford's much larger fund just before the stock market crashed. Making matters worse, foundations that once contributed to the center have tightened the purse strings. "They're not interested in paying for people to come here for a few months and maybe write a book, and I don't blame them," Kosslyn says.

Kosslyn thinks shifting the focus to real-world applications of behavioral science will make the center more appealing to donors. One way he wants to do this is by creating "impact networks" of six to eight scholars, including resident fellows and outside collaborators, to work on specific problems. One proposed network, for example, would study how to design software for elderly people that accounts for age-related changes in vision, memory, and coordination. Another team would identify the daily grievances that most foster resentment and mistrust between Palestinians and Israelis and obstruct the path to peace. Kosslyn hopes to fund these and a handful of other projects he's proposed through a combination of federal grants and donations from foundations and individual donors.

Kosslyn also hopes to create "center institutes," each headed by a resident scholar, that would tackle broader issues. His ideas for these include a war crimes archive and a center on personalized data mining that would examine how search engine and other companies that collect personal data online could use it to benefit the people who provided it. Kosslyn envisions these centers generating specific questions to be tackled by future "impact networks" of scholars.

At the same time, Kosslyn says he wants to preserve and encourage the interdisciplinary discourse the center has always provided. One day last fall, fellows gathered for a panel discussion, part of a new series Kosslyn started to foster crosstalk among disciplines. The topic was culture and economics, and the panel comprised two Stanford economists, Peter Reiss and Frank Wolak, and Jing Tsu, who studies Chinese language and culture at Yale University. They discussed how to define culture and determine its influence on economic activity (and vice versa) and whether cultural scholars might use tools from economics to quantify culture.

Kosslyn realizes that preserving the center's idyllic environment and getting scholars talking to each other will be the easy part. His plans to establish the center as a hub for translational social science research will require raising money in extremely difficult times. But he says the amounts are fairly modest, perhaps $200,000 per year for an impact network and $300,000 per year for a center institute. He thinks he can convince potential donors that it would be money well spent. The line between philanthropy and investment is getting blurrier, Kosslyn says, and the center has to prove that it can give something back. Its future may depend on it.

–GREG MILLER

Downloaded from www.sciencemag.org on January 27, 2012

Published by AAAS





LETTERS

edited by Jennifer Sills

Pause on Avian Flu Transmission Research

THE CONTINUOUS THREAT OF AN INFLUENZA PANDEMIC REPRESENTS ONE OF THE BIGGEST CHALlenges in public health. Influenza pandemics are known to be caused by viruses that evolve from animal reservoirs, such as in birds and pigs, and can acquire genetic changes that increase their ability to transmit in humans. Pandemic preparedness plans have been implemented worldwide to mitigate the impact of influenza pandemics. A major obstacle in preventing influenza pandemics is that little is known regarding what makes an influenza virus transmissible in humans. As a consequence, the potential pandemic risk associated with the many different influenza viruses of animals cannot be assessed with any certainty.

Recent research breakthroughs identified specific determinants of transmission of H5N1 influenza viruses in ferrets. Responsible research on influenza virus transmission using different animal models is conducted by multiple laboratories in the world using the highest international standards of biosafety and biosecurity practices that effectively prevent the release of transmissible viruses from the laboratory. These standards are regulated and monitored closely by the relevant authorities. This statement is being made by the principal investigators of these laboratories.



In two independent studies conducted in two leading influenza laboratories at the University of Wisconsin–Madison and Erasmus MC in Rotterdam, the Netherlands, investigators have proved that viruses possessing a hemagglutinin (HA) protein from highly pathogenic avian H5N1 influenza viruses can become transmissible in ferrets. This is critical information that advances our understanding of influenza transmission. However, more research is needed to determine how influenza viruses in nature become human pandemic threats, so that they can be contained before they acquire the ability to transmit from human to human, or so that appropriate countermeasures can be deployed if adaptation to humans occurs.

Despite the positive public health benefits these studies sought to provide, a perceived fear that the ferret-transmissible H5 HA viruses may escape from the laboratories has generated intense public debate in the media on the benefits and potential harm of this type of research. We would like to assure the public that these experiments have been conducted with appropriate regulatory oversight in secure containment facilities by highly trained and responsible personnel to minimize any risk of accidental release. Whether the ferret-adapted influenza viruses have the ability to transmit from human to human cannot be tested.

We recognize that we and the rest of the scientific community need to clearly explain the benefits of this important research and the measures taken to minimize its possible risks. We propose to do so in an international forum in which the scientific community comes together to discuss and debate these issues. We realize that organizations and governments around the world need time to find the best solutions for opportunities and challenges that stem from the work. To provide time for these discussions, we have agreed on a voluntary pause of 60 days on any research involving highly pathogenic avian influenza H5N1 viruses leading to the generation of viruses that are more transmissible in mammals. In addition, no experiments with live H5N1 or H5 HA reassortant viruses already shown to be transmissible in ferrets will be conducted during this time. We will continue to assess the transmissibility of H5N1 influenza viruses that emerge in nature and pose a continuing threat to human health.

RON A. M. FOUCHIER,[1]* ADOLFO GARCÍA-SASTRE,[2] YOSHIHIRO KAWAOKA,[3] WENDY S. BARCLAY,[4] NICOLE M. BOUVIER,[5] IAN H. BROWN,[6] ILARIA CAPUA,[7] HUALAN CHEN,[8] RICHARD W. COMPANS,[9] ROBERT B. COUCH,[10] NANCY J. COX,[11] PETER C. DOHERTY,[12] RUBEN O. DONIS,[13] HEINZ FELDMANN,[14] YI GUAN,[15] JAQUELINE KATZ,[16] H. D. KLENK,[17] GARY KOBINGER,[18] JINHUA LIU,[19] XIUFAN LIU,[20] ANICE LOWEN,[21] THOMAS C. METTENLEITER,[22] ALBERT D. M. E. OSTERHAUS,[23] PETER PALESE,[24] J. S. MALIK PEIRIS,[25] DANIEL R. PEREZ,[26] JÜRGEN A. RICHT,[27] STACEY SCHULTZ-CHERRY,[28] JOHN STEEL,[29] KANTA SUBBARAO,[30] DAVID E. SWAYNE,[31] TORU TAKIMOTO,[32] MASATO TASHIRO,[33] JEFFERY K. TAUBENBERGER,[34] PAUL G. THOMAS,[35] RALPH A. TRIPP,[36] TERRENCE M. TUMPEY,[37] RICHARD J. WEBBY,[38] ROBERT G. WEBSTER[39]

[1]Department of Virology, Erasmus MC, 3000CA Rotterdam, 3015GE Rotterdam, Netherlands. [2]Department of Microbiology, Mount Sinai School of Medicine, New York, NY 10029, USA. [3]Department of Pathobiological Sciences, School of Veterinary Medicine, University of Wisconsin-Madison, Madison, WI 53711, USA. [4]Department of Medicine, Imperial College, London, UK. [5]Division of Infectious Diseases and Department of Microbiology, Mount Sinai School of Medicine, New York, NY 10029, USA. [6]Virology Department, Animal Health and Veterinary Laboratories Agency, Addlestone, KT15, UK. [7]Istituto Zooprofilattico

Letters to the Editor

Letters (~300 words) discuss material published in *Science* in the past 3 months or matters of general interest. Letters are not acknowledged upon receipt. Whether published in full or in part, Letters are subject to editing for clarity and space. Letters submitted, published, or posted elsewhere, in print or online, will be disqualified. To submit a Letter, go to www.submit2science.org.

CREDIT: GREG KNOBLOCH/CDC

Downloaded from www.sciencemag.org on January 27, 2012

Published by AAAS



Prion transmission

411



IBI Prize Essay

418

Sperimentale delle Venezie, 35020, Padova, Italy. [8]Harbin Veterinary Research Institute, CAAS, Harbin 150001, China. [9]Influenza Pathogenesis and Immunology Research Center, Emory University, School of Medicine, Atlanta, GA 30322, USA. [10]Department of Molecular Virology and Microbiology, Baylor College of Medicine, Houston, TX 77030, USA. [11]Centers for Disease Control and Prevention, Influenza Division, Atlanta, GA 30333, USA. [12]Department of Immunology, St. Jude Children's Research Hospital, Memphis, TN 38105, USA. [13]Molecular Virology and Vaccines Branch, Influenza Division, Centers for Disease Control and Prevention, Atlanta, GA 30333, USA. [14]Laboratory of Virology, National Institute of Allergy and Infectious Diseases, National Institutes of Health, Rocky Mountain Laboratories, Hamilton, MT 59840, USA. [15]State Key Laboratory of Emerging Infectious Diseases, The University of Hong Kong, Hong Kong SAR. [16]Immunology and Pathogenesis Branch, Influenza Division, Centers for Disease Control and Prevention, Atlanta, GA 30333, USA. [17]Institut für Virologie, 35043 Marburg, Germany. [18]National Microbiology Laboratory, Public Health Agency of Canada, Winnipeg, Manitoba R3E 3R2, Canada. [19]Department of Preventative Veterinary Medicine, China Agricultural University, Beijing, China. [20]Animal Infectious Disease Laboratory, School of Veterinary Medicine, Yangzhou University, Yangzhou, Jiangsu 225009, China. [21]Department of Microbiology and Immunology, Emory University School of Medicine, Atlanta, GA 30322, USA. [22]Friedrich-Loeffler-Institut, D-17493 Greifswald-Insel Riems, Germany. [23]Department of Virology, Erasmus MC, Rotterdam, Netherlands. [24]Department of Microbiology, Mount Sinai School of Medicine, New York, NY 10029-6574, USA. [25]Department of Microbiology and HKU-Pasteur Research Centre, The University of Hong Kong, Pokfulam, Hong Kong SAR. [26]Department of Veterinary Medicine, University of Maryland, College Park, College Park, MD 20742, USA. [27]College of Veterinary Medicine, Kansas State University, Manhattan, KS 66506, USA. [28]Department of Infectious Diseases, St. Jude Children's Research Hospital, Memphis, TN 38105, USA. [29]Department of Microbiology and Immunology, Emory University, School of Medicine, Atlanta, GA 30322, USA. [30]Emerging Respiratory Viruses Section, Laboratory of Infectious Diseases, National Institute of Allergy and Infectious Diseases, National Institutes of Health, Bethesda, MD 20892-3203, USA. [31]Southeast Poultry Research Laboratory, USDA/Agricultural Research Service, Athens, GA 30605, USA. [32]Department of Microbiology and Immunology, University of Rochester Medical Center, Rochester, NY 14642, USA. [33]National Institute of Infectious Diseases, Influenza Virus Research Center, Tokyo, 208-001, Japan. [34]Viral Pathogenesis and Evolution Section, Laboratory of Infectious Diseases, National Institute of Allergy and Infectious Diseases, National Institutes of Health, Bethesda, MD 20892-3203 USA. [35]Department of Immunology, St. Jude Children's Research Hospital, Memphis, TN 38105-3678, USA. [36]Department of Infectious Diseases, College of Veterinary Medicine, University of Georgia, Athens, GA 30602, USA. [37]Influenza Division, Centers for Disease Control and Prevention, Atlanta, GA 30333, USA. [38]Department of Infectious Diseases, St. Jude Children's Research Hospital, Memphis, TN 38105-3678, USA. [39]Division of Virology, Department of Infectious Diseases, St. Jude Children's Research Hospital, Memphis, TN 38105, USA.

*To whom correspondence should be addressed. E-mail: r.fouchier@erasmusmc.nl

Published online 20 January 2012; 10.1126/science.1219412

CORRECTIONS AND CLARIFICATIONS

News Focus: "America's lost city" by A. Lawler (23 December 2011, p. 1618). On p. 1623, Indiana University–Bloomington was referred to incorrectly as the University of Indiana.

Reports: "Empathy and pro-social behavior in rats" by I. B.-A. Bartal *et al*. (9 December 2011, p. 1427). On p. 1428, the last full paragraph of column 1 was incorrect. The paragraph should be replaced by this corrected text: "All female rats (6/6) and most male rats (17/24) in the trapped condition became door-openers. Female rats in the trapped condition opened the restrainer door at a shorter latency than males on days 7 to 12 ($P < 0.01$, MMA, Fig. 3A), consistent with suggestions that females are more empathic than males (*7*, *12*, *13*). Furthermore, female rats were also more active than males in the trapped condition ($P < 0.001$, ANOVA) but not in the empty condition (Fig. 3B)."

TECHNICAL COMMENT ABSTRACTS

Comment on "Dynamics of Dpp Signaling and Proliferation Control"

Gerald Schwank, Schu-Fee Yang, Simon Restrepo, Konrad Basler

Wartlick *et al*. (Research Articles, 4 March 2011, p. 1154) reported that growth rates in the *Drosophila* wing disc correlate with increasing Dpp signaling levels, suggesting that the rate of Dpp increase determines the cell-cycle length. Contradicting their model, we found that cells in which the increase of Dpp signaling levels was genetically abrogated grew at rates comparable to wild-type cells.

Full text at www.sciencemag.org/cgi/content/full/335/6067/401-b

Response to Comment on "Dynamics of Dpp Signaling and Proliferation Control"

Ortrud Wartlick, Peer Mumcu, Frank Jülicher, Marcos González-Gaitán

Schwank *et al*. challenge the temporal growth model with an experiment in which Dpp signal transduction is abrogated. They claim that in this condition, cellular Dpp signaling levels do not increase over time but that cells do grow normally. We repeated this experiment and observed an increase of signaling over time. The results are consistent with a temporal model of growth control.

Full text at www.sciencemag.org/cgi/content/full/335/6067/401-c

Recognizing Existing Models

IN THEIR EDITORIAL "ADDRESSING SCIENtific fraud" (2 December 2011, p. 1182), J. Crocker and M. L. Cooper suggest that we need to develop better systems to report suspected misconduct and fraud. They overlook useful current models that institutions and investigators can follow. For example, David Goodstein, a respected physicist and former vice-provost at CalTech, has recently published a book (*1*) that discusses the issue of investigator misconduct in considerable detail. He presents, as an appendix, the text of the CalTech policy, which is closely aligned with that of the federal government.

There is simply no excuse for any institution or journal to be without a clear policy on misconduct or a clear procedure for handling allegations of misconduct. This is not a subject to be thought through after an allegation. No institution should think that this topic only arises somewhere else or in some other research environment.

WILLIAM JOSEPH ROSENBERG

Bruce Drive Solutions, 820 Bruce Drive, Palo Alto, CA 94303–3643, USA. E-mail: billrosenberg@earthlink.net

Reference

1. D. Goodstein, *On Fact and Fraud* (Princeton Univ. Press, Princeton, NJ, 2010).

Portugal's Age of Enlightenment

IN 2001, *SCIENCE* PUBLISHED AN ARTICLE heralding the arrival of a scientific "age of enlightenment" in Portugal (*1*). This culture of science was impressive considering that Portugal has virtually no historical foundation for scientific research (unlike other European countries with identical demographic or cultural indicators). In the decade that has passed since that article, Portuguese R&D has taken advantage of the increase in national and European Union funding and harnessed the talents of new and younger leaders. However, there are signs of trouble despite the advances.

The Portuguese national funding agency, Fundação para a Ciência e a Tecnologia (FCT), which had previously financed proj-

Downloaded from www.sciencemag.org on January 27, 2012

ect grants and fellowships only sporadically, has instead called for grants and fellowships on an almost yearly basis. However, FCT grants have a limit of 200,000, typically for 3 years, including equipment, consumables, maintenance, travel, portions of salaries, and institutional overheads; most of these expenses are taxed with a 23% value-added consumption tax (which is not waived for publicly funded research costs, as in other EU countries). Because individual researchers can only be the principal investigators of two such projects at the same time, it is difficult to invest money in the purchase of large equipment. Unfortunately, the last call for specific re-equipment grants opened in 2001, with results in July 2004. The past decade also witnessed several delays on the receipt of contracted funds, and most of the host institutions lacked the capital necessary to buffer such delays.

Variability in the quality of Portuguese research is perpetuated by a system that allows unsuccessful research groups to continue, despite years (or even decades) without producing deliverables. Furthermore, some disciplines have not succeeded in reaching the average level of output of their European colleagues.

Portuguese R&D still produces few academia-industry partnerships. Not many companies in Portugal have the size, capital, interest, and foresight to make research-oriented investments for the development of new and innovative products. Portuguese universities also suffer from historical social isolation, lack of focus on entrepreneurship in student training, and limited experience with new and emerging technology-transfer platforms. Most universities are now adopting policies to address these limitations, such as creating technology-transfer offices and including entrepreneurship in some curricula.

Due to the economic crisis, in 2011 faculty and researchers experienced a cut of more than 10% in annual income, with an additional 14% reduction already announced for 2012. Hundreds of researchers are working on 5-year contracts funded by the Ciência 2007 and Ciência 2008 initiatives of the former Ministry of Science, Technology, and Higher Education (MCTES). Initially, they hoped to be hired directly by their host institutions at the end of their contracts. However, this is now unlikely considering that several Portuguese universities and research centers are already struggling to pay the salaries of their present employees and will face a new funding cut of 8.5% in 2012.

The change in government last June has added to the feeling of uncertainty. MCTES and the Ministry of Education have merged but, for the first time, this year's calendar for grants and fellowships calls has been published in advance. Nevertheless, the budget for these calls is still unknown.

The Portuguese research community is now facing its first "stress test" after the progress and consolidation of the past 15 years. Portugal-based researchers are highly qualified and will surely do their best to overcome these hurdles, and Portugal's institutions have the necessary facilities and intellectual environment to do good science. Now is the time for Portugal's science community to show that the country's "age of enlightenment" is not at an end.

NUNO C. SANTOS

Instituto de Medicina Molecular, Faculdade de Medicina da Universidade de Lisboa, Portugal. E-mail: nsantos@fm.ul.pt

Reference

1. R. Stone, *Science* **291**, 1889 (2001).

Learn how current events are impacting your work.

***Science*Insider, the new policy blog from the journal *Science*,** is your source for breaking news and instant analysis from the nexus of politics and science.

Produced by an international team of science journalists, *Science*Insider offers hard-hitting coverage on a range of issues including climate change, bioterrorism, research funding, and more.

Before research happens at the bench, science policy is formulated in the halls of government. Make sure you understand how current events are impacting your work. Read *Science*Insider today.

www.ScienceInsider.org



*Science*Insider

Breaking news and analysis from the world of science policy



Science AAAS

Downloaded from www.sciencemag.org on January 27, 2012

Comment on "Dynamics of Dpp Signaling and Proliferation Control"

Gerald Schwank,* Schu-Fee Yang, Simon Restrepo, Konrad Basler†

Wartlick *et al.* (Research Articles, 4 March 2011, p. 1154) reported that growth rates in the *Drosophila* wing disc correlate with increasing Dpp signaling levels, suggesting that the rate of Dpp increase determines the cell-cycle length. Contradicting their model, we found that cells in which the increase of Dpp signaling levels was genetically abrogated grew at rates comparable to those of wild-type cells.

Patterning and growth of organs are regulated by morphogen gradients. In a recent work, Wartlick *et al.* (*1*) analyzed the formation of the anterior-posterior (A-P) Decapentaplegic (Dpp) gradient during *Drosophila* wing disc development. The authors found that the amplitude and the decay length of the morphogen gradient increase during development and that the gradient scales with tissue size. Because cell proliferation is spatially uniform, and the relative position of a cell within the disc does not change, their finding implies that all cells sense the same relative increase of Dpp levels during wing disc growth. This relative increase of Dpp signaling levels was found to be about 50% during each cell cycle. Wartlick *et al.* thus proposed a model in which the temporal increase of Dpp signaling controls growth: The cell cycle length is determined by how fast a 50% increase of cellular Dpp signal is reached. Their model therefore enables them to explain how position-independent growth rates can be achieved by the Dpp morphogen gradient. However, it is difficult to reconcile this model with previously published data. Several independent studies had demonstrated that Dpp plays a permissive role in growth regulation, allowing proliferation by suppressing the expression of the growth repressor Brk (*2*–*4*). Moreover, it has been demonstrated that wing discs mutant for hypomorphic *dpp* and *brk* alleles overgrow (*5*, *6*), and recently Hamaratoglu *et al.* showed that the Dpp signaling gradient does not scale to the same extent throughout the wing disc (*7*). Here, we reassessed the growth model by generating clones in which the Dpp signaling pathway was fully abrogated. Our results demonstrate that Dpp signaling levels in such clones did not increase, yet growth was normal. These findings therefore clearly imply that an increase in Dpp signaling is not required to drive cell proliferation.

In *Drosophila*, Dpp signaling is mediated by the sole Smad protein Mad (*8*). Upon phosphorylation via the typeI-typeII Dpp receptor complex, Mad binds to Medea and translocates to the nucleus to regulate target gene expression (*8*, *9*). Whereas some target genes are activated by Dpp signaling, others are repressed (*3*). One such repressed target is *brk*, which encodes a transcriptional repressor that is a key mediator for Dpp-dependent patterning and growth (*2*, *4*, *5*). To create a situation where Dpp signaling levels are constant, we fixed Dpp signaling genetically by removing the transcription factor *Mad* as well as

Institute of Molecular Life Sciences, University of Zurich, Zurich, Switzerland.

*Present address: Hubrecht Institute for Developmental Biology and Stem Cell Research, and University Medical Centre, Utrecht, Netherlands.

†To whom correspondence should be addressed. E-mail: basler@imls.uzh.ch

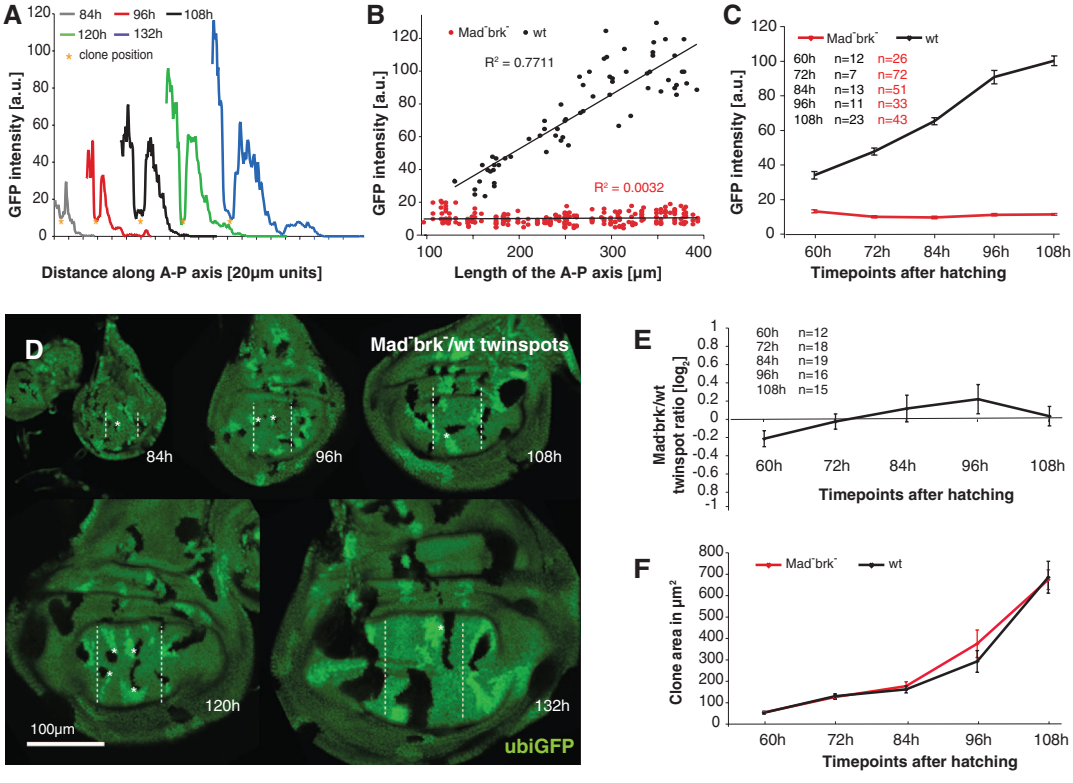


Fig. 1. *Mad*^{12}*brk*^{M68} clones: Constant *dad-GFP* levels and wild-type growth rates. The generation of *Mad brk* mutant clones has been described previously (*15*). Clones were induced at 36 hours after hatching. Mutant clones are marked by the loss of *arm-lacZ* (A to C) or by the loss of *ubi-nGFP* (D to F). (**A**) Examples for posterior *dad-GFP* gradients of wing discs containing *Mad*^{12}*brk*^{M68} mutant clones. (**B**) *dad-GFP* levels in medial *Mad brk* mutant clones (red) and the amplitude of *dad-GFP* levels at the A-P axis in wild-type discs (black), plotted according to the length of the discs. (**C**) Same measurements as in (B), but plotted according to the time points when the discs were collected. No trend toward increasing dad-GFP levels in mutant clones was observed (60 hours, 13.0 ± 0.9; 72 hours, 9.7 ± 0.3; 84 hours, 9.3 ± 0.4; 96 hours, 10.9 ± 0.7; 108 hours, 11.1 ± 0.5). (**D**) Examples for wing discs containing *Mad*^{12}*brk*^{M68}/wild-type twin spots at different time points after hatching. Only medial twin spots that did not fuse with neighboring clones (marked with asterisks) were used for the statistical analysis. The medial area is illustrated by the dashed lines. (**E**) Average size-ratio of the individual *Mad*^{12}*brk*^{M68}/wild-type twin spots for the different time points when discs were collected. The difference remains within 20%. (**F**) Average area of mutant clones and the wild-type twin spots for the different time points. All error bars represent the mean ± SEM.

Downloaded from www.sciencemag.org on January 27, 2012

the target *brk*. We used the Mad^{12} allele (*10*)—which comprises a premature stop codon upstream of the Dpp receptor phosphorylation site and therefore represents a situation in which Dpp responsiveness is completely abrogated (*11*)—and the amorphic brk^{M68} allele (*2*).

We first tested whether Dpp signaling levels in $Mad^{12}brk^{M68}$ mutant cells are indeed constant during development and compared the dynamics of Dpp signaling levels in mutant versus wild-type wing disc cells. We focused our analysis on the medial area (defined as the area within the decay length of *dad* from the Dpp source), where Dpp signaling levels are high and the increase can be measured accurately (*1*). Moreover, in the medial area *brk* is normally repressed by high Dpp signaling levels so that medial $Mad^{12}brk^{M68}$ clones differ from the wild type only in their lack of Mad. As a transcriptional read-out for Dpp signaling activity, we used a *dad-nGFP* reporter (*12*), which contains the same *dad* enhancer that Wartlick *et al*. used. We first analyzed *dad-nGFP* levels in wild-type discs. The increasing levels during development correlate with wing disc size (Fig. 1A-C) and thus support the hypothesis of a dynamic Dpp gradient (*1*). However, when monitoring *dad-GFP* in $Mad^{12}brk^{M68}$ mutant clones, reporter expression remained constant at low levels throughout development (Fig. 1A-C). These findings therefore confirm that Dpp signaling levels do not increase in such clones and validate the use of this tool to test the growth model of Wartlick *et al*. (*1*).

Next, we measured the growth rates of medial $Mad^{12}brk^{M68}$ mutant clones during wing disc development and compared them with those of their wild-type twin spots. Strikingly, $Mad^{12}brk^{M68}$ mutant clones and wild-type clones grew at the same rate (Fig. 1, D to F), as assessed at the population level (Fig. 1F) and when the ratios of mutant and corresponding wild-type twin spots were compared directly (Fig. 1E). Thus, our experiments reveal that increasing Dpp signaling levels are not necessary for driving cell proliferation. Rather, the results are in agreement with previously suggested models, in which Dpp signaling plays a permissive role in allowing proliferation by repressing the expression of the growth inhibitor Brk (*6*, *13*, *14*). In these models, position-independent growth rates are explained by the integration of complementary signals from additional growth modulators (*14*).

Taken together, our results confirm the observation that Dpp signaling levels increase during wild-type wing disc development but contradict the model in which this increase is the cause for cell proliferation. It will be interesting to find out why the Dpp signaling activity adopts to the disc size with increasing amplitudes.

References and Notes

1. O. Wartlick *et al*., *Science* **331**, 1154 (2011).
2. A. Jaźwińska, N. Kirov, E. Wieschaus, S. Roth, C. Rushlow, *Cell* **96**, 563 (1999).
3. T. Marty, B. Müller, K. Basler, M. Affolter, *Nat. Cell Biol.* **2**, 745 (2000).
4. M. Minami, N. Kinoshita, Y. Kamoshida, H. Tanimoto, T. Tabata, *Nature* **398**, 242 (1999).
5. G. Campbell, A. Tomlinson, *Cell* **96**, 553 (1999).
6. G. Schwank, S. Restrepo, K. Basler, *Development* **135**, 4003 (2008).
7. F. Hamaratoglu, A. M. de Lachapelle, G. Pyrowolakis, S. Bergmann, M. Affolter, *PLoS Biol* **9**, e1001182 (2011).
8. J. Kim, K. Johnson, H. J. Chen, S. Carroll, A. Laughon, *Nature* **388**, 304 (1997).
9. J. B. Hudson, S. D. Podos, K. Keith, S. L. Simpson, E. L. Ferguson, *Development* **125**, 1407 (1998).
10. J. J. Sekelsky, S. J. Newfeld, L. A. Raftery, E. H. Chartoff, W. M. Gelbart, *Genetics* **139**, 1347 (1995).
11. E. Eivers *et al*., *PLoS ONE* **4**, e6543 (2009).
12. N. Ninov *et al*., *Curr. Biol.* **20**, 513 (2010).
13. F. A. Martín, A. Pérez-Garijo, E. Moreno, G. Morata, *Development* **131**, 4921 (2004).
14. G. Schwank *et al*., *Dev. Cell* **20**, 123 (2011).
15. G. Schwank *et al*., *PLoS Biol.* **9**, e1001111 (2011).

Acknowledgments: We thank G. Hausmann and M. Affolter for comments on the manuscript. This work was supported by the European Research Council, the SystemsX.ch initiative, and the Swiss National Science Foundation.

11 July 2011; accepted 13 December 2011
10.1126/science.1210997

Downloaded from www.sciencemag.org on January 27, 2012

Response to Comment on "Dynamics of Dpp Signaling and Proliferation Control"

Ortrud Wartlick,[1] Peer Mumcu,[2] Frank Jülicher,[2] Marcos Gonzalez-Gaitan[1]*

Schwank *et al*. challenge the temporal growth model with an experiment in which Dpp signal transduction is abrogated. They claim that in this condition, cellular Dpp signaling levels do not increase over time but that cells do grow normally. We repeated this experiment and observed an increase of signaling over time. The results are consistent with a temporal model of growth control.

In a recent study (*1*) we found that, in the *Drosophila* wing disc, the cell proliferation rate correlates with the relative temporal increase in signaling levels of the morphogen Dpp and that, therefore, relative temporal changes in signaling could control proliferation [among other possibilities discussed in the supporting online material (SOM) of (*1*) (text beginning on p. 79 and figure S46)]. A new experiment by Schwank *et al*. challenges this temporal growth model. These authors claim that clones of cells lacking the Dpp signal transducers Mad and Brk do not experience temporal increases in signaling but grow at the same rate as wild-type cells (*2*). They conclude that Dpp signaling is "permissive" for growth control.

In our recent paper, we did study a similar experimental condition: a brk^{XA} $dpp^{d12/d14}$ mutant (*1*). We found that the output of the Dpp signaling pathway, as measured by the transcriptional reporter dad-RFP, was strongly position-dependent and did increase over time in this condition [SOM of (*1*) (text beginning on p. 86 and figure S50)]. This difference from the recent findings by Schwank *et al*. in brk^{M68} mad^{12} clones could in principle be explained by either

[1]Departments of Biochemistry and Molecular Biology, Faculty of Sciences, University of Geneva, 30 Quai Ernest Ansermet, 1211 Geneva, Switzerland. [2]Max Planck Institute for the Physics of Complex Systems, Nöthnitzer Strasse 38, 01187 Dresden, Germany.

*To whom correspondence should be addressed. E-mail: marcos.gonzalez@unige.ch

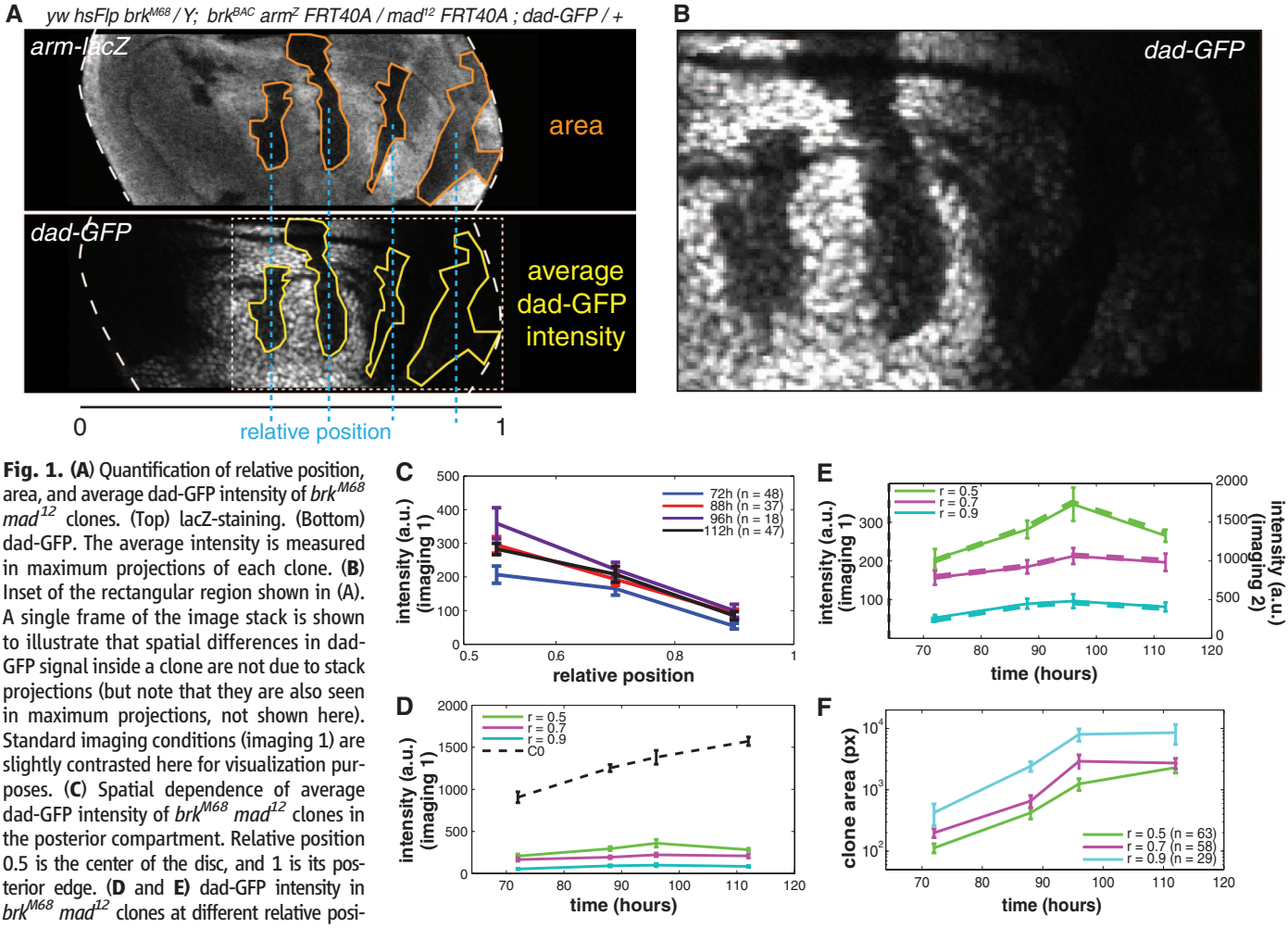


Fig. 1. (**A**) Quantification of relative position, area, and average dad-GFP intensity of brk^{M68} mad^{12} clones. (Top) lacZ-staining. (Bottom) dad-GFP. The average intensity is measured in maximum projections of each clone. (**B**) Inset of the rectangular region shown in (A). A single frame of the image stack is shown to illustrate that spatial differences in dad-GFP signal inside a clone are not due to stack projections (but note that they are also seen in maximum projections, not shown here). Standard imaging conditions (imaging 1) are slightly contrasted here for visualization purposes. (**C**) Spatial dependence of average dad-GFP intensity of brk^{M68} mad^{12} clones in the posterior compartment. Relative position 0.5 is the center of the disc, and 1 is its posterior edge. (**D** and **E**) dad-GFP intensity in brk^{M68} mad^{12} clones at different relative positions (r) over time, as compared to the amplitude of the endogenous gradient (C_0) (measured at the anterior-posterior boundary, not in wildtype clones), when imaged with standard imaging conditions (imaging 1) [(D) and dashed lines in (E)] and imaging conditions adjusted to low signaling levels in clones (imaging 2) [solid lines in (E)]. Independently of the imaging conditions, the signal intensity increases in clones (E). (**F**) Area over time for clones at different relative positions (r).

Downloaded from www.sciencemag.org on January 27, 2012

(i) the genotype—the brk^{M68} allele is amorphic, whereas brk^{XA} is hypomorphic; (ii) the imaging conditions—signaling levels are around an order of magnitude lower in the mutant cells than in wild-type tissue. The temporal model is based on relative temporal changes: ΔC/C rather than ΔC. Even small absolute increases in the signal (ΔC) lead to large relative temporal changes (ΔC/C) when the concentration (C) is small. When imaged with the standard imaging conditions used to quantify the wild-type dad-GFP profile, the dynamic range of the signal in brk^{M68} mad^{12} mutant clones might be too small to quantify temporal increases above noise levels. (We discussed this previously for the brk^{XA} $dpp^{d12/d14}$ mutant in the SOM of (*1*) (text beginning on p. 86 and figure S50); or (iii) the quantification method: Because the signal has a strong spatial dependence [see SOM of (*1*), figure S50, and Fig. 1, A to C], whether the minimum, maximum, or average signal intensity in the clone is measured will influence the result.

To address the genotype issue, we repeated the brk^{M68} mad^{12} mutant clone experiment with the fly lines kindly provided by Schwank *et al*. Like in our previous work (*1*), we quantified the average dad-GFP signal intensity and area of clones as a function of time and relative position. We found that, independently of imaging conditions, signaling levels in brk^{M68} mad^{12} clones (i) are position-dependent (Fig. 1, A to C) and (ii) increase over time (Fig. 1, C to E). Signal increases are accompanied by an increase in clone area (Fig. 1F). Consistent with a temporal growth model, the signal increase is statistically significant in medial clones where the signal (C) is higher and therefore its absolute increase (ΔC) is bigger [$P < 0.05$, two-way analysis of variance (ANOVA) (Fig. 1E). Laterally, where the average dad-GFP signal in clones is lower, the absolute increase is also smaller. Because we used the fly lines of Schwank *et al*. and the results were independent of imaging conditions, the differences between our results and those of Schwank *et al*. are most likely due to the quantification method (Fig. 1A).

The hypothesis that Dpp signaling is only permissive for growth was based on the observation that *tkv brk* or *mad brk* double-mutant clones grow, whereas *tkv* or *mad* mutant clones do not (*3*–*5*). This observation and the assumption that, when brk is mutated, Dpp targets are maximally and uniformly activated led to the hypothesis that growth is implemented by Brk and that spatial differences or temporal changes in Dpp are irrelevant for growth (*6*). However, as Schwank *et al*., we, and others have shown, the output of the Dpp signaling pathway is neither maximal nor uniform in space nor constant in time in brk^{XA} and brk^{XA} $dpp^{d12/d14}$ discs, or indeed in brk^{M68} mad^{12} mutant clones (*1*, *3*–*7*) (Fig. 1). Therefore, these conditions cannot be used as evidence for a permissive Dpp role.

The fact that Dpp signaling levels are not maximal but are very low in brk^{M68} mad^{12} and brk^{XA} $dpp^{d12/d14}$ mutant cells compared with wild type (Fig. 1, A and B) [see also SOM of (*1*), figure S50, and figure 1B in (*2*)] shows that removal of Brk is not sufficient to achieve full activation of Dpp target genes. This is consistent with the observation that both P-Mad and Brk regulate the enhancer of the Dpp target Dad (*8*). Furthermore, in *brk* mutants, dad-RFP expression levels are still graded in space and the repressive activity of Brk apparently has only a minor effect on the level of known output signals (Spalt and Dad) in lateral positions of the disc where extra proliferation effects are seen [see figure S1, H and J in (*6*) and figures S11F and S50A in the SOM of (*1*); discussed in (*9*)]. This is also difficult to reconcile with the permissive model by Schwank *et al*. (*6*), where Dpp signaling and its role in growth critically depend on absolute Brk activity levels.

The brk^{M68} mad^{12} clone experiments highlighted two key features of the Dpp system: (i) the Dpp output (dad-GFP levels) in the complete absence of Dpp input (Mad and Brk) is neither maximal nor zero but is very low and neither constant in space nor time, and (ii) the Dpp input is not essential for proliferation, because brk^{M68} mad^{12} clones still grow. It is worth noting, however, that growth is no longer homogeneous: lateral clones are larger than medial clones (Fig. 1F) [see also, e.g., (*1*, *6*)]. The increase in Dpp target gene expression over time in brk^{M68} mad^{12} clones shows that this experiment is consistent with a model in which growth is regulated by (normally Dpp-dependent) relative temporal increase in the expression of target genes implicated in proliferation. However, the fact that growth can occur in the absence of Dpp input uncovers another interesting aspect of growth control. We speculate that, in brk^{M68} mad^{12} clones, Dpp target genes respond to other inputs that dominate in this particular situation and can lead to growth in the absence of Dpp input. What would temporal changes in Dpp input achieve then in the wild-type situation? Because of scaling of the Dpp gradient, it would ensure position-independent growth and determine the decay time of the proliferation rate, the timing of growth arrest, and therefore the correct final size of the tissue.

References

1. O. Wartlick *et al*., *Science* **331**, 1154 (2011).
2. G. Schwank, S.-F. Yang, S. Restrepo, K. Basler, *Science* **335**, 401 (2012); www.sciencemag.org/cgi/content/full/335/6067/401-b.
3. A. Jaźwińska, N. Kirov, E. Wieschaus, S. Roth, C. Rushlow, *Cell* **96**, 563 (1999).
4. T. Marty, B. Müller, K. Basler, M. Affolter, *Nat. Cell Biol.* **2**, 745 (2000).
5. M. Minami, N. Kinoshita, Y. Kamoshida, H. Tanimoto, T. Tabata, *Nature* **398**, 242 (1999).
6. G. Schwank, S. Restrepo, K. Basler, *Development* **135**, 4003 (2008).
7. G. Campbell, A. Tomlinson, *Cell* **96**, 553 (1999).
8. A. Weiss *et al*., *Nat. Struct. Mol. Biol.* **17**, 69 (2010).
9. O. Wartlick, P. Mumcu, F. Jülicher, M. Gonzalez-Gaitan, *Nat. Rev. Mol. Cell Biol.* **12**, 594 (2011).

19 September 2011; accepted 13 December 2011
10.1126/science.1211373

Downloaded from www.sciencemag.org on January 27, 2012

ARCHAEOLOGY

Ecocide or Utopia on Easter Island?

Robin Torrence

The presence of iconic, gigantic stone statues on tiny, remote Easter Island (Rapa Nui) is frequently labeled a mystery because in the 18th century this stony, barren island hosted a warring population considered too small and impoverished to have produced such monuments. The standard account of Rapa Nui has been well popularized (*1*–*3*). Humans arrive; populations grow; intergroup competition leads to ever-larger statues whose transport demands more trees be cut down, leading to environmental destruction, warfare, and social disruption. That narrative might support certain views of how modern civilization could end up, but, according to the recent research summarized in *The Statues That Walked*, it is wrong on almost all counts. Forget previous claims for aliens or willful ecocide. Instead, archaeologists Terry Hunt and Carl Lipo argue, ancient Easter Island was a well-adapted, quasi-utopian world.

Building on a large body of archaeological, environmental, and paleobotanical findings, Hunt and Lipo unfold a story of how puzzling results from their fieldwork led them to alternative explanations. Combining new dating from excavations at key sites and a reassessment of previous work, they conclude that humans arrived only about 1200 CE. Their revision fits much better with dates for the expansion of Polynesian settlement to other far-flung locations such as Hawaii and New Zealand. Rats that also traveled on the boats fed on the nuts of the island's giant *Jubaea* palm and over 600 years helped drive them to extinction. Rather than degenerating into warfare, the islanders responded to deforestation by developing an effective gardening system aided by small walled gardens enhanced by composting and stone mulching. This productive use of stones provided a sustainable subsistence despite the harsh effects of unpredictable and low levels of rainfall, no permanent water sources, and high, drying winds.

The Polynesian colonists also brought with them the practice of building large stone platforms with statues, from which the concept of the Rapa Nui *ahu* and *moai* were derived but highly elaborated. Many solutions for transporting the multitonne statues about the island from their quarry have been suggested. Hunt and Lipo favor a previous hypothesis that statues were "walked" vertically, just as one person can move a refrigerator by tilting and twisting. New evidence for the existence of a system of roads across the island with just the right angles for moving upright statues up and down slopes supports their view. An important implication is that the movement and erection of *moai*, even those weighing many tonnes, could be achieved by a small group of people. Having developed a rationale for small, egalitarian groups, the book takes a big step away from previous scholarship.

The Statues That Walked
Unraveling the Mystery of Easter Island
by Terry Hunt and Carl Lipo
Free Press (Simon and Schuster), New York, 2011. 251 pp. $26, C$29.99. ISBN 9781439150313.

At European contact, the construction and use of large-scale religious stone structures in other parts of Polynesia supported a hierarchical social structure and intergroup fighting was common. *The Statues That Walked* poses the radical alternative for Rapa Niu that cultural elaboration was achieved without concomitant social complexity, competition, and aggression. The authors muster the absence of defensive structures, weapons, or damage on skeletons from fighting together with arguments from evolutionary theory to predict pacificism as a beneficial strategy for a small and highly interrelated population that must cope with an especially harsh environment.

If not to support chiefs, why were *moai* made? Following their mentor, Robert Dunnell (*4*), Hunt and Lipo propose the statues were a form of costly signaling. The size of monuments demonstrated which groups were most successful and so not worth challenging, thereby avoiding damaging warfare. Furthermore, they argue that *moai* (and also costly stone mulching) were consequences of bet-hedging in which investment in a "wasteful" activity diverted effort from productive tasks and helped prevent the population from outgrowing the limited resources on the island.

No Rapa Nui story would be complete without a catastrophe. In this telling, that was generated by the arrival of Europeans. Drawing on early Dutch accounts, Hunt and Lipo argue that Rapanui culture had not succumbed to environmental disaster by the early part of the 18th century but was flourishing because it was well adapted to the limited resources on the island. As in other revisions of early European contact (*5*), they paint a positive picture in which goods introduced by the visitors became "the new costly signals communicating access to new wealth and technology." Responding to opportunities, the islanders created rituals focused on European boats and items that diverted their attention from the *moai*, which quickly collapsed largely through neglect rather than warfare. Ultimately, collapse was inevitable as disease led to massive population decline, which, when combined with slavery and other abuses, led to social disintegration.

Hunt and Lipo depict a utopia in which culture acts



Toppled *moai*.

CREDIT: MICHAEL SNELL/ALAMY

The reviewer is at the Australian Museum, 6 College Street, Sydney, New South Wales 2010, Australia. E-mail: robin.torrence@austmus.gov.au

Downloaded from www.sciencemag.org on January 27, 2012

Published by AAAS

in seemingly strange ways to reduce population and sustain people stranded on a small, isolated island with a marginal environment. Whereas over the rest of Polynesia statue and monument building was integral to competition and warfare, they propose that on Easter Island these activities were turned in the opposite direction, resulting in a highly adapted, stable society. Their argument that the "story of Rapa Nui is one not of ecological suicide but of persistence and resilience in which the islanders employed innovative approaches" is certainly persuasive. But whether this supposedly perfectly adapted society was the product of the ritual and ideology surrounding giant stone statues hangs on the theories on which the authors' interpretation is based: functionalist cultural ecology and notions of altruism and group selection. One can reasonably question whether the pendulum has swung too far from self-induced catastrophe to utopia. The debates arising from *The Statues That Walked* raise critical issues about the relative roles of environmental determinism, evolutionary processes, and human agency in shaping human pasts and futures. These ensure that archaeological research on tiny, remote Easter Island will continue to play an important role in broader scientific scholarship.

References

1. J. Diamond, *Collapse: How Societies Choose to Fail or Succeed* (Viking, New York, 2005).
2. J. Diamond, *Science* **317**, 1692 (2007).
3. J. Flenley, P. Bahn, *The Enigmas of Easter Island: Island on the Edge* (Oxford Univ. Press, Oxford, ed. 2, 2003).
4. R. Dunnell, *J. Anthropol. Archaeol.* **18**, 243 (1999).
5. J. Pollard, A. Paterson, K. Welham, *World Archaeol.* **42**, 562 (2010).

10.1126/science.1216863

HISTORY OF MEDICINE

The Pursuit of Love

Beth Ann Malow

Understanding Autism examines the rich and colorful history of a condition that has gained the attention of scientists and the public alike due to its dramatically increasing rate of diagnosis, its mystifying constellation of symptoms, and its underpinnings spanning multiple disciplines. As Chloe Silverman recounts, autism has been "treated alternatively as a psychological, neurological, behavioral, or genetic disorder, often paralleling trends in medical research and popular interest." A multicolored heart on the book's cover reflects the metaphor of love that she employs throughout her history of this enigmatic condition.

Silverman (a historian at Penn State) begins her narrative with Leo Kanner's 1943 introduction of the diagnostic category of autism in his case series of 11 children who exhibited an "*inability to relate themselves* in the ordinary way to people and situations from the beginning of life" (*1*). The next year brought Hans Asperger's account of isolated and self-sufficient individuals—we learn that he took "pains to emphasize the talents and potential of the children." The psychogenic theory embraced by many practitioners, and popularized in a best-selling 1967 book by Bruno Bettelheim (*2*), linked autism to "refrigerator mothers." The tide shifted back when Kanner "delighted" parents at the 1969 meeting of the National Society for Autistic Children, "declaring 'I hereby acquit you people as parents' while dismissing Bettelheim and his 'empty book.'" His affirmation of the dedication and commitment of parents to the development of their children is one example of love's powerful influence in autism.

Understanding Autism
Parents, Doctors, and the History of a Disorder
by Chloe Silverman
Princeton University Press, Princeton, NJ, 2012. 352 pp. $35, £24.95. ISBN 9780691150468.

Subsequent decades witnessed an explosion in autism neuroscience—including the study of genetic disorders associated with autistic features, such as Rett syndrome; the development of animal models; and advances in diagnostic assessment tools, imaging techniques, and brain tissue studies. The science was fueled by federal funding but also by parent-based foundations. These research advances provide a second example of love—that as a practice which, in psychologist Erich Fromm's words, demands "discipline, concentration, and patience" (*3*). One finds these qualities in the scientists struggling with critical research questions, the practitioners facing challenging and treatment-refractory patients, and the parent groups devoted to raising public awareness and funding for autism research.

The author highlights how parents have influenced autism research and treatment in positive ways. One example is the Parents Speak column, introduced by editor-in-chief Eric Schopler, that ran from 1974 to 1985 in the *Journal of Autism and Developmental Disorders* and its predecessor. It "revealed parents eager to share their knowledge and ideas in an academic forum, aware that they had data that clinicians and researchers didn't possess." Mary Akerley, the column's first editor, held that parents' "observations, interpretations, and suggestions for research and/or treatment are perhaps more likely to represent the problems of the autistic child than the specialized professional concerns." In this "remarkable column," parents described the effect of high fevers on improved behavior, the phenomenon of children with autism asking the same questions over and over, and the success of operant conditioning on improving communication and behavior (and they speculated on why this approach was successful).

No history of autism would be complete without discussion of the debate over vaccine safety. Silverman presents this controversial section in a sensitive and balanced fashion. She accurately describes the *Lancet*'s retraction (*4*) of Andrew Wakefield's work related to the measles-mumps-rubella vaccine yet also explains why some parents continue to question vaccine safety.

As she notes, proponents of biomedical treatments for autism, such as psychologist and parent advocate Bernard Rimland, have been valuable in bringing relevant and important areas of research (e.g., potential links to gastrointestinal disorders and other medical conditions) to the forefront. She makes a plea for "respectful dialogue.... because all of these groups—parents, self-advocates, researchers, and clinicians—need to share their particular insights to arrive at the best ways to understand, respect, and nurture people on the autism spectrum." Her remarks emphasize a third role of love: as a powerful force that allows those with contentious views to come together in a productive way that moves a field forward. Passion and deep commitment to the field, when shared openly, debated, and discussed, can be transformative.

Comprehensive, well annotated, and fascinating to read, *Understanding Autism* will appeal to readers from a broad variety of disciplines. Silverman provides an honest and refreshing perspective on encouraging dialogue about a condition that will likely continue to be in the public spotlight for decades to come.

References

1. L. Kanner, *Nervous Child* **2**, 217 (1943).
2. B. Bettelheim, *The Empty Fortress: Infantile Autism and the Birth of the Self* (Free Press, New York, 1967).
3. E. Fromm, *The Art of Loving* (Harper and Row, New York, 1956).
4. *Lancet* **375**, 445 (2010).

10.1126/science.1217237

The reviewer is at the Departments of Neurology and Pediatrics and the Kennedy Center, Vanderbilt University Medical Center, Nashville, TN 37232–2551, USA. E-mail: beth.malow@vanderbilt.edu

Downloaded from www.sciencemag.org on January 27, 2012

Published by AAAS

GLOBAL FOOD SUPPLY

Mixed Messages on Prices and Food Security

We need a more nuanced debate on how prices and policies affect food security; neither high nor low prices are panaceas.

Johan Swinnen[1,2] and Pasquamaria Squicciarini[1]*

Spikes in food prices have pushed food security to the top of the global policy agenda. Price increases have mixed effects on poverty and hunger: They increase the cost of food for consumers but increase incomes of farmers, who represent the bulk of the world's poor. Net effects will differ depending on whether poor households or countries buy or import, or sell or export food (infrastructure, institutions, and market imperfections will play roles, as well) (*1*–*4*). Policies to influence prices imply winners and losers, not just between rich and poor, but also among the poor. These nuances are too often absent in public debate, to the detriment of policy-making. Moreover, the arguments put forward today, that high food prices generally hurt the poor, are in contrast with those put forward a few years ago, that low food prices were hurting the poor.

As recently as 2005, the United Nations Food and Agricultural Organization (FAO) explained: "The long-term downward trend in agricultural commodity prices threatens the food security of hundreds of millions of people …" (*5*). The dramatic increase of food prices in 2008 caused a major turnaround in opinion. FAO wrote: "Rising food prices … worsen the … food deprivation suffered by 854 million people" (*6*). This reversal of opinion was fairly widespread with some extreme examples coming from non-governmental organizations (NGOs) (*7*). In 2005 Oxfam stated: "Low prices [on world markets make] it impossible for farmers in developing countries to compete. As a consequence, over 900 millions of farmers are losing their livelihoods" (*8*). Three years later, Oxfam argued: "[Higher] food prices … have pushed millions of people in developing countries further into hunger and poverty" (*9*).

Some might argue that improvements in modeling and measurement (see the chart) have improved understanding of impacts of prices and thus influenced changes in messages. Although this may play a role in some cases (e.g., regarding the impact of biofuel policies on food prices), we believe that, more often, detailed analytical reports with nuanced conclusions are turned into simplistic messages (*10*–*12*). In our view, it can be hard to find a relation between underlying analytical work and the policy messages sent by communications departments. For example, the background document for the 2008 FAO Summit on Soaring Food Prices explained that the impact of soaring food prices on the poor may be positive or negative, depending on how much they produce and consume food, and that it may represent an opportunity for promoting agricultural development (*13*). The FAO press communication at the summit does not mention potential benefits and focuses exclusively on how high prices hurt the poor (*14*). Studies by World Bank researchers show complex effects of food price changes on poverty in developing countries (*15*–*18*), yet official World Bank communications at the time of the crisis largely emphasize how rising prices hurt the poor (*19*).



Food price index. Weighted average of meat, dairy, cereals, oil and fat, and sugar price indices. The average during 2002–04 is set to 100. Data from UN FAO, deflated using the World Bank Manufactures Unit Value Index.

One reason for this may be fundraising. In a world where development organizations need to compete for donor funding and attention, there is pressure to demonstrate the relevance and importance of their work (*20*, *21*). Arguing that changes in food prices hurt the poor may help in raising funds. Because donors, like TV viewers and newspaper readers, tend to pay more attention to negative news (*22*, *23*), development organizations have an incentive to portray events negatively (*24*). This effect is reinforced by other factors, such as the need to be concise in communicating to policy-makers and the public and the pressure for researchers in large organizations to "stay on message." That is, once an organization has taken a public stance, it will be reluctant to promote research conflicting with this message.

Mass media also play an important role in influencing the policy agenda (*25*). Emotionally charged media coverage, typically concentrated around "events" or "shocks" (*26*), invokes public responses, which induce politicians and governments to act (*27*, *28*).The absence of media coverage reduces priority for items on the policy or donor agenda (*29*). Sudden changes with dramatic effects, such as the 2008 food crisis, not only present challenges to development organizations and experts but also opportunities for them to capture media attention and signal their importance to donors and the public. These factors create incentives to emphasize negative implications and to deemphasize the positive effects.

Bad News but Good Policies?

Development organizations may argue that, although they have changed their messages, they have not changed their basic policy advice. This is true to some extent. Many organizations have maintained their policy prescriptions to invest in agriculture and support small farmers. They have been consistent in their trade policy advice; some favor trade liberalization, others advise against it. However, there are also important shifts in advice.

For example, in 2003 the World Bank emphasized how low prices hurt developing-

[1]Centre for Institutions and Economic Performance (LICOS) and Department of Economics, University of Leuven, Leuven, Belgium. [2]Center for Food Security and the Environment, Stanford University, Palo Alto, CA USA.

*Author for correspondence: mara.squicciarini@econ.kuleuven.be

Downloaded from www.sciencemag.org on January 27, 2012

Published by AAAS

country farmers, with little mention of potential benefits for urban consumers or how an increase in prices would hurt many poor people in rural areas who are net consumers (*30*). In 2008 and later, the World Bank argued that the largest number of poor, including rural smallholders, are net buyers and are hurt by increasing prices, with little attention paid to benefits from high prices for farmers (*19*, *31*).

In trade policy, development organizations have largely held their line. Some (such as FAO, the Organisation for Economic Co-operation and Development, and the World Bank) have continued to emphasize the importance of trade liberalization and of the conclusion of the Doha Round of international trade negotiations. NGOs such as ActionAid and Oxfam have continued to recommend reduction of subsidies and elimination of import tariffs in rich countries and the need for import tariffs to protect poor countries. The consistency of this advice is problematic.

If high food prices are hurting urban consumers and many poor rural households in developing countries, NGOs' "consistent" policy advice may yield the wrong effect. Elimination of import tariffs and export subsidies of rich countries and the use of import tariffs in poor countries could increase food prices, hurting the poor and worsening food security, according to the oft-used NGO argument. Arguments that poor countries should use such protections not when prices are high but when they are low are inconsistent with claims that most poor farmers are net consumers. If they are net consumers when prices are high, they will likely be net consumers when prices are low and would suffer from import tariffs. One reason why development organizations have advocated trade liberalization was because it would increase prices for poor farmers (*32*, *33*), at odds with current claims that high food prices hurt the poor, including many farmers.

Implications

Before 2005, recommendations to help developing-country farmers by cutting subsidies in the European Union and the United States typically ignored the fact that this could hurt consumers and net food-consuming farmers in developing countries. The recent reversal in messages, that high prices are bad for the poor, is providing ammunition for those wanting to keep farm subsidies in rich countries. Several food exporting countries, such as India, China, and Russia, blocked exports after global price increases (*34*). This led to proposals to constrain the use of such export policies (e.g., tariffs, bans, and quotas) under World Trade Organization (WTO) rules. Here, too, there are costs and benefits. For example, export restrictions in rice-exporting countries have been blamed for hurting poor consumers in rice-importing countries. However, several rice-exporting countries like China, India, and Indonesia have many poor consumers at home (who benefit from the policies).

We need to be more honest about what we do and do not know. One striking example is the use of the number of hungry people in the world and how the food crisis changed this. Some development organizations have announced that 1 billion people are hungry (*35*). Experts have challenged these numbers (*36*, *37*). Impacts of price changes on the number of hungry people are projections, based on models and assumptions, which include uncertainties and should be interpreted with caution. New studies suggest that the number of hungry may have declined, possibly by many millions, despite the food price increase (*37*). Combined effects of price changes, economic growth, market imperfections, and policy interventions may have resulted in more subtle gradations in the effects on food security even in the poorest countries of Africa (*38*). In parts of Asia, growth in wages and remittances has been stronger than increases in food prices (*39*).

We need a more nuanced debate on how global developments and policies affect food security. All changes cause winners and losers, also among the poor. If the objective is to assist those who are hurt by price changes, this is no excuse for simplistic messages.

References and Notes

1. A. Panagariya, Agricultural liberalisation and the least developed countries: Six fallacies. *World Econ.* **28**, 1277 (2005).
2. J. C. Bureau, S. Jean, A. Matthews, The consequences of agricultural trade liberalization for developing countries: Distinguishing between genuine benefits and false hopes. *World Trade Rev.* **5**, 225 (2006).
3. T. W. Hertel, R. Keeney, M. Ivanic, L. A. Winters, Distributional effects of WTO agricultural reforms in rich and poor countries. *Econ. Policy* **22**, 289 (2007).
4. R. L. Naylor, W. P. Falcon, Food security in an era of economic volatility. *Popul. Dev. Rev.* **36**, 693 (2010).
5. FAO, Agriculture commodity prices continue long-term decline [press release]; www.fao.org/newsroom/EN/news/2005/89721/index.html.
6. FAO, Food prices remain high despite higher output [press release]; www.fao.org/newsroom/EN/news/2008/1000845/index.html.
7. J. F. M. Swinnen, The right price of food. *Dev. Policy Rev.* **29**, 667 (2011).
8. OXFAM International, International celebrities get dumped on at the WSF [news] (2005); www.oxfam.org/en/node/283.
9. OXFAM International, Agriculture campaign—Global food prices in 2011: Questions & answers; www.oxfam.org/en/campaigns/agriculture/food-price-crisis-questionsanswers.
10. L. Christiaensen, L. Demery, *Down to Earth: Agriculture and poverty reduction in Africa* (World Bank, Washington, DC, 2007).
11. T. Hertel, L. A. Winters, Eds., *Poverty and the WTO* (Palgrave Macmillan, London, and the World Bank, Washington, DC, 2006).
12. A. Sarris, J. Morrison, Eds., *Food Security in Africa* (Edward Elgar, Cheltenham, UK, 2010).
13. FAO, *Soaring Food Prices: Facts, Perspective, Impacts and Actions Required* (FAOHLC/08/INF/1, FAO, Rome, 2008).
14. FAO, High food prices—supporting the poor and re-launching agriculture [news]; www.fao.org/newsroom/en/news/2008/1000847/index.html.
15. K. Anderson, W. Martin, Eds., *Agricultural Trade Reform and the Doha Development Agenda* (Palgrave Macmillan, London, and World Bank, Washington, DC, 2007).
16. T. W. Hertel, R. Keeney, M. Ivanic, L. A. Winters, Distributional effects of WTO agricultural reforms in rich and poor countries. *Econ. Policy* **22**, 289 (2007).
17. M. Ivanic, W. Martin, Implications of higher global food prices for poverty in low-income countries (Working Paper Series 4594, World Bank, Washington, DC, 2008).
18. T. Hertel, J. Reimer, Predicting the poverty impacts of trade reform. *J. Int. Trade Econ. Dev.* **14**, 377 (2005).
19. World Bank, Food price surge could mean '7 lost years' in poverty fight, Zoellick says [news] (World Bank, Washington, DC, 2008).
20. J. Andreoni, A. A. Payne, Do government grants to private charities crowd out giving or fund-raising? *Am. Econ. Rev.* **93**, 792 (2003).
21. S. Rose-Ackerman, Charitable Giving and "Excessive" Fundraising. *Q. J. Econ.* **97**, 193 (1982).
22. L. L. Marshall, R. F. Kidd, *Soc. Behav. Pers.* **9**, 223 (1981).
23. R. F. Baumeister, E. Bratslavsky, C. Finkenauer, K. D. Vohs, Bad is stronger than good. *Rev. Gen. Psychol.* **5**, 323 (2001).
24. J. J. McCluskey, J. F. M. Swinnen, Political Economy of the Media and Consumer Perceptions of Biotechnology. *Am. J. Agric. Econ.* **86**, 1230 (2004).
25. J. J. McCluskey, J. F. M. Swinnen, in *The Oxford Handbook of Government and Business*, D. Coen, W. Grant, G. Wilson, Eds. (Oxford Univ. Press, Oxford, 2010), pp. 643–662.
26. J. F. M. Swinnen, N. Francken, Summits, Riots and Media Attention: The Political Economy of Information on Trade and Globalisation. *World Econ.* **29**, 637 (2006).
27. L. Marks, N. Kalaitzandonakes, L. Zakharova, *J. Agribusiness* **21**, 1 (2003).
28. V. Hawkins, The Other Side of the CNN Factor: The media and conflict. *Journalism Stud.* **3**, 225 (2002).
29. P. V. Jakobsen, Focus on the CNN Effect misses the point: The real media impact on conflict management is invisible and indirect. *J. Peace Res.* **37**, 131 (2000).
30. World Bank, Reaching the Rural Poor (World Bank, Washington, DC, 2003).
31. World Bank, *Implementing Agriculture for Development: World Bank Group Agriculture Action Plan: FY2010–2012* (World Bank, Washington, DC, 2009).
32. Cline's book (*33*) on how trade would help 500 million people escape poverty has been an influential theoretical foundation supporting trade liberalization policies.
33. W. Cline, *Trade Policy and Global Poverty* (Center for Global Development and Institute for International Economics, Washington, DC, 2004).
34. A. Bouët, D. L. Debucquet, Economics of export taxation in a context of food crisis (IFPRI Discussion Paper 00994, International Food Policy and Research Institute, Washington, DC, 2010).
35. FAO, *The State of Food Insecurity in the World* (FAO, Rome, 2009).
36. A. Banerjee, E. Duflo, *Poor Economics: A Radical Rethinking of the Way to Fight Global Poverty* (Public Affairs, New York, 2011).
37. D. Headey, Was the global food crisis really a crisis? Simulations versus self-reporting (IFPRI Discussion Paper 01087, IFPRI, Washington, DC, 2011).
38. M. Verpoorten, A. Arora, J. F. M. Swinnen, Self-reported food insecurity in Africa during the food price crisis (LICOS Discussion Paper 303, LICOS, Leuven, Belgium, 2012).
39. J. F. M. Swinnen, K. Van Herck, Food security and the transition region (Working Paper, FAO Investment Centre, Rome, 2011); www.eastagri.org/publications/pub_docs/Food%20security_Web.pdf.

40. We thank S. Rozelle, T. Vandemoortele, D. McElroy, J. Pieters, other colleagues, and reviewers. The work was supported by the KU Leuven Methusalem project.

10.1126/science.1210806

Downloaded from www.sciencemag.org on January 27, 2012

Published by AAAS

IMMUNOLOGY

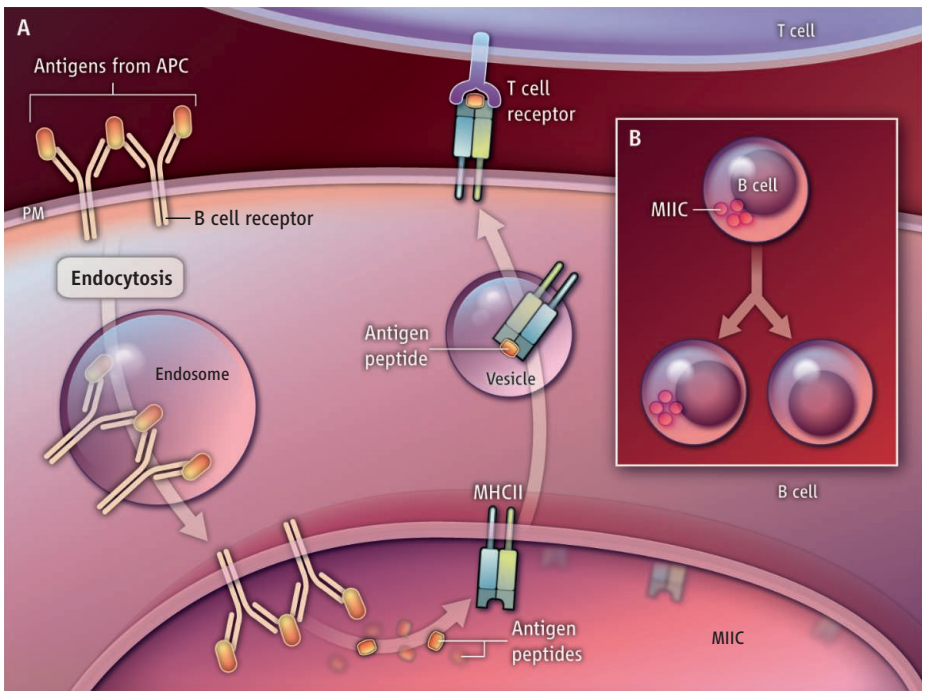
Antigen Feast or Famine

Michael L. Dustin[1] and Michael Meyer-Hermann[2,3]

The asymmetric distribution of antigen during B cell division affects the fate of B cells and their function.

Humoral immunity is critical for host defense and depends upon the generation of secreted antibodies with high affinity for antigens. The generation of high-affinity antibodies is a Darwinian process in which cycles of mutation in the genes encoding an antibody and the selection of antibodies for antigen binding lead to many-fold increases of antibody affinity. On page 475 in this issue, Thaunat *et al*. (*1*) report that B cells inherit antigen in an asymmetric manner during cell division, leaving all but one daughter cell starved of antigen while the cells are otherwise dividing symmetrically. This has implications for models of the humoral response that can be further explored.

The cell biology of antigen handling by B cells is well studied because of its central importance in humoral responses. B cells use the antibodies that they make as receptors to deliver antigen to internal organelles that harbor major histocompatibility complex (MHC) class II molecules. When the B cell receptor binds to an antigen, the antigen is extracted from the presenting cell and internalized by the B cell through endocytosis. Once an antigen-derived peptide forms a complex with MHC class II molecules in a compartment called the MHC class II compartment (MIIC), it is transported to the B cell surface where it is presented to, and selected by, T cells (*2*–*5*) (see the figure). Antigen presentation to T cells triggers B cell activation and differentiation into antibody-secreting cells (plasma cells). The MIIC serves as a "timed-release" system such that an antigen depot is maintained over a period of days. Using imaging cytometry, Thaunat *et al*. demonstrate that the MIIC is largely indivisible and is often inherited entirely by one daughter cell during mitosis. This means that most daughters suffer "antigen famine" and are perfectly prepared to mutate their receptors—the outcome is that they will only survive if a high-affinity antibody is generated that can capture more antigen. The single daughter that feasts on the MIIC can continue to receive help from T cells without a need for new antigen capture, which is not compatible with an effective natural selection scheme and suggests that this cell has a different fate.



Antigen polarization. (**A**) A B cell extracts antigen from an antigen-presenting cell (APC) and delivers it to MIIC, where antigen-derived peptides are generated. These combine with MHC class II molecules, which are delivered from the endoplasmic reticulum, and are transported back to the plasma membrane (PM) to interact with cognate T follicular helper cells. (**B**) In asymmetric MIIC (red) inheritance, only one daughter B cell receives the compartment, and thus, all the antigen.

The anatomic site in which high-affinity antibodies are made is the germinal center, located within lymphoid tissues. In iterative cycles, B cells divide and mutate their receptors and subsequently acquire antigen from follicular dendritic cells to get selected by T follicular helper (TFH) cells. Plasma cells are generated throughout the course of a humoral response with short-lived plasma cells arising prior to germinal center formation and long-lived plasma cells generated during the germinal center reaction (*6*). Germinal center B cells express the master regulatory transcription factor Bcl6, whereas that expressed by plasma cells is Blimp1 (*7*). In addition to containing antigen, the MIIC activates Erk and Akt kinases (*8*). Akt represses Bcl6 as well as activation-induced cytidine deaminase, which is required to mutate antibody genes (*9*); Erk activation is required for Blimp-1 expression (*10*). Although the consequences of MIIC signaling need to be tested more directly in this setting, it is possible to incorporate rules based on these observations into mathematical models.

Thaunat *et al*. demonstrated that the daughter cell inheriting MIIC can undergo additional interactions with TFH cells without further antigen collection. However, the actual fate of MIIC-inheriting B cells in germinal centers is not obvious, and two further scenarios may be considered. In one case, MIIC-inheriting B cells may collect more antigen from follicular dendritic cells. Thus, the inherited MIIC provides a competitive advantage regardless of the affinity of the potentially mutated receptor for interaction with TFH cells. In another scenario, the MIIC is a signal for differentiation to plasma cells without further interaction with TFH cells.

It was predicted by mathematical models (*11*) and verified by experiments (*12*) that help by TFH cells is a critical and limiting factor for B cell selection. This model (*13*) can be modified to incorporate additional

[1]Skirball Institute for Molecular Medicine, New York University School of Medicine, New York, NY 10016, USA. [2]Department Systems Immunology, Helmholtz Centre for Infection Research, Braunschweig, Germany. [3]Biocenter for Life Science, University of Technology, Braunschweig, Germany. E-mail: michael.dustin@med.nyu.edu

Downloaded from www.sciencemag.org on January 27, 2012

CREDIT: B. STRAUCH/*SCIENCE*

Published by AAAS

rules based on asymmetric MIIC inheritance and to predict the effect of each of the three scenarios on antibodies in terms of plasma cell quality and quantity (see SOM text). It shows that asymmetric MIIC inheritance only weakly affects the affinity of antibodies produced by plasma cells, with less than a 20% change. If MIIC inheritance turns off mutation, then affinity is increased while it is reduced in the case of unaffected mutation rates. By contrast, the model also predicts that asymmetric antigen inheritance can have a profound impact on plasma cell numbers. Based on simulations with comparable germinal center population kinetics, if the MIIC-inheriting daughter always differentiates into a plasma cell, the number of plasma cells derived from a germinal center reaction is 5- to 10-fold greater than in the other models in which this choice is made probabilistically (see fig. S1). This is because in the latter model, TFH selection events produce plasma cells only 10 to 20% of the time. In the scenario in which every B cell selected by TFH divides asymmetrically and one of the daughters differentiates to a plasma cell, 100% of TFH selection events produce a plasma cell. This substantial increase in early plasma cells may be critical for control of pathogens as higher-affinity antibodies are selected.

That plasma cells would also automatically inherit antigen fits with recent data suggesting that plasma cell presentation of antigen to T cells provides negative feedback on germinal center reactions (*14*). Thus, the results of Thaunat *et al*. provide a deterministic element in B cell differentiation that was previously missing and should inspire many in silico and in vivo experiments in the near future.

References and Notes

1. O. Thaunat *et al*., *Science* **335**, 475 (2012).
2. S. Amigorena, J. R. Drake, P. Webster, I. Mellman, *Nature* **369**, 113 (1994).
3. A. Tulp, D. Verwoerd, B. Dobberstein, H. L. Ploegh, J. Pieters, *Nature* **369**, 120 (1994).
4. K. Siemasko, B. J. Eisfelder, E. Williamson, S. Kabak, M. R. Clark, *J. Immunol.* **160**, 5203 (1998).
5. T. A. Gondré-Lewis, A. E. Moquin, J. R. Drake, *J. Immunol.* **166**, 6657 (2001).
6. A. Radbruch *et al*., *Nat. Rev. Immunol.* **6**, 741 (2006).
7. S. L. Nutt, N. Taubenheim, J. Hasbold, L. M. Corcoran, P. D. Hodgkin, *Semin. Immunol.* **23**, 341 (2011).
8. A. Chaturvedi, R. Martz, D. Dorward, M. Waisberg, S. K. Pierce, *Nat. Immunol.* **12**, 1119 (2011).
9. S. A. Omori *et al*., *Immunity* **25**, 545 (2006).
10. T. Yasuda *et al*., *Sci. Signal.* **4**, ra25 (2011).
11. M. E. Meyer-Hermann, P. K. Maini, D. Iber, *Math. Med. Biol.* **23**, 255 (2006).
12. G. D. Victora *et al*., *Cell* **143**, 592 (2010).
13. A. Garin *et al*., *Immunity* **33**, 84 (2010).
14. N. Pelletier *et al*., *Nat. Immunol.* **11**, 1110 (2010).

15. M.M.H. was supported by the BMBF GerontoSys initiative (GerontoMitoSys and GerontoShield) and the Human Frontier Science Program. M.L.D. was supported by NIH grant AI072529.

Supporting Online Material

www.sciencemag.org/cgi/content/full/335/6067/408/DC1
SOM Text
Fig. S1

10.1126/science.1218165

PHYSIOLOGY

A Clearer View from Fuzzy Images

Jumping spiders use defocus as a gauge of depth perception to locate prey.

Marie E. Herberstein and Darrel J. Kemp

Blurred vision is caused by an image not being focused correctly on the retina. In humans, blurred vision retards our ability to accurately perceive the world, and we go to great lengths to correct unfocused vision. In some spiders, however, images are deliberately defocused on the retina to provide for the crucial depth perception that allows high-precision jumps. On page 469 of this issue, Nagata *et al*. (*1*) elegantly demonstrate this novel form of depth perception in jumping spiders through a combination of molecular, electrophysiological, and behavioral experiments.

Humans receive information about depth mostly from their binocular stereoscopic vision; this feature of human vision is exploited in 3D movie technology by feeding slightly different images into each eye. Many animals, such as insects, do not have the same degree of binocular vision and instead use motion parallax, by moving their heads side to side, as a guide to how near or far a given object is (*2*). Jumping spiders (see the figure) possess admirable acuity in their principal eyes, which are also characteristically enlarged (*3*, *4*). The other two or three pairs of secondary eyes also have good acuity and are effective motion detectors (*5*). Jumping spiders are, as the name suggests, excellent jumpers and are capable of performing precision jumps over gaps or onto prey (*6*). However, jumping spiders are not known to use binocular stereoscopy or motion parallax. How, then, do they gain depth information from the environment?

The unusual "staircase" retina of the jumping spider anterior eye, described in the 1980s (*7*), provided a clue. Rather than having a single layer of photoreceptor cells, these eyes have a multitiered retina with four distinct photoreceptor layers. Nagata *et al*. investigated the spectral sensitivity of these retinal layers using a combination of molecular biology and electrophysiology. Opsins, a group of genes coding for specific color sensitivity (*8*, *9*), were identified in the four retinal layers by gene sequencing, expression analysis, and in situ hybridization. Electrophysiology revealed that layers 1 and 2 are maximally sensitive to green light, whereas layers 3 and 4 are maximally sensitive in the ultraviolet. These sensitivities matched the identified opsin genes in the retinal layers. Curiously, however, even though layers 1 and 2 contain primarily green-sensitive photoreceptors, the effect of chromatic aberration means that incoming green light is only clearly focused on layer 1. This means that the second main green-sensitive retinal layer (layer 2) receives a defocused or "fuzzy" image. Nagata *et al*. suggest that the spiders obtain depth cues from the amount of defocus in this layer, which is proportional to the distance of the object to the lens.



Gotcha! The jumping spider determines the distance to its prey according to green-light images focused differentially within its multilayered retina.

CREDIT: AJAY NARENDRA/AUSTRALIAN NATIONAL UNIVERSITY, CANBERRA

Department of Biological Sciences, Macquarie University, Sydney, NSW 2109, Australia. E-mail: marie.herberstein@mq.edu.au

Downloaded from www.sciencemag.org on January 27, 2012

Published by AAAS

To test this hypothesis, Nagata *et al*. set up an experiment in which jumping spiders had to accurately jump at prey under different light conditions. If defocus in the green channel is important, spiders should not be able to accurately judge a jumping distance in the absence of green light. As predicted, the spiders made accurate jumps onto prey under green light, but they consistently underestimated jump distances under red illumination (in which all shorter-wave light, such as green or blue, is removed). Taken together, the data provide strong evidence that jumping spiders use the novel method of image defocus for depth perception. The exact neural mechanism involved in integrating focused and unfocused images is, however, unknown.

Understanding how animals perceive the world poses a major challenge for vision research. The study by Nagata *et al*. exemplifies the complex nature of animal vision and highlights the crucial role of behavioral studies in honing our understanding of this phenomenon. Vision researchers have achieved exceptional progress in describing eye structure and in identifying light receptors with the use of sophisticated molecular and physiological approaches (*10*). Inferences regarding animal perception based on such data nevertheless remain as essentially untested hypotheses in the absence of ground-truthing from behavioral experiments. Nagata *et al*.'s study demonstrates the precision with which molecular and physiological techniques can be applied, and the great insights that can be gained as a result, but their ultimate test still required behavioral experimentation with whole, live animals. Against a background of increasingly popular technological approaches in visual research, Nagata *et al*.'s study therefore shows how these approaches complement—but do not replace—behavioral studies of animal vision.

References

1. T. Nagata *et al*., *Science* **335**, 469 (2012).
2. K. Kral, *Behav. Processes* **64**, 1 (2003).
3. M. F. Land, *J. Exp. Biol.* **51**, 443 (1969).
4. R. F. Foelix, *Biology of Spiders* (Oxford Univ. Press, Oxford, ed. 3, 2011).
5. D. B. Zurek, A. J. Taylor, C. S. Evans, X. J. Nelson, *J. Exp. Biol.* **213**, 2372 (2010).
6. R. R. Jackson, S. D. Pollard, *Annu. Rev. Entomol.* **41**, 287 (1996).
7. A. D. Blest, R. C. Hardie, P. Mcintyre, D. S. Williams, *J. Comp. Physiol.* **145**, 227 (1981).
8. K. Palczewski *et al*., *Science* **289**, 739 (2000).
9. Y. Shichida, T. Matsuyama, *Philos. Trans. R. Soc. London Ser. B* **364**, 2881 (2009).
10. A. Kelber, M. Vorobyev, D. Osorio, *Biol. Rev. Camb. Philos. Soc.* **78**, 81 (2003).

10.1126/science.1216887

EVOLUTION

The Role of Coevolution

Coevolution of a virus and a bacterium leads to the emergence of a key adaptive innovation.

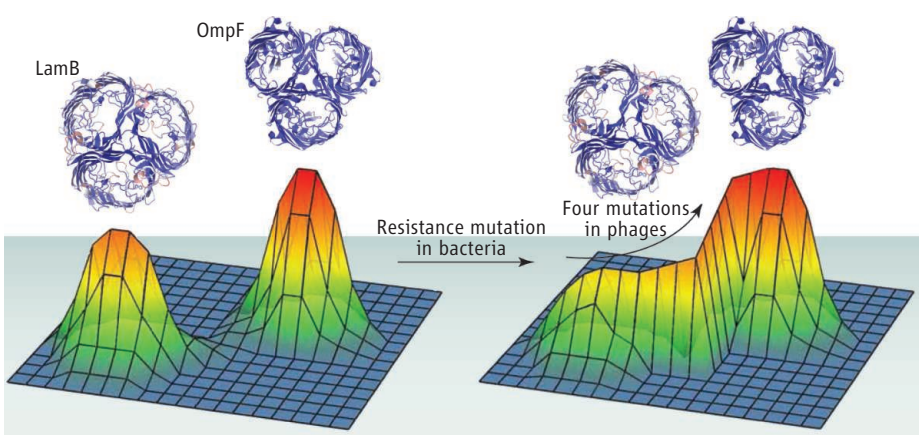
John N. Thompson

One of the great metaphors of evolutionary biology, introduced by Sewall Wright (*1*), is that populations evolve toward adaptive peaks separated by adaptive valleys. The peaks are combinations of genes that confer high Darwinian fitness on individuals, whereas the valleys are combinations that confer low fitness (see the figure). But how can a population move from one peak to another, perhaps higher, peak, across an adaptive valley in which gene combinations are presumed to be maladaptive? On page 428 of this issue, Meyer *et al*. (*2*) show that coevolution may favor key innovations that guide a population quickly onto the slope of a different adaptive peak.

Almost half a century ago, Ehrlich and Raven (*3*) argued that coevolution could drive the diversification of life by sequentially favoring key innovations in coevolving lineages. Each innovation in one lineage leads to subsequent diversification, which, in turn, favors key innovations in the other lineage. Ever since then, biologists have been trying to understand under which conditions coevolution can directly favor innovations and diversification rather than simple improvements in current adaptations (*4*, *5*).

Department of Ecology and Evolutionary Biology, University of California, Santa Cruz, Santa Cruz, CA 95064, USA. E-mail: jnthomp@ucsc.edu

The experiments by Meyer *et al*. show not only that coevolution can be instrumental in shaping a key innovation but also why coevolution is important. The authors study the coevolution of a virus, λ bacteriophage, and the bacterium *Escherichia coli*. Natural selection on coevolving interactions between bacteria and phages is often focused on the ability of a phage to adsorb to the surface of a bacterium and the ability of bacteria to prevent this adsorption. λ bacteriophages attach to *E. coli* bacteria using a tail protein called J,



How to cross an adaptive valley. In an adaptive landscape, some genetic combinations have high Darwinian fitness (adaptive peaks) and others have low fitness (adaptive valleys). In the coevolving interaction between λ bacteriophages and *E. coli* bacteria reported by Meyer *et al*., the phages normally attach to the bacterial surface protein LamB. It takes the co-occurrence of four mutations to allow the phages to shift their attachment site to OmpF rather than LamB. Coevolution of the phage population with LamB fortuitously makes it possible for that unlikely combination of mutations to come together. This all-or-nothing combination of mutations creates, in effect, a gene combination that forms a narrow ridge between the two peaks, allowing the phage population to shift from using LamB to using OmpF. The ridge could eventually disappear as selection acts to favor resistant forms of the OmpF protein. The figure is intended heuristically; the full fitness landscape was not measured in the study and cannot be captured in three dimensions.

Downloaded from www.sciencemag.org on January 27, 2012

Published by AAAS

To test this hypothesis, Nagata *et al*. set up an experiment in which jumping spiders had to accurately jump at prey under different light conditions. If defocus in the green channel is important, spiders should not be able to accurately judge a jumping distance in the absence of green light. As predicted, the spiders made accurate jumps onto prey under green light, but they consistently underestimated jump distances under red illumination (in which all shorter-wave light, such as green or blue, is removed). Taken together, the data provide strong evidence that jumping spiders use the novel method of image defocus for depth perception. The exact neural mechanism involved in integrating focused and unfocused images is, however, unknown.

Understanding how animals perceive the world poses a major challenge for vision research. The study by Nagata *et al*. exemplifies the complex nature of animal vision and highlights the crucial role of behavioral studies in honing our understanding of this phenomenon. Vision researchers have achieved exceptional progress in describing eye structure and in identifying light receptors with the use of sophisticated molecular and physiological approaches (*10*). Inferences regarding animal perception based on such data nevertheless remain as essentially untested hypotheses in the absence of ground-truthing from behavioral experiments. Nagata *et al*.'s study demonstrates the precision with which molecular and physiological techniques can be applied, and the great insights that can be gained as a result, but their ultimate test still required behavioral experimentation with whole, live animals. Against a background of increasingly popular technological approaches in visual research, Nagata *et al*.'s study therefore shows how these approaches complement—but do not replace—behavioral studies of animal vision.

References

1. T. Nagata *et al*., *Science* **335**, 469 (2012).
2. K. Kral, *Behav. Processes* **64**, 1 (2003).
3. M. F. Land, *J. Exp. Biol.* **51**, 443 (1969).
4. R. F. Foelix, *Biology of Spiders* (Oxford Univ. Press, Oxford, ed. 3, 2011).
5. D. B. Zurek, A. J. Taylor, C. S. Evans, X. J. Nelson, *J. Exp. Biol.* **213**, 2372 (2010).
6. R. R. Jackson, S. D. Pollard, *Annu. Rev. Entomol.* **41**, 287 (1996).
7. A. D. Blest, R. C. Hardie, P. Mcintyre, D. S. Williams, *J. Comp. Physiol.* **145**, 227 (1981).
8. K. Palczewski *et al*., *Science* **289**, 739 (2000).
9. Y. Shichida, T. Matsuyama, *Philos. Trans. R. Soc. London Ser. B* **364**, 2881 (2009).
10. A. Kelber, M. Vorobyev, D. Osorio, *Biol. Rev. Camb. Philos. Soc.* **78**, 81 (2003).

10.1126/science.1216887

EVOLUTION

The Role of Coevolution

Coevolution of a virus and a bacterium leads to the emergence of a key adaptive innovation.

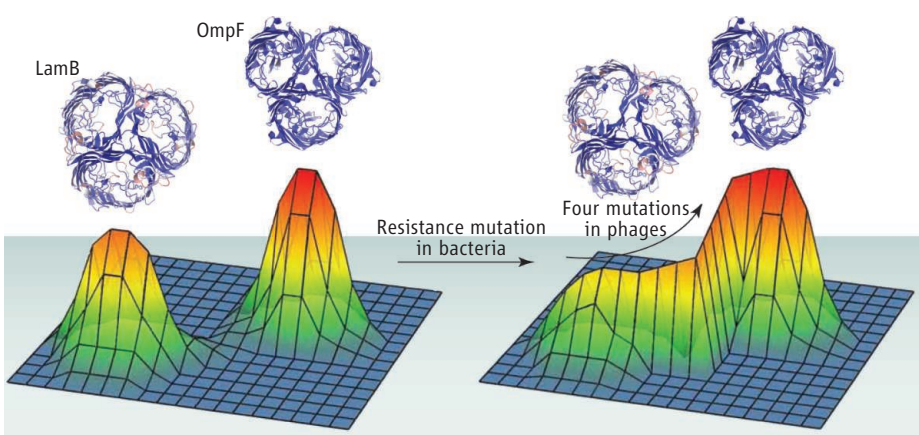
John N. Thompson

One of the great metaphors of evolutionary biology, introduced by Sewall Wright (*1*), is that populations evolve toward adaptive peaks separated by adaptive valleys. The peaks are combinations of genes that confer high Darwinian fitness on individuals, whereas the valleys are combinations that confer low fitness (see the figure). But how can a population move from one peak to another, perhaps higher, peak, across an adaptive valley in which gene combinations are presumed to be maladaptive? On page 428 of this issue, Meyer *et al*. (*2*) show that coevolution may favor key innovations that guide a population quickly onto the slope of a different adaptive peak.

Almost half a century ago, Ehrlich and Raven (*3*) argued that coevolution could drive the diversification of life by sequentially favoring key innovations in coevolving lineages. Each innovation in one lineage leads to subsequent diversification, which, in turn, favors key innovations in the other lineage. Ever since then, biologists have been trying to understand under which conditions coevolution can directly favor innovations and diversification rather than simple improvements in current adaptations (*4*, *5*).

Department of Ecology and Evolutionary Biology, University of California, Santa Cruz, Santa Cruz, CA 95064, USA. E-mail: jnthomp@ucsc.edu

The experiments by Meyer *et al*. show not only that coevolution can be instrumental in shaping a key innovation but also why coevolution is important. The authors study the coevolution of a virus, λ bacteriophage, and the bacterium *Escherichia coli*. Natural selection on coevolving interactions between bacteria and phages is often focused on the ability of a phage to adsorb to the surface of a bacterium and the ability of bacteria to prevent this adsorption. λ bacteriophages attach to *E. coli* bacteria using a tail protein called J,



How to cross an adaptive valley. In an adaptive landscape, some genetic combinations have high Darwinian fitness (adaptive peaks) and others have low fitness (adaptive valleys). In the coevolving interaction between λ bacteriophages and *E. coli* bacteria reported by Meyer *et al*., the phages normally attach to the bacterial surface protein LamB. It takes the co-occurrence of four mutations to allow the phages to shift their attachment site to OmpF rather than LamB. Coevolution of the phage population with LamB fortuitously makes it possible for that unlikely combination of mutations to come together. This all-or-nothing combination of mutations creates, in effect, a gene combination that forms a narrow ridge between the two peaks, allowing the phage population to shift from using LamB to using OmpF. The ridge could eventually disappear as selection acts to favor resistant forms of the OmpF protein. The figure is intended heuristically; the full fitness landscape was not measured in the study and cannot be captured in three dimensions.

Downloaded from www.sciencemag.org on January 27, 2012

Published by AAAS

which targets a single protein, LamB, on the bacterial outer surface. The key innovation in the phage population is the evolution of a mutant form of J that attaches to a different bacterial surface protein, OmpF. This bacterial protein has a crystal structure similar to LamB, even though its amino acid sequence is quite different. The mutant phages thus circumvent the evolution of resistance at the LamB protein by shifting their attack to a bacterial surface protein that happens to be structurally similar to their normal site of attachment. No previous studies have found this mutation in λ, despite decades of study of this phage.

The key innovation in λ occurred while the bacteria and phage were coevolving in flasks, and it occurred repeatedly within several weeks in different populations. Additional experiments and sequencing of the phage genome showed that a phage population needs to acquire four mutations to shift to the OmpF protein. Coevolution fortuitously made that possible. The evolution of resistant forms of LamB favored retention of an initial mutation in some phage populations, which, in turn, favored two other mutations. These three mutations needed to be in place before selection could favor the final mutation allowing the shift to OmpF. The coevolutionary process essentially created a very narrow ridge of high fitness between the adaptive peaks that could be attained only by phages with all four mutations (see the figure).

The experiments also show that there is nothing inevitable about the trajectory of coevolution. Under the same coevolutionary conditions, the key innovation appeared in only a subset of the phage populations. Hosts evolved resistance in more than one way. Although one resistant form created a selective advantage for phage mutants that target the new receptor, another resistant form blocked that potential advantage. Coevolution therefore shifted some populations to a new trajectory of adaptive change, but prevented other populations from following that trajectory.

Those trajectories, as the experiments show, can favor novel traits rather than just escalation in current defenses or counter-defenses. This is becoming an increasingly important theme in coevolutionary biology (*6*). If coevolution of parasites and hosts were only about escalating arms races, life might have coevolved to extinction eons ago. Coevolution may rarely have the opportunity to favor novelty through major key innovations, such as that found in these experiments, but it often has the opportunity to cyclically favor uncommon, minor deviations in traits to which the coevolving partner is not currently adapted.

The populations in Meyer *et al*.'s experiments coevolved in ecologically simple environments. Whether key innovations are more likely, or less likely, in populations evolving in more genetically and ecologically variable environments is a question for future research. Spatial structuring of coevolving populations, for example, often generates coevolutionary dynamics that differ qualitatively and quantitatively from those observed in locally coevolving populations (*7*, *8*). Because selection differs among coevolving populations and they exchange genes periodically, the pace, trajectories, and dynamics of evolving traits are not a simple sum of the events within local populations. Therefore, one of the next questions to answer is how the evolution of entirely new functions (that is, key innovations) proceeds in interactions coevolving as a geographic mosaic of traits and fitnesses.

The results of Meyer *et al*. show that microbial populations can evolve key innovations on time scales of several weeks, when those populations are evolving in environments that favor them. The same laboratory has previously reported that, in the absence of coevolution, a subset of experimental populations of *E. coli* developed a key innovation in resource use within about 30,000 generations (*9*). Taken together, the two studies suggest that key innovations may not be limited in nature by genetic variation. Instead, they are more likely limited by lucky sequences of events in which selection has the opportunity in a particular ecological setting to favor multiple genetic variants in a row. Coevolution may increase the number of lucky opportunities.

References

1. S. Wright, *Proc. 6th Int. Congr. Genet.* **1**, 356 (1932).
2. J. R. Meyer *et al*., *Science* **335**, 428 (2012).
3. P. R. Ehrlich, P. H. Raven, *Evolution* **18**, 586 (1964).
4. R. E. Ricklefs, *Proc. Natl. Acad. Sci. U.S.A.* **107**, 1265 (2010).
5. J. B. Yoder, S. L. Nuismer, *Am. Nat.* **176**, 802 (2010).
6. L. T. Morran, O. G. Schmidt, I. A. Gelarden, R. C. Parrish, II, C. M. Lively, *Science* **333**, 216 (2011).
7. J. N. Thompson, *The Geographic Mosaic of Coevolution* (Univ. Chicago Press, Chicago, 2005).
8. M. A. Brockhurst, A. D. Morgan, P. B. Rainey, A. Buckling, *Ecol. Lett.* **6**, 975 (2003).
9. Z. D. Blount, C. Z. Borland, R. E. Lenski, *Proc. Natl. Acad. Sci. U.S.A.* **105**, 7899 (2008).

10.1126/science.1217807

CELL BIOLOGY

The Risk of Prion Zoonoses

John Collinge

Transmission of prions between species through both lymphoid and neural tissues has implications for public health and risk management.

Prions are lethal infectious pathogens that cause neurodegenerative diseases in humans and animals (*1*). They can pass from one species to another but with greater difficulty than transmission within the same species because of the so-called species barrier effect. Such barriers protect humans from developing prion disease after dietary or other exposure to animal reservoirs of infection. These include endemic scrapie of sheep and goats, chronic wasting disease (CWD) of deer and elk, and bovine spongiform encephalopathy (BSE) or "mad cow disease" (*1*). On page 472 of this issue, Béringue *et al*. (*2*) show that in transgenic mice expressing ovine or human prion protein (PrP), lymphoid tissue is more susceptible to cross-species transmission than neural tissue (brain), which may prompt a reevaluation of the effectiveness of species barriers.

Prions consist of polymers of a misfolded form of a host-encoded PrP and propagate by recruiting normal PrP monomers (*3*); fission of the polymer produces more "seeds." Multiple prion strains can propagate in the same host type and produce different disease phenotypes associated with distinct abnormal PrP conformations. A prion strain, however, consists of a molecular ensemble or quasispecies maintained under host selection pressure (*3*, *4*) that comprise a dominant component together with lower-abundance subspecies. Minor components might preferentially propagate in a new host, resulting in strain shifting or mutation, or in a different tissue within the same host where factors determining rates of propagation and clearance favor such a subcomponent (*3*).

MRC Prion Unit, UCL Institute of Neurology, London WC1N 3BG, UK. E-mail: j.collinge@prion.ucl.ac.uk

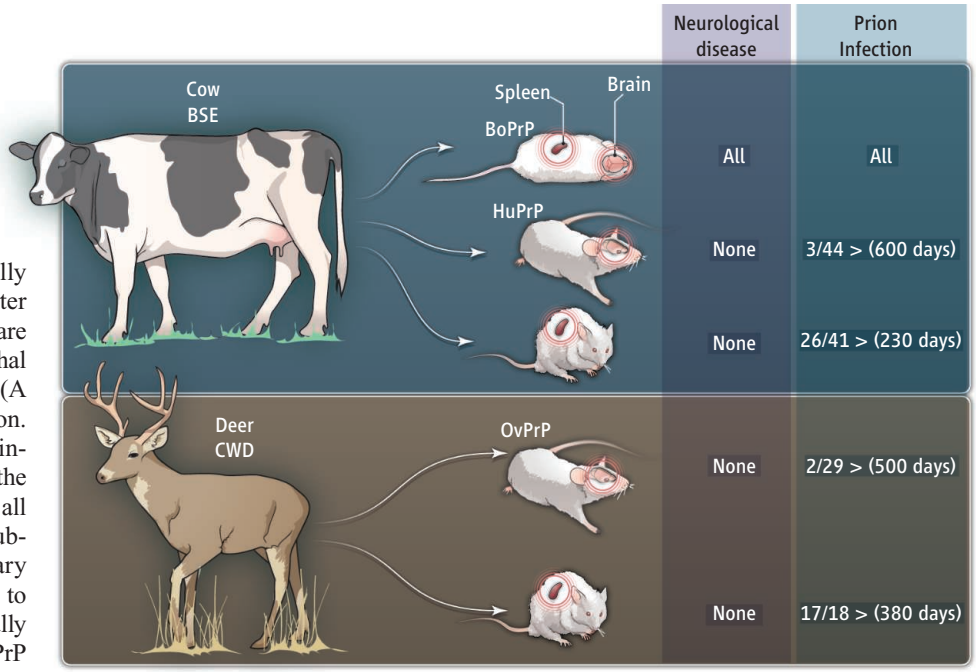
Downloaded from www.sciencemag.org on January 27, 2012

Published by AAAS

Species barriers, or transmission barriers, may be quantified by measuring the change in incubation periods as prions adapt to a new host. Although prions from one species (A) may infect another species (B), this is usually inefficient; subsequent exposure of species B to species B–passaged prions typically results in 100% lethality with much shorter incubation periods. Alternatively, barriers are assessed by comparing the LD_{50} (dose lethal to half the animals inoculated) on primary (A to B) and secondary (B to B) transmission. The strain type is also crucial in determining the transmission barrier. According to the conformational selection model (*3*, *5*), of all the possible prion strain types, only a subset is compatible with a given PrP primary structure, and transmission barriers relate to the degree of overlap of thermodynamically allowed or preferred conformers between PrP in the host and donor species.

However, measuring transmission barriers by scoring the onset of clinical disease in inoculated animals is inadequate and may be misleading (*6*). The barrier between mice and hamsters was thought to be complete, but disease-related PrP (PrP^{Sc}) is detectable in all hamster prion-inoculated mice living beyond 650 days, and such mice have brain prion titers comparable to those of animals dying of conventional prion infection (*6*). Such subclinical infections are now recognized following cross-species prion inoculation or low-dose same-species oral prion exposure (*6*–*8*). Although the barrier to developing clinical disease may be very large, the barrier to silent infection of the host (with production of prions composed of host PrP) may be modest but not detectable by PrP^{Sc} or infectivity assays until prolonged periods, which may approach the natural life span of the inoculated animals, have elapsed. The failure to develop the rapidly lethal neurological syndrome in such subclinically infected animals may relate to the slow kinetics of prion propagation, such that associated toxic species do not reach critical thresholds (*3*).

Béringue *et al*. have taken such investigations further by using several prion strains [including the BSE strain that causes variant Creutzfeldt-Jakob disease (vCJD) in humans, and CWD, in which there are concerns of zoonotic potential] in transgenic mice expressing ovine or human PrP (see the figure). In many prion infections, including natural sheep scrapie and vCJD, as well as experimental rodent models, prions propagate in the lymphoreticular system (LRS: spleen, lymph nodes, tonsil, appendix, and other gut-associated lymphoid tissues), and this may precede (and in some cases be necessary for) neuroinvasion (*9*, *10*). They found that no clinical disease resulted when they challenged mice expressing ovine PrP with CWD prions; however, almost all mice had evidence of LRS prion infection at death. Only a small minority of mice, which lived more than 500 days, had detectable brain PrP^{Sc}. The transmission barrier was more readily crossed in the LRS than in the brain. Inoculation of these ovine PrP mice with hamster prions and serial passage studies indicated strain differences between prions propagating in brain and spleen consistent with tissue-specific strain selection or mutation.



Cross species prion infection. Transgenic mice expressing human (Hu) or sheep (Ov) PrP, inoculated, respectively, with BSE or CWD prions, do not generally develop clinical disease, and were observed to end of life or culled for examination (*2*). The majority examined beyond 300 days showed evidence of prion infection in the spleen, whereas only a few mice had detectable brain infection beyond 500 days after inoculation. Bo, bovine.

The principal transmission barrier of concern to public health is that between humans and cattle (and possibly sheep and goat) BSE prions. Béringue *et al*. found little evidence of clinical disease in the human PrP–expressing transgenic mice challenged with BSE prions, but a high proportion had infection in the spleen; less than 10% had brain infection after more prolonged incubation periods.

Although subclinical infection by foreign prions may not be detrimental, prion titers may be comparable to those seen in animals dying of a conventional prion disease. Such prions have adapted to the new host species and show high lethality to other individuals of that species (*6*). This is relevant to public health in that individuals silently colonized with vCJD prions would pose a risk to others were they blood and other tissue donors, and via contamination of surgical instruments (*11*–*14*).

The arrival of vCJD in 1996, caused by exposure to the BSE strain (*1*), led to major public health concerns. The subsequent decline in vCJD and small overall numbers (around 200) led to reassurance that the bovine BSE–to–human transmission barrier was, fortuitously, substantial, thereby avoiding a major epidemic. However, concerns have persisted of a silent infection rate in the community because of the range of incubation periods in human prion diseases [partly genetically determined (*15*), and which can exceed 50 years (*16*)] and the possibility of subclinical carrier states. Based on an early study in which 3 out of ~12,000 archived surgical appendix samples were found positive (*17*), a UK government advisory committee proposed a figure of 1 in 4000 of the UK population infected for risk management assessments (*18*). Interim data from a repeat appendix survey have reported 4 positives from ~14,000 (*19*).

There has been considerable debate about the "discrepancy" between numbers of clinical vCJD cases and estimates of population prevalence of infection in LRS tissues. The data of Béringue *et al*. could explain such a discrepancy if BSE exposure led to LRS colonization in many individuals, but progressed to neuroinvasive disease in very few. These data may also mean that apparent prevalence of subclinical prion infection will increase in BSE-exposed cohorts because it may take years to develop to a point detectable by these methods. All efforts should be made to assess

CREDIT: Y. HAMMOND/*SCIENCE*

Downloaded from www.sciencemag.org on January 27, 2012

Published by AAAS

the prevalence of prion infection in the UK population by analyzing surgical and autopsy LRS and neural tissues, and investigating whether blood-based tests for vCJD can detect silent infection, both to assess prevalence of infection in donors, and if necessary, to ensure safety of blood and blood products and to avoid iatrogenic transmission during surgical and medical procedures (*20*, *21*). From a public health perspective, transmission barriers to infection, and not disease, matter for risk management as iatrogenic transmission will occur from healthy individuals, not those identified already as posing a risk by virtue of their clinical diagnosis of prion disease.

References

1. J. Collinge, *Annu. Rev. Neurosci.* **24**, 519 (2001).
2. V. Béringue *et al.*, *Science* **335**, 472 (2012).
3. J. Collinge, A. R. Clarke, *Science* **318**, 930 (2007).
4. J. Li *et al.*, *Proc. Natl. Acad. Sci. U.S.A.* **327**, 869 (2010).
5. J. Collinge, *Lancet* **354**, 317 (1999).
6. A. F. Hill *et al.*, *Proc. Natl. Acad. Sci. U.S.A.* **97**, 10248 (2000).
7. R. Race *et al.*, *J. Virol.* **75**, 10106 (2001).
8. A. M. Thackray *et al.*, *J. Virol.* **77**, 7991 (2003).
9. H. Fraser, M. E. Bruce, D. Davies, C. F. Farquhar, P. A. McBride, in *Prion Dis. of Humans and Animals*, S. B. Prusiner, J. Collinge, J. Powell, B. Anderton, Eds. (Ellis Horwood, London, 1992), chap. 22.
10. J. D. Wadsworth *et al.*, *Lancet* **358**, 171 (2001).
11. A. Peden *et al.*, *Haemophilia* **16**, 296 (2010).
12. S. J. Wroe *et al.*, *Lancet* **368**, 2061 (2006).
13. P. Brown *et al.*, *Neurology* **55**, 1075 (2000).
14. C. Bernoulli *et al.*, *Lancet* **1**, 478 (1977).
15. S. Lloyd, S. Mead, J. Collinge, *Top. Curr. Chem.* **305**, 1 (2011).
16. J. Collinge *et al.*, *Lancet* **367**, 2068 (2006).
17. D. A. Hilton *et al.*, *J. Pathol.* **203**, 733 (2004).
18. "SEAC position statement: Prevalence of subclinical variant Creutzfeldt-Jakob disease infections" (2008); http://webarchive.nationalarchives.gov.uk/20110316162913/http://www.seac.gov.uk/statements/state-cjd-infections.pdf.
19. Health Protection Report, Health Protection Agency (2011) www.hpa.org.uk/hpr/archives/2011/news3611.htm.
20. J. A. Edgeworth *et al.*, *Lancet* **377**, 487 (2011).
21. L. Gregori, *Lancet* **377**, 444 (2011).

10.1126/science.1218167

MATERIALS SCIENCE

Creating New Types of Carbon-Based Membranes

Graphene oxide membranes can show unusually high water permeability, and diamond-like carbon membranes exhibited ultrafast permeation of organic solvents.

Donald R. Paul

Carbon-based membranes (*1*) for gas separations, which can be produced by pyrolysis of various precursor polymers, have had limited commercial use to date, in part because of their high cost and fragile mechanical nature. In this issue, unusual permeation behavior is reported for membranes made from two quite different forms of carbon that make them attractive for molecular separations or perhaps other uses. On page 442, Nair *et al.* (*2*) describe extremely rapid permeation of water through graphene oxide (GO) membranes that are essentially impermeable to other liquids and to helium, while on page 444, Karan *et al.* (*3*) report ultrafast permeation of organic solvents through diamond-like carbon nanosheets that reject larger dissolved molecules.

Unlike current carbon membranes, polymeric membranes are used on large scales commercially (*4*) for gas separation (e.g., production of nitrogen from air), as well as desalination of seawater and filtration of dissolved macromolecules and suspended particles. Permeation through membranes of all types can be described by two limiting mechanisms, either pore flow (large molecules are blocked by smaller pores) or solution-diffusion (molecules dissolve into and diffuse through the membrane at different rates) (*4*, *5*). However, both mechanisms may be operating in some cases [see, for example, (*4*, *6*, *7*)]. For solid carbon-based membranes, pore-flow mechanisms are often expected, but if pores or channels are extraordinarily small (~1 nm in size), conventional notions of pore flow may not apply.

Nair *et al*. describe procedures for fabricating membranes from graphene oxide, in which oxidized graphene sheets have openings and edges that bear hydroxyl, epoxy, and other hydrophilic functional groups. The membranes have thicknesses ranging from 0.1 to 10 μm (area ~1 cm^2) and likely have a layered structure (see the figure, panel A). Mass-spectrometry techniques for measuring helium permeation show submicrometer-thick GO films (when dry) to be less permeable than a 1-mm-thick glass (*8*). The permeation of liquids was tested by a simple gravimetric technique. A liquid creates a saturated vapor in a feed chamber on one side of the membrane; the vapor can then pass through the membrane and evaporate into a dry sealed chamber. No permeation could be detected for several polar and nonpolar organic liquids through 1-μm-thick GO membranes. However, the membranes were highly permeable to water; for submicrometer GO membranes, the evaporation rate of water was essentially the same as when no membrane was in place, and even a 10-μm-thick membrane only reduced the evaporation rate by a factor of 2.

The authors suggest that functional groups on the surface of GO layers prop open the layers and that permeation occurs between layers through percolating regions of "empty space" where the sheets are not oxidized. The spacing between GO layers depended on relative humidity (RH); at about 10% RH, the spacing was ~6 to 7 Å but steadily increased to ~10 to 12 Å at 100% RH as water molecules intercalated into the void spaces (*9*). When GO membranes were reduced by annealing in a hydrogen atmosphere, the layer spacing was reduced to 4 Å, and they became much less permeable to water.

Nair *et al*. repeated the water permeation by adding salts to the water to lower the RH in the feed chamber. The resulting decrease in GO layer spacing greatly reduced the permeation of water, much more than could be explained by the reduced driving force with lower RH. Helium permeated humidified GO membranes at measurable rates, but at high RH, water permeated 10^5 times faster than helium. The authors used atomistic simulations of water dynamics in two-dimensional graphene capillaries to support their experimental results and hypotheses, and discuss the connection to the fast transport of water through carbon nanotubes [see, for example, (*10*, *11*)].

More detailed studies will be needed to sort out material variables, such as the effects of oxidation chemistry, as well as more refined measurements of permeation that eliminate the effects of external mass transfer resistance (which could compare

Department of Chemical Engineering, University of Texas at Austin, Austin, TX 78712, USA. E-mail: drp@che.utexas.edu

Downloaded from www.sciencemag.org on January 27, 2012

Published by AAAS

changes in the material versus changes in driving force for permeation) and studies at different temperature to elucidate the energetics of permeation.

Karan *et al*. fabricated free-standing, diamond-like carbon (DLC) nanosheets, with thicknesses of 10 to 40 nm, by plasma chemical vapor deposition of various organic compounds. Carbon-13 nuclear magnetic resonance measurements show that the membranes consist of about equal numbers of sp^3 (diamond lattice) and sp^2 (graphite lattice) carbon atoms (*12*), as typical for hydrogenated amorphous carbon (a-C:H soft). Their DLC membranes are stiff, and have elastic moduli ~50 times greater than that of engineering thermoplastics and only about 10 times less than that of diamond. These nanosheets contain pores traversing their thickness, and high-resolution transmission electron microscopy indicates ~12% surface porosity with pore sizes that seem to be no more than 1 nm. These pores are much smaller than the 9- to 35-nm ones reported for porous nanocrystalline silicon membranes having thicknesses of ~10 nm (*13*).

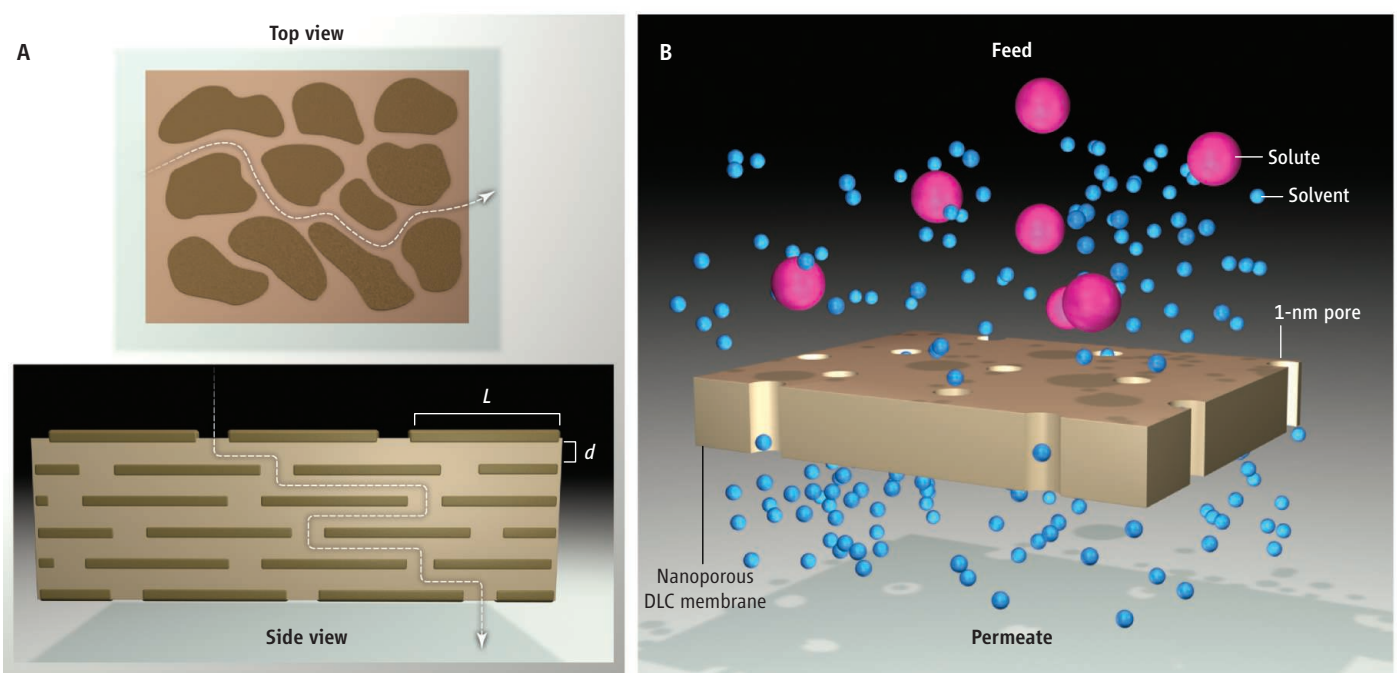
The authors demonstrate ultrafast permeation of organic solvents through these DLC membranes and rejection of organic solute molecules larger than, or comparable in size to, the 1-nm pores (see the figure, panel B). The membranes are apparently quite resistant to the organic solvents examined and exhibit stable performance. In some cases, the solvent flux through these membranes is about three orders of magnitude greater than for commercially available nanofiltration membranes suitable for use with organic solvents; the rejection of solute molecules seems to have a sharp cutoff based on molecular size. Perhaps most surprising is that the observed fluxes vary inversely with solvent viscosity, but not with any other measured characteristic of the solvent. Thinner membranes had higher fluxes, as expected, and Karan *et al*. discuss the flow through these ~1-nm pores in terms of the classical Hagen-Poiseuille equation for viscous flow derived from continuum fluid mechanics (*14*). Many avenues remain to be explored about the relation between the performance of these membranes and the materials chemistry and fabrication, especially tuning pore size and porosity.

For applications, the GO membranes of Nair *et al*. have characteristics that are of interest for dehumidifying gas streams before compression or for energy savings in air-conditioning systems. For the DLC membranes of Karan *et al*., all of the areas where membranes are currently used for nanofiltration from organic media are possibilities. Such membranes could also be used in the production of high-value products to reduce the amount of solvent in reaction mixtures before further purification. Any large-scale application of either of these new material concepts will require appreciable efforts to learn how to make large areas of membranes, to support them, and to package them in modules (*4*). In the near term, very small scale, niche applications are more likely.

References

1. A. F. Ismail, D. Rana, T. Matsuura, H. C. Foley, *Carbon-Based Membranes for Separations* (Springer, New York, 2011).
2. R. R. Nair, H. A. Wu, P. N. Jayaram, I. V. Grigorieva, A. K. Geim, *Science* **335**, 442 (2012).
3. S. Karan, S. Samitsu, X. Peng, K. Kurashima, I. Ichinose, *Science* **335**, 444 (2012).
4. R. W. Baker, *Membrane Technology and Applications* (Wiley, Chichester, UK, ed. 2, 2004).
5. Y. Yampolskii, I. Pinnau, B. D. Freeman, *Materials Science of Membranes for Gas and Vapor Separation* (Wiley, Chichester, UK, 2006).
6. R. Srinivasan, S. R. Auvil, P. M. Burban, *J. Membr. Sci.* **86**, 67 (1994).
7. T. Okada, T. Matsuura, *J. Membr. Sci.* **59**, 133 (1991).
8. F. J. Norton, *J. Am. Ceram. Soc.* **36**, 90 (1953).
9. A. Lerf, A. Buchsteiner, J. Pieper, S. Schöttl, I. Dekany, T. Szabo, H. P. Boehm, *Phys. Chem. Solids* **67**, 1106 (2006).
10. J. A. Thomas, A. J. H. McGaughey, *Nano Lett.* **8**, 2788 (2008).
11. X. Qin, Q. Yuan, Y. Zhao, S. Xie, Z. Liu, *Nano Lett.* **11**, 2173 (2011).
12. J. Robertson, *Mater. Sci. Eng.* **R37**, 129 (2002).
13. C. C. Striemer, T. R. Gaborski, J. L. McGrath, P. M. Fauchet, *Nature* **445**, 749 (2007).
14. R. B. Bird, W. E. Stewart, E. N. Lightfoot, *Transport Phenomena* (Wiley, New York, ed. 2, 2002).

10.1126/science.1216923



Permeation through carbon-based membranes. (**A**) In order to permeate through graphene oxide (GO) membranes reported by Nair *et al*., water molecules must take a tortuous path (dotted lines) within the "empty space" of unoxidized areas between GO sheets (with a narrow spacing *d*). The water molecules wiggle around the oxidized regions (see top view) and then around the GO sheets (with longer dimensions *L*) to get into the next interlayer space (see side view). (**B**) Solvent molecules permeate through the nanopores of diamond-like carbon (DLC) membranes fabricated by Karan *et al*. by viscous flow, but larger solute molecules cannot get through these 1-nm pores.

CREDIT: P. HUEY/*SCIENCE*

Downloaded from www.sciencemag.org on January 27, 2012

Published by AAAS

NEUROSCIENCE

Another Remembered Present

Could conscious perception reflect a memory process?

Kaspar Meyer



Intuition tells us that perceptual experience—the seamless flow of conscious images of vision, sound, touch, and so forth—reflects the external world. Accordingly, information flow along the brain's sensory pathways has been thought to follow a caudo-rostral direction, away from the ports of entry, toward integrative cortices in the anterior parts of the frontal and temporal lobes. However, this view of a unidirectional, "bottom-up" processing cascade is challenged by findings which suggest that there is also information transfer in the opposite, "top-down" direction, from association areas toward early sensory cortices. A particularly intriguing observation is that while the initial bottom-up activation sweep along the sensory pathways can accomplish stimulus processing of considerable complexity and yield certain automated behaviors, conscious awareness of a sensory object appears to depend on top-down signals (*1*–*3*), as observed in the visual (*4*), auditory (*5*), and somatosensory (*6*) systems. Why is this the case?

Bidirectional signaling figures prominently in two influential theories of consciousness. According to the "dynamic core hypothesis," two fundamental characteristics of consciousness are differentiation and integration (*7*). The high differentiation of a conscious state is evident from the fact that we can imagine a practically unlimited number of such states without any two of them being identical. Integration, on the other hand, refers to the observation that a conscious state cannot be decomposed into independent constituents: We see a red rose, rather than a colorless shape paired with a shapeless color. Computer stimulations suggest that the amount of integrated information (and, therefore, consciousness) that a system can generate is greater when information flow among the system's elements is bidirectional than when it is strictly feed-forward. Although fronto-parietal association cortices, rather than the early sensory relays, are considered most crucial for information integration, the dynamic core hypothesis could, in principle, offer an explanation for the importance of top-down signals in conscious perception.

According to the "global neuronal workspace model," there are two distinct computational spaces in the brain (*8*). The first space consists of a collection of separate and anatomically confined processors, each of which is specialized in a particular function (e.g., visual motion processing). These functions are carried out nonconsciously. The second space consists of a network of global workspace neurons that distinguish themselves from the local processors by their reciprocal, long-range anatomical interconnections. Information encoded in the workspace therefore is available to many brain regions at once, including those responsible for motor behavior or verbal report. According to the model, this "global availability of information (…) *is* what we subjectively experience as a conscious state" (*9*). The model suggests the global workspace to comprise prefrontal, cingulate, and parietal cortices, in particular, but attributes high importance to top-down signals from these regions to the individual processors located in lower-level cortices. The top-down signals would act as "generators of diversity," dynamically selecting the brain networks that participate in a conscious state at any given moment.

A third, somewhat less prominent hypothesis that implicates top-down signals along the sensory pathways is the model of "multiregional retroactivation" (*10*). This model emphasizes that perception and memory recall are inseparable processes. Any sensory object we perceive automatically triggers the re-experience of associated images, in both the same and other modalities: Reading the word "mother" may evoke a visual image of your mother's face, an auditory image of her voice, etc. These associated images are stored in dispositional form in so-called convergence-divergence zones (CDZs) in the association cortices. To be consciously re-experienced, the images have to be reconverted to their explicit form by being reconstructed, via top-down signals, in the early sensory cortices. A loose analogy would be that of a movie which may be stored on a chip (the CDZs) but, to be watched, must be projected onto a screen (the early sensory cortices). Multiregional retroactivation offers a possible explanation for the importance of top-down signals for conscious perception if we assume that all the images we experience (and not just those manifestly triggered by association) are reconstructed based on records held in CDZs. The stream of consciousness would be nothing other than a "remembered present" (*11*).

Intriguingly, the idea that perceptual images are not a direct reflection of the environment has precedence. Consciousness has been described as "an intrinsic property arising from the expression of existing dispositions of the brain to be active in certain ways. It is a close kin to dreaming, where sensory input by constraining the intrinsic functional states specifies, rather than informs, the brain of those properties of external reality that are important for survival" (*12*). Along similar lines, it was suggested that "from a top-down perspective, feedback is provided by the bottom-up stream" (*6*). Taking this view of conscious perception, the images we experience would result from signals that descend through the sensory systems, just as behavior results from signals that descend along the motor pathways.

Brain and Creativity Institute, University of Southern California, Los Angeles, CA 90089, USA. E-mail: kaspar.meyer@usc.edu

CREDIT: Y. HAMMOND/*SCIENCE*

Downloaded from www.sciencemag.org on January 27, 2012

Published by AAAS

Neuroanatomical and neurophysiological findings from animal studies are generally compatible with this view. Connectivity along the sensory pathways is reciprocal at all levels and in all modalities, perhaps even dominated by top-down projections (*13*). Top-down signals can excite pyramidal neurons located as deep as layer V in their target area, although they contact mainly apical dendrites in the most superficial cortical layers (*6*). Top-down projections target almost exclusively pyramidal cells and induce an excitatory postsynaptic potential with little or no subsequent inhibition, whereas the fraction of terminals on inhibitory interneurons is considerably greater for bottom-up projections, and the excitation they induce is followed by an inhibitory hyperpolarization (*6*, *14*, *15*). Furthermore, neuroimaging studies show that nonstimulated regions of V1 contain information about stimuli presented elsewhere in the visual field, and that these activity patterns are induced via cortico-cortical top-down projections, rather than lateral projections within V1 (*16*, *17*). Along the same lines, purely visual stimuli that imply sound or touch induce content-specific neural patterns in the early auditory and somatosensory cortices, respectively, in the absence of any direct stimulation in those modalities (*18*, *19*). Taken together, such data suggest that top-down signals, contrary to their common designation as "feedback signals," have more than a modulatory function: They can reconstruct neural representations of considerable resolution in the early sensory cortices.

Why would the conscious mind be grounded in dispositional records held in CDZs, rather than the "raw" version of reality initially established in the early sensory cortices through bottom-up signals from the thalamus? One potential answer is tied to prediction: The brain "constantly and internally [generates] varieties of hypotheses and [tests] them upon the outside world, instead of having the environment impose (instruct) solutions directly upon the internal structure of the brain" (*20*).

References and Notes

1. D. A. Pollen, *Cereb. Cortex* **9**, 4 (1999).
2. V. A. F. Lamme, *Brain Mind* **1**, 385 (2000).
3. J. Bullier, *Trends Cogn. Sci.* **5**, 369 (2001).
4. T. Ro, B. Breitmeyer, P. Burton, N. S. Singhal, D. Lane, *Curr. Biol.* **13**, 1038 (2003).
5. M. Boly *et al.*, *Science* **332**, 858 (2011).
6. L. Cauller, *Behav. Brain Res.* **71**, 163 (1995).
7. G. Tononi, G. M. Edelman, *Science* **282**, 1846 (1998).
8. S. Dehaene, J.-P. Changeux, in *Cognitive Neurosciences*, M. S. Gazzaniga, Ed. (MIT Press, Cambridge, MA, ed. 3, 2004).
9. S. Dehaene, J.-P. Changeux, *Neuron* **70**, 200 (2011).
10. A. R. Damasio, *Cognition* **33**, 25 (1989).
11. G. Edelman, *Ann. N. Y. Acad. Sci.* **929**, 111 (2001).
12. R. R. Llinás, D. Paré, *Neurosci.* **44**, 521 (1991).
13. P.-A. Salin, J. Bullier, *Physiol. Rev.* **75**, 107 (1995).
14. R. R. Johnson, A. Burkhalter, *J. Comp. Neurol.* **368**, 383 (1996).
15. Z. Shao, A. Burkhalter, *J. Neurosci.* **16**, 7353 (1996).
16. M. A. Williams *et al.*, *Nat. Neurosci.* **11**, 1439 (2008).
17. F. W. Smith, L. Muckli, *Proc. Natl. Acad. Sci. U.S.A.* **107**, 20099 (2010).
18. K. Meyer *et al.*, *Nat. Neurosci.* **13**, 667 (2010).
19. K. Meyer, J. T. Kaplan, R. Essex, H. Damasio, A. Damasio, *Cereb. Cortex* **21**, 2113 (2011).
20. J.-P. Changeux, S. Dehaene, *Cognition* **33**, 63 (1989).
21. This work was supported by the Mathers Foundation and by the NIH (NIH/NINDS 5P50NS019632).

10.1126/science.1214652

STRUCTURAL BIOLOGY

The Inner Workings of a Dynamic Duo

Structures of two–pore domain potassium channels reveal key differences from the more widely found tetrameric channels.

Hanne Poulsen and Poul Nissen

More than 60 years ago, Hodgkin and Huxley showed that neurons maintain their negative resting membrane potential by leaking potassium ions (*1*). In most cells, the Na^+- and K^+-dependent adenosine triphosphatase (Na^+, K^+-ATPase) builds up high concentrations of extracellular sodium and intracellular potassium, and because the membrane is more permeable to potassium, there is a net flow of positive ions out of the cell. The channels responsible for the permeability were much later identified to be the two–pore domain potassium (K2P) channels (*2*). On pages 432 and 436 of this issue, Miller and Long (*3*) and Brohawn *et al*. (*4*) report the structures of the human K2P channels TWIK-1 and TRAAK.

Most potassium channels are tetrameric, but K2Ps are dimers with four transmembrane helices and two pore domains per subunit (see the figure, panel A). The new structures may suggest a structural basis for how K2Ps, in addition to their role as "leak channels," can be regulated by a wide variety of stimuli including pH, membrane stretch, and anesthetics (*5*).

The first ion channel visualized at high resolution was the tetrameric bacterial homolog of mammalian potassium channels, KcsA. The KcsA structure revealed how exquisite ion selectivity is achieved by a membrane-embedded filter formed by four symmetrically arranged hairpins, with backbone oxygens lining a channel. Because the potassium ions are optimally coordinated by the backbone oxygens, they can become dehydrated as they pass (*6*).

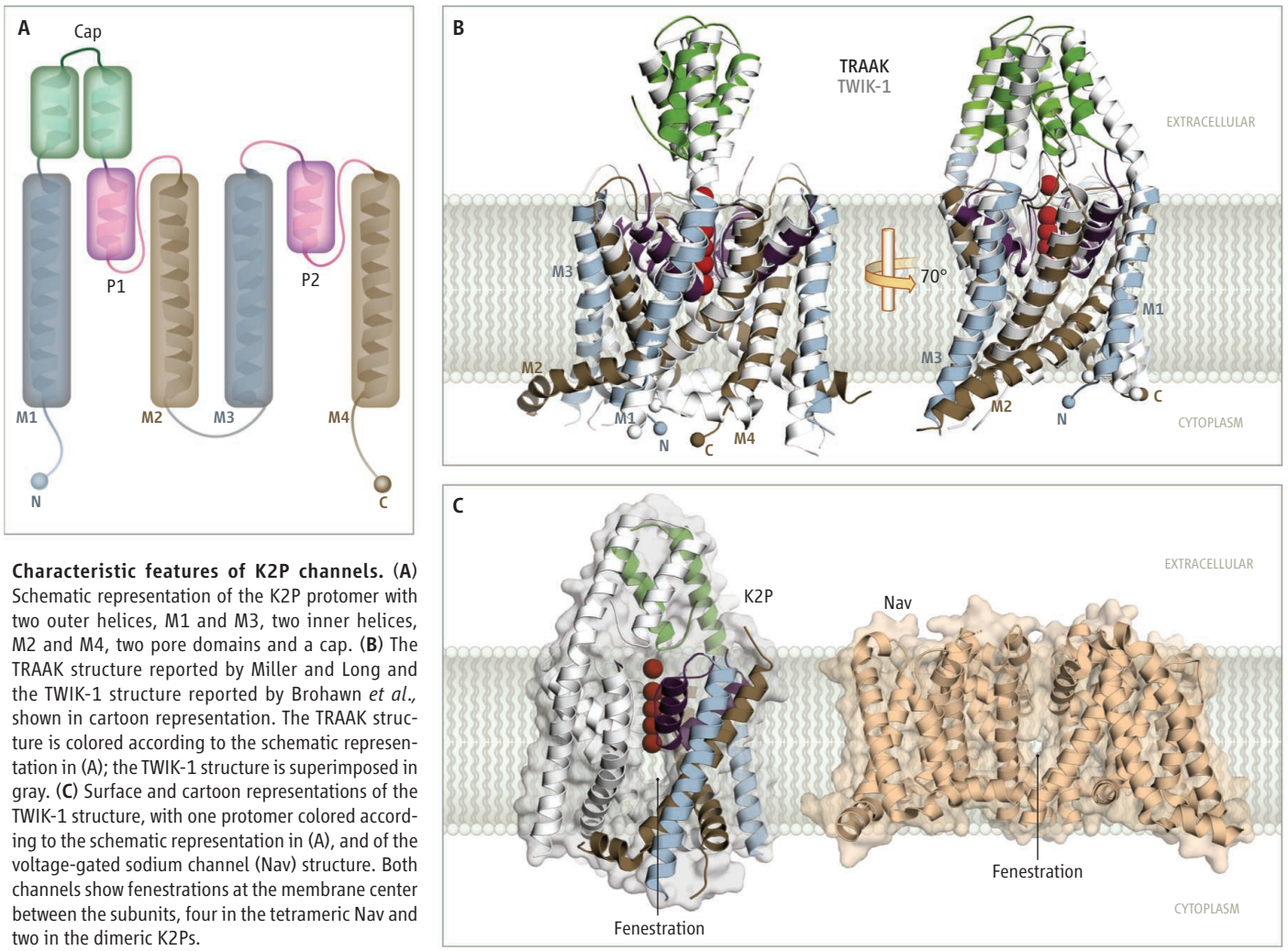
A highly conserved feature of tetrameric potassium channels is the selectivity filter sequence Thr-X-Gly-Tyr-Gly-Asp (where X denotes a hydrophobic residue). In K2P channels, only threonine and the first glycine are strictly conserved, but the new structures (*3*, *4*) show that the K2P selectivity filter approaches four-fold symmetry, and K^+ is coordinated in the same way as in the tetrameric potassium channels. The sequence variation of the two filters in each subunit offers a way to tweak the K2P pore. For example, TWIK-1 becomes Na^+-permeable at low extracellular K^+ levels, a characteristic that depends on a threonine residue after the conserved threonine residue in the first pore domain (*7*). Two recent studies have suggested that opening and closing of K2Ps depend mainly or solely on the pore and its vicinity (*8*, *9*). The diversity in the filter motifs may thus reflect variations in gating.

Both of the new structures show a potassium-conducting channel with the intracellular gate open, but the two inner helices forming the gate from each K2P subunit differ markedly from those of the tetrameric channels (see the figure, panel B): The M2 helix is longer and bends in the middle of the membrane; M4 is shorter and more perpendicular to the membrane plane. The C-terminal part of either M2 (in TRAAK) or M4 (in TWIK-1) localizes to the cytosolic membrane interface.

Centre for Membrane Pumps in Cells and Disease–Pumpkin, Danish National Research Foundation, and Department of Molecular Biology and Genetics, Aarhus University, Gustav Wieds Vej 10C, DK-8000 Aarhus C, Denmark. E-mail: hp@mb.au.dk, pn@mb.au.dk

Downloaded from www.sciencemag.org on January 27, 2012

Published by AAAS



Characteristic features of K2P channels. (**A**) Schematic representation of the K2P protomer with two outer helices, M1 and M3, two inner helices, M2 and M4, two pore domains and a cap. (**B**) The TRAAK structure reported by Miller and Long and the TWIK-1 structure reported by Brohawn *et al.*, shown in cartoon representation. The TRAAK structure is colored according to the schematic representation in (A); the TWIK-1 structure is superimposed in gray. (**C**) Surface and cartoon representations of the TWIK-1 structure, with one protomer colored according to the schematic representation in (A), and of the voltage-gated sodium channel (Nav) structure. Both channels show fenestrations at the membrane center between the subunits, four in the tetrameric Nav and two in the dimeric K2Ps.

This peculiar symmetry suggests that K2P channels may be regulated by coordinated association and dissociation of the inner helices with the membrane.

A notable difference between the TWIK-1 and TRAAK structures is at the helical cap, a characteristic feature of K2P channels on the extracellular side above the pore exit. The cap comes after M1, which is either a very long continuous helix or, in one of the TRAAK subunits, two helices connected by a short loop. Crystal packing may have caused the M1 asymmetry in the TRAAK structure, but the differences (see the figure, panel B) indicate that the connection of the cap to the rest of the channel is flexible.

Both K2P structures have marked fenestrations in the membrane plane (see the figure, panel C), a feature described extensively in the voltage-gated sodium channel (*10*). Hydrophobic compounds such as arachidonic acid and anesthetics can modulate members of both channel families, but it has been unclear how. The new structures suggest a simple explanation: that the compounds enter via the lipid membrane. The regulation of some K2P channels by stretch and lipids could also depend on the fenestrations.

The C-terminal segment is important for K2P responses to modulators such as intracellular pH, membrane stretch, and phosphorylation (*9*). The segment is highly variable among K2P channels, and most of it was deleted from the crystallized proteins. Brohawn *et al*. show that their channel does respond to stretch and arachidonic acid, suggesting that the truncated protein is fully functional as a channel. The C termini of both constructs are disordered in the crystals, but the structures suggest that the C-terminal segment of an intact K2P channel is close to the cytosolic entrance and may thus affect gating.

Many questions regarding regulation of the K2Ps await structural answers to how the C-terminal conformation is affected by the various stimuli. This information may also shed further light on whether the M2 and M4 helices change conformations in synchrony, whether they can form a closed gate, or whether changes at the C terminus are translated to the pore region. Nonetheless, with their two new K2P structures, Miller and Long and Brohawn *et al*. have brought us much closer to an understanding of why potassium channels do not have to depend on four identical subunits, but can be assembled in a dynamic duo to offer new possibilities for highly variable regulation.

References and Notes

1. A. L. Hodgkin, A. F. Huxley, *J. Physiol.* **106**, 341 (1947).
2. F. Lesage *et al*., *EMBO J.* **15**, 1004 (1996).
3. A. N. Miller, S. B. Long, *Science* **335**, 432 (2012).
4. S. G. Brohawn, J. del Mármol, R. MacKinnon, *Science* **335**, 436 (2012).
5. N. P. Franks, E. Honoré, *Trends Pharmacol. Sci.* **25**, 601 (2004).
6. D. A. Doyle *et al*., *Science* **280**, 69 (1998).
7. L. Ma, X. Zhang, H. Chen, *Sci. Signal.* **4**, ra37 (2011).
8. P. L. Piechotta *et al*., *EMBO J.* **30**, 3607 (2011).
9. S. N. Bagriantsev, R. Peyronnet, K. A. Clark, E. Honoré, D. L. Minor Jr., *EMBO J.* **30**, 3594 (2011).
10. J. Payandeh, T. Scheuer, N. Zheng, W. A. Catterall, *Nature* **475**, 353 (2011).
11. We thank R. Schmidt Kjærgaard for help with the figures.

10.1126/science.1217679

Downloaded from www.sciencemag.org on January 27, 2012

Published by AAAS

IBI* SERIES WINNER

An Inquiry-Based Curriculum for Nonmajors

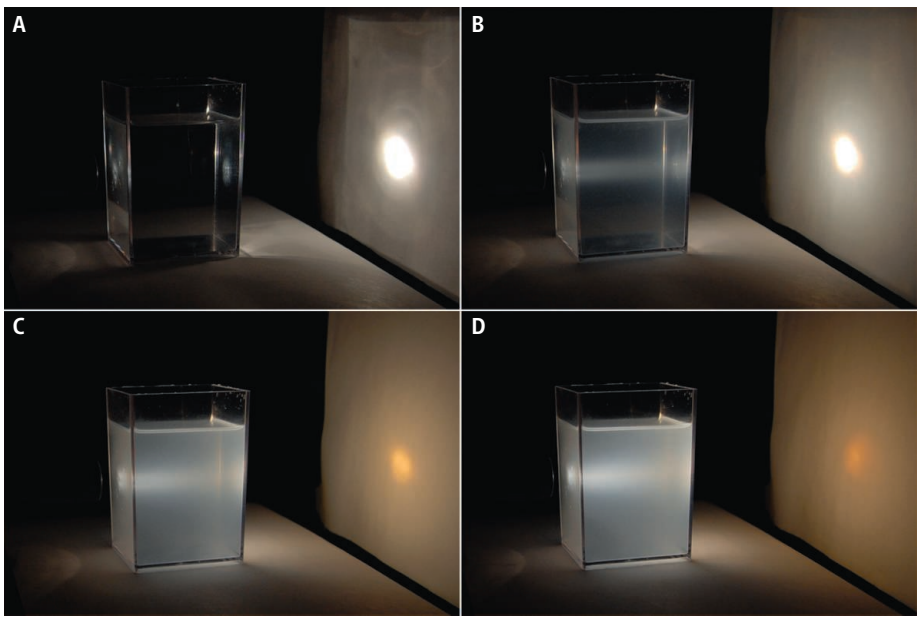
Light, Sight, and Rainbows, the IBI prize-winning module, provides questions for exploring simple atmospheric phenomena.

David P. Jackson,[1†] Priscilla W. Laws,[1] Scott V. Franklin[2]

Only 28% of the U.S. adult population is considered scientifically literate. Although this is the second highest among 35 developed countries, a fact attributed to postsecondary science requirements (*1*), it should not be considered satisfactory, and improvement is critical to our future. A trend of many U.S. colleges and universities is to offer courses for nonmajors that cover a wide range of material via lectures, with few opportunities for students to engage in hands-on learning. This is particularly disturbing given that "a growing body of science educators has found that students' attitudes toward science, their motivation for learning, and their conceptual development … can all be enhanced by engagement in real scientific investigations" (*2*).

Explorations in Physics (EiP) is an inquiry-based curriculum designed to increase the scientific literacy of those who are not science majors and to impart a fundamental understanding of the nature of scientific investigation (*3*). The curriculum consists of a series of stand-alone units that use guided-inquiry instruction and culminate with student-directed projects (see the table). Each unit has undergone extensive testing and revision at Dickinson College, Santa Clara University, and Rochester Institute of Technology. More information is available on the EiP Web site, http://physics.dickinson.edu/EiP (*4*).

A defining feature of EiP is the emphasis on student-directed projects. After working through the "core material" on one or two topics, students embark on projects of their own design. Each group of three or four students is required to submit a proposal, design and conduct experiments, take and analyze data, draw conclusions, present their results in class, and submit a final written report. This requires a significant investment in student and instructor time. Hence, during the project phase, 100% of in-class time is spent working on these projects. Just as actual scientists do, students come face to face with ambiguity and the task of formulating concrete understanding in the face of measurement errors and other uncertainties. The repeatability of their measurements and whether or not these results can be convincingly extrapolated are what give students a true sense of how science progresses. It is precisely this type of understanding that we believe is necessary for citizens to be able to make informed judgments on the scientific issues they will face in the future.



Light through a simulated atmosphere. A flashlight beam through a container of water with varying amounts of milk. (**A**) No milk, (**B**) two drops, (**C**) six drops, and (**D**) eight drops.

Explorations in Physics Units

Published units

A. Force, Motion, and Scientific Theories
B. Light, Sight, and Rainbows
C. Heat, Temperature, and Cloud Formation
D. Buoyancy, Pressure, and Flight

Unpublished units available on the EiP Web site

E. Atoms, Crystals, and Snowflakes
F. Sound, Vibrations, and Music
G. Population, Climate, and Mathematical Modeling
H. Magnets, Charge, and Electric Motors

One of our favorite units is Light, Sight, and Rainbows (*5*). As is typical of all our units, this unit is designed to help students address phenomena that physics education researchers have determined to be difficult to understand. Our own research and that of others, most prominently the Physics Education Group at the University of Washington (*6*), has revealed that students have tremendous difficulty with the concept of sight and the necessity of light impinging on the eye in order to see. Our unit begins with the simple question, "Can you see in the dark?" This never fails to produce a rich discussion of what it means to see and the difference between self-luminescent and reflecting objects. Some students assert that sight will return once their eyes become dark-adapted. Others accept that they cannot see in the dark, but attribute to light a passive catalyst role to illuminate the object and allow our "sight" to become active. True to the experimental nature of the curriculum, once students have considered and discussed

[1]Department of Physics and Astronomy, Dickinson College, Carlisle, PA 17013, USA. [2]Rochester Institute of Technology, Rochester, NY 14623, USA.

*IBI, *Science* Prize for Inquiry-Based Instruction; www.sciencemag.org/site/feature/data/prizes/inquiry/. †Author for correspondence. E-mail: jacksond@dickinson.edu

CREDIT: DAVID P. JACKSON

Downloaded from www.sciencemag.org on January 27, 2012

Published by AAAS

this question with each other, we plunge them into a "completely" darkened room (*7*). As students continue to argue, comment, and adapt to the dark, they gradually begin to distinguish fire-alarm LEDs and slivers of light around the edges of covered windows, but they still can't see an object sitting in the middle of the room. It finally dawns on them—in the absence of light, there is no sight!

Thus begins a journey in which students investigate how light travels, bounces, and bends and how images are formed with pinholes, lenses, and the human eye. The unit concludes with a study of color and dispersion that enables students to understand blue skies, orange sunsets, and the details of rainbow formation.

Topics in Light, Sight, and Rainbows often reappear with increasing complexity. For example, early in the unit, students shine a flashlight through clear water and note that although they cannot see the beam of light in the water, they do see a bright spot on a viewing screen placed beyond the tank. Adding a few drops of milk or a small amount of powdered creamer to the water makes the beam visible, but at the expense of the spot's brightness (and color, as the spot turns orange). Later in the unit, we return to this experiment to measure the relative amount of red and blue light transmitted through the water. Applying the concepts of reflection, scattering, and spectral composition, students use the results of this experiment to explain why the sky is blue and sunsets are orange (see the first figure). Subsequent student projects involving light include investigations of polarizing sunglasses, lenses, colored light on colored objects, and the "temperature" of color.

Student projects often combine themes from two units. For example, after completing guided inquiry on the light and heat units, one group of students constructed low-cost solar ovens out of Styrofoam packing crates (see the second figure). One was lined with flat black construction paper and another with reflective craft paper. The question was whether or not thermal absorption would be more effective than reflectivity. The students used mirrors to direct sunlight into the ovens and monitored interior and exterior temperatures with computer-interfaced sensors while baking cookies. To their surprise, the cookies really did bake! Their measurements revealed that the chamber with the black interior maintained a higher internal temperature, resulting in a shorter baking time for the cookies. The beauty of such an experiment is not so much the final result. It is that students gain a thorough and concrete understanding of a scientific topic by designing and carrying out an independent investigation.



Solar ovens constructed by students. The black one reaches a higher temperature. Both were capable of baking cookies.

CREDITS: (LEFT) HANS PFISTER; (RIGHT, TOP AND MIDDLE) VIRGINIA L. JACKSON; (RIGHT, BOTTOM) SUE WEISLER/RIT

Since the development of EiP began, many activities from our units have been described in publications (*8*–*12*). One important lesson we learned early in our development is that students need sufficient time to realize the benefits of the inquiry-based activities. It is all too easy to rush through activities and not give students the time necessary to make careful observations and to interpret their results. This is particularly important if students are expected to conduct meaningful self-directed projects. A typical unit requires between 18 and 24 hours of class time, with a similar amount of in-class time spent on projects.

Explorations in Physics has fulfilled our goal of increasing the scientific literacy of those who are not science majors in a way that encourages self-directed exploration. We hope the future brings this opportunity to students everywhere, helping them use investigative skills in their future endeavors and serve as scientifically literate citizens who contribute to the creation of a better world.

About the authors



David P. Jackson is Associate Professor of Physics at Dickinson College where he studies pattern formation in magnetic fluids and develops inquiry-based activities for physics majors and nonmajors. He has co-organized two Gordon Research Conferences on Physics Research and Education and is currently editor of the *American Journal of Physics*.

Priscilla Laws is research professor of Physics at Dickinson College where she has been developing activity-based curricular materials informed by the outcomes of Physics Education Research for introductory physics students. She has authored the *Workshop Physics Activity Guide* series and coauthored the *RealTime Physics Active Learning Laboratory Modules*, and *Physics with Video Analysis*.





Scott Franklin is professor of Physics at Rochester Institute of Technology where he conducts research in soft matter or granular materials and physics education. He was cofounding editor of the *Physics Education Research Conference Proceedings* and is currently secretary-treasurer of the American Physical Society Forum on Education and a founding member of Rochester Institute of Technology's Science and Mathematics Education Research Collaborative.

References and Notes

1. J. Miller, paper presented at the annual meeting of the American Association for the Advancement of Science, San Francisco, CA, 16 February 2007.
2. R. L. DeHaan, *J. Sci. Educ. Technol.* **14**, 253 (2005).
3. Explorations in Physics was developed with funding from the Charles A. Dana Foundation, the National Science Foundation (NSF), and the U.S. Department of Education's Fund for the Improvement of Post-Secondary Education (FIPSE).
4. D. P. Jackson, P. W. Laws, S. V. Franklin, *Explorations in Physics: An Activity-Based Approach to Understanding the World* (Wiley, New York, 2003).
5. This unit is available as supporting online material on *Science* Online.
6. For more information on the Physics Education Group at the University of Washington, visit their Web site www.phys.washington.edu/groups/peg/.
7. It is extremely difficult to completely darken a room. Fortunately, although the room needs to be quite dark, the room does not need to be 100% light tight for this demonstration to have an impact on students.
8. D. P. Jackson, P. W. Laws, in *The Changing Role of Physics Departments in Modern Universities* (American Institute of Physics, Woodbury, NY, 1997), pp. 623–630.
9. R. A. Morrow, A. Grant, D. P. Jackson, *Phys. Teach.* **37**, 412 (1999).
10. D. P. Jackson, P. W. Laws, *Am. J. Phys.* **74**, 94 (2006).
11. K. P. Browne, P. W. Laws, *Phys. Educ.* **38**, 115 (2003).
12. K. P. Browne, D. P. Jackson, *Phys. Teach.* **45**, 425 (2007).
13. The authors thank K. Browne (Rivendell Academy, Orford, NH) and H. Pfister (Dickinson College) for valuable contributions to the EiP Project.

Supporting Online Material
www.sciencemag.org/cgi/content/full/335/6067/418/DC1

10.1126/science.1213444

Downloaded from www.sciencemag.org on January 27, 2012

Published by AAAS

AAAS 2012 PRESIDENT

William H. Press: Seeking the Possible in Difficult Times

Support for science might be expected to suffer in a year of election-driven partisanship and a tough fiscal environment. But as he prepares to assume the presidency of AAAS, William Press sees some positive aspects: bipartisan agreement on key U.S. science policy goals, a renewed national focus on science education, a strong set of international collaborations, and new chances to share the beauty and benefits of science with the public.



William H. Press

While news reports and campaigns stress conflict, members of both parties recognize that investments in innovation and education are vital to American success and generally agree on the need for federal research funding, said Press, a professor of computer science and integrative biology at the University of Texas at Austin.

"The political debate now is not about whether basic, fundamental research is worth supporting," he said in a recent interview. "It's about doing enough of it, and, wherever possible, coupling it to the economy." When partisan arguments arise, Press said, they will reflect political and philosophical differences about government's role in transforming basic research into applications.

And that, he said, suggests an important role for U.S. AAAS members and other scientists and engineers: They can join the effort to resolve complex policy problems—from a comprehensive energy plan to a modernized health care system—by visiting congressional offices in their home districts. Although individual scientists may have partisan leanings, "science is intrinsically nonpartisan," he said. "We can educate our members of Congress and their staffs on what we believe are the facts, and how certain we are about them."

As a member of the President's Council of Advisors on Science and Technology (PCAST) for the past 2 years, Press has played an active role in bringing science to bear on national policies. A noted researcher whose work has spanned a remarkable range of disciplines—from computer science to genomics, statistical methods, astrophysics, and international security—he also served as deputy laboratory director for science and technology at the Los Alamos National Laboratory from 1998 to 2004.

Press will succeed Nina V. Fedoroff as president when the AAAS Annual Meeting closes on 20 February. Fedoroff will begin a 1-year term as chairperson of the AAAS Board.

As an astrophysicist at Harvard University from 1976 to 1998, Press was best known for his collaboration on the Press-Schechter formalism, which predicts the masses of galaxies within the universe, as well as his work on supernovae to estimate cosmic distances, which helped clear a path to the discovery that the expansion of the universe is accelerating. The power of computational science is the constant in his career, from his *Numerical Recipes* books on scientific computing and more recent projects in molecular biology and clinical trials.

"I had such fun, and was productive riding this wave in the physical sciences," he said, "that I just could never forgive myself if I didn't take the opportunity to stay on this same wave and do computational biology."

Press's eclectic interests make him an excellent ambassador for a message that he wants the public to understand: Science doesn't proceed in a neat or linear fashion. Who could have predicted, he asked, that a probability distribution algorithm worked out by Google's founders would become the backbone of a cultural and economic giant? "When we have a national and global scientific enterprise that is out there building terrain...that can become fertile ground on which all kinds of applications can grow."

AAAS has been instrumental in building this terrain through international science initiatives, and Press said that continued support for these programs is a critical counterbalance against the notion that global collaborations are a "luxury rather than an economic necessity."

U.S. graduate school programs still attract researchers from around the world, he noted, but PCAST, AAAS, and others are now offering ideas about improving undergraduate science education. "We need to admit that we're not doing a good job in those first 2 years" of undergraduate study, he said. "People aren't going to be attracted to science by a freshman course in which they're just going to be sitting in a large lecture hall. But they are attracted when we can get them out into research laboratories and they see what research really is."

Press cited several polls showing that the American public remains committed to science and sees scientists as trustworthy and prestigious citizens. With this in mind, he thinks voters will be very interested to hear what the 2012 presidential candidates have to say about their own plans for science.

"There's a broad segment of the American public that's interested in science and innovation, both the beauty and benefits of it," he said. "One of our goals should be to find ways to allow those things to move forward, and not have them brought down by things we can't agree on." —*Becky Ham*

AAAS

Call for Nomination of 2012 Fellows

AAAS Fellows who are current members of the association are invited to nominate members for election as Fellows. A Fellow is defined as a member "whose efforts on behalf of the advancement of science or its applications are scientifically or socially distinguished." A nomination must be sponsored by three AAAS Fellows (who are current in their membership), two of whom must have no affiliation with the nominee's institution.

Nominations undergo review by the steering groups of the association's sections

CREDIT: SARA PRESS

Downloaded from www.sciencemag.org on January 27, 2012

Published by AAAS

(the chair, chair-elect, retiring chair, secretary, and four members-at-large of each section). Each steering group reviews only those nominations designated for its section. Names of Fellow nominees who are approved by the steering groups are presented to the AAAS Council for election.

Nominations with complete documentation must be received by 11 April 2012. Nominations received after that date or nominations that are incomplete as of the deadline will not move forward, but may upon request be held for the following year. Complete instructions and a copy of the nomination form are available at www.aaas.org/aboutaaas/fellows/instructions.shtml. To request a hard copy of the nomination form, please contact the AAAS Executive Office, 1200 New York Avenue, NW, Washington, DC, 20005, USA; at 202-326-6468; or at kobrien@aaas.org.



Pacific Rim S&T. The AAAS Annual Meeting will convene for the first time in Vancouver, British Columbia.

ANNUAL MEETING

Solving Challenges by "Flattening the World"

It is a question that frames the 21st-century scientific enterprise: As the world population moves toward 9 billion, will it be possible to provide food, water, and energy for everyone without dangerously depleting natural resources and damaging the environment? These challenges will be the focus of the 178th AAAS Annual Meeting, which convenes from 16 to 20 February in Vancouver, British Columbia.

The meeting will feature top scientists, engineers, educators, policy-makers, and science journalists from some 50 nations and a full spectrum of disciplines. More than 170 plenary addresses, lectures, seminars, and symposia are scheduled under the theme "Flattening the World: Building the Global Knowledge Society."

"The theme…is intended to focus the program on the complex, interconnected challenges of the 21st century and on pathways to global solutions through international, multidisciplinary efforts," said AAAS President Nina V. Fedoroff in her letter of invitation.

The program will be rich and ambitious: Among the daily plenary events will be a panel of influential journalists and scientists—including NASA climate expert James Hansen—discussing the challenges of communicating climate change, and an address by Ismail Serageldin, the eminent director of the Library of Alexandria, Egypt, on "Science and Democracy."

Some of the world's leading experts will offer topical lectures on water security, the science of science education, international science collaboration, molecular motors, and other issues. Sessions in the seminar "Unlocking Biology's Potential" will look at predictive medicine and delivering on the promise of the Human Genome Project.

2012 marks the first AAAS Annual Meeting in Vancouver—there have been seven other meetings in Canada, starting with Montreal in 1857—and this one will have a strong focus on Canada, the Arctic, and the northeastern Pacific Ocean. A full-day seminar will focus on climate change in the northern latitudes. And among many Canadian speakers at the meeting will be Mike Lazaridis, president and co-CEO of Research In Motion and founder/chairman of Perimeter Institute for Theoretical Physics, whose plenary address will explore "The Power of Ideas."

For registration and program information, see www.aaas.org/meetings. The site http://news.aaas.org will serve as a portal for Annual Meeting news from *Science*Now, Science Update, www.aaas.org, AAAS MemberCentral, and EurekAlert! The AAAS Facebook page and Twitter (#AAASmtg) also will feature news from Vancouver.

COMMUNICATION

AAAS, Kavli Name Science Journalism Award Winners

Stories on the potential impact of climate change in two localities and on the secret lives of scientists and engineers are among the winners of the 2011 AAAS Kavli Science Journalism Awards.

Large Newspaper—(Circulation ≥100,000): Mark Johnson and Kathleen Gallagher, Milwaukee *Journal Sentinel,* for "One in a Billion: A Boy's Life, A Medical Mystery" (series), 19, 22, 26 December 2010.

Small Newspaper—(Circulation <100,000): Christine Peterson, Kerry Huller, Wes Watson, *Casper Star-Tribune* (Wyoming), for "On Thinning Ice: A Look at Wind River Range's Shrinking Glaciers" (series), 23 to 25 January 2011.

Magazine: Adam Rogers, *Wired,* for "The Angels' Share," June 2011.

Television—(Spot News/Feature Reporting, ≤20 minutes): Rachel Silverman, Craig Miller, Lindsay Kelliher, Linda Peckham, Amy Miller, Paul Rogers, KQED QUEST/Climate Watch (San Francisco), for "Going Up: Sea Level Rise in San Francisco Bay," 31 August 2010.

Television—(In-Depth Reporting, >20 minutes): Two winning entries:
Richard Burke-Ward, Robert Strange, Callum Macrae, Stuart Carter, Howard Swartz, WGBH/NOVA, for "Japan's Killer Quake," 30 March 2011.

Mark J. Davis, National Geographic Channel, for "Death of a Mars Rover," 2 June 2011.

Radio: Gabriel Spitzer, with Michael De Bonis, WBEZ Chicago, for "Clever Apes" (series), 26 July and 24 November 2010; 24 May 2011.

Online: Joshua Seftel, Tom Miller, Susan K. Lewis, Lauren Aguirre, PBS NOVA Online, for "The Secret Life of Scientists and Engineers" (series), 6 October 2010; 2 and 16 February 2011.

Children's Science News: Jeanne Miller, *ODYSSEY* Magazine, for "Skywalking for Science: Aloft in Redwood Space," April 2011.

The awards, administered by AAAS since their inception in 1945, go to professional journalists for distinguished reporting for a general audience. The Kavli Foundation, based in Oxnard, California, provided a generous endowment in 2009 that ensures the future of the awards program.

Independent panels of science journalists pick the winners, who will receive $3000 and a plaque at the 2012 AAAS Annual Meeting in Vancouver, British Columbia, in February.

—*Earl Lane*

CREDIT: THOM QUINE/WWW.COMMONS.WIKIMEDIA.ORG

Downloaded from www.sciencemag.org on January 27, 2012

Published by AAAS

The Centrosome in Cells and Organisms

Michel Bornens

The centrosome acts as the main microtubule-nucleating organelle in animal cells and plays a critical role in mitotic spindle orientation and in genome stability. Yet, despite its central role in cell biology, the centrosome is not present in all multicellular organisms or in all cells of a given organism. The main outcome of centrosome reproduction is the transmission of polarity to daughter cells and, in most animal species, the sperm-donated centrosome defines embryo polarity. Here I will discuss the role of the centrosome in cell polarity, resulting from its ability to position the nucleus at the cell center, and discuss how centrosome innovation might have been critical during metazoan evolution.

The centrosome of animal cells is a cytoplasmic organelle formed around a core structure made of two microtubule-based cylinders of defined length and diameter, the centrioles, with a highly conserved ninefold radial symmetry (*1*). The centriole pair displays structural and functional asymmetry due to the generational difference between each member of the pair: The old, fully mature, mother centriole is distinguished by two sets of nine appendages at its distal end while the young, immature, daughter centriole, assembled during the previous cell cycle, is about 80% the length of the mother centriole (Fig. 1). Both centrioles nucleate microtubules in their vicinity, but only the mother centriole can anchor microtubules at the subdistal appendages (*2*). In resting cells, the mother centriole can turn into a so-called basal body, by docking to the plasma membrane through the distal appendages (Fig. 1), where it templates a nonmotile primary cilium that serves as a sensory organelle (*3*). The basal body from the sperm flagellum triggers the assembly of the zygote centrosome during fertilization.

The centriole/basal body associated with a (9+2) flagellum is present in the common unicellular ancestor of eukaryotic cells (*3*, *4*). It participates in three major cell functions: locomotion, sensory reception, and division. The innovation of the centrosome as a cytoplasmic organelle, no longer permanently associated with an axoneme, has taken place essentially in the unikont lineage. Centrosome evolution among divergent eukaryotes must reflect cellular variations in locomotion, sensory reception, or division underlying the adaptive evolution of organisms.

The Centrosome, Yesterday and Today

The centrosome, described as a "polar corpuscle," was suspected from the start to have a role in cell symmetry breaking and the maintenance of cell polarity. Early experiments exploiting centrosome activity paved the way to the chromosomal theory of heredity. The fertilization of sea urchin eggs with two sperm cells results in the formation of a quadripolar mitotic spindle and the division of the egg into four blastomeres with an uneven segregation of chromosomes. When dissociated from each other at the four-cell stage, normal blastomeres form a dwarf embryo. Analyzing the development of blastomeres obtained after dispermy, Boveri could conclude that both the individuality of each chromosome and their continuity in the interphasic nucleus were important. The centrosome was seen as the organ coordinating karyokinesis and cytokinesis. The absence of centrosome in the unfertilized egg was seen as an efficient way to avoid parthenogenetic development. This contention was experimentally supported much later (*5*).

In the last decade, the molecular composition of the isolated centrosome in the human and fly has revealed a number of proteins conserved across eukaryotes (*3*, *4*). Functional genomics in nematodes and flies has identified a small set of conserved proteins required for the initiation of centriole/basal body assembly and for centrosome reproduction. Recently, the structural basis of the highly conserved ninefold radial symmetry of the centriole/basal body has been elucidated (*6*, *7*). Unexpectedly, it rests on the oligomerization of a single coiled-coil protein, SAS-6/Bld12p, which forms a cartwheel structure acting as a scaffold for centriole/basal body assembly.

The structural complexity of the centrosome is reflected in its biochemical composition: More than 100 proteins are localized either in the centrioles or in the centrosomal matrix (*8*, *9*), among which several are disease gene products. For example, all genes involved in microcephaly syndromes so far encode centrosomal proteins (*10*).

The Centriole/Basal Body Defines Embryo Polarity at Fertilization

Besides restoring diploidy, egg fertilization in animals involves the resetting of egg polarity through the conversion of the sperm head–associated basal body into the male pronucleus-associated centrosome.

Egg symmetry breaking. The polarization of the zygote by the sperm-donated centrosome has been studied in great detail in the nematode *Caenorhabditis elegans*. The sperm centrosome triggers the cortical flow that establishes the anterior and posterior cortical polarity domains through two redundant mechanisms (*11*). One acts on the contractility of the cortex itself, via local inactivation of the small GTP-binding protein Rho. The other acts by localizing the polarity-associated protein PAR-2 to the cortex and antagonizing PAR-3–dependent recruitment of myosin. These findings exemplify the centrosome's ability to trigger global spatial control by concentrating effectors locally.

Centrosome positioning at the egg's center. In large eggs, the centrosome centers itself independently of aster-cortex contact (*12*), and the spindle assembles between a pair of centrosomes prepositioned by the preceding interphase aster centers (*13*). The microtubule-dependent orientation of nuclear stretching and division axis in sea urchin eggs forced into microfabricated chambers of defined geometry has been quantitatively modelized (*14*). Pulling forces appear to be nearly proportional to the cubic length of microtubules. This result suggests a "volume sensing" model in which the probability for a motor encountering a microtubule of a given length is proportional to a cone-shaped volume around the microtubule. The demonstration in *C. elegans* egg of a dynein-dependent cytoplasmic pulling anchored on moving organelles could provide a physical basis to this model (*15*). Alternatively, cytoplasmic actin could exert pulling forces on astral microtubules, as shown in cultured mitotic cells (*16*).

Blastomere individuation. Unfertilized *Xenopus* egg cleavage can be triggered by the injection of a somatic centrosome, whether from the same or from divergent vertebrate species, whereas activation of the egg by pricking triggers cell cycle resumption but does not lead to cleavage despite an equivalent complement of microtubules in the egg (Fig. 2) (*17*). Centrosome-dependent astral organization of the microtubule array is thus necessary for egg cleavage. It is also sufficient in eggs where growth requirements have been met during oogenesis: Enucleation experiments on starfish eggs after fertilization lead to individuation of the control number of enucleated blastomeres due to the sequential duplication of the sperm centrosome (Fig. 2) (*18*). This result supports the contention that the coevolution of the centrosome able to nucleate a microtubule aster, and of a cortical acto-myosin network, has been critical for the selection of cell division by fission (*19*).

Centrosome generational asymmetry and embryo development. Centrosome reproduction overlaps two cell-division cycles and gives rise to a generational asymmetry so that a centrosome always consists of a mother and a daughter centriole (Fig. 1). These features are exploited to segregate mRNAs or transcription factors localizing to the centrosomal matrix in a microtubule- and cell cycle–dependent manner. For example, in spiralian mollusc embryos, mRNAs of patterning genes are centrosomally located, which leads to the production of cells that differ in size, cleavage pattern, and fate (*20*). In the *C. elegans* embryo, PIE-1 protein localizes to the germline blastomeres throughout early development and maintains

Institut Curie, UMR144 du Centre Nationale de la Recherche Scientifique, 26 rue d'Ulm, 75248 Paris Cedex 05, France. E-mail: mbornens@curie.fr

Downloaded from www.sciencemag.org on January 27, 2012

their totipotency by repressing the somatic state. PIE-1 initially associates with both centrosomes of the mitotic spindle (*21*), then rapidly disappears from the centrosome destined for the somatic daughter after spindle rotation, and persists in the centrosome of the daughter that becomes the next germline blastomere. A similar centrosome-based asymmetric degradation has been documented in dividing human embryonic stem cells in which the duration of signaling by the Smad1 transcription factor is terminated by proteasomal degradation (*22*). Centrosome-based asymmetric division is widely used in maintaining polarized tissue morphogenesis (*23*) and has been particularly well documented in the developing neocortex (*24*).

The Centriole/Basal Body in Somatic Cell Polarity

The three functional facets of cell polarity associated to the ancestral basal body/axoneme—namely, sensation, motion, and division—were preserved during metazoan multicellularity through the innovation of the centrosome organelle (*19*). The centrosome controls the maintenance of cell polarity during migration, tissue growth, and homeostasis. In many tissues, the primary cilium is a sensory organelle channeling signal transduction in several major pathways (*8*). A great range of stimuli seem to be collected in this way, and the primary cilium is thus critical for embryo development. Dysfunction of the primary cilium is

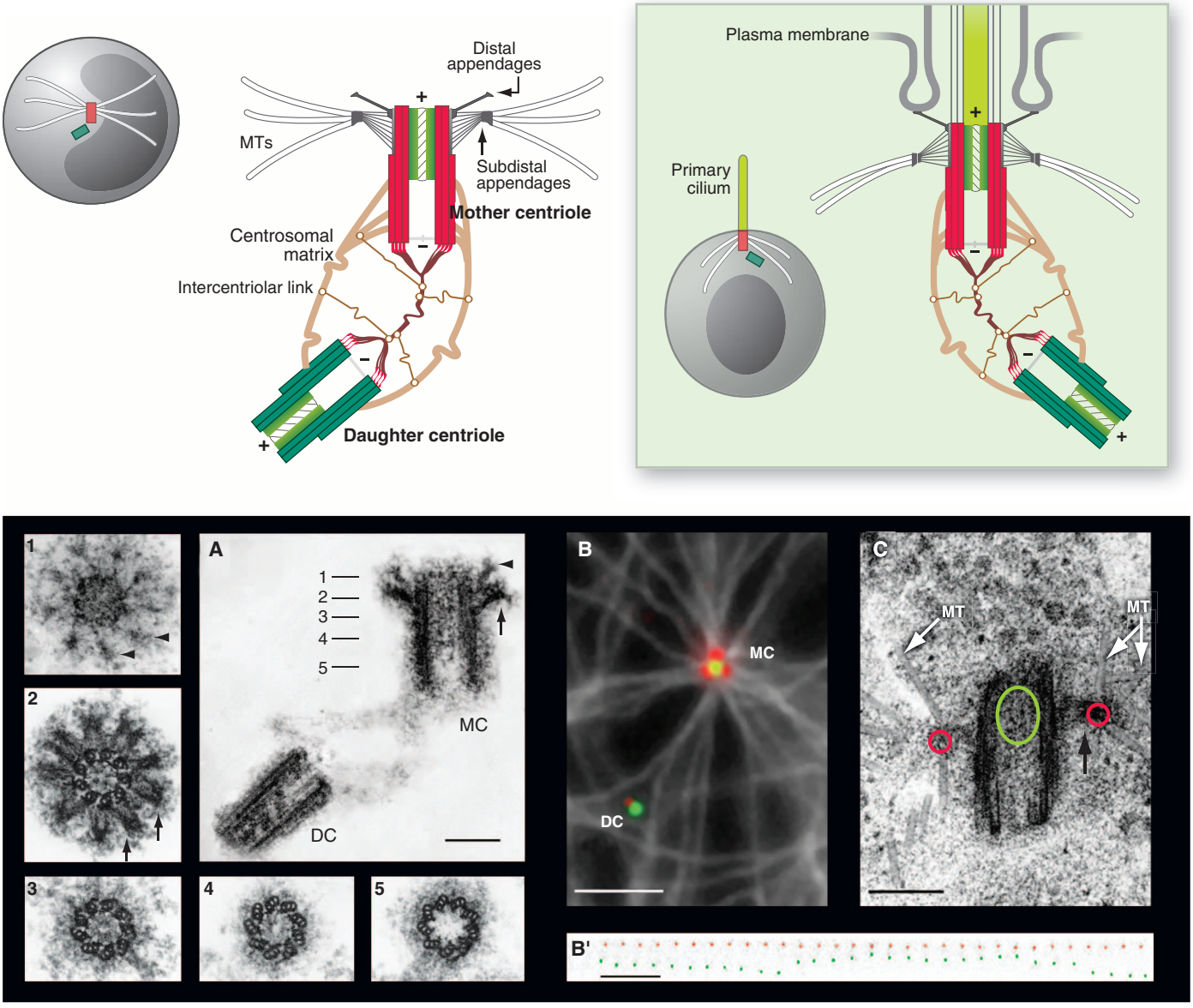


Fig. 1. The centrosome of human cells. In nonadherent lymphoblasts (left), the centrosome at the cell center deforms the nucleus. It contains a structurally and functionally asymmetric pair of centrioles, the mother centriole (red) and a daughter centriole (green). When isolated, the centrosome displays ultrastructural features shown in (**A**) and indicated in the cartoon at the top. The mother centriole (MC) is distinguished by two sets of nine appendages at its distal end, which are required for anchoring microtubules (MTs) and for docking the mother centriole at the plasma membrane during ciliogenesis in quiescent cells (inset). The proximo-distal differentiation of the MC is demonstrated on the left and at the bottom by serial sections according to the lettering shown in (A) [adapted from (*40*)]. The proximal part of centrioles displays nine microtubule triplets, which turn clockwise when viewed from the distal end, whereas the distal part displays nine microtubule doublets oriented in a tangential manner, like ciliary doublets. DC, daughter centriole. Bar: 0.2 μm. (**B**) The centrosome in situ observed by immunofluorescence light microscopy shows microtubules (white) and ninein (red), which marks the subdistal appendages of the MC in a cell line stably expressing centrin–green fluorescent protein (GFP). Bar: 3 μm. (**B'**) Movements of MC (red) and DC (green) over a period of 20 min. Bar: 1 μm. [Adapted from (*2*)] (**C**) Ultrastructural view of a mother centriole in situ showing numerous microtubules abutting at the tip of subdistal appendages where ninein (red) localizes. Centrin (green) localizes into the distal lumen of both centrioles. Bar: 0.2 μm.

Downloaded from www.sciencemag.org on January 27, 2012

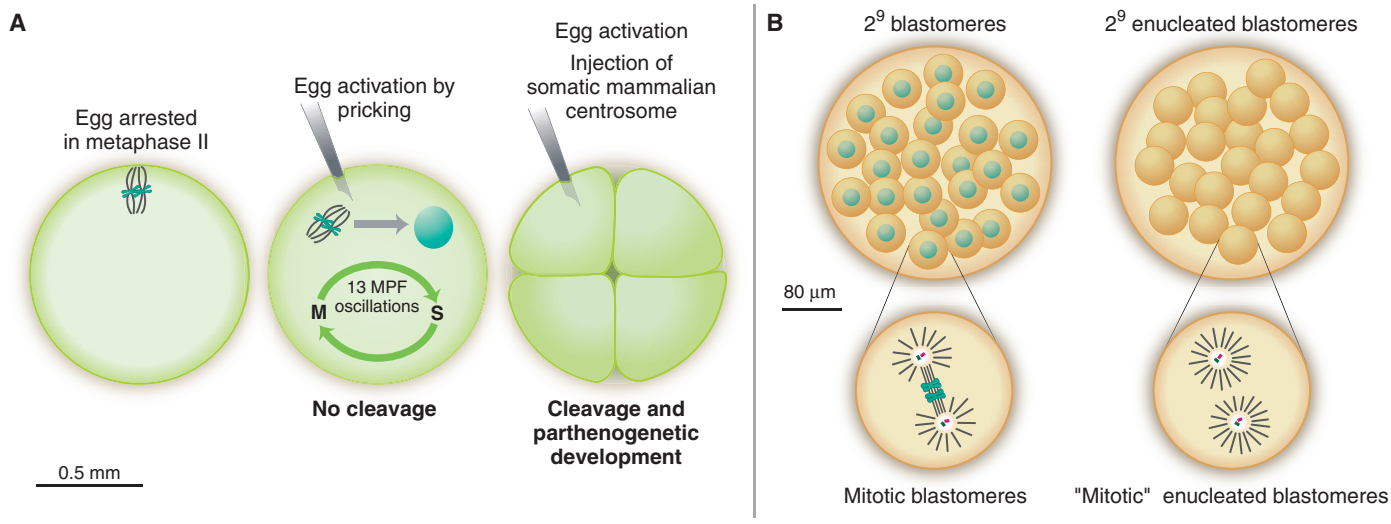


Fig. 2. Centrosome-dependent blastomere individuation. (**A**) Centrosome-induced parthenogenesis in the frog *Xenopus laevis*. Oocytes, arrested in metaphase II of meiosis, are activated by pricking: 13 embryonic cell cycles ensue in this species, monitored by maturation promoting factor (MPF) activity, but no cleavage occurs in the absence of a sperm cell. Parthenogenetic cleavage and development can be triggered by the injection of a heterologous centrosome, isolated from mammalian cells [see (*17*)]. (**B**) Complete cleavage of enucleated early embryos in the star fish *Astropecten aranciacus*. Pronuclei have been removed after fertilization, leaving the sperm-donated centrosome. Cartoon depicting control (left) and enucleated embryos (right) after the nine embryonic cell cycles in this species: The control number of enucleated blastomeres is observed in the enucleated embryo. At the bottom, cartoon depicting single blastomeres in M phase: the sequential reproduction of the sperm-donated centrosome is sufficient to trigger complete cleavages. [Adapted from (*18*)]

responsible for many human pathologies previously thought to be unrelated (*8*). The molecular pathways that regulate the conversion of centrioles to basal bodies and vice versa, as well as the transcriptional controls involved, are being actively investigated (*9*).

Centrosome positioning in migrating cells and in tissues. Mitotic centrosomes are compact, with the typical replicative orthogonal configuration between parental and daughter centrioles at each pole. By contrast, centrosomes in somatic cells have a considerable intrinsic flexibility during interphase (*2*): The two centrioles are disengaged and held together by a flexible linker between their proximal ends, and the intercentriolar distance continually changes (Fig. 1). Only the mother centriole can center the centrosome (*2*). How the intercentriolar linker length is regulated is not known. More is known about the separation of the two centrosomes at the onset of mitosis: The linker contains not only Nek2 kinase substrates such as C-Nap1 and Rootletin but also β-catenin, an effector of the Wnt pathway, which participates in the reorganization of the linker upon Nek2 phosphorylation (*25*). Nek2 association with the centrosome at this step is also regulated by components of the Hippo signaling pathway involved in growth control (*26*).

How do somatic cells sense their shape and size? There is evidence in many cell systems that interaction of dyneins with the lateral surface of microtubules is an important component of the centrosome positioning (*27*). Through its phys-

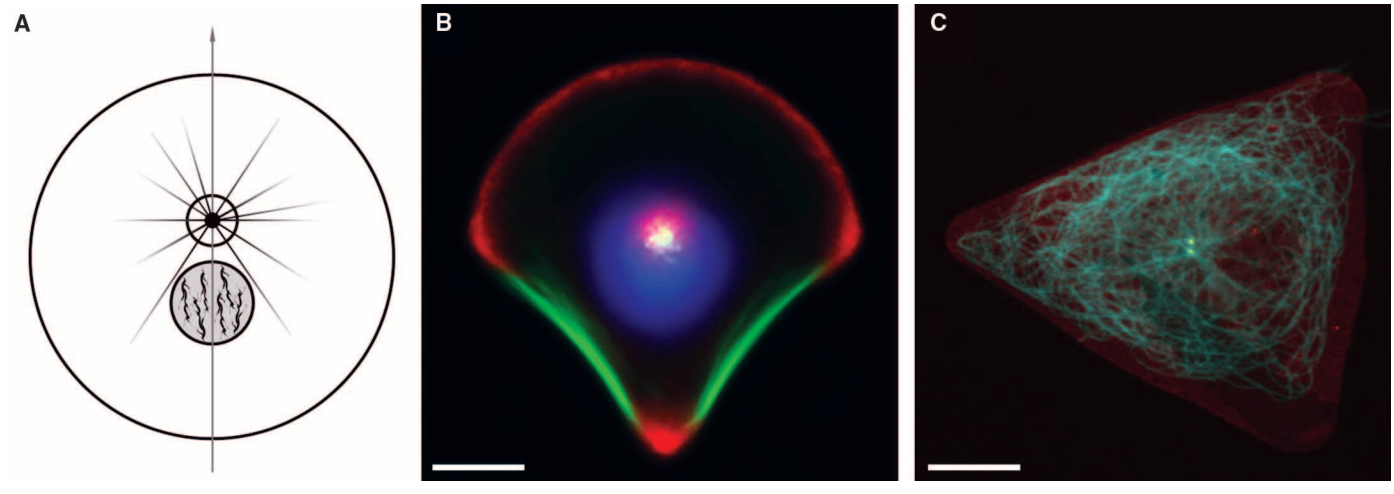


Fig. 3. The nucleus–centrosome axis as a marker of cell symmetry breaking. (**A**) A drawing from Van Beneden in 1883. (**B**) The centrosome positioning in cultured cells is tightly controlled as can be demonstrated by controlling cell adhesion. The figure shows the superimposition of 75 cells adhering to a cross-bow–shaped pattern: All centrosomes appearing as yellow-white dots are found in a 2-μm-diameter area. The Golgi apparatus appears in red. The nucleus positioning is more variable as judged by the blurring of the blue staining. The cortical labeling corresponds to regions of actin assembly on adhesive edges (cortactin in red decorates lamellipodia) and of acto-myosin contraction on nonadhesive edges (phalloidin in green decorates stress fibers). [Adapted from (*28*)] (**C**) In an enucleated cell, here adhering to a triangular micropattern, the centrosome sits precisely at the cell center and the microtubule network is symmetrically distributed. [From (*41*)] Bars: 10 μm

Downloaded from www.sciencemag.org on January 27, 2012

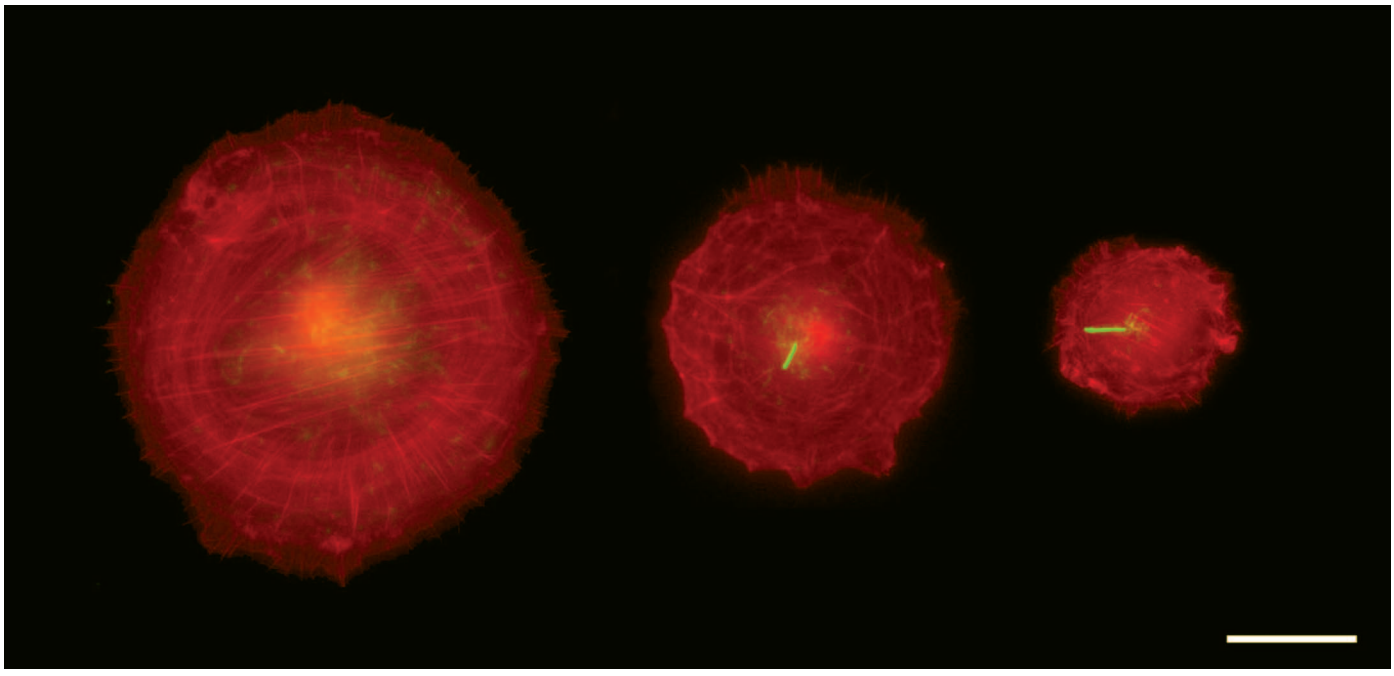


Fig. 4. Cell spreading controls ciliogenesis in serum-starved human pigment epithelial retinal cells. The transition from a cytoplasmic centrosome located at the cell center to a plasma membrane–associated centrosome in which the mother centriole acts as a basal body is modulated by the balance between assembly and contraction of the actin network. From left to right: fully adhesive discs with an area of 3500, 1500, and 500 μm^2. Cells were stained for F-actin (red) and for actetylated tubulin (green) to show the primary cilium. Bar: 10 μm. [Adapted from (*30*)]

ical association with the nucleus, the centrosome controls nuclear positioning, thus creating an internal asymmetry in the distribution of organelles: the nuclear volume is left out from the cell space in which microtubule-dependent centrosome positioning is taking place (Fig. 3). In nonadherent lymphocytes, or in enucleated adherent cells, the centrosome sits precisely at the cell's center. The mutual positioning of the centrosome and nucleus of adherent cells during migration indicates where the center of cytoplasmic mass is repositioning to. The control of centrosome positioning is tightly regulated in individual cultured cells when adhesion is controlled (Fig. 3) (*28*), which should also be the case for cells in tissues. Adhesion proteins can shuttle to the centrosome and regulate its activity in a cell cycle–dependent manner and thus could participate in centrosome positioning. Centrosome repositioning is also involved in the repositioning of the pericentrosomal Golgi ribbon. Breaking the polarity axis by disconnecting the Golgi ribbon from the centrosome has a more pronounced effect on directional cell migration than disrupting the Golgi ribbon (*29*), supporting the idea that centrosome repositioning could also depend on lateral interaction of microtubules with the three-dimensional (3D) network of intracellular membranes.

The switch to primary cilium–dependent cell polarity. Primary cilium formation is correlated with cell cycle exit, but has long been thought to depend also on cell-cell contacts because ciliogenesis in culture is dependent on cell density. The use of adhesive micropatterns of increasing size to control individual cell spreading has demonstrated instead that cell spreading is a major parameter of ciliogenesis (Fig. 4) (*30*). Only cells confined on small patterns express a robust polarity, and a full-length primary cilium. The switch between nonciliated and ciliated states in animal cells appears to be a global cell response integrating different types of information. This is not an all-or-none transition, but rather a progressive transition in which the cilium length itself can be smoothly tuned (*30*).

Actin contractility could modulate ciliogenesis in many ways. About 50 gene products can facilitate or inhibit primary cilium growth (*31*). These are proteins regulating vesicle trafficking and actin dynamics, including components of focal adhesion that participate in cell signaling. A compact pericentrosomal structure revealed by recycling endocytic markers apparently stores transmembrane proteins required for the early steps of ciliogenesis. This pericentrosomal compartment appears to be an important regulator of pre-ciliogenesis, but its relationship to the pericentrosomal Golgi apparatus is unclear. Disrupting Golgi ribbon integrity at the centrosome or disconnecting the Golgi ribbon from the centrosome inhibits ciliogenesis (*29*).

Centriole/basal body and tissue differentiation. We are far from understanding how the centriole/basal body switch is regulated in the different cell lineages of animal organisms. Some lineages never make primary cilia—like the immune system, which instead uses centrosome activity to build transient immune synapses (*32*). Kidney epithelia grow primary cilia that have a critical role in the physiology of the organ, whereas gut epithelia do not grow primary cilia but instead develop conspicuous actin-based microvilli. Myoblast-derived multinucleated myotubes cannot make primary cilia because centrosomes are eliminated during the differentiation process, while monocyte-derived multinucleated osteoclasts keep all centrosomes associated with their respective nuclei but do not make cilia (*33*). How cell polarity is controlled, or lost, in each case is unclear.

The Evolution of the Centrosome

Conserved and yet different centrosomes among divergent species. The centrosome has experienced many secondary variations that correlate with the fate of the axoneme. When the axoneme is no longer fully functional, the basal body structure becomes less constrained. When axonemes are absent, basal bodies/centrioles are also absent and different centrosomal structures can be observed, such as the nucleus-associated body in cellular slime molds, or the spindle pole body in higher fungi. In the metazoan ecdysozoa (arthropods and nematodes), the basal body/centriole structure can depart largely from the canonical structure, showing short centrioles with doublets or singlets and a correlative loss of a large number of centrosomal proteins (*3*, *4*). Accordingly, cilia are modified and involved only in sensory reception. The only beating axoneme in *Drosophila* is the sperm flagellum. In *C. elegans*, the sperm has centrioles but no flagellum. Centrosomes are robust microtubule-nucleating organelles during embryonic development and reproduce via the conserved orthogonal centriole duplication. However, somatic centrosomes are either absent or poor microtubule-nucleating centers during interphase. A fly acentriolar cell line, although prone to chromosome loss, was derived

Downloaded from www.sciencemag.org on January 27, 2012

years ago (*34*), and more recently it has been demonstrated that ablating genes necessary for centriole or centrosome assembly is compatible with the adult fly development (*35*). Thus, constraints on the centrosome may be reduced in the larval and adult organisms of this taxon, as if the evolution of an exoskeleton would have reduced the need of a robust cell polarity.

The flagellar apparatus–nucleus connection of the unicellular ancestor has been proposed to be a critical feature in evolving the centrosome in opisthokonts (*19*). The requirement of centrin, a very ancient protein closely related to calmodulin, for centrosome reproduction in many species seems to be due to its participation in mechanisms that ensure nucleus–centrosome connection through cell division. As observed for the centrosome, evolutionary constraints on centrin proteins have also been relaxed in Ecdysozoa (*19*).

Can we learn from the lower animal organisms? Organisms that exhibit variations from the usual pattern of centrosome behavior or reproduction could help to demonstrate cellular and developmental implications of centrosomes. Animals among the early branching taxa—cnidaria, ctenophora, and bilateria—in which one can hope to trace the origin of features defining animal body plans are good candidates. For example, planarians have lost the orthogonal duplication mode of centriole/basal body assembly and the centrosome organelle as well (*36*).

Planarians move and feed using multiciliated ventral and pharyngeal cells. As expected from the presence of canonical basal body/(9+2) axonemes, the genome of the freshwater planarian *Schmidtea mediterranea* contains most of the genes associated with centriole/basal body in other species. The vast majority of these genes are apparently required in planarians for the assembly and function of the basal bodies in multiciliated cells (*36*). Depletion of planarian homologs of proteins essential for centriole duplication such as *Sas-4* and *Plk4* abolished basal body assembly in multiciliated cells, but the depleted animals showed no observable regeneration defect. Accordingly, wild-type animals do not possess centrioles in cells other than multiciliated cells, including in dividing neoblasts (*36*). The centrosome was apparently lost in the lineage leading to planarians. A small set of centrosome signature proteins absent in planarians are present in lower organisms, including in the early flatworm *Macrostomum lignano*, which has centrioles at the mitotic poles of neoblasts and some, although limited, regenerative ability (*36*).

These results raise a burning question: Does the complete absence of a centrosome in animals really matter? Multicellularity is believed to have started by the transition from a colonial stage of unicellular flagellated cells to a true multicellular assembly of cells nonpermanently ciliated due to the constraints of synthesizing and maintaining a flagellum (*37*). Perhaps during this transition, individual cell polarity had to be preserved to control the stability of the novel multicellular organism, as in tissues of modern organisms. Selective pressure to maintain individual cell polarity could have triggered the transition from one type of "polar corpuscle," the plasma membrane–associated basal body/flagellum, to another, the cytoplasmic centrosome, which could switch back to the former type of cell polarity by growing a primary cilium.

What could be the developmental consequences of the absence of centrosome-based polarity in individual cells of an animal organism? Planarians depart from most animal multicellular organisms, including lower flatworms expressing centrosomes, like *M. lignano*, which undergo exclusive sexual reproduction: *S. mediterranea* can exist as sexual and asexual strains. The latter reproduce by transverse fission, do not differentiate germline or the somatic copulatory apparatus, and can generate abundant clonal progeny in controlled conditions (*38*). Possibly, reproduction by transverse fission of the body is incompatible with robust centrosome-dependent polarity of individual cells. Similarly, the long-range antero-posterior polarity system observed during asexual regeneration of planarians, or after experimental transection, to initiate head or tail formation could reflect the lack of polarity in individual cells.

If this view is correct, the absence of centrosomes in planarians would not conflict with, but rather support, the conclusion drawn from other organisms, in which the centrosome is an organ required for the stable individuation of polarized cells and for the transmission of polarities through cell division. Indeed, planarian embryonic cleavage has not retained the stereotypical pattern of cell division orientation of the ancestral spiral cleavage (*36*). Another possible consequence of evolving a centrosome in metazoa may be to preclude asexual reproduction. If further supported, this conclusion could have an important evolutionary implication as it would suggest that the centrosome's innovation has contributed to the very early differentiation and sequestration of the germ line observed in animal development (*39*).

Concluding Remarks

It is likely that the transition to multicellularity in the animal lineage has preserved cell polarity and cell individuation by internalizing the cortical microtubule network of the unicellular choanoflagellate-like ancestor and by evolving the centrosome. Actin-dependent amoeboid cells able to interact with each other, in which centrosome positioning through microtubules allows cells to sense their shape and size, are the real innovation allowing the unfolding of animal morphogenesis.

The evolutionary success of the centriole/basal body structure is striking. Centriole duplication according to orthogonal budding is observed in all ancient unicellular organisms. Did this puzzling mechanism evolve to control cell polarity, as a structural mechanism integrating 3D spatial information? The proximo-distal polarity and circumferential anisotropy of the chiral centriole/basal body structure could also specify connectivity with other cell compartments.

The selective pressure for the ninefold symmetry could come from the axoneme beating constraints. When the axoneme is no longer functional, the basal body structure becomes less constrained. Are there other functions for basal body, besides growing the axoneme and controlling the entry of flagellar complexes? Does it also participate in the beating or in the signaling control? Is there an intracentriole/basal body dynamics required for such a control or for centriole functions in the centrosome? These are questions for future work.

References and Notes

1. Y. Bobinnec *et al.*, *J. Cell Biol.* **143**, 1575 (1998).
2. M. Piel, P. Meyer, A. Khodjakov, C. L. Rieder, M. Bornens, *J. Cell Biol.* **149**, 317 (2000).
3. Z. Carvalho-Santos, J. Azimzadeh, J. B. Pereira-Leal, M. Bettencourt-Dias, *J. Cell Biol.* **194**, 165 (2011).
4. J. Azimzadeh, W. F. Marshall, *Curr. Biol.* **20**, R816 (2010).
5. J. Maller *et al.*, *Exp. Cell Res.* **99**, 285 (1976).
6. D. Kitagawa *et al.*, *Cell* **144**, 364 (2011).
7. M. van Breugel *et al.*, *Science* **331**, 1196 (2011).
8. E. A. Nigg, J. W. Raff, *Cell* **139**, 663 (2009).
9. T. Kobayashi, B. D. Dynlacht, *J. Cell Biol.* **193**, 435 (2011).
10. T. L. Megraw, J. T. Sharkey, R. S. Nowakowski, *Trends Cell Biol.* **21**, 470 (2011).
11. S. Zonies, F. Motegi, Y. Hao, G. Seydoux, *Development* **137**, 1669 (2010).
12. M. Hamaguchi, Y. Hiramoto, *Dev. Growth Differ.* **28**, 143 (1986).
13. M. Wühr, E. S. Tan, S. K. Parker, H. W. Detrich III, T. J. Mitchison, *Curr. Biol.* **20**, 2040 (2010).
14. N. Minc, D. Burgess, F. Chang, *Cell* **144**, 414 (2011).
15. K. Kimura, A. Kimura, *Proc. Natl. Acad. Sci. U.S.A.* **108**, 137 (2011).
16. J. Fink *et al.*, *Nat. Cell Biol.* **13**, 771 (2011).
17. F. Tournier, M. Bornens, *Methods Cell Biol.* **67**, 213 (2001).
18. A. Picard, M. C. Harricane, J. C. Labbe, M. Doree, *Dev. Biol.* **128**, 121 (1988).
19. M. Bornens, J. Azimzadeh, *Adv. Exp. Med. Biol.* **607**, 119 (2007).
20. J. D. Lambert, L. M. Nagy, *Nature* **420**, 682 (2002).
21. C. C. Mello *et al.*, *Nature* **382**, 710 (1996).
22. L. C. Fuentealba, E. Eivers, D. Geissert, V. Taelman, E. M. De Robertis, *Proc. Natl. Acad. Sci. U.S.A.* **105**, 7732 (2008).
23. C. Gonzalez, *Curr. Opin. Cell Biol.* **20**, 694 (2008).
24. X. Wang *et al.*, *Nature* **461**, 947 (2009).
25. S. Bahmanyar *et al.*, *Genes Dev.* **22**, 91 (2008).
26. B. R. Mardin *et al.*, *Nat. Cell Biol.* **12**, 1166 (2010).
27. J. Zhu, A. Burakov, V. Rodionov, A. Mogilner, *Mol. Biol. Cell* **21**, 4418 (2010).
28. M. Théry *et al.*, *Proc. Natl. Acad. Sci. U.S.A.* **103**, 19771 (2006).
29. L. Hurtado *et al.*, *J. Cell Biol.* **193**, 917 (2011).
30. A. Pitaval, Q. Tseng, M. Bornens, M. Théry, *J. Cell Biol.* **191**, 303 (2010).
31. J. Kim *et al.*, *Nature* **464**, 1048 (2010).
32. J. C. Stinchcombe, E. Majorovits, G. Bossi, S. Fuller, G. M. Griffiths, *Nature* **443**, 462 (2006).
33. M. Moudjou, M. Lanotte, M. Bornens, *J. Cell Sci.* **94**, 237 (1989).
34. A. Szöllösi, H. Ris, D. Szöllösi, A. Debec, *Eur. J. Cell Biol.* **40**, 100 (1986).
35. D. Gogendeau, R. Basto, *Semin. Cell Dev. Biol.* **21**, 163 (2010).
36. J. Azimzadeh *et al.*, *Science* **335**, xxx (2012).
37. N. King, *Dev. Cell* **7**, 313 (2004).
38. P. A. Newmark, A. Sánchez Alvarado, *Nat. Rev. Genet.* **3**, 210 (2002).
39. L. W. Buss, *The Evolution of Individuality* (Princeton Univ. Press, Princeton, 1987.
40. M. Paintrand, M. Moudjou, H. Delacroix, M. Bornens, *J. Struct. Biol.* **108**, 107 (1992).
41. M. Théry, M. Bornens, unpublished data.

Acknowledgments: I thank J. Sillibourne, R. M. Rios, and two reviewers for critical reading of the manuscript, and M. Théry for providing some of the figures. This work is funded by both CNRS and Institut Curie. M.B. is acting as the chief scientific officer for "CYTOO Cell Architects," Grenoble, France.

10.1126/science.1209037

Downloaded from www.sciencemag.org on January 27, 2012

Broadband Light Bending with Plasmonic Nanoantennas

Xingjie Ni, Naresh K. Emani, Alexander V. Kildishev, Alexandra Boltasseva, Vladimir M. Shalaev*

The phase of a light wave can be controlled by using bulk optical elements like lenses and mirrors to modify the wavefront of the propagating light. These elements introduce an additional spatially nonuniform phase in the incoming wave, thereby affecting its propagation characteristics. However, the amount of phase change is limited by the optical properties of the materials, and an appreciable change typically requires a propagation length comparable to or larger than the wavelength. Although metamaterials can be fabricated that are capable of bending light in unusual ways and have enabled many fantastic applications, such as negative refraction (*1*), superresolution lenses (*2*, *3*), and cloaking (*4*), the capabilities of phase control and light bending are still dictated by the material parameters as governed by the conventional Snell's law. However, the newly discovered generalized version of Snell's law ushers in a new era of light manipulation (*5*):

$$\sin(\theta_t)n_t - \sin(\theta_i)n_i = \lambda\nabla\Phi/2\pi \quad (1)$$

$$\sin(\theta_r) - \sin(\theta_i) = n_i^{-1}\lambda\nabla\Phi/2\pi \quad (2)$$

These expressions indicate that a gradient in a phase discontinuity, $\nabla\Phi$, along an interface between two media with refractive indices n_t and n_i can modify the direction of the refracted and the reflected waves by design and that this can occur in a very thin layer. Another more general interpretation of this is that $\nabla\Phi$ is essentially an additional momentum contribution that is introduced by breaking the symmetry at the interface; hence, in order to conserve momentum, the light wave has to bend accordingly. Note that when there is no phase gradient $\nabla\Phi$ along the interface, Eqs. 1 and 2 reproduce the conventional Snell's law. This is conceptually different from the diffraction formula for a periodic grating because the bent light is caused by a unidirectional phase discontinuity, which is not a particular order of diffraction. Thus by designing and engineering a phase discontinuity along an interface, one can fully control the bending of a light wave beyond what the conventional Snell's law predicts. Such an interface has been realized at a wavelength of 8 μm (*5*). We extend that work and demonstrate wavefront control in a broadband wavelength range from 1.0 to 1.9 μm, accomplished with a relatively thin 30-nm (~λ/50) plasmonic nanoantenna interface.

We used a plasmonic nanoantenna array similar to that in (*5*) and consisting of V-shaped gold antennas (Fig. 1A) to introduce an abrupt phase discontinuity at the interface. This type of antenna supports antisymmetric modes, which provide a tunable phase delay for cross-polarized light (whose polarization is perpendicular to the incident polarization) by appropriately choosing the design parameters. A unit cell of the nanoantenna array consists of eight antennas providing a phase shift from 0 to 2π in the x direction. Full-wave finite element method simulation results indicate that the designed antennas have the desired phase change (from 0 to 2π with π/4 intervals) for cross-polarized scattered light (*6*).

We fabricated a nanoantenna array sample on a double-sided polished silicon substrate with standard electron-beam lithography and lift-off processes. The height of the nanoantennas was about 30 nm, and the arm width was 40 nm. Four large arrays with different periods were fabricated on the same substrate (Fig. 1B). We measured the sample by using an ellipsometer, and the experimental measurements indicate that the reflection and refraction of the cross-polarized light are both "negative" in a broad range of incidence angles (Fig. 1, C and D, and fig. S2). In addition, wavelength-dependent measurements showed the broadband behavior of the observed phenomenon for wavelengths from 1.0 to 1.9 μm. All the experimental data match quite well with the theoretical predictions given by the generalized Snell's law, Eqs. 1 and 2, and the three-dimensional full-wave simulation results of the entire array (*6*).

The designed plasmonic interface consisting of a nanoantenna array provides a phase shift and enables us to modify the optical wavefront within an extremely thin layer. Hence, designers can now have unparalleled control of anomalous reflection and refraction, including negative refraction. The design works for a rather broad range of wavelengths, from 1.0 to 1.9 μm. This technique could lead to a variety of applications, such as spatial phase modulation, beam shaping, beam steering, and plasmonic lenses, and it also could have an impact on transformation optics and on-chip optics.

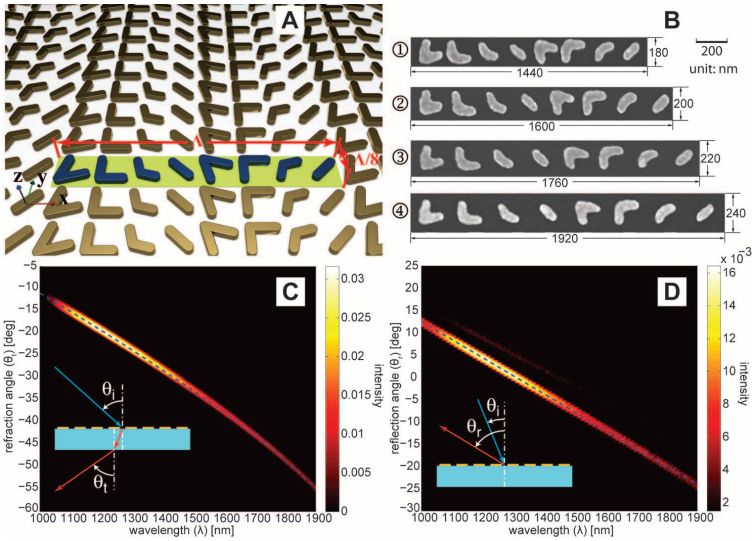


Fig. 1. (**A**) Schematic view of a representative antenna array. The unit cell of the plasmonic interface (in blue) consists of eight gold V-antennas of 40-nm arm width and 30-nm thickness, repeated with a periodicity of Λ in the x direction and Λ/8 in the y direction. The phase delay for cross-polarized light increases along the x axis from right to left. (**B**) Scanning electron microscope images of the unit cells of four antenna arrays with different periodicities fabricated on a single silicon wafer. (**C** and **D**) The false-color maps indicate the experimentally measured relative intensity profiles for the antenna array labeled ① [in (B), Λ = 1440 nm] with x-polarized excitation. The dashed line shows the theoretical prediction of the peak position using the generalized Snell's law. (C) Refraction angle θ_t versus wavelength λ for cross-polarized light with 30° incidence angle θ_i. (D) Reflection angle θ_r versus wavelength for cross-polarized light with 65° incidence angle.

References and Notes

1. V. G. Veselago, *Sov. Phys. Usp.* **10**, 509 (1968).
2. J. B. Pendry, *Phys. Rev. Lett.* **85**, 3966 (2000).
3. Z. Liu, H. Lee, Y. Xiong, C. Sun, X. Zhang, *Science* **315**, 1686 (2007).
4. J. B. Pendry, D. Schurig, D. R. Smith, *Science* **312**, 1780 (2006).
5. N. Yu *et al.*, *Science* **334**, 333 (2011); 10.1126/science.1210713.
6. See supporting online material available on *Science* Online.

Acknowledgments: This work was supported by Multidisciplinary University Research Initiative grants (Air Force Office of Scientific Research, FA9550-10-1-0264; Office of Naval Research, N00014-10-1-0942), Air Force Research Lab–Materials and Manufacturing Directorate, and NSF Division of Materials Research (1120923).

Supporting Online Material

www.sciencemag.org/cgi/content/full/science.1214686/DC1
Materials and Methods
Figs. S1 and S2

30 September 2011; accepted 13 December 2011
Published online 22 December 2011;
10.1126/science.1214686

School of Electrical and Computer Engineering and Birck Nanotechnology Center, Purdue University, West Lafayette, IN 47907, USA.

*To whom correspondence should be addressed. E-mail: shalaev@purdue.edu

Downloaded from www.sciencemag.org on January 27, 2012

Repeatability and Contingency in the Evolution of a Key Innovation in Phage Lambda

Justin R. Meyer,[1,2]* Devin T. Dobias,[3] Joshua S. Weitz,[4] Jeffrey E. Barrick,[2,5] Ryan T. Quick,[6] Richard E. Lenski[1,2,6]

The processes responsible for the evolution of key innovations, whereby lineages acquire qualitatively new functions that expand their ecological opportunities, remain poorly understood. We examined how a virus, bacteriophage λ, evolved to infect its host, *Escherichia coli*, through a novel pathway. Natural selection promoted the fixation of mutations in the virus's host-recognition protein, J, that improved fitness on the original receptor, LamB, and set the stage for other mutations that allowed infection through a new receptor, OmpF. These viral mutations arose after the host evolved reduced expression of LamB, whereas certain other host mutations prevented the phage from evolving the new function. This study shows the complex interplay between genomic processes and ecological conditions that favor the emergence of evolutionary innovations.

Throughout the history of life, evolving lineages have acquired qualitatively new functions that enable organisms to expand their ecological opportunities and, in many cases, to undergo further diversification (*1*). Explaining how these transitions have occurred is usually difficult, both because the responsible events typically occurred in the distant past and because their rarity suggests that they might involve atypical evolutionary processes. For example, natural selection is critical for the process of adaptation, yet its role in producing key innovations is less clear because, by fixing variants that improve existing functions, selection might strand populations on local adaptive peaks and thereby prevent them from discovering new functions (*2*). Darwin was well aware of the difference between improving an existing trait and evolving a new one (*3*), and he reasoned that new traits originate by co-opting previously existing structures and functions. Without an understanding of genetic mechanisms, however, he could not provide a detailed account of how this process happens. Since then, others have proposed more explicit models of the origin of new functions that vary in two main respects: the structure of the adaptive landscape—including its dimensionality (*2*), genetic connectivity (*4*), and fluctuations caused by changing environments (*5*), including interactions with coevolving species (*6*)—and the relative importance of natural selection and random drift (*2*, *4*, *7*). However, no consensus has been reached owing, at least in part, to the paucity of cases with sufficient genetic and ecological data (*8*).

To that end, we examine the evolutionary forces responsible for the emergence of a novel trait in a microbial system, including data bearing on the genetic architecture of the adaptive landscape in which the novel capacity arose. Microbes are well suited for such research because their evolution can be observed in real time, experiments are easily replicated, and transitional states can be studied by reviving samples stored at different times during an experiment (*9*, *10*). We investigated how a virus evolved the ability to infect its host through a new receptor that the ancestral virus cannot use. We tested competing hypotheses about the evolution of this new trait by determining the conditions that promoted its evolution, the mutations that conferred the new function, and the evolutionary forces that drove its emergence.

Study system. Viruses are genetically and morphologically diverse, and they infect all groups of organisms (*11*, *12*). Viruses initiate infections by binding to receptors on the surface of host cells. The physicochemical properties of viral ligands determine which receptors they target and thereby influence the host range and ecological niche of the virus (*13*). Mutations in viral genes that encode the production of ligands can cause shifts in host range and thus are often associated with emerging diseases (*14*, *15*). The evolution of the ability to infect through a new receptor represents a key innovation for a virus.

The virus we studied, a strictly lytic derivative of phage λ called cI26 (*16*) (table S1), is only known to infect one bacterial species, *Escherichia coli*, and has a specialized ligand, the J protein, at the end of its tail (*17*). J targets a single protein, LamB, on the *E. coli* outer membrane (*17*, *18*). Phage λ requires only LamB to attach (*19*), and LamB is the only outer-membrane protein that affects λ reproduction (*20*).

Given interest in the fundamental question of how organisms evolve novel traits and in the practical problem of how emerging pathogens evolve to target new host receptors, we sought to determine whether λ could evolve to infect through an alternative receptor. Phage λ is well studied and amenable to experimentation (*21*). A related phage (Ur-λ) has side-tail fibers and can infect *E. coli* through a second receptor OmpC (*22*, *23*), which suggested that other receptors might be accessible to evolving λ populations. Moreover, we identified conditions that seemed suitable for promoting the use of a novel receptor. In particular, when *E. coli* and λ were cultured

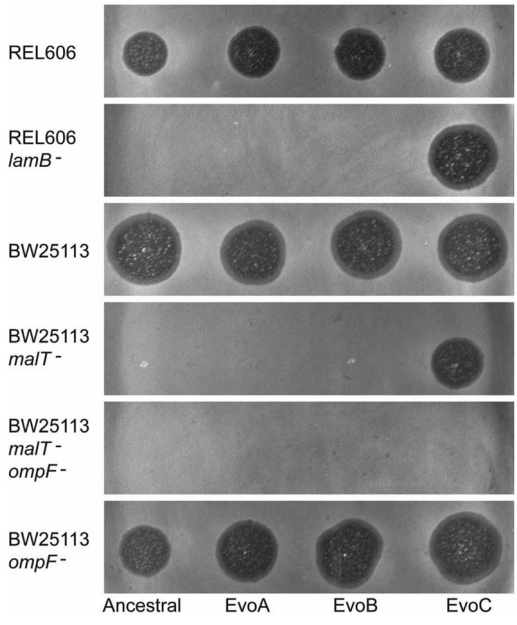


Fig. 1. Infection assay for four λ isolates tested on six *E. coli* strains. Each panel shows a bacterial lawn with aliquots of the phage applied to it; darker regions indicate successful infections that clear the lawn. The phage isolates include the ancestor and three clones isolated from the same population on day 8 of the initial evolution experiment, including one, EvoC, that can use the OmpF receptor. The bacterial strains include mutants that differ in the expression of LamB and OmpF porins on two genomic backgrounds, REL606 (the ancestral strain in the evolution experiments) and BW25113 (a derivative of K12). The *malT*⁻ strains do not express LamB at appreciable levels.

[1]Department of Zoology, Michigan State University, East Lansing, MI 48824, USA. [2]BEACON Center for the Study of Evolution in Action, Michigan State University, East Lansing, MI 48824, USA. [3]Department of Biology, Washington University, St. Louis, MO 63130, USA. [4]School of Biology and School of Physics, Georgia Institute of Technology, Atlanta, GA 30332, USA. [5]Department of Chemistry and Biochemistry, Institute for Cellular and Molecular Biology, The University of Texas, Austin, TX 78712, USA. [6]Department of Microbiology and Molecular Genetics, Michigan State University, East Lansing, MI 48824, USA.

*To whom correspondence should be addressed. E-mail: justin.raymond.meyer@gmail.com

Downloaded from www.sciencemag.org on January 27, 2012

together in a glucose-limited environment, the bacteria evolved resistance by mutations in *malT*, which interfered with its role as a transcription factor that promotes *lamB* expression (*23*). The mutants arose and fixed within 8 days, generating highly resistant populations (fig. S1), although the phage did not go extinct but instead persisted at densities of about 10^6 to 10^7 phage per ml or about one phage per 10^2 to 10^3 host cells (fig. S2). The phage evidently persisted on a subpopulation of cells that, despite their *malT* mutations, experienced spontaneous induction of the LamB protein (*24*). This explanation was confirmed by showing that phage were also sustained when they were grown on a *malT* mutant, whereas the phage went extinct when cultured with a *lamB* mutant that lacks the potential to produce the LamB protein (fig. S3). We reasoned that mutant viruses able to infect through some protein other than LamB would be favored after *malT* mutants arose because they could infect the entire host population rather than a small minority of cells.

Initial evolution experiment. We cocultured a virulent (nonlysogenic) derivative of λ and *E. coli* B in 10 ml of a minimal glucose medium in six replicate flasks for 28 days with daily transfers of 1% of each community into a flask containing fresh medium, and we preserved samples weekly by freezing 10% of the mixture (*16*). We tested whether the phage could infect cells through a new receptor by taking samples of the phage populations (typically ~5×10^4 virions) and inoculating them onto the surface of agar plates infused with a *lamB* mutant that does not produce the LamB receptor. A spot of clearing (lysis of host cells) provided evidence that some phage had evolved the ability to infect through a receptor other than LamB (Fig. 1). Such spots were observed in only one population, but this ability evolved quickly, such that ~0.01% of the phage could infect the *lamB*-negative mutants by day 8, including the isolate designated EvoC, and the majority did so by day 15.

Identification of the novel receptor. We used seven knockout strains (derivatives of K12 BW25113), each missing a gene encoding a different outer-membrane protein, to identify the new receptor (*16*, *25*). We then introduced *malT* mutations to these strains so that they also would not express the native LamB receptor. We inferred which one was the new receptor by testing the ancestral and evolved λ against these double mutants to see which ones were resistant to the various phage isolates. The only host that was resistant to the EvoC isolate was the *ompF malT* double mutant that lacked expression of both OmpF and LamB (Fig. 1 and table S2), which indicated that OmpF was the new receptor. This evolved phage could still infect the host strain expressing LamB but not OmpF, which showed that the phage retained the ability to infect through its native receptor (Fig. 1).

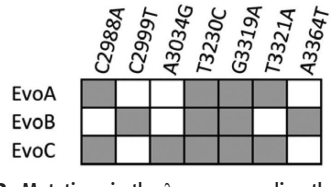


Fig. 2. Mutations in the λ gene encoding the J protein in three isolates from the same population on day 8 of the initial evolution experiment. The isolates are shown in rows and the mutations in columns, with the first letter being the ancestral nucleotide, the number the nucleotide position, and the last letter the evolved nucleotide. The gray fill indicates that the phage isolate has the corresponding mutation.

Both LamB and OmpF form trimeric porins composed of three identical β barrels (*26*, *27*). This overall structure is probably essential for the J protein in the λ tail to bind because J, too, forms a trimer and is thought to attach with radial symmetry across the three pore domains (*28*). Although OmpF has the most similar crystal structure to LamB of any *E. coli* protein determined to date (*29*), they are not the most similar pair by amino acid sequence (table S3). This discordance suggests that the overall structure is at least as important for λ binding as the identity of specific amino acid residues. Also, OmpF is the sole major porin in the *E. coli* B strain used in this study, and B expresses it constitutively during growth (*30*, *31*). Hence, OmpF provided a substantial ecological opportunity to phage that evolved the ability to target it.

Genome evolution. We sequenced the genome of the evolved phage EvoC in order to identify the mutations that allowed it to use the OmpF receptor (*16*). There were five mutations in total, and all of them were in the J gene (Fig. 2). Targeted sequencing of J showed that a single substitution (A to G at position 3034) differentiated EvoC from another evolved isolate from the same time point, EvoA, that could use only the ancestral LamB receptor, which indicated that mutation contributed to the new receptor function. Another LamB-dependent phage from the same day, EvoB, differed from EvoC at five sites in the J protein.

Large-scale evolution experiment. We repeated our first experiment with 96 more communities to identify general principles of how λ evolves the capacity to target an alternative receptor (*16*). We sampled daily for finer resolution of the evolutionary dynamics. As before, only some phage populations (24 out of 96) evolved the ability to use a second receptor. This ability emerged about the same time (median 12 days; range 9 to 17 days) (fig. S4), and all isolates with altered receptor function infected hosts through the OmpF protein.

Parallel molecular evolution. We sequenced J alleles from 24 phage isolates that independently evolved the ability to target OmpF during the large-scale evolution experiment to determine whether the mutation at position 3034 or any others were required to use that receptor. The isolates were taken the same day the new function was detected (*16*). For comparison, we sequenced phage from 24 populations that never evolved this trait; these isolates were sampled on the same days as those that evolved the new trait, so that the elapsed times were the same.

In total, there were 241 single-nucleotide polymorphisms (SNPs) across the 48 J alleles, but no insertions or deletions (Fig. 3). However, there were only 40 unique mutations because many arose repeatedly in replicate populations. Moreover, all of them were nonsynonymous. The alleles for phage able to target OmpF had on average 6.63 [± 0.51 95% confidence interval (CI)] SNPs, whereas the phage that required LamB had only 3.42 (± 0.50 95% CI) SNPs. This difference is highly significant on the basis of a paired comparison between the two types of phage matched for the day of their isolation and, in the case of multiple equivalent pairs, matched arbitrarily by position in the experiment ($t = 9.144$, 23 df, two-tailed test; $P < 0.0001$) (table S4). Also, across both classes of phage, more than 97% of the mutations were in the last 25% of the protein (C-terminal end), the region known to interact with LamB (*32*).

There are four striking cases of parallel evolution of the J protein in the phage that target OmpF. In two cases, the mutations were identical across all 24 populations; in two others, there were slight variations (Fig. 3). In particular, all J alleles from phage able to infect through OmpF had the A-to-G mutation at nucleotide position 3034 and G-to-A mutation at position 3319. Also, all of them had a mutation at either position 3320 or 3321, affecting the same codon (amino acid residue 1107) as the mutation at position 3319. Finally, all J alleles had at least one mutation between positions 2969 and 2999 (amino acid residues 990 to 1000).

Each of these mutations or classes of mutations were also found in at least one of the phage that retained the ancestral host-range, although none of them had all four together (Fig. 3). Two LamB-dependent isolates, F2 and H4, had three of the mutations, as did EvoA from the initial experiment (Fig. 2), yet none produced clearing on lawns of *lamB* mutants.

The correspondence between the use of the OmpF receptor and the presence of these four mutations, coupled with the observation that phage having only three of the four cannot use OmpF, provides evidence that all four are required for λ to infect through OmpF. We performed two additional assays to confirm that only phage with all four mutations can infect *lamB* mutants (*16*). The assays were performed using isolates EvoA, F2, and H4 that each had three of the four canonical mutations and D7 that had all four and no others. Only D7 exhibited a measurable adsorption rate on *lamB* mutant cells (fig. S5), and it was also the only one that reproduced on *lamB* mutants in the medium used in the evolution experiments (fig. S6). These findings indicate an "all-or-none" form of epistasis among the four mutations responsible for the novel receptor phenotype.

Role of natural selection. In the λ population that evolved to use OmpF in the initial experiment, the A3034G mutation was the fourth

Downloaded from www.sciencemag.org on January 27, 2012

and final step, and it was clearly advantageous because it conferred the ability to infect the entire cell population. However, the all-or-none epistasis among the mutations means that selection for that new capacity per se was not responsible for the rise of the three prior mutations. Nonetheless, there are several lines of evidence that selection drove their rise. First, all 248 independent mutations in the 51 sequenced J alleles were nonsynonymous, whereas the expected ratio of nonsynonymous to synonymous changes is 3.19:1 under the null model for the ancestral J sequence (*16*). This great excess is evident even if we include only the 82 nonsynonymous mutations in the 24 isolates that did not evolve the new receptor function. Second, the mutations are highly concentrated in the region of the J protein that interacts directly with LamB (*18*). Third, there was parallel evolution at the genetic level across the populations. For those phage that evolved to exploit OmpF, an average of 61% (4.06 out of 6.63) of mutations were shared across independently derived pairs (fig. S7), which greatly exceeds the fraction expected under a conservative randomization test (*16*) that used only the variable sites in J ($P < 10^{-5}$). Pairs of phage that remained dependent on LamB shared on average 17% (0.58 out of 3.42) of their mutations (fig. S7), and this fraction is again significant under the same test ($P < 10^{-5}$). Thus, it is clear that selection acted on the J protein even before the new capacity evolved. This selection presumably improved the interaction of the phage tail with LamB.

Stochasicity and contingency. All of the λ populations had the same ecological incentive to exploit an alternative receptor, but only some evolved that ability. Why were some populations successful and others not? One possibility is that all of them would eventually have evolved that function but that there was insufficient time to do so. This explanation is consistent with the facts that the LamB-dependent isolates had fewer mutations than those able to target OmpF, and that the two groups shared many mutations. Alternatively, the evolution of the new receptor function might have been contingent on earlier events (*33*–*35*), such that particular changes in the phage or the host promoted or impeded the subsequent evolution of that function. To test these hypotheses, we replayed evolution (*35*, *36*) using various combinations of phage and bacteria.

First, we tested whether certain mutations in the phage that might enhance performance on LamB would impede the evolution of the new OmpF function. We inoculated flasks with the ancestral bacteria and one of six phage isolates. Three of the six phage isolates had different sets of three mutations that were present in multiple isolates that evolved to use the OmpF receptor, including one, zero, and two of the four canonical mutations. The other three isolates had three, two, and one mutations that were not observed in any isolate that previously evolved the ability to use OmpF; these isolates also each had one of the canonical mutations. The first set provided a positive control; the second set had candidate mutations for impeding the evolution of the new function. For each phage, we propagated 12 communities for 10 days and surveyed daily the phage's ability to lyse *lamB* mutant cells. There were as many or more successes in evolving the new function among the three phages that had the potentially interfering mutations as among the positive controls (Fig. 4, top). This experiment thus provides no evidence that some phage failed to evolve the new function because they had mutations that prevented them from doing so.

Next, we asked if the outcome was contingent on mutations in the evolving bacteria. To that end, we performed a similar replay experiment except that the initial phage type was held constant while the starting bacterial isolate was varied. For the phage, we used EvoA, an isolate that was one mutation away from using OmpF (Fig. 2).

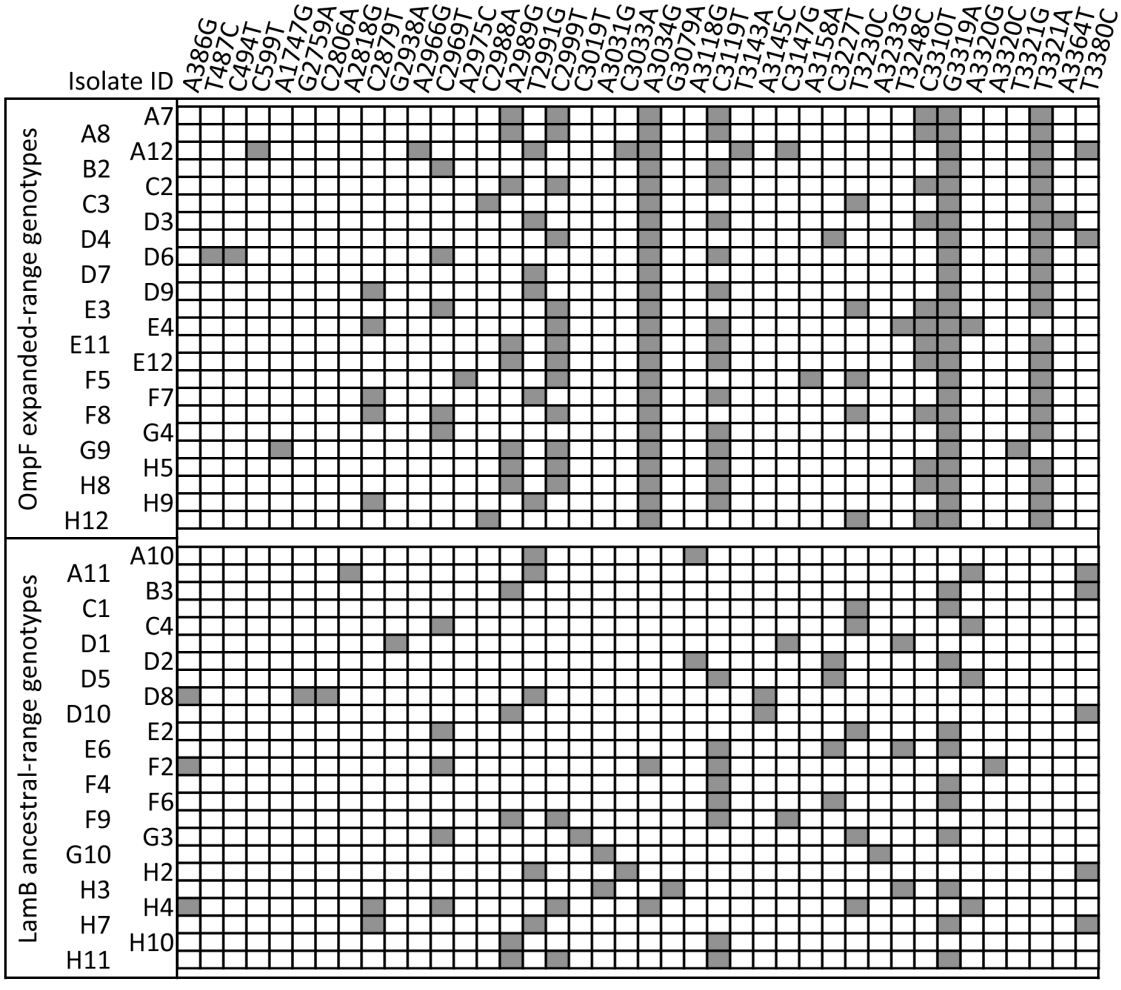


Fig. 3. Mutations affecting the J protein in phage isolates from 48 independent populations of the large-scale experiment. Isolates are shown in rows (with alternate labels offset for readability) and mutations in columns; gray fill indicates that an isolate has the mutation. The top 24 rows show phage isolates that can target the new OmpF receptor; the bottom 24 rows show phage that remain dependent on LamB.

Downloaded from www.sciencemag.org on January 27, 2012

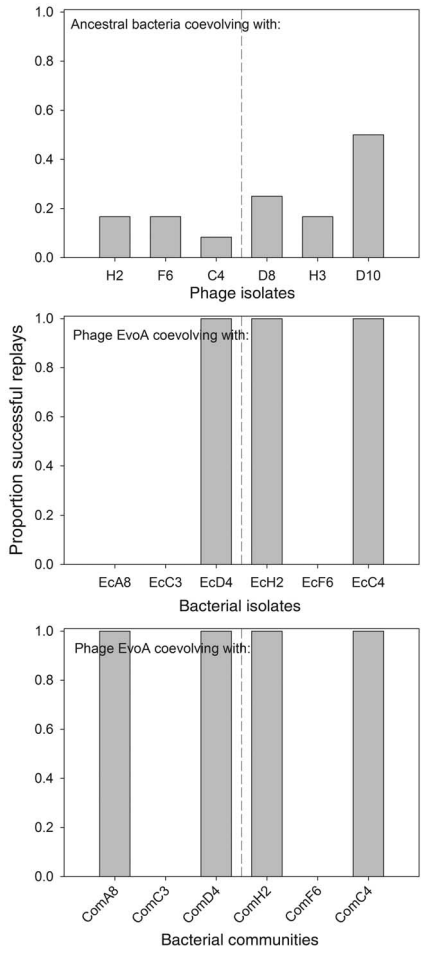


Fig. 4. Replay experiments using different combinations of phage and bacteria. For each panel, the *y* axis shows the proportion of replicate replays that produced phage able to target the new OmpF receptor. (**Top**) Replays were initiated with the ancestral bacteria and six phage isolates. Each combination was replicated 12-fold. Three of the phage (H2, F6, and C4) had mutations shared by multiple lineages that evolved the capacity to target OmpF in the large-scale experiment. The other three (D8, H3, and D10) had mutations that were never observed in phage that targeted OmpF. The latter mutations were candidates for impeding the evolution of the new function, but that hypothesis was not supported. (**Middle**) Replays were initiated with phage EvoA (which needs only one more mutation to use OmpF) and six bacterial clones. Each combination was replicated fourfold. Three clones (EcA8, EcC3, and EcD4) were isolated from flasks in which phage evolved the capacity to target OmpF in the large-scale experiment. The other three (EcH2, EcF6, and EcC4) came from flasks in which phage did not evolve that function. The replay outcomes did not support these categories, but sequencing the bacterial genomes identified mutations that uniquely determined whether the phage would evolve the OmpF function. See text for details. (**Bottom**) Replays were initiated using the same phage and bacteria used in the middle panel, except with full bacterial communities rather than individual clones. Each combination was replicated 12-fold. The different outcomes for one bacterial clone (EcA8, middle) and its source community (ComA8, bottom) show the effect of bacterial diversity on phage evolution.

For the bacteria, we used six clones: three from communities where λ evolved to use OmpF, and three where the phage retained their dependence on LamB. We observed a striking "all-or-none" pattern of outcomes, although not in accordance with our categories (Fig. 4). In particular, all 36 λ populations evolved the final mutation required to use OmpF in communities with three bacterial clones, whereas none of the phage evolved that ability in 36 communities with the three other clones. For two of the latter class (EcA8 and EcF6), the phage were unable to reproduce and went extinct; in the other case (EcC3), phage persisted but none of the replays yielded phage able to use OmpF. It is clear that bacterial characteristics determined whether the phage would evolve the new receptor function. However, the bacteria that promoted that outcome did not necessarily come from communities in which λ had previously evolved to exploit OmpF.

We sequenced the full genomes of these six bacteria to identify the mutations responsible for the differences in phage evolution. The six genomes harbor a total of 15 mutations (table S5). Five have similar deletions that affect the *rbs* operon, which confers the ability to grow on ribose; previous work has shown that these deletions occur at an unusually high rate owing to a nearby insertion-sequence element in the ancestral strain (*37*). All 10 other mutations are directly related to the interaction with λ. As expected, all six genomes have mutations in *malT* that confer resistance to the ancestral phage, as described earlier. One genome from a community where λ evolved to use the OmpF receptor has a nonsynonymous mutation in the *ompF* gene, which might confer partial resistance to the evolved phage. The three remaining mutations disrupt *manY* or *manZ*, and they uniquely differentiate the three strains that prevented phage from evolving to use OmpF from the three strains that allowed that change (table S5). The *manY* and *manZ* genes encode the transmembrane channel of the ManXYZ mannose permease, which is required for λ DNA to cross the inner membrane (*38*–*40*). These mutations thus confer resistance by blocking a later step during infection, and they would render ineffective any phage mutations that altered the receptor function. Therefore, the evolution of phage that target OmpF is promoted by bacterial mutations in *malT* but impeded by mutations in *manYZ*, which indicated contingency dependent on the host-parasite coevolution.

After discovering the *manYZ* mutations, we screened all 96 bacterial populations from the large-scale experiment to determine how many harbored mannose-deficient mutants that would block λ infections (*16*). At least 80 populations (table S6) had such mutations, including many from communities in which λ evolved the ability to exploit the OmpF receptor. However, these mutations rarely fixed; instead, susceptible subpopulations persisted in 77 of the 80 communities that allowed the phage to continue to evolve. This finding suggests a complex interplay between coevolving phage and bacteria, one that depends on the entire community and its diversity. To test this hypothesis, we repeated the second replay experiment using the same phage and bacteria, except with bacterial communities instead of clones (*16*). Once again, some bacteria consistently impeded the evolution of phage that used OmpF while others consistently promoted that change (Fig. 4, bottom). Moreover, those outcomes differed for one clone (EcA8) (Fig. 4, middle) and its community (ComA8) (Fig. 4, bottom), which confirmed the effect of bacterial diversity on the phage's evolution.

Repeatability, contingency, and the evolution of a key innovation. Phage λ often, but not always, evolved the ability to infect its *E. coli* hosts by targeting a new receptor, OmpF. Figure 5 summarizes the important steps in this process, including some that promoted this key innovation and others that impeded it. The fact that several mutations are required for λ to use OmpF may explain why no previous studies have reported this change, despite decades of intense study of this phage. However, by running evolution experiments rather than mutational screens, we observed 25 cases in which this new function evolved. Our experiments are not the first to demonstrate evolutionary transitions in viruses (*13*, *41*–*43*); one study found that a single mutation allowed phage φ6 to infect a new host

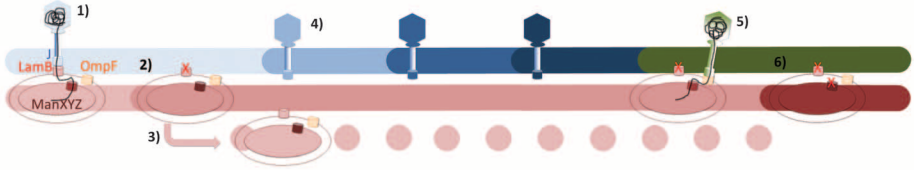


Fig. 5. Steps in the coevolution of phage λ and its *E. coli* host leading to the phage's ability to target a new receptor, OmpF. 1) The ancestral phage targets the LamB porin using the J protein and injects its DNA into the periplasm, then the DNA is transported into the cytoplasm via the ManXYZ permease. 2) The bacteria evolve resistance by mutations in *malT*, a positive regulator of LamB expression. 3) However, spontaneous inductions of LamB generate a subpopulation of phenotypically sensitive cells that can sustain the phage population. 4) The phage evolves mutations in the J protein that improve performance on the LamB receptor. Some of these mutations are also required for the phage to target OmpF. 5) The phage eventually evolves the four mutations that enable it to use OmpF. 6) However, the bacteria may evolve additional resistance by mutations in *manY* or *manZ* that prevent transport of the phage DNA into the cytoplasm. When these mutants become sufficiently common, there is little or no benefit to mutant phage that can use OmpF.

Downloaded from www.sciencemag.org on January 27, 2012

species (*13*), and a study of phage SBW25Φ2 showed that coevolution experiments were more effective at producing host-range shifts than were screens using new hosts (*43*). The rich and complex dynamics of coevolving species may thus sometimes facilitate key innovations (*6*, *44*).

More generally, our study shows some of the challenges that make it difficult to observe and explain the origin of many new functions, including the requirement for multiple mutations, the complex interactions of mutations within and between species, and the resulting historical contingency that can enable or impede the outcome of interest depending on the order in which mutations occur. The "all-or-none" epistasis among the four canonical phage mutations implies that it would have been unlikely for the new function to evolve on the scale of our experiments, except for the lucky fact that some of the mutations were beneficial to the phage in performing their current function, thereby pushing evolution toward the new function. The mutations in the bacteria, and how they influenced the phage's evolution, were also important. In particular, the initial resistance mutation generated a physiological subpopulation of hosts that allowed the phage to persist and adapt to the original receptor and, thereby, to accumulate the required mutations. Yet, as fortuitous as these circumstances were, another mutation could—and often did—derail the emergence of the new function: Namely, a mutation that conferred an alternative mode of host resistance eliminated the advantage to the phage of targeting the OmpF receptor. The interactions between bacteria and phage, which contributed so much to the development of microbial genetics and molecular biology (*45*, *46*), continue to serve as powerful models to study ecology and evolution (*47*, *48*).

References and Notes

1. E. Mayr, *Animal Species and Evolution* (Belknap Press, Cambridge, MA, 1963).
2. S. Gavrilets, in *Toward an Extended Evolutionary Synthesis*, M. Pigliucci, G. Muller, Eds. (MIT Press, Cambridge, MA, 2010).
3. C. Darwin, *The Origin of Species* (Murray, London, 1859).
4. R. A. Fisher, *The Genetical Theory of Natural Selection* (Clarendon Press, Oxford, 1930).
5. U. Dieckmann, M. Doebeli, J. A. J. Metz, Eds., *Adaptive Speciation* (Cambridge Univ. Press, Cambridge, UK, 2004).
6. J. N. Thompson, *The Geographic Mosaic of Coevolution* (Univ. Chicago Press, Chicago, 2005).
7. S. Wright, *Genetics* **16**, 97 (1931).
8. M. Pigliucci, *Philos. Sci.* **75**, 887 (2008).
9. J. J. Dennehy, *Trends Microbiol.* **17**, 450 (2009).
10. S. F. Elena, R. E. Lenski, *Nat. Rev. Genet.* **4**, 457 (2003).
11. R. A. Edwards, F. Rohwer, *Nat. Rev. Microbiol.* **3**, 504 (2005).
12. V. Torsvik, L. Øvreås, T. F. Thingstad, *Science* **296**, 1064 (2002).
13. S. Duffy, C. L. Burch, P. E. Turner, *Evolution* **61**, 2614 (2007).
14. K. M. Pepin, S. Lass, J. R. C. Pulliam, A. F. Read, J. O. Lloyd-Smith, *Nat. Rev. Microbiol.* **8**, 802 (2010).
15. E. C. Holmes, *Annu. Rev. Ecol. Evol. Syst.* **40**, 353 (2009).
16. Materials and methods are available as supporting material on *Science* Online.
17. I. Katsura, in *Lambda II*, R. W. Hendrix, Ed. (Cold Spring Harbor Laboratory Press, Cold Spring Harbor, NY, 1981).
18. E. Berkane *et al.*, *Biochemistry* **45**, 2708 (2006).
19. P. Grayson, L. Han, T. Winther, R. Phillips, *Proc. Natl. Acad. Sci. U.S.A.* **104**, 14652 (2007).
20. N. D. Maynard *et al.*, *PLoS Genet.* **6**, e1001017 (2010).
21. R. W. Hendrix, Ed., *Lambda II* (Cold Spring Harbor Laboratory Press, Cold Spring Harbor, NY, 1983).
22. R. W. Hendrix, R. L. Duda, *Science* **258**, 1145 (1992).
23. R. Gallet, S. Kannoly, I. N. Wang, *BMC Microbiol.* **11**, 181 (2011).
24. C. Braun-Breton, M. Hofnung, *Mol. Gen. Genet.* **159**, 143 (1978).
25. T. Baba *et al.*, *Mol. Syst. Biol.* **2**, 2006, 0008 (2006).
26. T. Schirmer, T. A. Keller, Y. F. Wang, J. P. Rosenbusch, *Science* **267**, 512 (1995).
27. G. Kefala *et al.*, *Protein Sci.* **19**, 1117 (2010).
28. P. A. Gurnev, A. B. Oppenheim, M. Winterhalter, S. M. Bezrukov, *J. Mol. Biol.* **359**, 1447 (2006).
29. R. Koebnik, K. P. Locher, P. Van Gelder, *Mol. Microbiol.* **37**, 239 (2000).
30. D. Schneider *et al.*, *BMC Microbiol.* **2**, 18 (2002).
31. E. Crozat *et al.*, *J. Bacteriol.* **193**, 429 (2011).
32. J. Wang, M. Hofnung, A. Charbit, *J. Bacteriol.* **182**, 508 (2000).
33. S. J. Gould, *Wonderful Life* (Norton, New York, 1989).
34. M. Travisano, J. A. Mongold, A. F. Bennett, R. E. Lenski, *Science* **267**, 87 (1995).
35. Z. D. Blount, C. Z. Borland, R. E. Lenski, *Proc. Natl. Acad. Sci. U.S.A.* **105**, 7899 (2008).
36. R. J. Woods *et al.*, *Science* **331**, 1433 (2011).
37. V. S. Cooper, D. Schneider, M. Blot, R. E. Lenski, *J. Bacteriol.* **183**, 2834 (2001).
38. B. Erni, B. Zanolari, H. P. Kocher, *J. Biol. Chem.* **262**, 5238 (1987).
39. P. E. J. Saris, E. T. Palva, *FEMS Microbiol. Lett.* **44**, 371 (1987).
40. M. Esquinas-Rychen, B. Erni, *J. Mol. Microbiol. Biotechnol.* **3**, 361 (2001).
41. R. L. Graham, R. S. Baric, *J. Virol.* **84**, 3134 (2010).
42. M. T. Ferris, P. Joyce, C. L. Burch, *Genetics* **176**, 1013 (2007).
43. A. R. Hall, P. D. Scanlan, A. Buckling, *Am. Nat.* **177**, 44 (2011).
44. J. N. Thompson, *The Coevolutionary Process* (Univ. of Chicago Press, Chicago, 1994).
45. D. I. Friedman, D. L. Court, *Curr. Opin. Microbiol.* **4**, 201 (2001).
46. J. Cairns, G. S. Stent, J. D. Watson, Eds., *Phage and the Origins of Molecular Biology* (Cold Spring Harbor Laboratory Press, Cold Spring Harbor, NY, 2007).
47. B. J. M. Bohannan, R. E. Lenski, *Ecol. Lett.* **3**, 362 (2000).
48. C. O. Flores, J. R. Meyer, S. Valverde, L. Farr, J. S. Weitz, *Proc. Natl. Acad. Sci. U.S.A.* **108**, E288 (2011).

Acknowledgments: This work was supported by the BEACON Center for the Study of Evolution in Action (NSF Cooperative Agreement DBI-0939454), the Defense Advanced Research Projects Agency (HR0011-09-1-0055 to R.E.L. and J.S.W.), and the NIH (R00GM087550 to J.E.B.). J.S.W. also acknowledges the support of the James S. McDonnell Foundation and the Burroughs Wellcome Fund. We thank N. Hajela and L. Zaman for help in the lab; D. Court for sharing phage cI26; the Michigan State University Research Technology Support Facility for help with genome sequencing; Z. Blount, T. Ferenci, C. Marx, L. Zaman, I. Wang, M. Kreitman, B. He, and J. Reinitz for discussions; and the anonymous reviewers for help revising. R.E.L. will make the evolved strains available to qualified recipients, subject to completion of a material transfer agreement that can be found at www.technologies.msu.edu/inventors/mta-cda/mta/mta-forms. The genome-sequence data for the phage and bacteria have been deposited in the National Center for Biotechnology Information, NIH, Sequence Read Archive (SRA043942). Other data and analysis scripts have been deposited at the Dryad Digital Repository (doi:10.5061/dryad.sh7rm2pt).

Supporting Online Material

www.sciencemag.org/cgi/content/full/335/6067/428/DC1
Materials and Methods
Tables S1 to S6
Figs. S1 to S7
References (*49*–*74*)

26 September 2011; accepted 15 December 2011
10.1126/science.1214449

Downloaded from www.sciencemag.org on January 27, 2012

Crystal Structure of the Human Two–Pore Domain Potassium Channel K2P1

Alexandria N. Miller[1,2] and Stephen B. Long[1]*

Two–pore domain potassium (K^+) channels (K2P channels) control the negative resting potential of eukaryotic cells and regulate cell excitability by conducting K^+ ions across the plasma membrane. Here, we present the 3.4 angstrom resolution crystal structure of a human K2P channel, K2P1 (TWIK-1). Unlike other K^+ channel structures, K2P1 is dimeric. An extracellular cap domain located above the selectivity filter forms an ion pathway in which K^+ ions flow through side portals. Openings within the transmembrane region expose the pore to the lipid bilayer and are filled with electron density attributable to alkyl chains. An interfacial helix appears structurally poised to affect gating. The structure lays a foundation to further investigate how K2P channels are regulated by diverse stimuli.

The high resting permeability of the plasma membrane to potassium ions (K^+) was appreciated for nearly 50 years (*1*–*3*) before these "background" K^+ currents were partially attributed to a family of two–pore domain K^+ (K2P) channels (*4*). A total of 15 K2P channels in humans can be divided into 6 K2P subfamilies based on sequence identity and functional characteristics: TWIK, TREK, TASK, TALK, THIK, and TRESK (*4*). Under normal physiological conditions, the K^+ gradient across the cellular membrane (~150 mM inside and ~5 mM outside) causes the net efflux of K^+ ions through K2P channels, which stabilizes the negative electrical potential (resting potential) of the cell (*4*). Expression of the K2P channel K2P1 (TWIK-1) has been detected in several tissues and plays important roles in excitable cells in the heart and brain (*5*–*7*). K2P1 has the unusual property that it becomes permeable to sodium ions (Na^+) under physiological conditions when the extracellular

[1]Structural Biology Program, Memorial Sloan-Kettering Cancer Center, 1275 York Avenue, New York, NY 10065, USA. [2]Louis V. Gerstner Jr. Graduate School of Biomedical Sciences, Memorial Sloan-Kettering Cancer Center, 1275 York Avenue, New York, NY 10065, USA.

*To whom correspondence should be addressed. E-mail: longs@mskcc.org

K^+ concentration is below normal levels (hypokalemia) (*7*). Hypokalemia occurs in up to 20% of hospitalized patients and increases the risk of sudden cardiac death (*8*). Because the extracellular concentration of Na^+ is higher than the intracellular concentration, this altered permeability of K2P1 allows the influx of Na^+ that has been shown to depolarize cardiomyocytes and may contribute to cardiac arrhythmia or arrest (*7*).

Although K2P channels were first considered simply "leak" channels, it has become clear that they are regulated by numerous factors (*4*). For example, TREK-1 is modulated by changes in temperature or pH, by membrane stretch, and by anesthetics and antidepressants (*9*–*13*). These regulatory properties may be involved in pain perception and neuroprotection (*4*). Regulation of TREK-1 activity by diverse stimuli has been partly ascribed to a C-terminal region of amino acids following the fourth transmembrane (M4) helix (*9*–*12*, *14*, *15*). Evidence suggests that the activity of K2P1 can be silenced by modification of a lysine residue in the corresponding C-terminal region (Lys^{274}) with a small ubiquitin-like modifier (SUMO), consistent with a role for this region in channel regulation (*16*, *17*) [although other studies have suggested that this modification does not occur (*18*, *19*)].

A K^+ channel pore is composed of four pore-forming (P) domains. Each P domain contains an outer transmembrane helix, a pore helix, a selectivity filter signature sequence, and an inner transmembrane helix (*20*). The crystal structures of K^+ channels determined to date are of tetrameric channels, with four identical subunits that each contain one P domain. The genes of K2P channels contain two P domain sequences (P domain 1 and P domain 2) arranged in tandem, and these channels assemble as dimers (*4*, *5*, *21*) (Fig. 1C). So, each K2P protomer contains four transmembrane helices (M1 to M4). M1 and M3 are the outer helices of P domains 1 and 2, respectively. M2 and M4 are the inner helices of P domains 1 and 2, respectively. Although tetrameric K^+ channels often have regulatory domains such as voltage sensors within the span of the membrane or ligand-binding domains located on the cytosolic side, they lack extracellular domains. K2P channels have an extracellular region of ~55 amino acids within P domain 1 (between M1 and pore helix 1) that is not present in P domain 2 or found in tetrameric K^+ channels (fig. S1A). The function of this region and whether or not it forms a structured domain are largely unknown. Although existing structures of K^+ channels give insights into principles of ion permeation, ion selectivity, and gating (*22*), structures of K2P channels are needed to understand the features specific to this class. Here, we present the crystal structure of human K2P1 (TWIK-1).

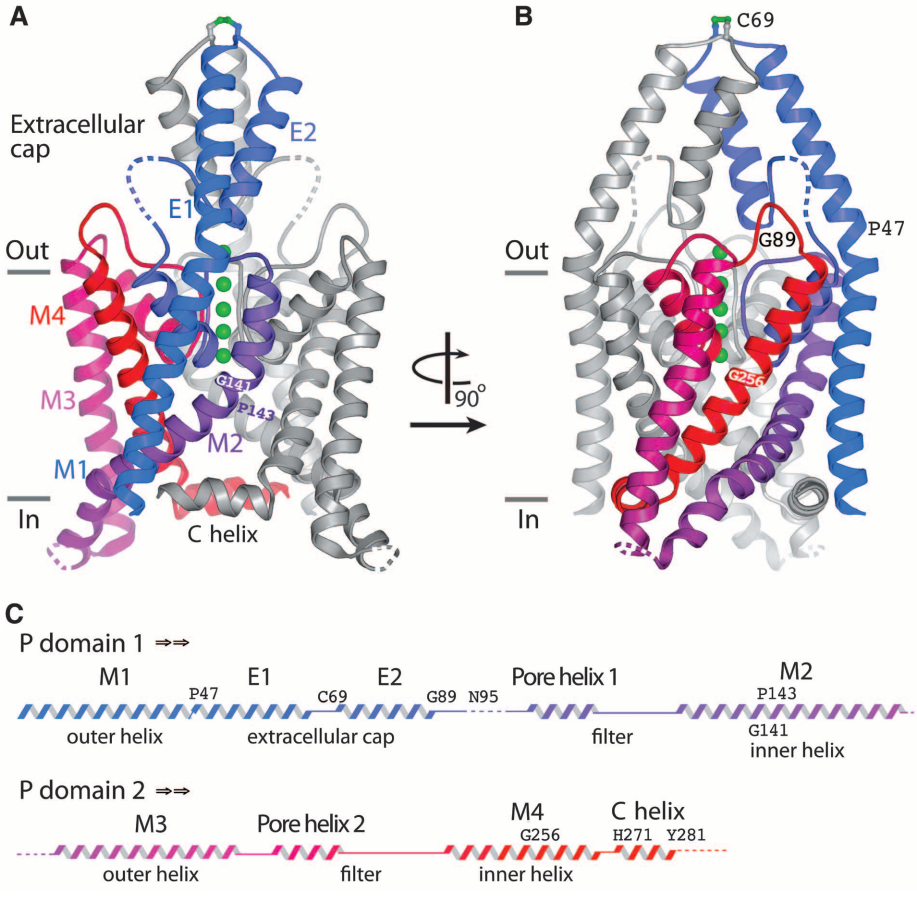


Fig. 1. Overall structure. (**A**) Tertiary structure of K2P1, showing a ribbon representation from the side. One subunit is colored blue-to-red from the N to the C terminus, and the other subunit is gray. K^+ ions are shown as green spheres. Approximate boundaries of the lipid membrane are shown as horizontal lines. The intersubunit disulfide bond (involving Cys^{69}) at the apex of the extracellular cap is colored green. Loop regions not included in the final model are indicated as dashed lines. The central cavity is located just below the K^+ ions along the symmetry axis (behind Gly^{141}). (**B**) An orthogonal view of the channel from the side. (**C**) Secondary structure of K2P1 colored according to (A). Dashed lines indicate disordered regions. Residues discussed in the text are labeled.

Structure determination. For crystallization, human K2P1 was truncated to amino acids 19 to 288 [removing 18 residues from the N terminus and 48 residues from the C terminus that are not well conserved among K2P channel families (fig. S1A)]. Cys^{22} and Asn^{95} were mutated to prevent nonspecific disulfide formation and glycosylation, respectively. The protein was expressed in *Pichia pastoris*, and a flux assay confirmed that the purified protein forms functional K^+ channels when reconstituted into lipid vesicles (fig. S2).

K2P1 crystallized in the $P2_1$ space group with four copies of the polypeptide in the asymmetric unit assembled into two channels. The crystals were grown in the presence of 150 mM K^+ and diffracted x-rays to 3.4 Å resolution. Experimental phases were derived from diffraction data collected from crystals containing mercury, gold, and thallium derivatives. The heavy atoms bound to cysteine residues within the M2, M3, and M4 transmembrane helices and served as guides in building the atomic model. Difference Fourier maps indicated that the thallium ions (Tl^+), which are usually permeant in K^+ channels (*23*), were bound within the selectivity filter. The phases, which were improved by noncrystallographic symmetry averaging, yielded an electron density map that allowed placement of the majority of the amino acid side chains (fig. S3). The coordinates were refined to yield a model with good stereochemistry and an R_{free} value of 27.9% (table S1).

Molecular architecture. Although dimeric, K2P1 recapitulates the fundamental architecture of tetrameric K^+ channels, and it also reveals differences that give insight into gating and ion permeation (Fig. 1). P domains 1 and 2 are arranged in a clockwise fashion when viewed from the extracellular side of the membrane. The ion conduction pathway below the selectivity filter is lined by inner helices that constitute the inner gate (also called the activation gate) in other K^+ channels (Figs. 1 and 2) (*24*). The inner helices of K2P1 are separated by >11 Å, suggesting that the channel is crystallized in an open conformation (Fig. 2B). Near the center of the membrane, the M2 inner helix is kinked by approximately 20° at a proline residue (Pro^{143}) that is conserved in K2P channels (except the THIK subfamily) (Fig. 1A and fig. S1A). As in tetrameric K^+ channels, a central cavity is located just below the selectivity filter, near the center of the membrane (Figs. 1 and 2B). Pore helices, which surround the selectivity filter, are arranged with the negative ends

Downloaded from www.sciencemag.org on January 27, 2012

of their helix-dipole moments oriented toward the central cavity and could serve to stabilize a cation within it (*20*, *25*, *26*).

In addition to an extracellular domain, the salient differences between the structure of K2P1 and those of other K^+ channels are an amphipathic helix located near the membrane/cytosol interface, a disparate extracellular ion pathway, and a subunit interface that exposes the central cavity to the lipid membrane.

Extracellular cap domain. In other K^+ channel families, the connection between the outer helix and the pore helix (called the turret) is typically 5 to 20 amino acids (fig. S1A) (*20*). In K2P1, the 56 amino acids between M1 and pore helix 1 form a structured domain that extends approximately 35 Å above the lipid membrane (Fig. 1, A and B). The domain, which we refer to as the extracellular cap, contains two helices (E1 and E2) from each subunit that form a structure resembling an A-frame that is positioned directly above the extracellular side of the selectivity filter. The proximity of the extracellular region to the selectivity filter was predicted from studies of the TASK-3 K2P channel (*27*), suggesting that this is a common element of K2P channels. A proline residue that is conserved among K2P channels (Pro^{47}) is located within a bend of ~30° between the M1 helix and the E1 helix (Fig. 1). Cys^{69}, which is located in the turn between the E1 and E2 helices at the apex of the extracellular cap and conserved in most K2P channels, forms a disulfide bond that covalently links the two subunits together. This disulfide cross-link was predicted from biochemical experiments (*21*). The E2 helices form a hydrophobic core within the extracellular cap through the interaction of hydrophobic amino acids along their length with both the E1 helix of the same subunit and the E2 helix of the adjacent subunit (Fig. 1 and fig. S1A). The C-terminal ends of the E2 helices, one from each subunit, are positioned with the negative ends of their helix dipole moments above and to either side of the selectivity filter. Residues following the E2 helix (90 to 93) extend away from the selectivity filter following a sharp bend that occurs at a conserved glycine (Gly^{89}) and pack against the E2 helix. This positions the remaining residues preceding pore helix 1 away from the selectivity filter. Several of these (94 to 99) are disordered. The extracellular cap creates an extracellular ion pathway that is markedly different from that observed in other K^+ channel structures (discussed in greater detail below).

Interfacial C helix and inner helix gating. Comparing crystal structures of K^+ channels with open and closed inner gates has allowed conformational changes underlying inner helix gating to be deduced (*24*). A glycine residue located on the inner helices near the midpoint of the membrane serves as a gating hinge that permits the inner helices to bend as they constrict and dilate the pore near the intracellular side (fig. S4, E and F) (*24*). In K2P channels, corresponding glycine residues (Gly^{141} and Gly^{256} in K2P1) are strictly conserved in both inner helices (Fig. 1 and fig. S1A), which suggests that the inner helices may move in analogous fashion. In the structure, the inner helices create a pore that has similar dimensions to other K^+ channels with open inner gates (Fig. 2B and fig. S4E). Some studies support the hypothesis that the inner gates of K2P channels function similarly to other K^+ channels (*28*, *29*). In a study of TREK-1, however, quaternary ammonium compounds such as tetrahexylammonium (THA) freely accessed the central cavity before channel activation, which was interpreted to mean that the inner gate is constitutively open (*30*). The structure of K2P1 raises the alternative possibility that THA, which is lipophilic, might also be able to access its binding site via openings in the transmembrane region that expose the central cavity to the membrane.

In the structure of the voltage-dependent K^+ channel Kv1.2, a helix at the membrane/cytosol interface (the S4-S5 helix) couples the voltage sensor to the inner gate (*31*, *32*). In K2P channels, amino acids following the M4 helix have been experimentally shown to play a role in gating (*9*–*12*, *14*, *15*, *33*). In K2P1, we find that these residues (His^{271}-Tyr^{281}) form an amphipathic helix (the C helix) at the membrane/cytosol interface that is reminiscent of the S4-S5 helix of Kv1.2 (Fig. 2). The C helix lies roughly parallel to the membrane, following a bend of ~80° (at Leu^{270}) from M4, with its hydrophobic and hydrophilic residues oriented toward and away from the membrane core, respectively (Fig. 2A). Lys^{274}, the potential site of SUMO modification (*16*, *17*), is located on it (Fig. 2A). The C-terminal end of the C helix reaches across the dimer interface and is positioned between the M1 and M2 helices of the adjacent subunit (Figs. 1A and 2). The C helix is therefore coupled to two inner helices: the M4 helix to which it is covalently connected and

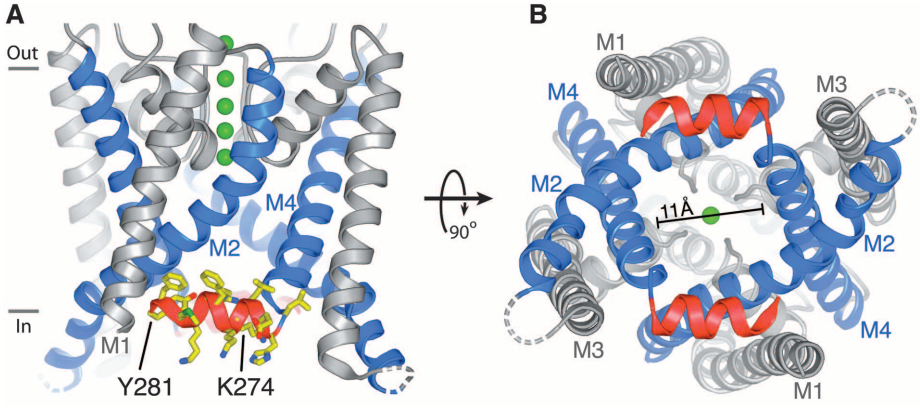
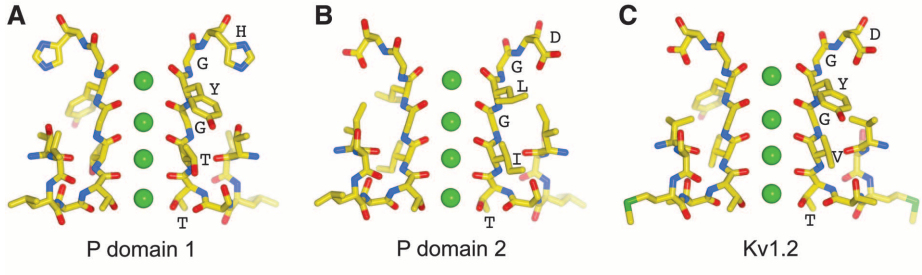


Fig. 2. Interfacial C helix. Ribbon representation of the transmembrane and intracellular regions of K2P1 viewed from the membrane (**A**) and intracellular side (**B**). The inner helices are colored blue, the C helices are red, and the remaining portions are gray. K^+ ions are shown as green spheres. In (A), residues on the C helix in the foreground are drawn as sticks (yellow, carbon; blue, nitrogen; red, oxygen; green, sulfur).



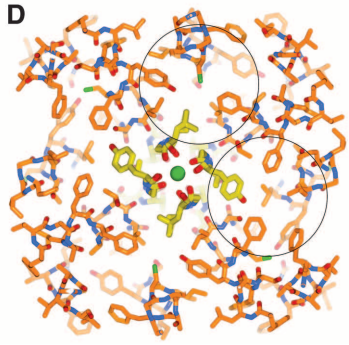


Fig. 3. Selectivity filter. (**A** to **C**) Conformation of amino acids comprising the selectivity filter from P domain 1 (A) and P domain 2 (B) compared with the selectivity filter of Kv1.2 (C) (PDB ID 2R9R). Two subunits are shown from the side, with the extracellular solution located above. The filter sequence is labeled in single-letter amino acid code (D, Asp; G, Gly; H, His; I, Ile; L, Leu; T, Thr; V, Val; Y, Tyr). Amino acids are drawn as colored sticks (yellow, carbon; blue, nitrogen; red, oxygen; and green, sulfur), and K^+ ions are depicted as green spheres. (**D**) Depiction of a ~10 Å–thick cross section of K2P1, viewed from the extracellular side, showing the packing of residues (orange-colored carbons) surrounding the selectivity filter (yellow-colored carbons). Circles highlight differences in packing surrounding the selectivity filter residues of P domains 1 and 2. K^+ ions are drawn as green spheres.

Downloaded from www.sciencemag.org on January 27, 2012

the M2 helix of the adjacent subunit (Fig. 2). The C helix appears structurally poised to affect inner helix gating.

The regions in other K2P channels that correspond to the C helix of K2P1 serve as part of the gating apparatus that responds to various stimuli, including certain phospholipids, intracellular acidification, and membrane stretch (*9*–*12*, *14*, *15*). This region of TREK-1, which is predicted to be helical from sequence analysis, associates with the plasma membrane in a dynamic manner that is correlated with channel gating, consistent with the idea that it may be a mobile gating element (*14*, *34*). In the conformation of K2P1 observed in the crystal structure, the C helix may stabilize an open gate by separating the inner helices. Further experiments are necessary to understand the coupling of this region to channel gating and determine whether these mechanisms vary among K2P channels.

Selectivity filter. In the selectivity filters of tetrameric K^+ channels, dehydrated K^+ ions are coordinated by backbone carbonyl oxygens and a threonine side chain that are arranged in a four-fold symmetric configuration that mimics the hydration of K^+ ions (*35*). In K2P1, the amino acid sequences comprising the selectivity filter differ between P domains 1 and 2 (TTGYGH and TIGLGD) and deviate from the "canonical" K^+ channel filter sequence TXGYGD, where X represents an aliphatic amino acid (Fig. 3 and fig. S1A). In the assembled channel, the packing of the side chains surrounding the selectivity filter is two-fold symmetric (Fig. 3D). However, at the limit of accuracy with which atomic positions can be determined in the K2P1 structure, the coordination of ions within the filter is four-fold symmetric and the amino acids comprising the selectivity filter adopt a conductive configuration (Fig. 3) (*35*). Thr^{118}, the second T of the TTGYGH filter sequence, is associated with the ability of K2P1 to conduct Na^+ when the extracellular K^+ concentration is below ~3 mM, which occurs during hypokalemia (*7*). In the crystal, which was grown in 150 mM K^+, the side chain of Thr^{118} occupies approximately the same three-dimensional space as aliphatic residues normally found in this position, and the backbone is indistinguishable from a canonical conductive conformation (Fig. 3, A to C). Whereas the conformation of the selectivity filter of the prokaryotic K^+ channel KcsA, which has a canonical sequence, has been shown to change when the K^+ concentration is low (*35*), the filter of another K^+ channel (MthK) maintains its conformation in low K^+ (*36*). What conformation the K2P1 filter adopts in low K^+, what effect Thr^{118} has on this, and how Na^+ permeates through it are undetermined. The selectivity filter observed in the dimeric K2P1 channel underscores the idea of a universal mode of K^+ selectivity that incorporates four-fold symmetry of K^+ ion coordination.

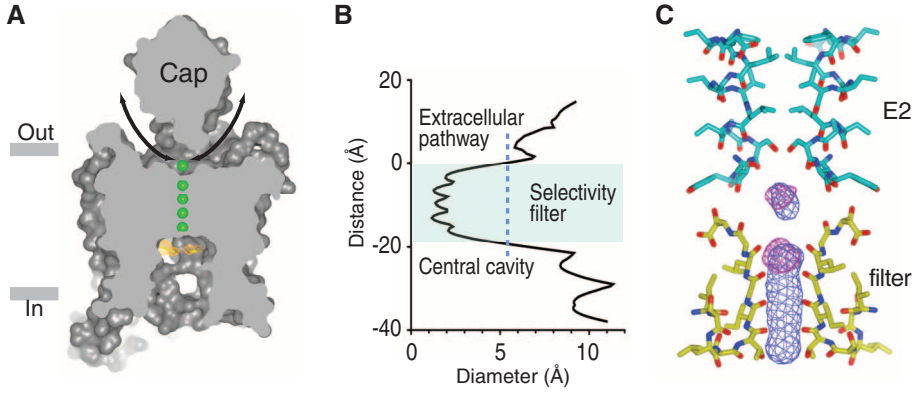


Fig. 4. Extracellular ion pathway. (**A**) Cutaway view of the molecular surface of K2P1 (gray) from the side with the approximate boundaries of the lipid membrane shown as horizontal lines. K^+ ions (four sites in the selectivity filter and one external site) are shown as green spheres. Side portals (arrows) located beneath the extracellular cap connect the selectivity filter with the extracellular solution. Orange mesh depicts electron density assigned to alkyl chains. (**B**) Diameter of the pore (measured as the separation between van der Waals surfaces) as a function of distance along the ion conduction pathway. A dashed line indicates the diameter of a K^+-H_2O complex. The 0 coordinate on the *y* axis corresponds to the location of the external K^+ ion. (**C**) Ion binding in the extracellular pathway. Amino acids of the selectivity filter (yellow-colored carbons, P domain 2) and E2 helices (cyan-colored carbons) are shown as sticks. The orientation is from the side, with a 90° rotation about the vertical axis with respect to (A). Electron density corresponding to potassium ions is shown from a simulated-annealing omit F_o-F_c map (blue mesh, calculated from 20 to 3.4 Å resolution and contoured at 4 σ). A Tl^+ isomorphous difference Fourier map is also shown (red mesh, calculated from 20 to 6.2 Å resolution and contoured at 4 σ).

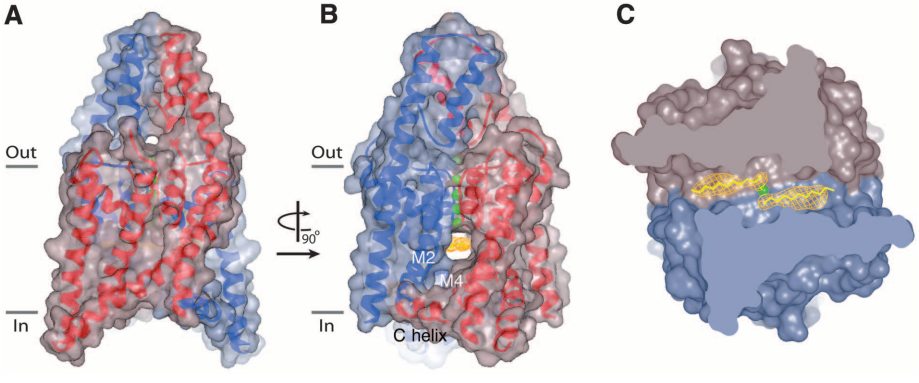


Fig. 5. Molecular surface and subunit interface. (**A**) View of the molecular surface, which has been made partially transparent to reveal a ribbon representation of the channel, from the side with the extracellular solution above. One subunit of the dimer is colored blue and the other red. (**B**) Orthogonal view from the side. Electron density (orange mesh, F_o-F_c simulated annealing omit map calculated from 20 to 3.4 Å resolution and contoured at 3 σ) is present within an opening between the subunits. Stereo representations of (A) and (B) are shown as supplementary information (fig. S5, A and B). (**C**) Cutaway view of the molecular surface viewed from the intracellular side, with one subunit colored blue and the other red. The intracellular-most K^+ ion in the selectivity filter is depicted as a green sphere (center). Electron density (orange mesh), calculated as in (B), is shown for what is interpreted as alkyl chains (yellow sticks).

Extracellular ion pathway. K2P1 has a distinct extracellular ion pathway compared with the structures of other K^+ channels (Fig. 4). The extracellular cap restricts access to the selectivity filter, allowing the passage of K^+ ions only through two side portals (Fig. 4A, arrows). The portals are funnel-shaped, and their narrow ends meet above the selectivity filter. The van der Waals surface of the opening at the narrow end is approximately 6 Å across (~9 Å measured between atom positions) (Fig. 4B). The size of the portals would allow K^+ ions to move through while remaining hydrated (Fig. 4B). The walls lining the side portals are predominantly negatively charged (contributed in part by Glu^{84}, Ser^{86}, Asn^{87}, Ser^{91}, and Glu^{235}) (fig. S5C). Notably, the C-terminal ends of the E2 helices (one from each subunit) also line the portals above the selectivity filter (Fig. 1B and Fig. 4C). The negative electrostatic potential at the C-terminal end of these helices, which arises from the helix dipole effect (*37*–*40*), would raise the local concentration of cations near the mouth of the selectivity filter while lowering the concentration of anions. The electron density maps are consistent with a K^+ ion that is coordinated by two water molecules bound in an external site outside the filter (Fig. 4C and fig. S6). This assignment is confirmed by the 6-σ peak in a difference Fourier electron density map calculated

Downloaded from www.sciencemag.org on January 27, 2012

using diffraction data from a crystal soaked in Tl^+, an electron-rich surrogate for K^+ (*23*) (Fig. 4C).

Sequence alignments indicate that several of the residues that line the side portals vary among K2P channels (fig. S1A). This may account for some of the electrophysiological differences between K2P channels (*4*) and suggests that it may be possible to block the extracellular ion pathway with channel-specific drugs. The presence of the extracellular cap explains why protein toxins that block the pores of many tetrameric K^+ channels from the extracellular side are ineffective against K2P channels (*5*, *41*, *42*). Members of the Kir family of tetrameric K^+ channels are also relatively insensitive to these toxins, and this is attributed to the particularly large turrets (containing ~20 amino acids) of these channels on the extracellular side (*43*). In addition to conferring resistance to toxins, it is possible that the extracellular cap serves as a binding site for endogenous extracellular factors that modulate K2P channel activity.

Subunit interface. K2P1 has an unusual transmembrane molecular surface that may have important functional consequences. The two P domains within each K2P1 subunit form a continuous molecular surface throughout the transmembrane region (Fig. 5A). However, the surface formed at the interface between the two subunits is markedly different from the intramolecular surface and from the transmembrane surfaces of tetrameric K^+ channel structures determined to date (Fig. 5B). In K2P1, openings between the subunits expose the central cavity to the hydrophobic core of the lipid membrane. The two openings, one on each side of the dimer, are sealed off at the top at the level of the selectivity filter and at the bottom by the C helix and consequently span much of what would correspond to the inner leaflet of the membrane. They are located between the M2 helix of one subunit and the M4 helix of the other (Figs. 1A and 5B). The separation between these helices arises from M4 being more perpendicular to the membrane than M2 and from a bend in M2 that occurs at Pro^{143}. Pro^{143} is conserved in most K2P channels, suggesting that analogous openings may be present in other K2P channels.

Electron density maps revealed tubes of density within the openings just below the selectivity filter (Fig. 5, B and C). The density is consistent with two alkyl chains of about 11 carbons each. The alkyl chains could arise from detergent used in purification or from bound lipids that copurified with K2P1. Two lines of evidence support the binding of alkyl chains within the openings. First, the recently determined crystal structure of a prokaryotic voltage-dependent Na^+ channel contains analogous openings (termed fenestrations) (*44*). The fenestrations were filled with electron density that could be attributed to lipid alkyl chains, suggesting that this may be a property common to other channels. Second, lipids are known to affect TREK-1 channel function, and residues that play a role in lipid sensing correspond to positions along the C helix of K2P1, which is located directly below the openings (*9*–*12*, *45*). The openings may provide a way for hydrophobic K^+ channel inhibitors, such as THA, to reach the central cavity via the membrane and suggest that screening of lipophilic compounds may be an effective strategy for ion channel drug discovery. The openings create a physical connection between the membrane and the ion pore and thus may be a means of coupling properties of the membrane such as lipid composition or mechanical tension with K2P channel function.

References and Notes

1. A. L. Hodgkin, A. F. Huxley, *J. Physiol.* **106**, 341 (1947).
2. A. L. Hodgkin, A. F. Huxley, *J. Physiol.* **117**, 500 (1952).
3. A. L. Hodgkin, B. Katz, *J. Physiol.* **108**, 37 (1949).
4. P. Enyedi, G. Czirják, *Physiol. Rev.* **90**, 559 (2010).
5. F. Lesage *et al.*, *EMBO J.* **15**, 1004 (1996).
6. M. Zhou *et al.*, *J. Neurosci.* **29**, 8551 (2009).
7. L. Ma, X. Zhang, H. Chen, *Sci. Signal.* **4**, ra37 (2011).
8. K. Kjeldsen, *Exp. Clin. Cardiol.* **15**, e96 (2010).
9. A. J. Patel *et al.*, *EMBO J.* **17**, 4283 (1998).
10. F. Maingret, A. J. Patel, F. Lesage, M. Lazdunski, E. Honoré, *J. Biol. Chem.* **274**, 26691 (1999).
11. A. J. Patel *et al.*, *Nat. Neurosci.* **2**, 422 (1999).
12. F. Maingret *et al.*, *EMBO J.* **19**, 2483 (2000).
13. A. Dedman *et al.*, *Eur. Biophys. J.* **38**, 293 (2009).
14. J. Chemin *et al.*, *EMBO J.* **24**, 44 (2005).
15. E. Honoré, F. Maingret, M. Lazdunski, A. J. Patel, *EMBO J.* **21**, 2968 (2002).
16. S. Rajan, L. D. Plant, M. L. Rabin, M. H. Butler, S. A. Goldstein, *Cell* **121**, 37 (2005).
17. L. D. Plant *et al.*, *Proc. Natl. Acad. Sci. U.S.A.* **107**, 10743 (2010).
18. S. Feliciangeli *et al.*, *J. Biol. Chem.* **285**, 4798 (2010).
19. S. Feliciangeli *et al.*, *Cell* **130**, 563 (2007).
20. D. A. Doyle *et al.*, *Science* **280**, 69 (1998).
21. F. Lesage *et al.*, *EMBO J.* **15**, 6400 (1996).
22. R. MacKinnon, *Angew. Chem. Int. Ed. Engl.* **43**, 4265 (2004).
23. Y. Zhou, R. MacKinnon, *J. Mol. Biol.* **333**, 965 (2003).
24. Y. Jiang *et al.*, *Nature* **417**, 523 (2002).
25. Y. Zhou, R. MacKinnon, *Biochemistry* **43**, 4978 (2004).
26. B. Roux, R. MacKinnon, *Science* **285**, 100 (1999).
27. C. E. Clarke, E. L. Veale, K. Wyse, J. I. Vandenberg, A. Mathie, *J. Biol. Chem.* **283**, 16985 (2008).
28. Y. Ben-Abu, Y. Zhou, N. Zilberberg, O. Yifrach, *Nat. Struct. Mol. Biol.* **16**, 71 (2009).
29. I. Ashmole *et al.*, *J. Physiol.* **587**, 4769 (2009).
30. P. L. Piechotta *et al.*, *EMBO J.* **30**, 3607 (2011).
31. S. B. Long, E. B. Campbell, R. Mackinnon, *Science* **309**, 897 (2005).
32. S. B. Long, E. B. Campbell, R. Mackinnon, *Science* **309**, 903 (2005).
33. Y. Kim, H. Bang, C. Gnatenco, D. Kim, *Pflugers Arch.* **442**, 64 (2001).
34. G. Sandoz, S. C. Bell, E. Y. Isacoff, *Proc. Natl. Acad. Sci. U.S.A.* **108**, 2605 (2011).
35. Y. Zhou, J. H. Morais-Cabral, A. Kaufman, R. MacKinnon, *Nature* **414**, 43 (2001).
36. S. Ye, Y. Li, Y. Jiang, *Nat. Struct. Mol. Biol.* **17**, 1019 (2010).
37. D. J. Lockhart, P. S. Kim, *Science* **260**, 198 (1993).
38. D. J. Lockhart, P. S. Kim, *Science* **257**, 947 (1992).
39. J. Aqvist, H. Luecke, F. A. Quiocho, A. Warshel, *Proc. Natl. Acad. Sci. U.S.A.* **88**, 2026 (1991).
40. D. Sali, M. Bycroft, A. R. Fersht, *Nature* **335**, 740 (1988).
41. P. Hidalgo, R. MacKinnon, *Science* **268**, 307 (1995).
42. M. Fink *et al.*, *EMBO J.* **17**, 3297 (1998).
43. X. Tao, J. L. Avalos, J. Chen, R. MacKinnon, *Science* **326**, 1668 (2009).
44. J. Payandeh, T. Scheuer, N. Zheng, W. A. Catterall, *Nature* **475**, 353 (2011).
45. J. Chemin *et al.*, *J. Biol. Chem.* **280**, 4415 (2005).

Acknowledgments: We thank the staff of beamlines X25 and X29 (National Synchrotron Light Source, Brookhaven National Laboratory) for assistance at the synchrotron; C. D. Lima, N. P. Pavletich, Z. Lu, and members of the Long laboratory for helpful discussions; and N. P. Pavletich, M. B. Long, and J. P. Greenfield for comments on the manuscript. This work was supported in part by a Burroughs Wellcome Career Award in the Biomedical Sciences and by a Gerstner Young Investigator Award to S.B.L. Coordinates and structure factors have been deposited in the Protein Data Bank (PDB ID 3UKM).

Supporting Online Material

www.sciencemag.org/cgi/content/full/335/6067/432/DC1
Materials and Methods
Figs. S1 to S6
Table S1
References (*46*–*62*)

29 August 2011; accepted 8 December 2011
10.1126/science.1213274

Crystal Structure of the Human K2P TRAAK, a Lipid- and Mechano-Sensitive K^+ Ion Channel

Stephen G. Brohawn, Josefina del Mármol, Roderick MacKinnon*

TRAAK channels, members of the two–pore domain K^+ (potassium ion) channel family K2P, are expressed almost exclusively in the nervous system and control the resting membrane potential. Their gating is sensitive to polyunsaturated fatty acids, mechanical deformation of the membrane, and temperature changes. Physiologically, these channels appear to control the noxious input threshold for temperature and pressure sensitivity in dorsal root ganglia neurons. We present the crystal structure of human TRAAK at a resolution of 3.8 angstroms. The channel comprises two protomers, each containing two distinct pore domains, which create a two-fold symmetric K^+ channel. The extracellular surface features a helical cap, 35 angstroms tall, that creates a bifurcated pore entryway and accounts for the insensitivity of two–pore domain K^+ channels to inhibitory toxins. Two diagonally opposed gate-forming inner helices form membrane-interacting structures that may underlie this channel's sensitivity to chemical and mechanical properties of the cell membrane.

Cellular electrical signaling relies on a resting potential difference that originates in the membrane's permeability to K^+ (*1*). Termed "potassium leakage" by Hodgkin and Huxley (*2*), cellular leak currents are approximated by the behavior of constitutively open

Downloaded from www.sciencemag.org on January 27, 2012

K^+-selective pores but deviate in detail, suggesting more complex underlying channel behavior. Leak K^+ currents are now recognized as resulting from the activity of two–pore domain K^+ ion channels (K2P channels) (*3*). Discovered as the final member of the K^+ channel family (*4*–*6*), K2P channels have remained less well characterized than other K^+ channels. Perhaps the prospect of studying simple "leakage" has somewhat delayed progress.

The view of K2P channels as passive K^+ leaks has recently changed. K2P channels control the resting potential in many cells, and their regulation can directly tune cellular excitability. K2P channels have among the most varied sets of ion channel modulators, including mechanical force, temperature, lipid interaction, voltage, pH, post-translational modification, and accessory protein interaction (*3*, *7*, *8*). Pharmacologically, K2P channels are targets of antidepressants, inhalational anesthetics, neuroprotective agents, and respiratory stimulants (*9*–*12*). Their deregulation underlies human pathophysiologies including Birk-Barel syndrome and familial migraine with aura (*13*, *14*).

K2P channels constitute one of five clades within the K^+ channel superfamily (fig. S1, A and B). Although their sequences are diverse (figs. S1C and S2), K2P channels have two shared characteristics. First, K2P channels contain two concatenated pore domains on a single protein chain protomer (fig. S1A); each pore domain contains an outer and inner membrane-spanning helix flanking a membrane-reentrant segment that forms a pore helix and K^+ selectivity filter. K^+ channels of known structure have one pore domain per protomer and form four-fold symmetric tetramers. Second, K2P channels contain a segment of ~60 amino acids on the extracellular side of the first pore domain. This segment has often been referred to as a "loop," and its role in channel function has been unknown.

The best-studied subfamily of K2P channels includes TRAAK (TWIK-related arachidonic acid–stimulated K^+ channel), TREK-1, and TREK-2 (fig. S3) (*15*–*17*). Unlike other K2P channels, they are mechanosensitive and modulated by polyunsaturated fatty acids and temperature (*18*–*21*). Physiologically, TRAAK and TREK-1 appear to regulate the noxious input threshold for temperature and pressure sensitivity in mouse dorsal root ganglia (*22*). These channels are highly sensitive to the structure and chemical composition of the lipid bilayer, but a mechanistic

Laboratory of Molecular Neurobiology and Biophysics and Howard Hughes Medical Institute, The Rockefeller University, 1230 York Avenue, New York, NY 10065, USA.

*To whom correspondence should be addressed. E-mail: mackinn@mail.rockefeller.edu

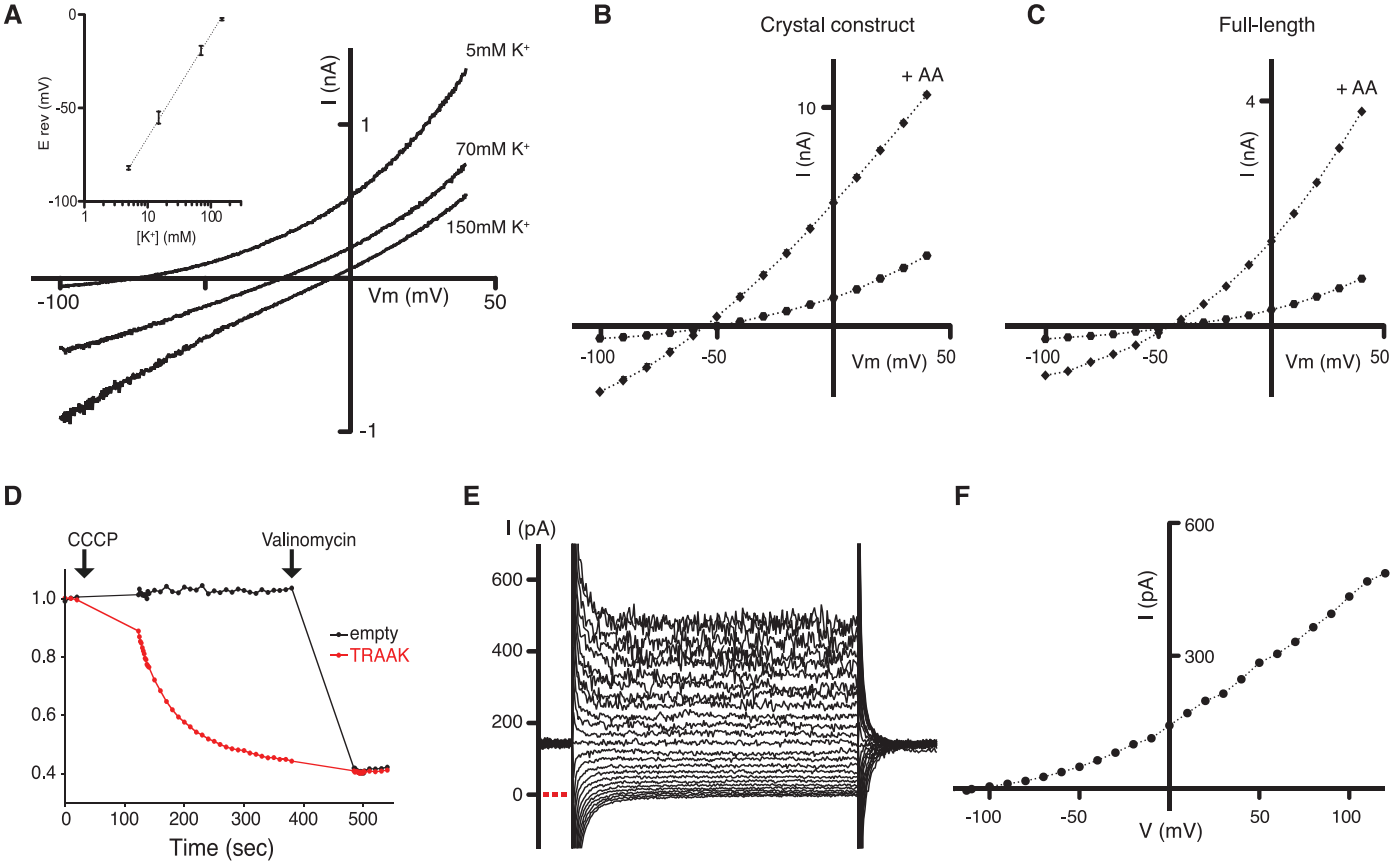


Fig. 1. Analysis of TRAAK channel activity. (**A**) Macroscopic currents from Chinese hamster ovary (CHO) cells expressing the crystal construct of TRAAK. Current was measured in whole-cell mode during a voltage ramp from –100 mV to 40 mV from a holding potential of –80 mV in 800 ms. Curves recorded from cells in 5, 70, and 150 mM external $[K^+]$ are displayed. The inset is a plot of reversal potential determined from voltage ramps recorded from cells in 5, 15, 70, and 150 mM external $[K^+]$. (**B**) Arachidonic acid activation of the crystal construct of the TRAAK channel. (**C**) Arachidonic acid activation of the full-length channel. Current-voltage relationship is plotted from whole-cell recordings during voltage pulses from –100 to 40 mV from a holding potential of –80 mV before and after perfusion of arachidonic acid (+AA). (**D**) K^+ flux assay in which K^+ efflux drives the carbonyl cyanide *m*-chlorophenyl hydrazone (CCCP)–mediated uptake of protons, which are detected by fluorophore 9-amino-6-chloro-2-methoxyacridine (ACMA). Vesicles were loaded with 150 mM K^+, 0 mM Na^+, and assayed in buffer with 0 mM K^+, 150 mM Na^+. Relative fluorescence change recorded from TRAAK-reconstituted (red) and empty (black) lipid vesicles is shown. Addition of the K^+ ionophore valinomycin results in flux from crystal construct TRAAK-reconstituted and empty vesicles. (**E**) Current recorded from TRAAK reconstituted into planar lipid bilayers under bi-ionic conditions. Current was recorded during voltage pulses from –120 to 120 mV from a holding potential of 0 mV with internal 150 mM K^+, 0 mM Na^+ and external 0 mM K^+, 150 mM Na^+ by electrophysiological convention. Zero current level is indicated by a dashed red line. (**F**) Current-voltage relationship plotted from data in (E).

Downloaded from www.sciencemag.org on January 27, 2012

rationale for these biophysical properties has not been possible in the absence of structural information.

Crystal structure of TRAAK. Human TRAAK was recombinantly expressed and purified from *Pichia pastoris*. Diffracting crystals were obtained by mutating two consensus N-linked glycosylation sites ($Asn^{104} \rightarrow Gln$, $Asn^{108} \rightarrow Gln$), and the predicted intrinsically unstructured C-terminal region was truncated (to Gln^{300}). Four complementary approaches were taken to assess the functional integrity of this modified construct. First, macroscopic currents were examined in cells expressing TRAAK (Fig. 1A). Channels displayed approximate time and voltage independence of activation. Current-voltage relationships did not indicate strong rectification. Expressed channels were K^+-selective, as demonstrated by the change in reversal potential as a function of external K^+ concentration [K^+] (Fig. 1A, inset). Second, channel activation by arachidonic acid and mechanical force was examined. TRAAK channels were robustly activated above basal levels after perfusion of arachidonic acid (Fig. 1B). The extent of activation above basal levels by arachidonic acid was comparable to that measured from full-length TRAAK channels (Fig. 1C). Application of positive pressure through the pipette to outside-out patches also activated TRAAK channels (fig. S4). [Future quantitative assessments of the gating response to mechanical perturbation will require simultaneous measurements of pressure and membrane curvature to ascertain tension as the independent variable (*23*).] Third, purified TRAAK was reconstituted into lipid vesicles and examined in a K^+ flux assay. A decrease in fluorescence indicative of K^+ flux was observed from TRAAK-reconstituted, but not empty, vesicles loaded with high [K^+] into buffer without K^+ (Fig. 1D). Fourth, recordings were made with planar lipid bilayers into which purified TRAAK channels were reconstituted (Fig. 1E). The bilayer recordings show voltage-independent channels exhibiting exquisite selectivity for K^+ over Na^+ (Fig. 1F). Taken together, these data show that the channel we have expressed, purified, and crystallized exhibits the fundamental biophysical properties of previously described TRAAK channels (*24*).

Crystals of TRAAK grown in 150 mM KCl diffracted to 3.8 Å. Initial attempts at molecular replacement using known K^+ channel structures were unsuccessful. The structure was thus solved with phases determined from a multiple-wavelength isomorphous replacement with anomalous scattering experiment using a crystal grown in the presence of $TlNO_3$ substituted for KCl. Additional register information was obtained from anomalous scattering data collected from crystals derivatized with CH_3Hg^+ to covalently label cysteine residues. The experimentally phased maps were of sufficient quality to model the majority of the structure (fig. S5), and the final TRAAK

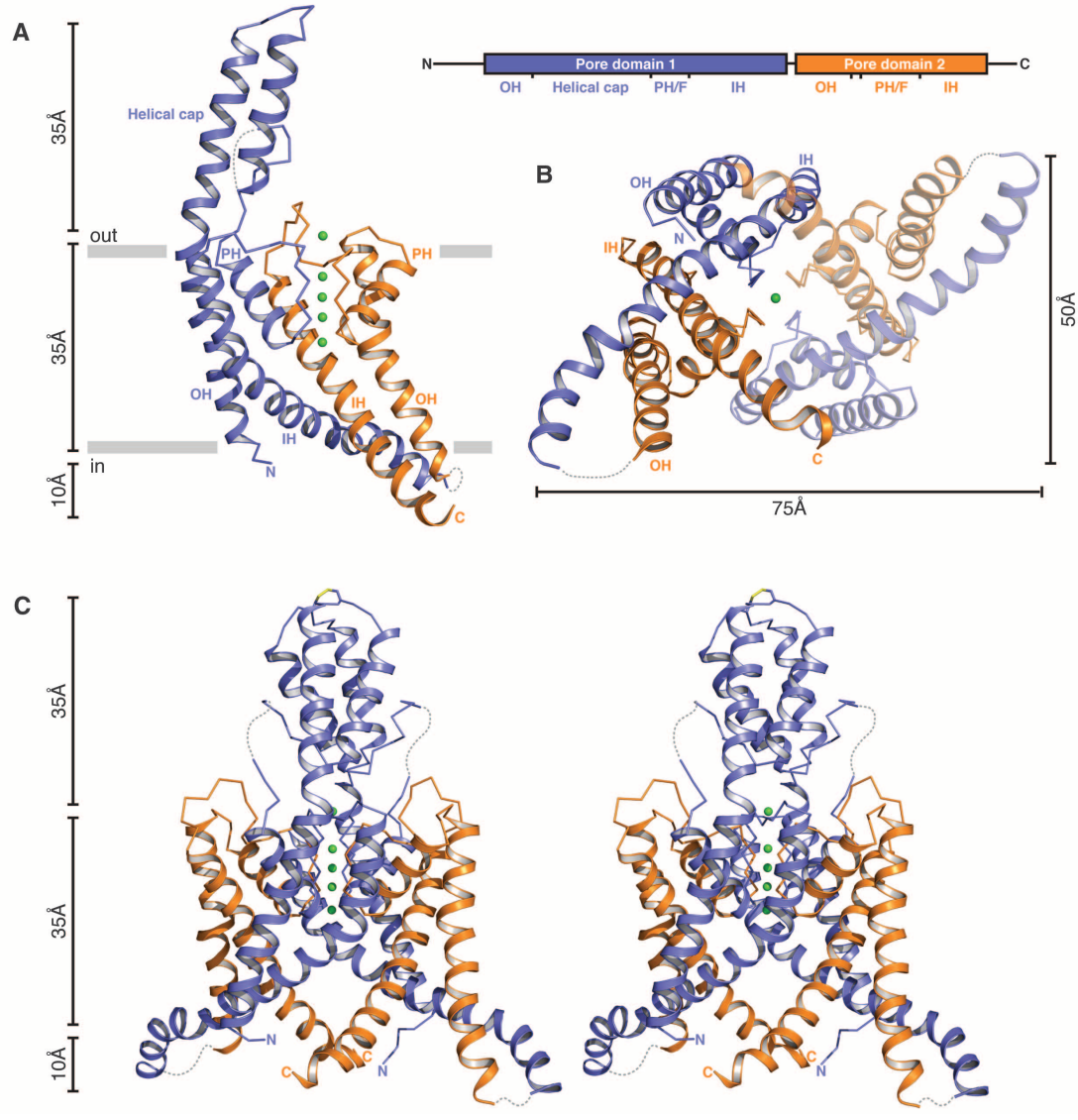


Fig. 2. Structure of TRAAK. (**A**) Left: Ribbon representation of a single TRAAK protomer viewed from the membrane plane with the extracellular solution above. Approximate positions of the lipid bilayer boundaries are indicated as gray bars. Pore domain 1 is colored blue, pore domain 2 is colored orange, and potassium ions are shown as green spheres. Right: Illustration of TRAAK protomer organization. Approximate boundaries of structural features are indicated in the illustration and labeled in the structure: N and C terminus, outer helix (OH), helical cap, pore helix (PH), selectivity filter (F), and inner helix (IH). (**B**) A view of the TRAAK channel from the cytoplasmic solution. The protomer shown in (A) is rotated 90° both into the page and clockwise, and the second protomer is half-transparent. (**C**) Stereo view of TRAAK viewed from the membrane plane with the protomer shown in (A) rotated 90°. The disulfide bond bridging the apex of the helical cap is shown in stick representation, with the cysteine sulfur colored yellow. Note that part of the cytoplasmic extension of protomer B (residues 180 to 187) is not present in the final TRAAK model because of weak electron density features. Here, it is modeled from a superposition of the well-defined region in protomer A for visual clarity. Loops not modeled in the structure because of a lack of interpretable electron density are drawn as dashed gray lines.

Downloaded from www.sciencemag.org on January 27, 2012

model was refined to R_{work}/R_{free} = 31.7/32.3% with good geometry (table S1).

TRAAK crystallized in space group $p2_12_12_1$ with two protomers, each containing two nonidentical pore domains—pore domain 1 and pore domain 2—in the asymmetric unit, forming a single K^+ channel with a molecular two-fold axis (along the K^+ conduction pathway) noncoincident with crystal symmetry axes (fig. S6). Viewed from the bilayer plane, the transmembrane region of the channel spans ~35 Å in height and is formed by the outer helix, pore helix, K^+ selectivity filter, and inner helix from the four pore domains (Fig. 2A). Extensions of the inner helices and the linker between pore domains 1 and 2 protrude ~10 Å further into the cytoplasmic side. On the extracellular side of the transmembrane region is a structural unit we term the helical cap, extending ~35 Å above the membrane. The helical cap is not observed in other ion channels of known structure. When viewed from the cytoplasmic side of the membrane, the channel is rhomboid-shaped; the inner helices of pore domain 1 are separated by ~75 Å across a long axis, whereas the inner helices of pore domain 2 are separated by ~50 Å across a short axis (Fig. 2B).

Structural asymmetry in TRAAK. Structural differences between pore domains 1 and 2 in each protomer of TRAAK result in deviation from the four-fold symmetry of known K^+ channel structures and generate an approximately two-fold symmetric channel instead (Fig. 2C). Differences between TRAAK pore domains 1 and 2 are most evident in three regions: the outer helix–pore helix connection, the filter–inner helix connection, and the inner helix (fig. S7A).

The difference between the outer helix–pore helix connections in pore domains 1 and 2 is shown in fig. S7B. In pore domain 1, the ~60–amino acid connection forms a two-helix hairpin extending ~35 Å into the extracellular solution. The helices from each protomer pack together to form the helical cap and are covalently linked by a disulfide bond between interhelix turns at the cap apex. A conserved glycine allows a tight turn at the bottom of the second helix leading to an extended loop containing the N-linked glycosylation sites and connecting to the pore helix. The outer helix–pore helix connection in pore domain 2 forms a short four-residue linker structurally similar to the corresponding "turret"

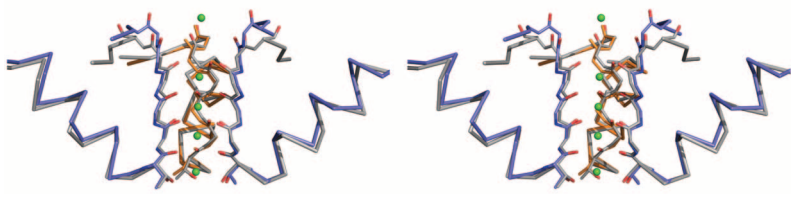


Fig. 3. Convergent symmetry of the TRAAK pore helices and selectivity filter. Stereo view, from the membrane plane with extracellular solution above, shows a comparison between the TRAAK and KcsA (*27*) pore helices and selectivity filters. Pore helices and selectivity filter chains closest to the viewer are removed. Pore helices are shown as wires and selectivity filters as backbone sticks. TRAAK pore domain 1 is blue, TRAAK pore domain 2 is orange, and KcsA is gray, with backbone carbonyl and threonine hydroxyl oxygen atoms from selectivity filter residues shown in red. K^+ positions in TRAAK (green spheres) occupy canonical positions S0 to S4 from the extracellular to the intracellular side.

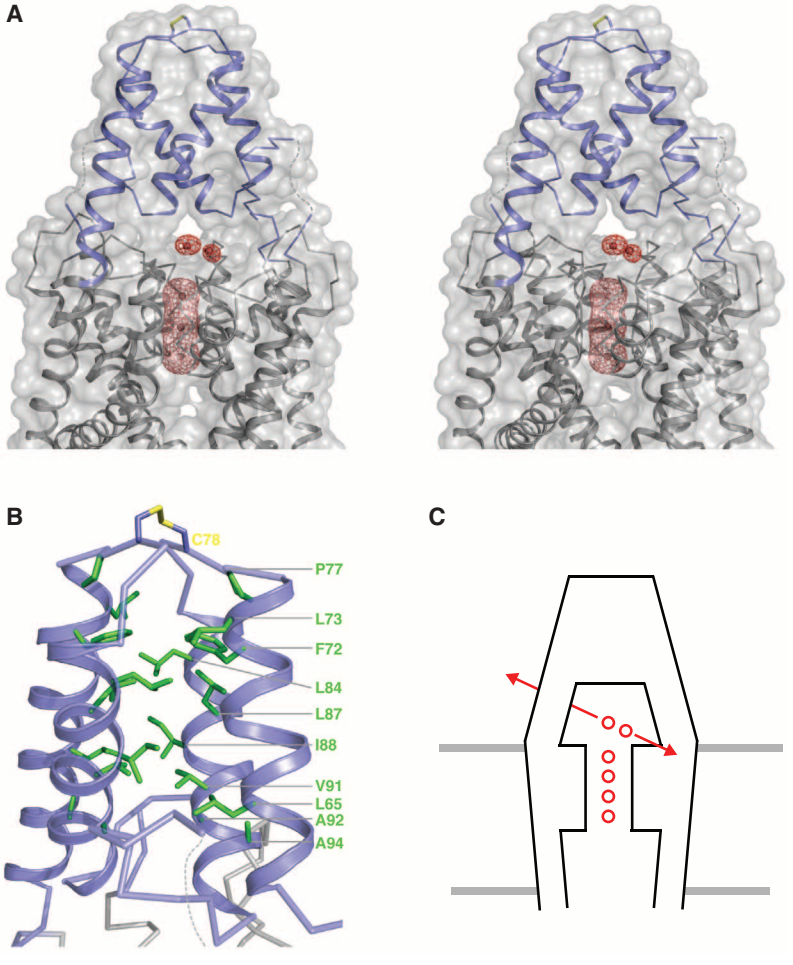


Fig. 4. The TRAAK helical cap. (**A**) Stereo view of the helical cap viewed from the membrane plane with the extracellular solution above. TRAAK is shown as gray ribbons, with the helical cap blue within a semitransparent surface representation. A Tl^+ anomalous-difference Fourier map (red mesh) calculated from 30 to 4.2 Å and contoured at 6σ is shown around Tl^+ ions (red spheres). (**B**) The hydrophobic core of the helical cap. The helical cap is shown as a blue ribbon with hydrophobic residues (L65, F72, L73, P77, L84, L87, I88, V91, A92, A94) as green sticks. The C78 disulfide bond is shown as blue sticks with yellow sulfur atoms. Abbreviations: A, Ala; C, Cys; F, Phe; I, Ile; L, Leu; P, Pro; V, Val. (**C**) Cartoon depiction of the bifurcated ion pathway created by the TRAAK helical cap. View is analogous to (A). TRAAK (black) in a membrane (gray) coordinates four ions (red circles) in the selectivity filter and one ion directly above in site S0. A sixth ion is present in one of the two possible extracellular access/egress pathways (red arrows) that extend into the page and toward the viewer. The TRAAK helical cap blocks ion access from above and laterally in the image plane.

Downloaded from www.sciencemag.org on January 27, 2012

regions in the prokaryotic K^+ channel MthK (*25*) and the nonselective cation channel NaK (*26*) (fig. S8).

The difference between the selectivity filter–inner helix connections in pore domains 1 and 2 is shown in fig. S7C. In pore domain 1, this connection is short and forms an interaction network conserved in most K^+ channel structures tethering the extracellular end of the outer helix and inner helix (fig. S9), whereas in pore domain 2, this connection is longer and forms an extended bridge to the inner helix. The interaction network observed in pore domain 1 is absent because of the extended linker and lateral displacement of the pore domain 2 inner helix from the channel core.

The difference between the inner helices in pore domains 1 and 2 is shown in fig. S7D. The pore domain 1 inner helix is kinked halfway through the bilayer and projects toward the cytoplasmic side at an angle ~25° more acute to the membrane plane than the pore domain 2 inner helix. Pro^{155}, two residues C-terminal to the hinge glycine conserved in all K^+ channels, permits this helix distortion because of its lack of a hydrogen bond donor at the backbone amide position. Pro^{155} is conserved in K2P channel pore domain 1 inner helices [except in THIK-1,2 (fig. S2)] and not observed in pore domain 2 or in other ion channels. The pore domain 1 inner helix is also longer by three helical turns that lead to the cytoplasmic connection between pore domains 1 and 2.

Convergent four-fold symmetry at the selectivity filter. The pore helix and selectivity filter are the most conserved regions of K^+ channels. The majority of K^+ channel selectivity filters share the canonical sequence Thr-x-Gly-Tyr-Gly-Asp-x (where x denotes a hydrophobic amino acid). In TRAAK, the selectivity filter is made from the sequences Thr-Val-Gly-Tyr-Gly-Asn-Tyr (pore domain 1) and Thr-Ile-Gly-Phe-Gly-Asp-Val (pore domain 2). Comparison of TRAAK to the prototypical K^+ channel KcsA (*27*) demonstrates that the overall two-fold symmetric channel converges to an essentially four-fold symmetric pore helix and selectivity filter (Fig. 3). Only minor deviations due to conservative side chain substitutions between the two TRAAK pore domains were observed. The atomic positions of K^+ coordinating oxygens from selectivity filter residues in TRAAK align well with those from KcsA (root mean square deviation = 0.6 Å). We modeled four K^+ ions in positions S1 to S4 and a fifth ion in the extracellular site S0 on the basis of observed electron density from native crystals grown in 150 mM KCl, Tl^+ positions in derivative crystals determined from anomalous scattering data, and chemical knowledge of the ion conduction pathway. The convergence to nearly perfect four-fold symmetry at the pore helix and selectivity filter in the two-fold symmetric TRAAK channel implies strong evolutionary pressures maintaining the integrity of nature's solution to highly selective K^+ conduction through an ion channel.

The TRAAK helical cap structure and implications for K^+ access and pharmacology. The helical cap is unprecedented in ion channel structures and is likely a conserved feature of K2P channels. The interface between protomers is large (~850 $Å^2$) and forms a complementary hydrophobic core (Fig. 4, A and B). The region is conserved in length among K2P channels, with residues that form the hydrophobic core more conserved than those that are solvent-exposed (fig. S2). The interprotomer disulfide-bonded cysteine is conserved in most K2P channels (fig. S2) and was correctly predicted to covalently link TWIK protomers (*28*). The TRAAK helical cap is modestly askew of the molecular two-fold axis along the ion conduction pathway. This is presumably the result of crystal packing between the helical cap from one channel and a neighboring channel in the crystal (fig. S6). As a result, residues 55 to 60 from one protomer are extended, whereas the rest of the cap displays approximate two-fold symmetry.

What might be the functional ramifications of the helical cap? The rigid helical bundle of the cap is positioned above the mouth of the channel pore tethered to pore domain 1 outer helices, bridging opposite sides of the channel. The surface of the helical cap is far enough above the pore entrance to allow unhindered K^+ access from two sides. However, the cap blocks K^+ access from above and from the two tethered sides, creating a bifurcated extracellular pathway for ions to the pore (Fig. 4, A and C). Consistently, we observed a Tl^+ ion along one branch of the split pathway to the pore in crystals grown in the presence of $TlNO_3$ in place of KCl (Fig. 4, A and C).

K2P channels are not responsive to known K^+ channel blockers including pore-blocking toxins from the extracellular side (*6*, *16*). The TRAAK structure provides a simple explanation for these observations: The presence of the helical cap above the pore would sterically prevent toxin access to the channel mouth. A similar steric occlusion mechanism was proposed for Kir2.2 on the basis of its atypically tall turrets surrounding the pore entrance (*29*). By fully preventing access to the mouth of the channel from above and two

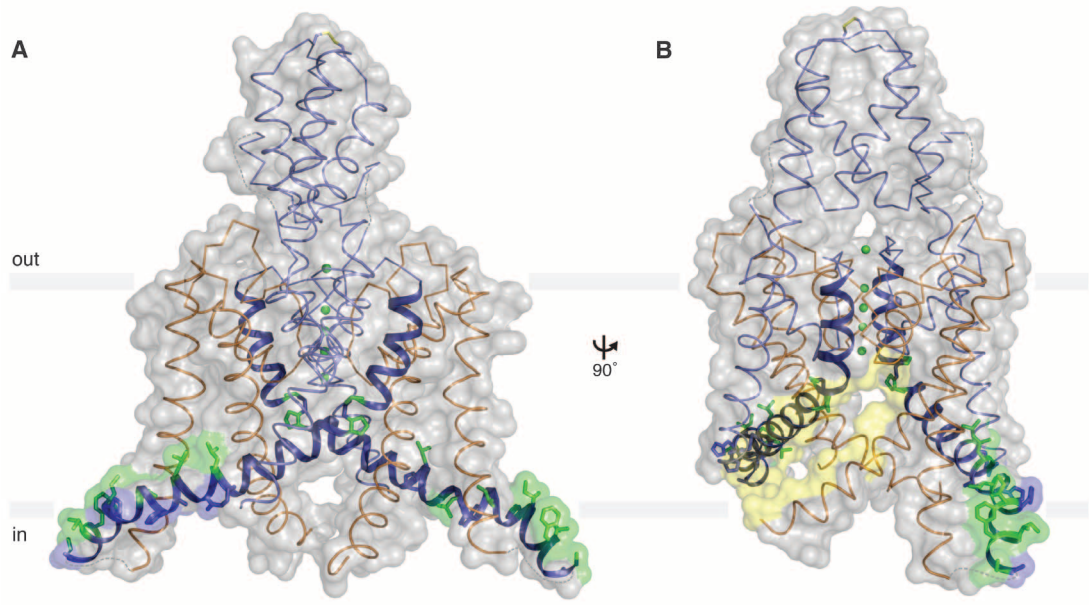


Fig. 5. TRAAK channel inner helices and gating implications. (**A**) View from the membrane, with extracellular solution above, of the amphipathic segment of the pore domain 1 inner helix (as in Fig. 1C). TRAAK is shown in wire representation with inner helices from pore domain 1 as ribbons and key residues as sticks within a semitransparent gray surface. Pore domain 1 is colored blue, pore domain 2 is colored orange, and K^+ ions are shown as green spheres. The hinge glycine (Gly^{153}), kink proline (Pro^{155}), and hydrophobic face of the amphipathic segment (Leu^{168}, Leu^{172}, Ile^{176}, Ile^{179}, Ile^{182}, Phe^{183}, Trp^{186}) are colored green. Basic residues conserved in TRAAK (Arg^{167}, Arg^{173}, His^{174}, His^{178}, Lys^{185}) on the solution accessible face of the amphipathic helix are colored blue. (**B**) A view rotated 90° with respect to (A). The lipid bilayer accessible surface of the lateral opening into the TRAAK channel central cavity closest to the viewer is additionally colored yellow.

Downloaded from www.sciencemag.org on January 27, 2012

sides, the helical cap in K2P channels more effectively restricts molecular access to the pore entryway.

Implications of TRAAK structure for channel gating. The crystal structure of TRAAK has an open inner helical gate (Fig. 2C). The central cavity under the selectivity filter is wide and forms a vestibule continuous with the cytoplasmic solution, presenting no steric hindrance to ion flux. The pore domain 1 inner helices are wide open, with the smallest constriction measuring ~12 Å, similar to the most open configuration observed in MthK (fig. S10) (*25*). The pore domain 2 inner helices are slightly less open, with the smallest constriction measuring ~10 Å, but this is still more open than observed in open-state Kv structures (fig. S10) (*30*).

It is interesting to speculate on the potential for inner helix gating in TRAAK. Recent studies have suggested that the closely related K2P TREK-1 has an inner gate that is constitutively open (*31*, *32*). Three features of the TRAAK pore domain 1 inner helix may be relevant if TRAAK has a similarly constitutively open inner gate: the presence of Pro^{155} that kinks the helix, the nature of the putative membrane interaction region (discussed below), and the peptide linkage to the pore domain 2 outer helix. The combination of these structural features may restrict the ability of the pore domain 1 inner helix to access a closed inner gate conformation.

TRAAK (and TREK) channels are exquisitely responsive to the chemical and mechanical properties of the lipid bilayer. Chemically, TRAAK is activated by arachidonic acid, other polyunsaturated fatty acids, and lysophosphatidic acid by an apparently direct mechanism (*16*, *33*–*35*). Mechanically, applying the equivalent to positive (and not negative) intracellular pressure through a patch pipette reversibly activates TRAAK and TREK (*21*, *34*), whereas hyperosmolarity-induced cell shrinkage reduces TREK currents (*20*). Pressure-induced activation of TRAAK is enhanced upon cytoskeletal disruption or patch excision, which suggests that TRAAK directly responds to the physical state of the bilayer (*21*).

What might be the molecular sensor(s) of the mechanical and chemical state of the bilayer in TRAAK? In TREK channels, a region immediately C-terminal to the intracellular end of the pore domain 2 inner helix has been demonstrated to be involved in activity modulation by mechanical force, lipids and fatty acids, acidic internal pH (pH_i), phosphorylation, and interaction with the accessory protein AKAP150 (*20*, *36*–*40*). The homologous C-terminal region in TRAAK is included in the crystal construct and is partially modeled as a cytoplasmic extension of the pore domain 2 inner helix (Fig. 2). However, this region has not been shown to be involved in TRAAK modulation: TRAAK is not activated by acidic pH_i, TRAAK does not interact with AKAP150, and chimeras exchanging this region with that from TASK K2P channels display unaltered response to arachidonic acid and mechanical force (*34*, *36*, *39*, *41*). Together, these data suggest that an alternative molecular sensor is used for TRAAK lipid activation and mechano-activation.

A distinctive structural feature of TRAAK is illustrated in Fig. 5A. After the kink at Pro^{155}, the pore domain 1 inner helix projects laterally and runs approximately parallel to the cytoplasmic membrane surface. Along this projection the helix is amphipathic. Hydrophobic residues point toward the lipid bilayer along one face opposite a series of basic residues (Arg^{167}, Arg^{173}, His^{174}, His^{178}) pointed toward the membrane-cytoplasm interface. An additional basic residue (Lys^{185}) farther along the helix is also directed toward the same plane. These five residues are conserved in basic character among TRAAK channels (fig. S3). The amphipathic helix is thus positioned to interact with both the hydrophobic tails and acidic head groups of membrane lipids. This structured extension of the pore domain 1 inner helix, which extends like a tendril out into the lipid membrane inner leaflet, may be related to this channel's ability to respond to both mechanical and chemical properties of the cell membrane.

Another consequence of the inner helix structure in TRAAK is illustrated in Fig. 5B. The relative orientation of inner helices creates an extended lateral opening to the central cavity from the membrane. Between the two protomers, a gap ~5 Å wide extends through the bilayer from the bottom of the selectivity filter to the ends of the pore domain 2 inner helix and pore domain 1 outer helix on the cytoplasmic side. Although we observed electron density from the central cavity to the lateral openings in TRAAK, we were not able to confidently assign and model a ligand at this resolution. Lateral openings have been observed in other ion channels, including the K^+ channel KcsA (*27*) and the voltage-gated sodium channel (*42*), but the size and shape of the openings in TRAAK are striking. This bilayer-facing opening results in a large protein surface accessible to the membrane and is a potential site for the interaction of lipids and other hydrophobic molecules with the TRAAK channel.

References and Notes

1. B. Hille, *Ion Channels of Excitable Membranes* (Sinauer, Sunderland, MA, 2001).
2. A. L. Hodgkin, A. F. Huxley, *J. Physiol.* **106**, 341 (1947).
3. P. Enyedi, G. Czirják, *Physiol. Rev.* **90**, 559 (2010).
4. K. A. Ketchum, W. J. Joiner, A. J. Sellers, L. K. Kaczmarek, S. A. Goldstein, *Nature* **376**, 690 (1995).
5. X. L. Zhou, B. Vaillant, S. H. Loukin, C. Kung, Y. Saimi, *FEBS Lett.* **373**, 170 (1995).
6. F. Lesage *et al.*, *EMBO J.* **15**, 1004 (1996).
7. A. Cohen, Y. Ben-Abu, N. Zilberberg, *Eur. Biophys. J.* **39**, 61 (2009).
8. A. Mathie, E. Al-Moubarak, E. L. Veale, *J. Physiol.* **588**, 3149 (2010).
9. A. J. Patel *et al.*, *Nat. Neurosci.* **2**, 422 (1999).
10. J. F. Cotten, B. Keshavaprasad, M. J. Laster, E. I. Eger 2nd, C. S. Yost, *Anesth. Analg.* **102**, 779 (2006).
11. F. Duprat *et al.*, *Mol. Pharmacol.* **57**, 906 (2000).
12. C. Heurteaux *et al.*, *Nat. Neurosci.* **9**, 1134 (2006).
13. R. G. Lafrenière *et al.*, *Nat. Med.* **16**, 1157 (2010).
14. O. Barel *et al.*, *Am. J. Hum. Genet.* **83**, 193 (2008).
15. H. Bang, Y. Kim, D. Kim, *J. Biol. Chem.* **275**, 17412 (2000).
16. M. Fink *et al.*, *EMBO J.* **17**, 3297 (1998).
17. M. Fink *et al.*, *EMBO J.* **15**, 6854 (1996).
18. D. Kang, C. Choe, D. Kim, *J. Physiol.* **564**, 103 (2005).
19. F. Maingret *et al.*, *EMBO J.* **19**, 2483 (2000).
20. A. J. Patel *et al.*, *EMBO J.* **17**, 4283 (1998).
21. F. Maingret, M. Fosset, F. Lesage, M. Lazdunski, E. Honoré, *J. Biol. Chem.* **274**, 1381 (1999).
22. J. Noël *et al.*, *EMBO J.* **28**, 1308 (2009).
23. L. R. Opsahl, W. W. Webb, *Biophys. J.* **66**, 75 (1994).
24. F. Lesage, F. Maingret, M. Lazdunski, *FEBS Lett.* **471**, 137 (2000).
25. S. Ye, Y. Li, Y. Jiang, *Nat. Struct. Mol. Biol.* **17**, 1019 (2010).
26. A. Alam, Y. Jiang, *Nat. Struct. Mol. Biol.* **16**, 30 (2009).
27. Y. Zhou, J. H. Morais-Cabral, A. Kaufman, R. MacKinnon, *Nature* **414**, 43 (2001).
28. F. Lesage *et al.*, *EMBO J.* **15**, 6400 (1996).
29. X. Tao, J. L. Avalos, J. Chen, R. MacKinnon, *Science* **326**, 1668 (2009).
30. S. B. Long, X. Tao, E. B. Campbell, R. MacKinnon, *Nature* **450**, 376 (2007).
31. S. N. Bagriantsev, R. Peyronnet, K. A. Clark, E. Honoré, D. L. Minor Jr., *EMBO J.* **30**, 3594 (2011).
32. P. L. Piechotta *et al.*, *EMBO J.* **30**, 3607 (2011).
33. F. Maingret, A. J. Patel, F. Lesage, M. Lazdunski, E. Honoré, *J. Biol. Chem.* **275**, 10128 (2000).
34. Y. Kim, H. Bang, C. Gnatenco, D. Kim, *Pflugers Arch.* **442**, 64 (2001).
35. J. Chemin *et al.*, *J. Biol. Chem.* **280**, 4415 (2005).
36. G. Sandoz *et al.*, *EMBO J.* **25**, 5864 (2006).
37. J. Murbartián, Q. Lei, J. J. Sando, D. A. Bayliss, *J. Biol. Chem.* **280**, 30175 (2005).
38. J. Chemin *et al.*, *EMBO J.* **24**, 44 (2005).
39. E. Honoré, F. Maingret, M. Lazdunski, A. J. Patel, *EMBO J.* **21**, 2968 (2002).
40. Y. Kim, C. Gnatenco, H. Bang, D. Kim, *Pflugers Arch.* **442**, 952 (2001).
41. F. Maingret, A. J. Patel, F. Lesage, M. Lazdunski, E. Honoré, *J. Biol. Chem.* **274**, 26691 (1999).
42. J. Payandeh, T. Scheuer, N. Zheng, W. A. Catterall, *Nature* **475**, 353 (2011).

Acknowledgments: We thank M. Becker, R. Sanishvili, and staff at beamline 23-IDB/D at the Advanced Photon Source (APS), F. Murphy, K. Rajashankar, and staff at beamline 24-IDC at APS, and H. Robinson and staff at beamline X29 at the National Synchrotron Light Source for assistance at the synchrotrons, and members of the MacKinnon laboratory for helpful discussions. S.G.B. is a postdoctoral fellow of the Helen Hay Whitney Foundation, J.d.M. is a Howard Hughes Medical Institute International Student Research Fellow, and R.M. is an investigator in the Howard Hughes Medical Institute. The authors declare no conflict of interest. The x-ray crystallographic coordinates and structure factors are available in the Protein Data Bank, entry 3UM7. S.G.B. purified and crystallized TRAAK; collected, processed, and refined crystallographic data; and performed the flux assay and analyzed data. J.M. performed and analyzed data from electrophysiology experiments in CHO cells. R.M. performed and analyzed data from bilayer experiments. S.G.B and R.M. wrote the paper.

Supporting Online Material

www.sciencemag.org/cgi/content/full/335/6067/436/DC1
Materials and Methods
Figs. S1 to S10
Table S1
References (*43*–*58*)

9 September 2011; accepted 8 December 2011
10.1126/science.1213808

Downloaded from www.sciencemag.org on January 27, 2012

Unimpeded Permeation of Water Through Helium-Leak–Tight Graphene-Based Membranes

R. R. Nair,[1,2] H. A. Wu,[1,3] P. N. Jayaram,[2] I. V. Grigorieva,[1] A. K. Geim[1,2]*

Permeation through nanometer pores is important in the design of materials for filtration and separation techniques and because of unusual fundamental behavior arising at the molecular scale. We found that submicrometer-thick membranes made from graphene oxide can be completely impermeable to liquids, vapors, and gases, including helium, but these membranes allow unimpeded permeation of water (H_2O permeates through the membranes at least 10^{10} times faster than He). We attribute these seemingly incompatible observations to a low-friction flow of a monolayer of water through two-dimensional capillaries formed by closely spaced graphene sheets. Diffusion of other molecules is blocked by reversible narrowing of the capillaries in low humidity and/or by their clogging with water.

Despite being only one atom thick, graphene is believed to be impermeable to all gases and liquids (*1*, *2*), which makes it tempting to exploit this material as a barrier film. Because of the ways graphene can currently be mass produced (*3*), films made from graphene oxide (GO) present a particularly interesting candidate. By using this graphene derivative, it is possible to make laminates, which are a collection of micron-sized GO crystallites forming an interlocked layered structure (*4*–*6*). This structure resembles that of nacre and exhibits great mechanical strength and flexibility, even for films of submicron thickness (*3*–*6*). In this Report, we investigate molecular permeation through such films.

Figure 1A shows an example of the studied GO membranes that were prepared as follows (*7*): We employed Hummer's method to obtain graphite oxide that was dispersed in water by sonication to make a stable suspension of GO crystallites (*4*–*6*). We then used this suspension to produce laminates by spray- or spin-coating (*7*). Scanning electron microscopy and x-ray analysis reveal that such GO films have a pronounced layered structure (Fig. 1B) and consist of crystals with typical sizes L of a few micrometers, which are separated by a typical distance d of ~10 Å (*4*–*6*). For permeation experiments, Cu foils of several centimeters in diameter were uniformly covered with the GO laminates. Then, we chemically etched Cu to produce apertures of diameter $D \approx 1$ cm fully covered by freestanding GO films (fig. S1). Finally, a metal container was sealed by using the Cu disks (fig. S2). We studied membranes with thicknesses h from 0.1 to 10 μm. Even submicrometer-thick membranes were strong enough to withstand a differential pressure ΔP up to 100 mbar.

As an initial test, we filled the containers with various gases under a small overpressure (<100 mbar) and recorded its changes over a period of several days. We observed no noticeable reduction in ΔP for any tested gas including He, H_2, N_2, and Ar. This allowed an estimate for the upper limit on their permeation rates Pr as $\approx 10^{-11}$ g/cm^2·s·bar, which is close to the value reported for micron-sized "balloons" made from continuous graphene monolayers (*1*). In an alternative approach, we used mass spectrometry (fig. S2) and found no detectable permeation of He (Fig. 1D). The accuracy was limited only by digital noise of our He spectrometer and a slightly fluctuating background, which yielded $Pr < 10^{-12}$ g/cm^2·s·bar. Using hydrogen mass spectrometry, no permeation was found either, albeit the accuracy was three orders of magnitude lower than for He, due to a larger background. A 12-μm-thick film of polyethylene terephthalate (PET) was used as a reference barrier and exhibited a He leakage rate 1000 times higher than our detection limit (Fig. 1D) yielding PET's bulk permeability $\prod_{He} = Pr \cdot h \approx 10^{-11}$ mm·g/cm^2·s·bar, in agreement with literature values. The measurements set up an upper limit on $\prod_{He}$ for GO laminates as $\approx 10^{-15}$ mm·g/cm^2·s·bar; that is, our submicrometer-thick films provide a higher He gas barrier than 1-mm-thick glass (*8*).

To evaluate the permeation barrier for liquid substances, we employed weight-loss measurements. Figure 2 shows examples for evaporation rates from a metal container with an aperture covered by a 1-μm-thick GO membrane. No weight loss could be detected with accuracy of <1 mg for ethanol, hexane, acetone, decane, and propanol in the measurements lasting several days (*7*). This sets an upper limit for their $\prod$ as $\approx 10^{-11}$ mm·g/cm^2·s·bar. Unexpectedly, we observed a huge weight loss if the container was filled with water. Moreover, the evaporation rate was practically the same as in the absence of the GO film; that is, for the open aperture (Fig. 2A and fig. S3).

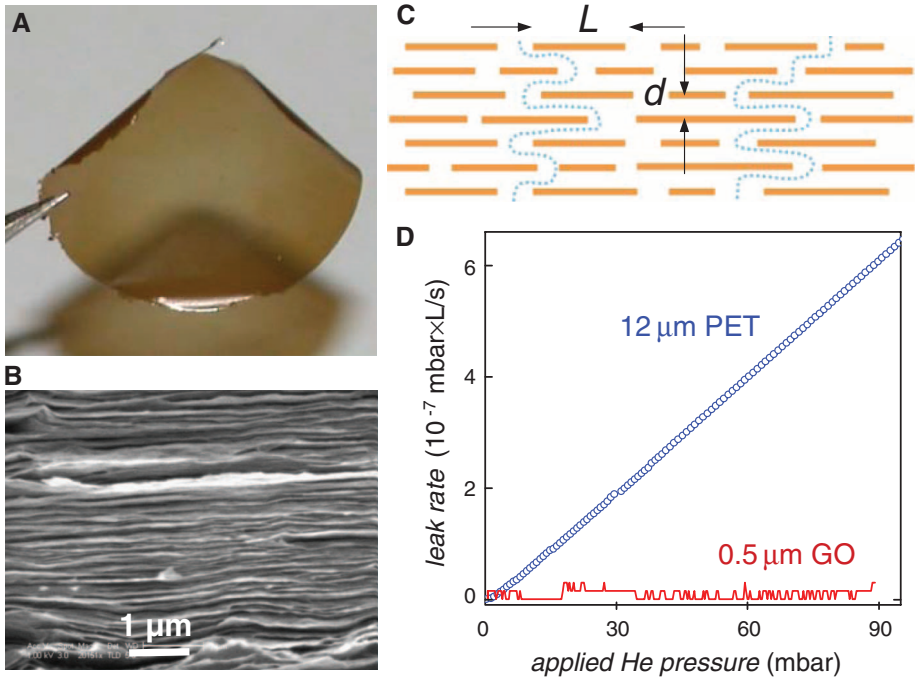


Fig. 1. He-leak–tight GO membranes. (**A**) Photo of a 1-μm-thick GO film peeled off of a Cu foil. (**B**) Electron micrograph of the film's cross section. (**C**) Schematic view for possible permeation through the laminates. Typical L/d is ~1000. (**D**) Examples of He-leak measurements for a freestanding submicrometer-thick GO membrane and a reference PET film (normalized per square centimeter).

[1]School of Physics and Astronomy, University of Manchester, Manchester M13 9PL, UK. [2]Centre for Mesoscience and Nanotechnology, University of Manchester, Manchester M13 9PL, UK. [3]Department of Modern Mechanics, Chinese Academy of Sciences Key Laboratory of Mechanical Behavior and Design of Materials, University of Science and Technology of China, Hefei, Anhui 230027, China.

*To whom correspondence should be addressed. E-mail: geim@manchester.ac.uk

Downloaded from www.sciencemag.org on January 27, 2012

The latter was confirmed directly by using the same aperture with and without a GO cover. Furthermore, the same membrane could be used many times for different liquids, always exhibiting unimpeded and zero evaporation for H_2O and other molecules, respectively. Also, after measurements with water, we checked the membranes for a He leak and found none. Only if we increased h to several micrometers could we observe a partial inhibition of water evaporation from the container (fig. S5), which yielded $\prod_{H2O} \approx 10^{-5}$ mm·g/cm^2·s·bar; that is, water permeates through GO films more than 10 orders of magnitude faster than He (Fig. 2B).

To elucidate the origin of the fast transport of water vapor through otherwise leak-tight GO films, we have carried out a number of additional experiments. First, we reduced GO by annealing it at 250°C in a hydrogen-argon atmosphere (*5*). The membranes became fragile and required extreme care to avoid cracks but nonetheless became 100 times less permeable to water (Fig. 2A). This can be attributed to structural changes such that d decreased from ≈10 to 4 Å, as shown by x-ray analysis and in agreement with earlier reports (*9*, *10*). The importance of the interlayer distance was also witnessed when the partial pressure of water inside the container was reduced (fig. S3). If the pressure dropped below 10 mbar, the permeation stopped (*7*), which again can be explained by changes in d in low humidity. X-ray analysis of GO in various humidity shows that this blockage occurs when d falls below ≈7 Å (*11*, *12*). The process of opening and closing the GO capillaries was found reversible with varying humidity (*7*).

Further insights into the permeation mechanism come from experiments using mixtures of H_2O with other gases and liquids. Mass spectroscopy showed that, in the presence of saturated water vapor, He did permeate through GO membranes (fig. S4). However, its rate was ≈five orders of magnitude slower than that of H_2O, in agreement with the rate calculated for He diffusion through an equivalent column of water (*7*). For other molecules (for example, ethanol and H_2), we were unable to detect their permeation along with H_2O (*7*). This shows that, despite somewhat larger d in high humidity, the intercalating water blocks, or at least impedes, other molecules from moving through GO.

In another series of experiments, we investigated why water permeated through GO film as fast as through an open aperture. To this end, membranes were placed on a support grid that allowed us to apply a water pressure of several bars without damaging them. The large ΔP did not result in any noticeable increase in Pr with respect to water vapor. On the other hand, if we increased humidity outside the container, Pr decreased. Furthermore, if we blew air at the GO membrane, this increased the weight loss rate. Also, Pr increased if the container was heated (we could increase temperature up to 40°C, above which the membranes had a tendency to develop cracks). The same changes in Pr happened when we changed temperature of the membrane only, without heating water inside. In all the cases, Pr changed similarly to the evaporation rate from an open-water surface under similar conditions. This suggests that permeation of water through our membranes was limited by evaporation from the wetted surface of GO.

To explain our findings, we recall that GO laminates consist of crystallites stacked on top of each other (Fig. 1C). The groups (for instance, hydroxyl, epoxy, etc.) attached to graphene sheets are responsible (*9*–*12*) for keeping the relatively large spacing d (fig. S6). Importantly, such groups tend to cluster and leave large, percolating regions of graphene sheets not oxidized (*5*, *7*, *13*, *14*). Therefore, GO laminates are likely to have empty spaces formed between nonoxidized regions of graphene sheets (fig. S6). Because d for reduced GO is ≈4 Å, the empty space's width δ can be estimated as ≈5 Å, which is sufficient to accommodate a monolayer of water (*15*, *16*). We speculate that these empty spaces form a network of pristine-graphene capillaries within GO laminates. By invoking the same water-permeation mechanism as previously used for small-diameter carbon nanotubes and hydrophobic nanopores (*17*–*25*), we suggest that the two-dimensional (2D) graphene nanocapillaries allow low-friction flow of monolayer water. At the same time, the oxidized regions that strongly interact with intercalating water are unlikely (*7*) to contribute to water permeation and, in our model, serve as spacers for the 2D capillary network (fig. S6).

To support our explanation, we used molecular dynamics (MD) simulations (*7*). Because a graphene monolayer is essentially impermeable, molecular transport in GO laminates should involve a permeation path through the network of graphene nanocapillaries as discussed above (Fig. 1C and fig. S6). The bottleneck in this process is the passage between graphene sheets separated by $d << L$ (figs. S6 and S7). For $d \leq 6$ Å (including the van der Waals thickness of graphene), our MD simulations show that water cannot fill the capillaries. On the other hand, for $d \geq 10$ Å, two layers of water start forming between the sheets. For intermediate d, water rushes into the capillaries (*21*, *22*) and forms a highly ordered monolayer shown (Fig. 2B, inset), in agreement with the previous analysis for 2D capillaries (*15*, *16*). Furthermore, the simulations enabled us to estimate the involved capillary pressure as on the order of 1000 bars (*7*), in qualitative agreement with the estimates based on van der Waals interaction between water and graphite (*26*). Such capillary pressures explain why the water permeation in our experiments was insensitive to ΔP of several bars. Similar to the case of nanotubes, our simulated water can move anomalously fast, with velocities reaching meters per second and, thus, sufficient to sustain the observed permeation rates (fig. S8). Finally, we mimicked the oxidized graphene regions by adding arrays of epoxy groups to the simulated capillaries and found the water permeation being strongly impeded for all $d \leq 10$ Å.

The observed unimpeded evaporation of water through He-leak–tight membranes resembles the permeation of protons (atomic hydrogen) through thin films of transition metals, a phenomenon known as superpermeability (*27*). Despite the analogy, our phenomenon is different and explained by a network of graphene nanocapillaries formed within GO laminates, which are filled with monolayer water under ambient conditions. A capillary-like pressure provides a sufficient flow to keep the external GO surface wetted so that the observed permeability is effectively limited by the surface evaporation (*28*). The described GO membranes can be used as barrier films in the design of filtration and separation materials and for selective removal of water (*7*).

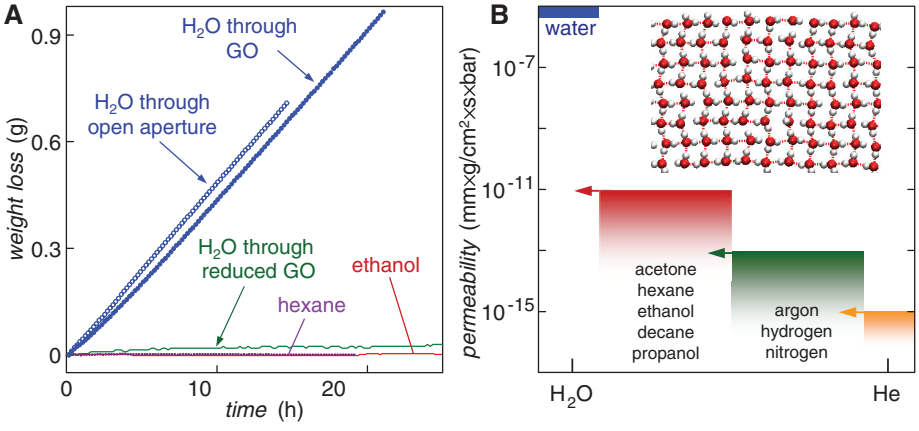


Fig. 2. Permeation through GO. (**A**) Weight loss for a container sealed with a GO film ($h \approx 1$ μm; aperture's area ≈ 1 cm^2). No loss was detected for ethanol, hexane, etc. (*7*), but water evaporated from the container as freely as through an open aperture (blue curves). The measurements were carried out at room temperature in zero humidity. (**B**) Permeability of GO paper with respect to water and various small molecules (arrows indicate the upper limits set by our experiments). (Inset) Schematic representation of the structure of monolayer water inside a graphene capillary with $d = 7$ Å, as found in our MD simulations (*7*).

Downloaded from www.sciencemag.org on January 27, 2012

References and Notes

1. J. S. Bunch *et al.*, *Nano Lett.* **8**, 2458 (2008).
2. O. Leenaerts, B. Partoens, F. M. Peeters, *Appl. Phys. Lett.* **93**, 193107 (2008).
3. A. K. Geim, *Science* **324**, 1530 (2009).
4. D. A. Dikin *et al.*, *Nature* **448**, 457 (2007).
5. G. Eda, M. Chhowalla, *Adv. Mater.* **22**, 2392 (2010).
6. J. T. Robinson *et al.*, *Nano Lett.* **8**, 3441 (2008).
7. See supporting material on *Science* Online.
8. F. J. Norton, *J. Am. Ceram. Soc.* **36**, 90 (1953).
9. M. J. McAllister *et al.*, *Chem. Mater.* **19**, 4396 (2007).
10. H. K. Jeong *et al.*, *Chem. Phys. Lett.* **470**, 255 (2009).
11. A. Lerf *et al.*, *J. Phys. Chem. Solids* **67**, 1106 (2006).
12. S. Cerveny, F. Barros-Bujans, Á. Alegría, J. Colmenero, *J. Phys. Chem. C* **114**, 2604 (2010).
13. N. R. Wilson *et al.*, *ACS Nano* **3**, 2547 (2009).
14. D. Pacilé *et al.*, *Carbon* **49**, 966 (2011).
15. R. Zangi, A. E. Mark, *Phys. Rev. Lett.* **91**, 025502 (2003).
16. N. Giovambattista, P. J. Rossky, P. G. Debenedetti, *Phys. Rev. Lett.* **102**, 050603 (2009).
17. J. K. Holt *et al.*, *Science* **312**, 1034 (2006).
18. M. Majumder, N. Chopra, R. Andrews, B. J. Hinds, *Nature* **438**, 44 (2005).
19. X. Peng, J. Jin, Y. Nakamura, T. Ohno, I. Ichinose, *Nat. Nanotechnol.* **4**, 353 (2009).
20. X. Qin, Q. Yuan, Y. Zhao, S. Xie, Z. Liu, *Nano Lett.* **11**, 2173 (2011).
21. M. Whitby, N. Quirke, *Nat. Nanotechnol.* **2**, 87 (2007).
22. J. C. Rasaiah, S. Garde, G. Hummer, *Annu. Rev. Phys. Chem.* **59**, 713 (2008).
23. J. Köfinger, G. Hummer, C. Dellago, *Proc. Natl. Acad. Sci. U.S.A.* **105**, 13218 (2008).
24. J. A. Thomas, A. J. H. McGaughey, *Phys. Rev. Lett.* **102**, 184502 (2009).
25. Y. Li, J. Xu, D. Li, *Microfluid. Nanofluid.* **9**, 1011 (2010).
26. F. Caupin, M. W. Cole, S. Balibar, J. Treiner, *Europhys. Lett.* **82**, 56004 (2008).
27. A. I. Livshits, M. E. Notkin, V. I. Pistunovich, M. Bacal, A. O. Busnyuk, *J. Nucl. Mater.* **220-222**, 259 (1995).
28. N. Goedecke, J. Eijkel, A. Manz, *Lab Chip* **2**, 219 (2002).

Acknowledgments: This work was supported by the Engineering and Physical Research Council (UK), the U.S. Office of Naval Research, the U.S. Air Force Office of Scientific Research, the Royal Society, and the Körber Foundation. We thank K. S. Novoselov, E. Hill, P. Blake, S. Neubeck, and R. Joshi for their help. H.A.W. is grateful for support from the National Science Foundation of China and Oversea Academic Training Funds–University of Science and Technology of China.

Supporting Online Material

www.sciencemag.org/cgi/content/full/335/6067/442/DC1
Materials and Methods
SOM Text
Figs. S1 to S8
References (*29*–*38*)

25 July 2011; accepted 17 November 2011
10.1126/science.1211694

Ultrafast Viscous Permeation of Organic Solvents Through Diamond-Like Carbon Nanosheets

Santanu Karan,[1] Sadaki Samitsu,[1] Xinsheng Peng,[1]* Keiji Kurashima,[1] Izumi Ichinose[1,2]†

Chemical, petrochemical, energy, and environment-related industries strongly require high-performance nanofiltration membranes applicable to organic solvents. To achieve high solvent permeability, filtration membranes must be as thin as possible, while retaining mechanical strength and solvent resistance. Here, we report on the preparation of ultrathin free-standing amorphous carbon membranes with Young's moduli of 90 to 170 gigapascals. The membranes can separate organic dyes at a rate three orders of magnitude greater than that of commercially available membranes. Permeation experiments revealed that the hard carbon layer has hydrophobic pores of ~1 nanometer, which allow the ultrafast viscous permeation of organic solvents through the membrane.

About 40 years ago, reverse-osmosis membranes applicable to seawater desalination were prepared by plasma polymerization of organic monomers (*1*). Membranes obtained from hydrophilic monomers showed high salt rejection and water permeability (*2*, *3*). The permeation mechanism was discussed in terms of the free-volume theory of polymers (*4*, *5*) or the hydrodynamic flow of water through micropores. However, initial expectations for the use of plasma-polymerized membranes gradually diminished with the improved performance of cross-linked polyimide membranes (*6*). Today, asymmetric polyimide membranes are mass-produced for organic solvent nanofiltration by the phase-inversion method. Meanwhile, thin supported carbon membranes made by various techniques are mainly used for gas separations (*7*, *8*).

Diamond-like carbon (DLC) was also made ~40 years ago by Aisenberg and Chabot (*9*). They prepared thin transparent films very similar to diamond by means of an ion-beam deposition technique. Currently, a widely used technique for DLC deposition is plasma chemical vapor deposition using organic compounds (*10*, *11*). In plasma polymerization of organic compounds, a highly cross-linked network of sp^3 carbons is obtained under certain conditions, which provides the resulting thin carbon films with mechanical stability broadly comparable to diamond. We have become interested in the process by which molecules permeate through such a highly cross-linked molecular network. By improving the permeability, we can thereby obtain extremely hard and thin carbon membranes with great advantages for separation technologies.

We demonstrate the ultrafast permeation of organic solvents through DLC nanosheets, free-standing amorphous carbon membranes with thicknesses ranging from 10 to 40 nm. In addition to their high permeability for various solvents, the membranes have excellent separation performance for organic solutes. Interestingly, the solvent flux was mainly affected by the viscosity of the solvents, not by their molecular size or dipole moment.

We prepared the uniform ultrathin DLC membrane on a sacrificial layer of cadmium hydroxide nanostrands (*12*) by using a parallel-plate plasma-enhanced chemical vapor deposition reactor [radio frequency (RF) power: 5 to 50 W at 13.56 MHz, deposition time: 10 to 370 s, pressure: 1 to 6 Pa] (figs. S1 to S3). To prevent damage of the nanostrands, the substrate temperature was maintained at –20°C. We carefully removed the sacrificial layer by treating it with an ethanolic solution of hydrochloric acid (Fig. 1, C to F). The configuration of the filtration membrane is shown in Fig. 1A. In this case, a 35-nm DLC membrane is formed on a 200-nm-pore alumina support. The membrane has a relatively porous layer of thickness ~10 nm where removal of the nanostrands occurred. However, the overall membrane was completely defect-free, as observed by scanning electron microscopy (SEM), and could be used for high-pressure filtration up to at least 2.0 MPa. Nano-indentation measurements confirmed that the membrane prepared from acetylene diluted in argon gas (RF power: 50 W) has a Young's modulus of 170 GPa and a hardness of 20.1 GPa (Table 1). In this case, the Young's modulus is one-seventh the elastic modulus of diamond (1050 to 1200 GPa) (*13*). Solid-state ^{13}C cross-polarization/magic angle spinning nuclear magnetic resonance (CP/MAS NMR) measurements revealed that the membrane contains 47% sp^3 carbons and 53% sp^2 carbons (fig. S4) (*14*). High-resolution transmission electron microscopy (HRTEM) observations confirmed that the acetylene membrane produced at a low substrate temperature (–20°C) was a typical hydrogenated amorphous carbon (a-C:H soft) (fig. S5) (*15*). Fourier-transform infrared measurements indicated the membrane has a relatively high hydrogen content (fig. S6). Furthermore, we estimated the carbon content to be 95.6 atomic % by x-ray photoelectron spectroscopy (XPS) (fig. S7 and table S1). Deconvolution of the C_{1S} spectra indicated that some of the carbon atoms had been oxidized to form ether (or alcohol), carbonyl, and ester (or carboxyl) groups. Based on these data, the internal chemical structure of the acetylene membrane is presumed to be as shown in Fig. 1B.

DLC membranes made from pyridine and hexamethyldisiloxane (HMDS) gave high elastic moduli of 106 and 91.8 GPa, respectively, and

[1]Polymer Materials Unit, National Institute for Materials Science, 1-1 Namiki, Tsukuba, Ibaraki 305-0044, Japan. [2]Japan Science and Technology Agency (JST), Core Research for Evolutional Science and Technology (CREST), 5 Sanbancho, Chiyoda-ku, Tokyo 102-0075, Japan.

*Present address: Department of Materials Science and Engineering, Zhejiang University, Hangzhou 310027, China.
†To whom correspondence should be addressed. E-mail: ichinose.izumi@nims.go.jp

Downloaded from www.sciencemag.org on January 27, 2012

had significant nitrogen or silicon content (Table 1 and figs. S8 and S9). The density of the membranes was in the range of 1.96 to 2.45 g/cm^3, which was generally higher than the value for general amorphous carbon (1.6 to 2.2 g/cm^3) (fig. S6) (*10*, *16*). These results indicate that dense, three-dimensional network structures are formed by considerable carbonization of the precursor monomers. Roughly speaking, our DLC membranes have elastic moduli ~50 times greater than the values for high-strength engineering plastics and ~10 times less than the value for diamond.

For the DLC membranes, we investigated the permeation properties of various organic solvents. In Fig. 2A, the fluxes of different solvents at a pressure difference of 80 kPa are plotted along with their viscosities. In the case of the 35-nm-thick acetylene membrane, hexane, with the smallest viscosity of 0.31 centipoise (cP), gave a surprisingly high flux of 382.9 liters per square meter·hour (L/m^2h). Acetonitrile (0.35 cP) gave the second highest value of 235.2 L/m^2h. In contrast, the relatively viscous liquid 1-butanol (2.95 cP) gave the lowest flux (27.8 L/m^2h). Thus, the solvent permeability increased in inverse proportion to the viscosity. The fluxes of chloroform, ethanol, and benzene also showed the same tendency (fig. S10 and table S2). The solvent polarity did not affect the permeation, at least in the range between acetonitrile and hexane. This is probably because the interaction from a hydrophobic pore is nonspecific to solvents. The HMDS membrane showed a similar inverse proportionality between solvent flux and viscosity (blue curve in Fig. 2A). In both cases, small deviations were observed only for methanol and toluene. The relatively bulky toluene had a flux around two-thirds that of methanol, despite having a slightly lower viscosity. It is apparent that these DLC membranes allow for fast permeation of organic solvents. The apparent viscosity dependence indicates that the hard network structure does not swell in the presence of these solvents. In fact, we confirmed that solvent flux does not change with time (fig. S11). For membranes with many pores of a few nanometers in size, viscous flow can be readily explained by the Hagen-Poiseuille (HP) equation (*17*, *18*)

$$J = \varepsilon\pi r_p^2 \Delta p/\delta\mu\delta\tau \quad (1)$$

Indeed, we observed that the flux (J) increases linearly with applied pressure (Δp), at least in the range 0.08 to 2.0 MPa (fig. S10) (ε, surface porosity; r_p, pore radius; μ, viscosity; δ, membrane thickness; τ, tortuosity). The diffusive transport of solvents that is usually seen in dense polymer membranes and generally gives very low solvent flux (*19*) does not occur with these DLC membranes. However, these membranes do not have any large pores to allow permeation of the solvents as a continuum flow. As confirmed by HRTEM observations, the pore size seems to be no more than 1 nm (fig. S5).

Figure 2B shows the filtration performance of an acetylene membrane for protoporphyrin-IX (PPh-IX) [molecular weight (MW): 562.7]. The membrane could completely reject the protoporphyrin with a molecular width of 1.47 nm (fig. S12), indicating that there are no pores larger than 1.4 nm. The membrane could also reject 99.8% of a fluorescent dye (MW: 389.4) with a width of 1.28 nm, and it rejected azobenzene (MW: 182.2), a small dye molecule with a width of 0.69 nm, to 93.3%. The rejection performance was very constant with time (fig. S13). As mentioned above, our acetylene membrane allows very fast permeation of toluene. However, azobenzene, with the same width and double the length of toluene, cannot permeate through the membrane. This is probably due to the tortuous structure of the solvent pathway through the ultrathin DLC membrane. Although we cannot necessarily assume that the solvents permeate as a continuum flow, it is important that we can analyze the flux in terms of the HP equation. That is, the viscosity-flux and pressure-flux dependencies strongly indicate that the HP equation is extendable to molecular-sized pores. From the rejection of azobenzene (94.4%), the pore size seems to be somewhat larger than the width (*20*, *21*). Supposing a pore size of 1.0 nm, we calculated the surface porosity (ε) of a 35-nm-thick acetylene membrane (RF power: 10 W) to be 12.4%, where an ethanol flux of 67.3 L/m^2h at a pressure difference (Δp) of 80 kPa, a viscosity (μ) of 1.19 × 10^{-3} Pa·s (1.19 cP) at 20°C, and a tortuosity (τ) of 1.25 were used for the calculation (*17*) (note that the viscosity and tortuosity have some uncertainty). The actual membrane would have a distribution of pore sizes. The blue circles in Fig. 1B represent a surface porosity of ~12% in area. Judging from the observed density of 2.45 g/cm^3, the nonpore regions are expected to be filled with dense hydrogenated amorphous carbon. The applicability of the HP equation to our membranes needs to be verified, because the molecular sizes of organic solvents are close to or no less than one-third the size of the pores in the membranes.

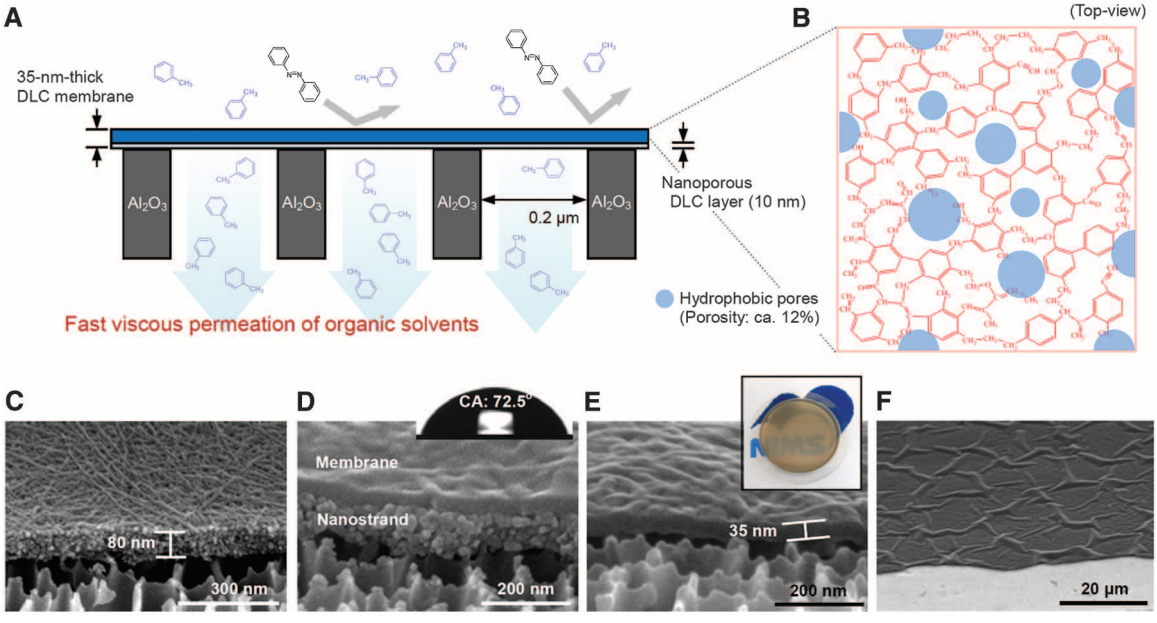


Fig. 1. (**A**) Schematic presentation of a free-standing DLC membrane formed on submicron pores of a porous alumina support. (**B**) Internal structure of the membrane inferred from ^{13}C CP/MAS NMR and XPS. Chemical structures are drawn at a magnification of 1.5, as compared with the hydrophobic pores. (**C** to **E**) Cross-sectional SEM images of a sacrificial 80-nm-thick nanostrand layer on a porous alumina support, a carbon layer deposited on the nanostrand layer, and 35-nm-thick DLC membrane obtained after removal of the nanostrands with HCl. (**F**) Low-magnification SEM image of (E). These images were taken after applying a 3-nm platinum coating. Inset in (D) shows a photographic image of a water droplet on the deposited DLC membrane (CA, contact angle). Inset in (E) shows the DLC membrane formed on a 25-mm porous alumina support.

Downloaded from www.sciencemag.org on January 27, 2012

However, it should be possible to say that our DLC membranes have an abundance of pores that are equivalent to ~12% porosity in the HP equation.

Table 2 summarizes the filtration performance of DLC membranes prepared from various precursor gases (monomers). In preparation at a substrate temperature of –20°C, methane gave membranes with pores of a few nanometers. The rejection values for azobenzene and a fluorescein derivative [fluorescein-4-isothiocyanate (FI)] were 23.0 and 41.3%, respectively. The allylamine membrane also gave low rejection values for these molecules. On the other hand, acetylene and pyridine gave rejection values of more than 90% for azobenzene. In a comparison of the three acetylene membranes, the membrane deposited at an RF power of 10 W gave the highest flux for ethanol and also the highest rejection value for azobenzene. The low RF power probably acts to help prevent complete carbonization of the growing DLC layer and to give a highly microporous structure. We confirmed that the performance of the DLC membranes varies widely with the preparation parameters. This indicates that there are many ways to design cross-linked network structures in DLC membranes in addition to controlling the composition and hydrophobicity. It is also important to stress that the filtration performance changes substantially with the membrane thickness. For example, a 10-nm-thick acetylene membrane allows hexane permeation at a flux of 2911 L/m^2h at a pressure difference of 80 kPa and completely rejects 5-nm gold nanoparticles from an ethanolic solution (fig. S14 and table S3). This membrane thus offers an innovative ultrafiltration membrane for organic solvents. The observed flux is overwhelmingly higher than those of other known ultrafiltration membranes with similar rejection properties.

More importantly, the ethanol flux through one of the 35-nm-thick acetylene membranes (67.3 L/m^2h) is about three orders of magnitude greater than those of commercially available organic solvent nanofiltration membranes [see supporting online material (SOM)]. This DLC membrane has an extremely sharp molecular weight cut-off, as indicated by a rejection value for azobenzene of more than 94% (Table 2 and fig. S15). From the viewpoint of applications in the chemical and petrochemical industries (*19*, *22*), the ultrafast permeation of organic sol-

Table 1. Composition and mechanical properties of acetylene, pyridine, and HMDS membranes. ND, not determined.

Monomers	Membrane atomic composition*					Density† (g/cm^3)	Young's modulus‡ (GPa)	Hardness‡ (GPa)
	C	N	O	Si	Ar			
Acetylene	95.6	ND	3.8	ND	0.6	2.45	170	20.1
Pyridine	87.8	7.9	4.3	ND	ND	2.08	106	12.3
HMDS	49.9	ND	20.7	29.4	ND	1.96	91.8	10.1

*DLC membranes were prepared at RF power of 50 W using 20% acetylene/Ar gas at 5 Pa, pyridine at 2 Pa, and HMDS at 1.5 Pa. The atomic composition was estimated by XPS measurements. †Density was estimated by a quartz crystal microbalance technique for 40- to 80-nm-thick membranes. ‡Young's modulus and hardness were measured by a nano-indentation technique for ~300-nm-thick membranes deposited on silicon wafers.

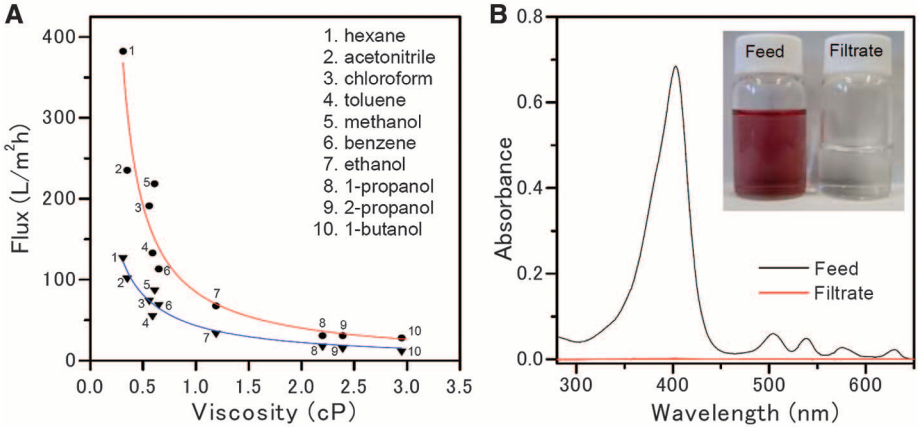


Fig. 2. (**A**) Relation between flux and viscosity of organic solvents showing inverse proportionality. Red curve, fit of fluxes of different solvents passed though a 35-nm-thick acetylene membrane deposited at 10 W; blue curve, fit of fluxes of different solvents though a 35-nm-thick HMDS membrane deposited at 50 W. The experiments were conducted at 20°C at 80 kPa. Note that the flux values were calculated for the membrane area covering the pores of the alumina support (porosity: 50%). (**B**) Ultraviolet-visible absorption spectra of PPh-IX ethanolic solution (0.05 mM) before and after filtration through a 35-nm-thick acetylene membrane (30 W). (Inset) Photograph of the feed and filtrate of the PPh-IX solution.

Table 2. Filtration performance of free-standing DLC membranes.

Monomer*	RF power (W)	Pressure (Pa)	Thickness (nm)	Contact angle (deg)	Ethanol flux† (L/m^2h)	AB‡ (0.69 nm)		FI‡ (1.28 nm)		PPh-IX‡ (1.47 nm)	
						Flux (L/m^2h)	Rejection (%)	Flux (L/m^2h)	Rejection (%)	Flux (L/m^2h)	Rejection (%)
Methane	10	5.0	35 ± 3	73.2 ± 2.1	201.1	188.8	23.0	179.8	41.3	129.7	81.5
Butadiene	20	5.0	35 ± 3	66.2 ± 1.4	45.8	35.9	86.6	32.3	99.3	25.5	100
Acetylene	10	5.0	35 ± 3	72.5 ± 1.1	67.3	51.5	94.4	47.8	99.6	44.6	100
Acetylene	30	5.0	36 ± 2	71.1 ± 1.2	54.4	40.2	93.3	32.7	99.8	31.1	100
Acetylene	50	5.0	35 ± 4	70.0 ± 1.4	21.0	10.3	87.2	7.5	100	7.2	100
Pyridine	50	2.0	35 ± 5	61.0 ± 1.1	37.8	32.1	92.7	21.4	99.8	18.9	100
HMDS	50	1.5	36 ± 4	93.8 ± 1.7	34.0	25.5	79.9	21.5	98.5	16.9	99.6
ATMS	50	1.5	36 ± 4	66.0 ± 0.8	38.2	35.2	85.7	31.8	99.6	19.4	100
Propylamine	10	5.0	40 ± 2	71.2 ± 0.6	24.3	20.1	87.0	15.2	99.8	12.5	100
Allylamine	20	6.0	50 ± 4	62.6 ± 1.4	25.5	16.9	48.2	10.2	60.9	3.9	99.3

*Butadiene and acetylene gases were introduced after diluting to 20% with Ar. ATMS, allyltrimethoxysilane. Monomer flow rates were 2.71 standard cubic centimeters per minute (sccm) for methane, 1.68 sccm for butadiene, 1.67 sccm for acetylene, and 1.40 sccm for HMDS and ATMS. †The valid area of the free-standing DLC membranes was 0.39 cm^2. ‡AB, azobenzene (0.5 mM in ethanol); FI, fluorescein-4-isothiocyanate (0.05 mM in ethanol); and PPh-IX, protoporphyrin-IX (0.05 mM in ethanol). A permeated volume of no less than 2 ml was collected to determine the rejection value. All the filtration experiments were conducted at 20°C at a pressure difference of 80 kPa.

Downloaded from www.sciencemag.org on January 27, 2012

vents contributes appreciably to improved energy efficiency in recovery of the solvents. A range of industries—including polymer synthesis (*23*), production of biofuels (*24*), environmental remediation (*25*), and oil extraction in the food industry (*19*)—have a strong demand for solvent-resistant nanofiltration membranes with superior permeability characteristics. For these purposes, nanoporous free-standing sheets of carbon nanotubes (*26*, *27*) and other inorganic membranes (*28*) have been studied globally. However, it has been a challenge to produce such membranes in an industrially applicable process. DLC membranes have been found to be extremely dense and suitable for use in gas barrier applications (*29*, *30*). In this Report, we demonstrate that DLC membranes can be prepared with extremely high solvent permeability while maintaining considerable mechanical strength.

References and Notes

1. K. R. Buck, V. K. Davar, *Br. Polym. J.* **2**, 238 (1970).
2. J. R. Hollahan, T. Wydeven, *Science* **179**, 500 (1973).
3. H. Yasuda, C. E. Lamaze, *J. Appl. Polym. Sci.* **17**, 201 (1973).
4. A. A. Bondi, *Physical Properties of Molecular Crystals, Liquids, and Glasses* (Wiley, New York, 1968).
5. D. W. Van Krevelen, *Properties of Polymers* (Elsevier, Amsterdam, 1990).
6. Y. H. See Toh, F. W. Lim, A. G. Livingston, *J. Membr. Sci.* **301**, 3 (2007).
7. M. Kiyono, P. J. Williams, W. J. Koros, *J. Membr. Sci.* **359**, 2 (2010).
8. A. F. Ismail, D. Rana, T. Matsuura, H. C. Foley, *Carbon-Based Membranes for Separation Processes* (Springer, New York, 2011).
9. S. Aisenberg, R. Chabot, *J. Appl. Phys.* **42**, 2953 (1971).
10. J. Robertson, *Mater. Sci. Eng. Rep.* **37**, 129 (2002).
11. X. D. Pan, E. A. Maydell, R. H. Milne, D. J. Fabian, *Vacuum* **41**, 1360 (1990).
12. I. Ichinose, K. Kurashima, T. Kunitake, *J. Am. Chem. Soc.* **126**, 7162 (2004).
13. M. Werner, S. Hein, E. Obermeier, *Diamond Relat. Mater.* **2**, 939 (1993).
14. We used the term of DLC to emphasize the mechanical stability of the membranes. However, the fraction of sp^2 carbon is relatively high and is close to that in disordered carbon (see SOM).
15. P. Koidl, Ch. Wild, B. Dischler, J. Wagner, M. Ramsteiner, *Mater. Sci. Forum* **52-53**, 41 (1990).
16. P. J. R. Honeybone, R. J. Newport, J. K. Walters, W. S. Howells, J. Tomkinson, *Phys. Rev. B* **50**, 839 (1994).
17. K. Li, *Ceramic Membranes for Separation and Reaction* (Wiley, West Sussex, UK, 2007).
18. Q. Zhang, S. Ghosh, S. Samitsu, X. Peng, I. Ichinose, *J. Mater. Chem.* **21**, 1684 (2011).
19. P. Silva, L. G. Peeva, A. G. Livingston, in *Advanced Membrane Technology and Applications*, N. N. Li, A. G. Fane, W. S. W. Ho, T. Matsuura, Eds. (Wiley, Hoboken, NJ, 2008), pp. 451–467.
20. J. L. Anderson, J. A. Quinn, *Biophys. J.* **14**, 130 (1974).
21. G. F. Froment, K. B. Bischoff, *Chemical Reactor Analysis and Design* (Wiley, New York, 1979).
22. P. Vandezande, L. E. M. Gevers, I. F. J. Vankelecom, *Chem. Soc. Rev.* **37**, 365 (2008).
23. S. So, L. G. Peeva, E. W. Tate, R. J. Leatherbarrow, A. G. Livingston, *Org. Process Res. Dev.* **14**, 1313 (2010).
24. R. Othman, A. W. Mohammad, M. Ismail, J. Salimon, *J. Membr. Sci.* **348**, 287 (2010).
25. I. C. Escobar, S. Hong, A. Randall, *J. Membr. Sci.* **175**, 1 (2000).
26. J. K. Holt *et al.*, *Science* **312**, 1034 (2006).
27. F. Fornasiero *et al.*, *Proc. Natl. Acad. Sci. U.S.A.* **105**, 17250 (2008).
28. C. C. Striemer, T. R. Gaborski, J. L. McGrath, P. M. Fauchet, *Nature* **445**, 749 (2007).
29. A. Shirakura *et al.*, *Thin Solid Films* **494**, 84 (2006).
30. G. A. Abbas, S. S. Roy, P. Papakonstantinou, J. A. McLaughlin, *Carbon* **43**, 303 (2005).

Acknowledgments: We gratefully acknowledge financial support from JST, CREST, and a grant-in-aid for scientific research from the Ministry of Education, Culture, Sports, Science and Technology, Japan (no. 23350105). A part of this Report was used for a Japanese patent [application no. (2010) 180194].

Supporting Online Material

www.sciencemag.org/cgi/content/full/335/6067/444/DC1
Materials and Methods
Figs. S1 to S15
Tables S1 to S3
References (*31*–*55*)

2 August 2011; accepted 7 November 2011
10.1126/science.1212101

Downloaded from www.sciencemag.org on January 27, 2012

An All-Silicon Passive Optical Diode

Li Fan,[1,2]* Jian Wang,[1,2]* Leo T. Varghese,[1,2]* Hao Shen,[1,2] Ben Niu,[1,2] Yi Xuan,[1,2] Andrew M. Weiner,[1,2] Minghao Qi[1,2,3]†

A passive optical diode effect would be useful for on-chip optical information processing but has been difficult to achieve. Using a method based on optical nonlinearity, we demonstrate a forward-backward transmission ratio of up to 28 decibels within telecommunication wavelengths. Our device, which uses two silicon rings 5 micrometers in radius, is passive yet maintains optical nonreciprocity for a broad range of input power levels, and it performs equally well even if the backward input power is higher than the forward input. The silicon optical diode is ultracompact and is compatible with current complementary metal-oxide semiconductor processing.

Nonreciprocal transmission is fundamental to information processing. Electrical nonreciprocity, or the diode effect, had been realized in integrated form with a semiconductor p-n junction. Optical nonreciprocity (ONR) is inherently difficult because of the time-reversal symmetry of light-matter interaction (*1*). Previously reported observations of ONR were based on the magneto-optic effect (*2*–*4*), optical nonlinearity (*5*–*8*), electro-absorption modulation (*9*), cholesteric liquid crystals (*10*), optomechanical cavities (*11*), indirect interband photonic transitions (*12*), and the opto-acoustic effect (*13*). However, complementary metal-oxide semiconductor (CMOS)–compatible passive optical diodes with a footprint and functionality analogous to those of p-n junctions have not been realized at the near-infrared wavelengths that are preferred for silicon (Si) photonics.

Our optical diode (Fig. 1A) is based on strong optical nonlinearity in high–quality factor (Q) Si microrings (*14*–*17*). It consists of a high-Q all-pass notch filter (NF) operating near the critical coupling regime (*17*) (Fig. 1B) and an add-drop filter (ADF) (*14*, *16*, *18*) with asymmetric power coupling to the bus waveguides (Fig. 1C). The resonant wavelength of the NF is thermally tuned to match that of the ADF through the thermo-optic effect of silicon (*19*).

A microring accumulates optical energy at its resonant wavelength. The schematics in Fig. 1, E and F, show that light couples into the microring in the ADF through two different gaps, G_2 and G_3. If we define forward and backward input power as $P_{c,f}$ and $P_{in,b}$, respectively, the optical energy stored in the microring near its resonant wavelength, λ_{ADF}, can be expressed as

$$U_{\text{forward}}(\lambda) = \frac{P_{c,f}}{Q_{G_2}} Q_{ADF}^2 K(\lambda) \qquad (1)$$

and

$$U_{\text{backward}}(\lambda) = \frac{P_{in,b}}{Q_{G_3}} Q_{ADF}^2 K(\lambda) \qquad (2)$$

where Q_{ADF} is the ring's loaded quality factor, Q_{G_2} and Q_{G_3} are power coupling quality factors that are exponentially proportional to the gap sizes, and $K(\lambda)$ represents all other terms that are independent of propagation direction for a linear system (*14*).

The energy enhancement factor in the ring depends on the propagation direction because of our asymmetric design ($Q_{G_2} \approx 300{,}000$, $Q_{G_3} \approx 192{,}000$, and $Q_{ADF} \approx 43{,}800$, all through curve-fitting), and $(U_{\text{forward}}/U_{\text{backward}}) = (Q_{G_3}/Q_{G_2}) = 0.64$ for $P_{c,f} = P_{in,b}$. With high input power at $\lambda_0 = \lambda_{ADF}$, the power density inside the ring will be amplified substantially because of its high Q factors and small radius; this induces optical nonlinearity in silicon (*20*–*23*) and a red shift in the ring's resonance ($\lambda'_{ADF} > \lambda_0$, Fig. 1F). Because less energy is stored in the ring during forward

[1]Birck Nanotechnology Center, Purdue University, West Lafayette, IN 47907, USA. [2]School of Electrical and Computer Engineering, Purdue University, West Lafayette, IN 47907, USA. [3]Shanghai Institute of Microsystem and Information Technology, Chinese Academy of Sciences, Shanghai 20050, China.

*These authors contributed equally to this work.
†To whom correspondence should be addressed. E-mail: mqi@purdue.edu

propagation, the amount of resonance shift in the forward direction is smaller than that in the backward direction. If we define wavelength detuning as $\delta_{ADF}(\lambda_0) = 2Q_{ADF}[(\lambda_0 - \lambda'_{ADF})/\lambda'_{ADF}]$, we have $|\delta_{ADF,forward}(\lambda_0)| < |\delta_{ADF,backward}(\lambda_0)|$. This leads to a case in which forward transmission, $T_{ADF,forward}(\lambda_0)$, exceeds backward transmission, $T_{ADF,backward}(\lambda_0)$, because

$$T_{ADF,\,forward}(\lambda_0) = \frac{1}{\delta^2_{ADF,\,forward}(\lambda_0) + 1} F \quad (3)$$

and

$$T_{ADF,\,backward}(\lambda_0) = \frac{1}{\delta^2_{ADF,\,backward}(\lambda_0) + 1} F \quad (4)$$

where $F = 4Q^2_{ADF}/Q_{G_2}Q_{G_3}$ is a constant that is independent of propagation direction. Therefore, an ADF with asymmetric power coupling can function as an ONR device for strong optical inputs, and we call it the ONR initiator.

For the NF, the power transmission near its resonance (λ_{NF}) is

$$T_{NF}(\lambda_0) = \frac{\delta^2_{NF}(\lambda_0) + [1 - (2Q_{NF}/Q_{G_1})]^2}{\delta^2_{NF}(\lambda_0) + 1} \quad (5)$$

where Q_{NF} is the loaded quality factor of the NF ring and $\delta_{NF}(\lambda_0) = 2Q_{NF}[(\lambda_0 - \lambda_{NF})/\lambda_{NF}]$ is wavelength detuning. Our design leads to $Q_{G_1} \approx$ 55,000 (*24*), and the fabricated NF ring (*25*) has $Q_{NF} \approx$ 27,000, so $[1 - (2Q_{NF}/Q_{G_1})] \approx 0$. A weak input will pass the NF with a strong attenuation of ~20 dB at $\lambda_0 = \lambda_{NF}$ because $\delta_{NF}(\lambda_0) = 0$. A strong input will red-shift the NF ring ($\lambda'_{NF} > \lambda_0$), resulting in a nontrivial $\delta'_{NF}(\lambda_0)$, and will pass the NF with a much smaller attenuation at λ_0 (Fig. 1D). We call the NF an ONR amplifier because it will significantly attenuate the weakened signal that has passed the ONR initiator in the backward direction.

When we cascade the ONR amplifier to an ONR initiator with similar onset power for nonlinearity (Fig. 1A), strong ONR can be achieved for a broad range of forward and backward input power levels. Without nonlinear effects (i.e., at a very low input power of ~85 nW at the device, with 1 μW measured at the input laser), our optical diode has a transmission that is independent of propagation direction (Fig. 1H).

With the input power increased to ~85 μW, a nonreciprocal transmission ratio (NTR) of ~20 dB was observed at $\lambda_0 = 1630$ nm (Fig. 1I). For forward propagation, input from port I enters the NF first and has sufficiently high power to red-shift the NF resonance, thus allowing it to pass with low attenuation at wavelength λ_0 (solid curve in Fig. 1D). When this input reaches the ADF, the optical energy accumulated in the ADF ring is not high enough to appreciably red-shift the resonance—that is, $\delta_{ADF,forward}(\lambda_0) \rightarrow 0$ in Eq. 3—because of the large gap of G_2 as well as the power reduction after passing the NF. Thus, light can transmit to the drop port through the resonance and achieve reasonably high transmis-

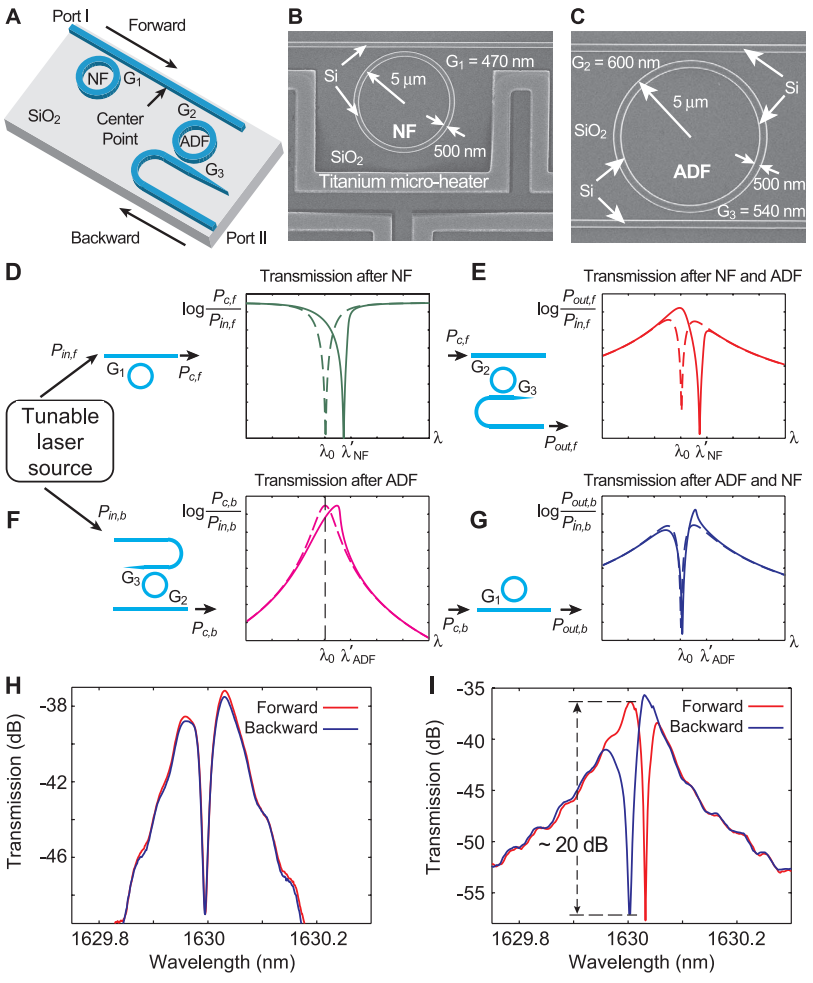


Fig. 1. (**A**) The optical diode consists of two resonance-matched filters: one notch filter (NF) and one add-drop filter (ADF). Input at port I and output at port II is defined as forward propagation; input at port II and output at port I is defined as backward propagation. (**B** and **C**) Fabricated NF and ADF showing the design parameters. A titanium heater allows tuning of the NF resonance to match that of the ADF. (**D** to **G**) Mechanism of passive ONR due to nonlinearity. The optical power at port I, center point, and port II are defined as $P_{in,f}$, $P_{c,f}$, and $P_{out,f}$ for forward propagation and as $P_{out,b}$, $P_{c,b}$, and $P_{in,b}$ for backward propagation. Dashed curves are the simulated transmission spectra in the linear regime (incident power ~85 nW); the solid curves are the simulated transmission spectra at a power level of ~85 μW, which is high enough to induce optical nonlinearity. (**H**) Forward and backward transmission spectra of the diode at ~85 nW incident power, showing reciprocity and good agreement with dashed curves in (E) and (G). (**I**) Forward and backward transmission spectra at input power level of ~85 μW, showing strong ONR and good agreement with solid curves in (E) and (G).

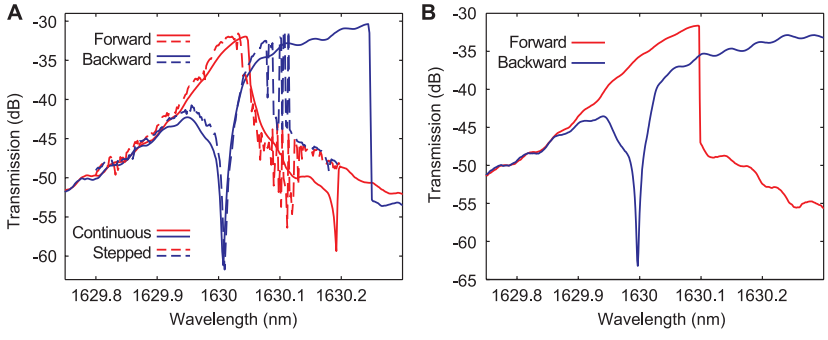


Fig. 2. Forward and backward transmission spectra of the all-silicon optical diode at relatively high input power levels. (**A**) Input power of ~850 μW (10 dBm at laser source). Solid curves denote data acquired through a continuous-mode scan; dashed lines denote data acquired through a stepped-mode scan. The NTR near 1630 nm is 27.3 dB for continuous-mode scan and 29 dB for stepped-mode scan. (**B**) Input power of ~2100 μW (14 dBm at laser source). The NTR near 1630 nm is 27 dB.

Downloaded from www.sciencemag.org on January 27, 2012

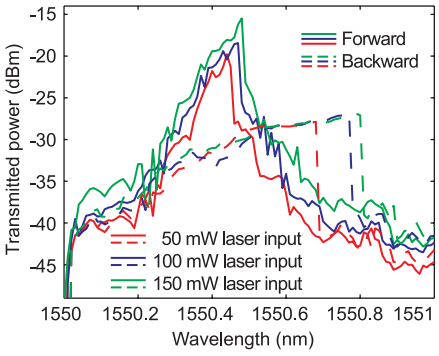


Fig. 3. Saturation of the backward-transmitted power near resonance in an ADF with coupling gaps of 420 nm and 630 nm.

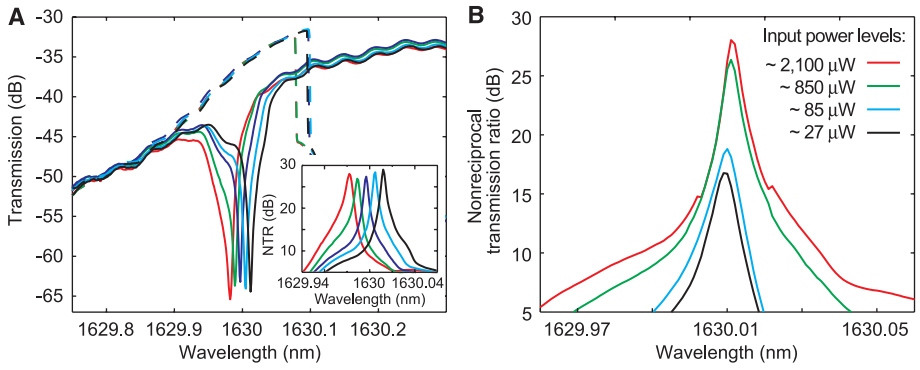


Fig. 4. (**A**) Wavelength tunability and tolerance of the mismatch between resonant wavelengths of the two filters. Dashed lines are forward transmissions; solid lines are backward transmissions. Input power was ~2100 μW. Inset explicitly shows the NTR. (**B**) The NTR at various input power levels with a fixed operating wavelength of 1630.011 nm.

sion in port II at λ_0 (solid curve in Fig. 1E). For backward propagation (input at port II), light will enter the ADF first. With the small gap, G_3, the energy in the ADF ring is high enough to red-shift its resonance—that is, $|\delta_{ADF,backward}(\lambda_0)| > 0$ in Eq. 4—and transmitted light at λ_0 will be reduced (Fig. 1F, solid curve). At the NF, the reduced light intensity, due to both the resonance shift and the insertion loss of the ADF, will not be able to red-shift the NF ring—that is, $\delta_{NF}(\lambda_0) \rightarrow 0$ in Eq. 5—and its intensity will be significantly reduced as it passes through the critically coupled NF at resonance ($\lambda_0 = \lambda_{NF}$, Fig. 1G).

At higher input power levels (~850 μW and ~2100 μW), larger NTRs up to 29 dB were observed (Fig. 2). This is due simultaneously to the increase of the NTR from the ADF (compared to Fig. 1F, which occurs at a rather moderate input power of ~85 μW) and to the sustained large NTR from the NF at high input power levels. Figure 3 shows the forward and backward transmissions of an individual ADF with coupling gaps of 420 nm and 630 nm (without a cascaded NF). In the forward direction, the transmitted power increases with the laser input power near resonance (~1550.4 nm), whereas the backward-transmitted power remains approximately the same, effectively increasing the NTR. In our optical diode (Fig. 1A), such saturation limits the backward input power entering the NF ($P_{c,b}$ in Fig. 1G). This restricts the nonlinearity in the NF and allows it to maintain high attenuation of the backward transmission.

The performance of our diode is independent of optical bistability (*7*, *20*, *26*) and is free from uncertainties caused by data acquisition schemes. In the spectra taken at two different scan modes of the tunable laser source (Fig. 2A), the solid lines are the spectra of a continuous-mode scan, which typically follows the upper trace of the hysteresis loop, whereas the dashed lines are the spectra of the stepped-mode scan (based on a step-by-step changing of operating wavelength), which generally follows the lower trace of the hysteresis loop. The rapid swing near 1630.1 nm indicates the transition between the upper and lower traces, possibly due to the fluctuations of laser power and wavelength in stepped-mode scan. Our optical diode does not operate in the bistability regime, and we observed almost identical NTRs with point measurements (i.e., fixing the laser at a specific wavelength and then measuring the transmitted power level at forward and backward directions) (table S1).

The device operation is robust against the mismatch of resonant wavelengths between the two filters, and it can achieve high NTR for various input power levels at a fixed wavelength. Within a resonance mismatch range of ~0.04 nm, the NTR remains over 25 dB (Fig. 4A). Given such tolerance, we were able to fix the operating wavelength of the diode by tuning the NF resonance in the backward direction to 1630.011 nm and achieved at least 18 dB of NTR for input power between 85 and 2100 μW (Fig. 4B).

An electronic diode blocks the backward current for a large range of applied backward voltages. Analogously, table S1 shows that our optical diode attenuates the backward-transmitted power to a low level (around –50 dBm) for a broad range of laser input power (5 to 14 dBm) at the operating wavelength of 1630.011 nm. The forward-transmitted power is more than 20 dB higher than the backward-transmitted power within this laser power range. Therefore, our optical diode tolerates not only input power variation, but also forward/backward input power disparity.

Similar to all resonance-enhanced optical devices, our all-silicon optical diode is bandwidth-limited. However, its operating wavelength can be thermally tuned (*19*) and should work across a large wavelength band. It also has a relatively high insertion loss after subtracting the coupling losses (~10.7 dB per facet). For laser input power levels between 5 and 10 dBm, the forward insertion losses were ~12 dB. This number could be reduced if the intrinsic quality factor of both rings is increased to 250,000 (*16*, *17*) and if the thermal isolation of the rings is improved, such as by suspending the NF ring away from the substrate (*27*).

The optical nonlinear effects in silicon include the Kerr effect (*28*, *29*), two-photon absorption (TPA) (*30*), the free carrier effect (FCE) (*31*), and the thermo-optic effect (*26*) from Joule heat generated through TPA, FCE, and linear absorption. Because of the large thermal dissipation time of the SiO_2 undercladding (~2 μs) (*21*–*23*) and the input power at tens of microwatts, the thermo-optic effect was dominant in our experiments. In addition to its role in enabling low-power operation, the thermo-optic effect (which reacts to optical powers averaged over a microsecond range) has a slow response time; this may benefit one-way transmission of data streams with high modulation speed, because the long integration time should desensitize nonlinear operation to fluctuations associated with rapidly varying data patterns or different modulation formats. Alternatively, when the slower thermal effect is mitigated through efficient thermal dissipation, fast nonlinearity such as FCE in silicon may dominate (*23*, *31*), opening doors to nonreciprocal high-speed optical signal processing where instantaneous response is required.

Our optical diode uses only the materials already used in CMOS processing and does not require external assistance such as magnetic fields, radio-frequency modulation, or optical pumping. The broad input power range within which our device performs may be sufficient for on-chip photonic applications. Its ability to block backward inputs that are much stronger than the forward inputs makes it functionally similar to electrical diodes. Our diode has an ultracompact footprint and is robust against resonance mismatch between the two microrings. These attributes make it attractive as a potential component for future highly integrated photonic information processing chips.

References and Notes

1. H. A. Haus, *Waves and Fields in Optoelectronics* (Prentice-Hall, Englewood Cliffs, NJ, 1984), pp. 56–61.
2. R. L. Espinola, T. Izuhara, M. C. Tsai, R. M. Osgood Jr., H. Dötsch, *Opt. Lett.* **29**, 941 (2004).
3. T. R. Zaman, X. Guo, R. J. Ram, *Appl. Phys. Lett.* **90**, 023514 (2007).
4. L. Bi *et al.*, *Nat. Photonics* **5**, 758 (2011).
5. S. F. Mingaleev, Y. S. Kivshar, *J. Opt. Soc. Am. B* **19**, 2241 (2002).

Downloaded from www.sciencemag.org on January 27, 2012

6. K. Gallo, G. Assanto, K. R. Parameswaran, M. M. Fejer, *Appl. Phys. Lett.* **79**, 314 (2001).
7. M. Soljačić, C. Luo, J. D. Joannopoulos, S. Fan, *Opt. Lett.* **28**, 637 (2003).
8. A. Rostami, *Opt. Laser Technol.* **39**, 1059 (2007).
9. S. K. Ibrahim, S. Bhandare, D. Sandel, H. Zhang, R. Noe, *Electron. Lett.* **40**, 1293 (2004).
10. J. Hwang *et al.*, *Nat. Mater.* **4**, 383 (2005).
11. S. Manipatruni, J. T. Robinson, M. Lipson, *Phys. Rev. Lett.* **102**, 213903 (2009).
12. Z. Yu, S. Fan, *Nat. Photonics* **3**, 91 (2009).
13. M. S. Kang, A. Butsch, P. S. J. Russell, *Nat. Photonics* **5**, 549 (2011).
14. B. E. Little, S. T. Chu, H. A. Haus, J. Foresi, J.-P. Laine, *J. Lightwave Technol.* **15**, 998 (1997).
15. Q. Xu, B. Schmidt, S. Pradhan, M. Lipson, *Nature* **435**, 325 (2005).
16. S. Xiao, M. H. Khan, H. Shen, M. Qi, *Opt. Express* **15**, 14467 (2007).
17. S. Xiao, H. Shen, M. H. Khan, M. Qi, *Conf. Lasers and Electro-Optics* CTuGG6 (2008); www.opticsinfobase.org/abstract.cfm?uri=CLEO-2008-CTuGG6.
18. T. Barwicz *et al.*, *Opt. Express* **12**, 1437 (2004).
19. M. H. Khan *et al.*, *Nat. Photonics* **4**, 117 (2010).
20. M. Soljačić, M. Ibanescu, S. G. Johnson, Y. Fink, J. D. Joannopoulos, *Phys. Rev. E* **66**, 055601 (2002).
21. P. E. Barclay, K. Srinivasan, O. Painter, *Opt. Express* **13**, 801 (2005).
22. T. Uesugi, B.-S. Song, T. Asano, S. Noda, *Opt. Express* **14**, 377 (2006).
23. Q. Xu, M. Lipson, *Opt. Lett.* **31**, 341 (2006).
24. J. Ouyang, X. Wang, M. Qi, Meep (MIT Electromagnetic Equation Propagation), http://nanohub.org/resources/2954 (2007).
25. See supporting material on *Science* Online.
26. V. R. Almeida, M. Lipson, *Opt. Lett.* **29**, 2387 (2004).
27. P. Sun, R. M. Reano, *Opt. Lett.* **35**, 1124 (2010).
28. X. Chen, N. C. Panoiu, I. Hsieh, J. I. Dadap, R. M. Osgood, *IEEE Photon. Technol. Lett.* **18**, 2617 (2006).
29. J. B. Driscoll *et al.*, *IEEE J. Sel. Top. Quantum Electron.* **16**, 1448 (2010).
30. M. Dinu, F. Quochi, H. Garcia, *Appl. Phys. Lett.* **82**, 2954 (2003).
31. A. C. Turner-Foster *et al.*, *Opt. Express* **18**, 3582 (2010).

Acknowledgments: We thank D. Leaird for experimental assistance and J. Ouyang for helpful discussions. Supported by Defense Threat Reduction Agency grant HDTRA1-10-1-0106, Air Force Office of Scientific Research grant FA9550-08-1-0379, NSF grant ECCS-0925759, and NIH grant 1R01RR026273-01. Finite-difference time domain simulation work was carried out through the Network for Computational Nanotechnology with resources available at www.nanohub.org. L.F. and L.T.V. fabricated and characterized the devices. J.W. performed simulation and selected device parameters. H.S. helped in device characterization. B.N. helped in the design. M.Q. conceived the idea and supervised the investigation. M.Q., L.T.V., L.F., and J.W. wrote the manuscript. All discussed the results and commented on the manuscript.

Supporting Online Material

www.sciencemag.org/cgi/content/full/science.1214383/DC1
Materials and Methods
Table S1

23 September 2011; accepted 6 December 2011
Published online 22 December 2011;
10.1126/science.1214383

Reversible Reduction of Oxygen to Peroxide Facilitated by Molecular Recognition

Nazario Lopez,[1] Daniel J. Graham,[1] Robert McGuire Jr.,[1] Glen E. Alliger,[1] Yang Shao-Horn,[2] Christopher C. Cummins,[1]* Daniel G. Nocera[1]*

Generation of soluble sources of peroxide dianion (O_2^{2-}) is a challenge in dioxygen chemistry. The oxidizing nature of this anion renders its stabilization in organic media difficult. This Report describes the chemically reversible reduction of oxygen (O_2) to cryptand-encapsulated O_2^{2-}. The dianion is stabilized by strong hydrogen bonds to N-H groups from the hexacarboxamide cryptand. Analogous stabilization of peroxide by hydrogen bonding has been invoked recently in crystalline saccharide and protein systems. The present peroxide adducts are stable at room temperature in dimethyl sulfoxide (DMSO) and *N*,*N*′-dimethylformamide (DMF). These adducts can be obtained in gram quantities from the cryptand-driven disproportionation reaction of potassium superoxide (KO_2) at room temperature.

Reduction of molecular oxygen to the level of peroxide dianion (O_2^{2-}) is typically accomplished in chemical and biological systems in the stabilizing coordination sphere of a transition metal (*1*). Such peroxide transition-metal complexes are important intermediates in natural oxidation processes (*2*–*4*), and they have long been used as reagents for organic synthesis (*5*). We hypothesized that peroxide dianion could be stabilized alternatively in a molecular environment of hydrogen bond donors so arranged as to completely surround O_2^{2-} with partial positive charge. A structural basis for peroxide stabilization via hydrogen bonding to organic matter has appeared recently in the context of sodium peroxide crystallization with 1,6-anhydro-β-maltose (*6*). The reported complex salt of formula $[Na_2(1,6\text{-anhydro-}\beta\text{-maltose})_2(H_2O)_3]O_2$ has a layered structure featuring six hydrogen bonds that encase each O_2^{2-} ion, with sugar O-H groups acting as the hydrogen-bond donors. This peroxide environment is reminiscent of that determined for $Na_2O_2 \cdot 8\,H_2O$, in which chains of edge-connected $[Na(OH_2)_6]^+$ octahedra are linked together by O–H···O peroxide/water hydrogen bonds (*7*). Now, we show that hexacarboxamide cryptand molecules of a type introduced originally as receptors for halide ions (*8*, *9*), and investigated by us as binucleating ligands for transition-metal ions (*10*, *11*), form soluble 1:1 complexes with peroxide dianion wherein O_2^{2-} resides in a molecular interior surrounded by six carboxamide N-H hydrogen bond donors in a trigonal antiprismatic array. The receptors stabilize peroxide dianion to such an extent that, if it is present in the same solution, superoxide (O_2^-) undergoes disproportionation to form O_2 and encapsulated O_2^{2-}, thus coupling the anion receptor molecular recognition phenomenon (*12*) to an oxidation-reduction process.

Preparation of the cryptand peroxide adduct can be achieved starting from either superoxide or O_2. Treatment of a slurry of *tert*-butyl–substituted hexacarboxamide cryptand (*m*BDCA-5t-H_6) with 2.2 equiv of KO_2 in *N*,*N*′-dimethylformamide (DMF) resulted in the formation of the O_2^{2-} adduct $[K_2(DMF)_5][(O_2)\subset m\text{BDCA-5t-}H_6]$ in 74% isolated yield (Fig. 1). Vigorous bubbling was observed immediately after adding KO_2; mass spectrometry (MS, fig. S1) establishes that the gas is a result of O_2 production from the cryptand-driven disproportionation of O_2^-. The ^{1}H nuclear magnetic resonance (NMR) spectrum (fig. S2) indicates the formation of a O_2^{2-} adduct in which the amide chemical shift is in the range of a normal charged hydrogen bond (NCHB) interaction (*13*). The generality of peroxide dianion recognition was probed by using the related 3,5-dipropoxyphenoxyl–substituted hexacarboxamide cryptand (*m*BDCA-5p-H_6) (*10*). Similar large downfield shifts of ^{1}H NMR signals for N-H [14.69 parts per million (ppm)] and aromatic protons (10.03 ppm) pointing inside the cavity were observed, indicative of O_2^{2-} encapsulation at room temperature (fig. S3). The $[(O_2)\subset m\text{BDCA-5t-}H_6]^{2-}$ adduct can also be obtained by reducing O_2 in situ with 2 equiv of cobaltocene ($CoCp_2$, where Cp is cyclopentadienyl) in the presence of 1 equiv of free cryptand in DMF (fig. S4), where the first reduction potential of $CoCp_2$ is coincident with the reduction of oxygen (fig. S5).

Both cryptand peroxide adducts were characterized by x-ray diffraction studies using single crystals obtained by vapor diffusion of diethyl ether into DMF solutions (Fig. 2 and figs. S6 and S7). A view down the pseudo-threefold axis of the adduct indicates that the cryptand adopts a propeller-like conformation (Fig. 2B and fig. S7b). The O–O bond lengths of 1.504 ± 0.0002 [1.504(2) (number in parentheses indicates the estimated standard deviation in the final digit) Å for $[K_2(DMF)_5][(O_2)\subset m\text{BDCA-5t-}H_6]$ and 1.499(2) Å for $(DMF)[K_2(DMF)_5][(O_2)\subset m\text{BDCA-5p-}H_6]$, which are comparable to that in ribonucleotide reductase Ib (1.47 Å) (*14*), in 1,6-anhydro-β-maltose adduct [1.496(2) Å] (*6*), and in Na_2O_2 (1.49 Å)

[1]Department of Chemistry, 77 Massachusetts Avenue, Massachusetts Institute of Technology (MIT), Cambridge, MA 02139–4307, USA. [2]Departments of Mechanical Engineering and Materials Science and Engineering, 77 Massachusetts Avenue, MIT, Cambridge, MA 02139–4307, USA.

*To whom correspondence should be addressed. E-mail: nocera@mit.edu (D.G.N.); ccummins@mit.edu (C.C.C.)

Downloaded from www.sciencemag.org on January 27, 2012

(*15*), are indicative of the peroxide character of the O_2 moiety. Both structures reveal identical interactions with O_2^{2-} where the complementarity of the six amide protons with the six lone pairs on the peroxide dianion results in N···O distances in the range of 2.64 to 2.73 Å and 2.63 to 2.71 Å for $[K_2(DMF)_5][(O_2)\subset mBDCA\text{-}5t\text{-}H_6]$ (table S1) and $(DMF)[K_2(DMF)_5][(O_2)\subset mBDCA\text{-}5p\text{-}H_6]$ (table S3), respectively, which are indicative of strong hydrogen bonds (*16*). The amide protons of the present cryptand adducts are directed toward the lone pairs on the peroxide with N···O–O angles ranging from 117.7° to 123.8° and from 118.3° to 121.9° for $[K_2(DMF)_5][(O_2)\subset mBDCA\text{-}5t\text{-}H_6]$ (table S1) and $(DMF)[K_2(DMF)_5][(O_2)\subset mBDCA\text{-}5p\text{-}H_6]$ (table S3), respectively (*17*). The aryl protons pointing inside the cavity also interact with peroxide, with C···O distances ranging from 3.16 to 3.23 Å and from 3.13 to 3.18 Å for $[K_2(DMF)_5][(O_2)\subset mBDCA\text{-}5t\text{-}H_6]$ (table S2) and $(DMF)[K_2(DMF)_5][(O_2)\subset mBDCA\text{-}5p\text{-}H_6]$ (table S4), respectively, distances indicative of weak hydrogen bonds (*16*). Thus, the peroxide dianion is stabilized by a combination of six strong hydrogen bonds to six amide protons and six weak hydrogen bonds to three aryl protons (Fig. 2 and Table 1).

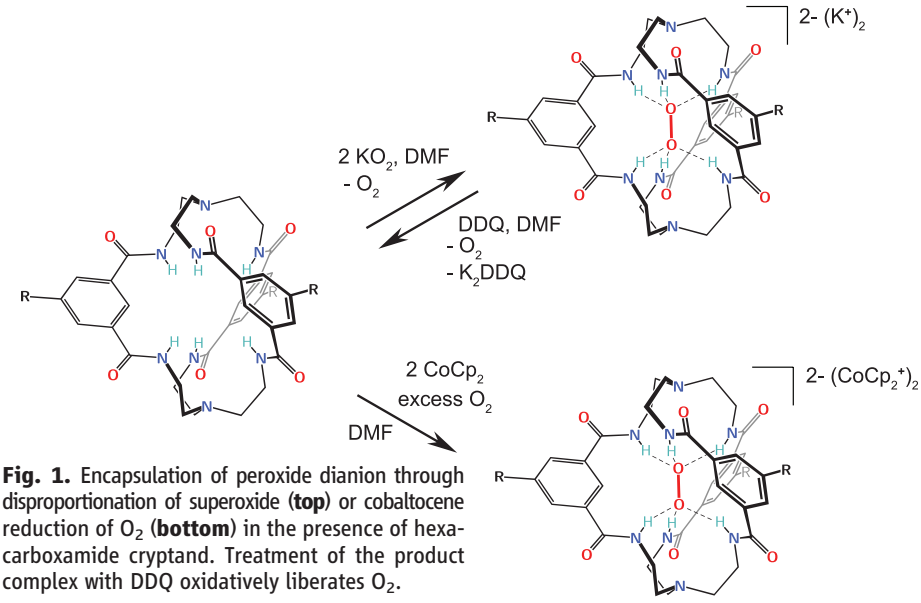


Fig. 1. Encapsulation of peroxide dianion through disproportionation of superoxide (**top**) or cobaltocene reduction of O_2 (**bottom**) in the presence of hexacarboxamide cryptand. Treatment of the product complex with DDQ oxidatively liberates O_2.

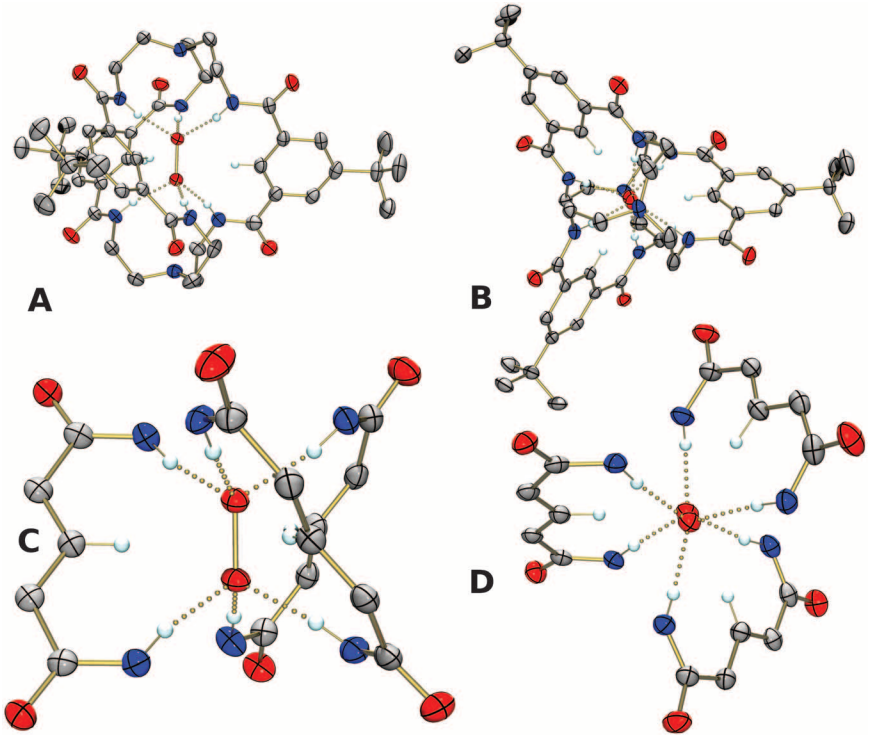


Fig. 2. Thermal ellipsoid plots at 50% probability level of $[K_2(DMF)_5][(O_2)\subset mBDCA\text{-}5t\text{-}H_6]$ peroxide adduct. (**A**) Side view and (**B**) view down the pseudo-threefold axis. Potassium ions, non–hydrogen-bonded hydrogen atoms, and DMF molecules have been omitted for clarity. (**C**) Side view and (**D**) view down the pseudo-threefold axis of cropped cryptand emphasizing the hydrogen-bonding interactions (dotted lines) with peroxide dianion. C is in gray; N, blue; O, red; H, light blue. Bond distance for $O\text{–}O_{peroxide}$ is 1.504(2) Å.

$[K_2(DMF)_5][(O_2)\subset mBDCA\text{-}5t\text{-}H_6]$ is stable in solution at room temperature for at least 1 month and remains intact even after heating for 100 min at 50°C (fig. S8). The molecular recognition of O_2^{2-} is reversible. Treatment of a solution containing 1 equiv of $[K_2(DMF)_5][(O_2)\subset mBDCA\text{-}5t\text{-}H_6]$ with 2 equiv of ferrocenium trifluoromethanesulfonate (FcOTf) results in quantitative production of free cryptand and ferrocene as indicated by ^1H NMR spectroscopy; no oxidation of the cryptand was observed (figs. S9 and S10). The cryptand fluoride adduct (*9*) is readily obtained through treatment of 1 equiv of $[K_2(DMF)_5][(O_2)\subset mBDCA\text{-}5t\text{-}H_6]$ with the convenient two-electron oxidant and fluoride source, xenon difluoride (XeF_2) (*18*) (figs. S11 and S12). The fluoride adduct, $[TBA][(F)\subset mBDCA\text{-}5t\text{-}H_6]$ (TBA is tetra-*n*-butylammonium cation), was independently obtained and structurally characterized (figs. S13 to S15). The fluoride is hydrogen-bonded to all amide protons and three aryl protons as is observed for the peroxide adduct. The behavior of $[K_2(DMF)_5][(O_2)\subset mBDCA\text{-}5t\text{-}H_6]$ upon chemical oxidation was found to depend on the nature of the oxidant. No gaseous products were observed upon addition of 2 equiv of FcOTf to $[K_2(DMF)_5][(O_2)\subset mBDCA\text{-}5t\text{-}H_6]$. Although gas chromatography (GC) and MS revealed substantial CO_2 and Xe but insignificant O_2 in the headspace above dimethyl sulfoxide (DMSO) solutions of $[K_2(DMF)_5][(O_2)\subset mBDCA\text{-}5t\text{-}H_6]$ after treatment with XeF_2, the slow addition of 1.1 equiv 2,3-dichloro-5,6-dicyano-1,4-benzoquinone (DDQ) resulted in the sole release of O_2 in 88% yield as determined by GC (fig. S16) and MS (fig. S17). Analysis of the reaction mixture by ^1H NMR spectroscopy indicates that DDQ^{2-} is hydrogen-bonded to $mBDCA\text{-}5t\text{-}H_6$ (fig. S18); this interaction can be overcome by the formation of the fluoride adduct $[(F)\subset mBDCA\text{-}5t\text{-}H_6]^-$ when 2 equiv of [TBA][F] are added (fig. S19).

Evidence for the release of O_2 upon oxidation of $[K_2(DMF)_5][(O_2)\subset mBDCA\text{-}5t\text{-}H_6]$ at a glassy carbon electrode was obtained from a 4.8 mM solution of cryptand peroxide adduct in DMF containing 0.1 M $[TBA][ClO_4]$ by using a rotating ring disk electrode, scanning the potential of the disk, and holding the ring potential constant (fig. S20). During a potential scan of the disk electrode, a collection current is observed only when the ring is fixed to a potential sufficient for O_2 reduction. In addition, the release of O_2 is observed in cyclic voltammograms of the same solution. Although no features are observed

Downloaded from www.sciencemag.org on January 27, 2012

during an initial scan to negative potentials, a reductive wave appears only after oxidation of the complex at the electrode (fig. S21).

The observed chemical reactivity for reversible peroxide encapsulation is supported by the electrochemistry of the cryptand in the presence of oxygen. The reduction of oxygen to O_2^- solvated by large cations such as TBA is reversible in aprotic solvents (*19*). Whereas *m*BDCA-5t-H_6 shows no redox features from 0.25 to –2.3 V versus Ag/Ag^+, several new features are observed in the cyclic voltammograms of the cryptand in the presence of oxygen as shown in Fig. 3A. Upon scanning cathodically, an additional sharp reduction wave appears positive of the free-oxygen reduction wave at ~–1.4 V. The red trace shows the reversible one-electron oxygen/superoxide (O_2/[TBA][O_2]) couple in the absence of *m*BDCA-5t-H_6. On the return anodic sweep, a broad oxidation process is observed, centered at –0.7 V, in addition to the oxidation of free superoxide ([TBA][O_2]) at ~–1.4 V. The current associated with these new reduction and oxidation waves increases with increasing concentration of the cryptand, whereas the oxidation associated with superoxide ([TBA][O_2]) decreases.

Table 1. Selected hydrogen-bonding distances (Å) and angles (°).

Donor — — — H···Acceptor	D — H	H···A	D···A	D—H···A (°)
N101 — — H101 ··O2	0.86(2)	1.85(2)	2.692(3)	168(3)
N102 — — H102 ··O1	0.88(2)	1.83(2)	2.698(3)	169(3)
N201 — — H201 ··O2	0.87(3)	1.78(3)	2.639(3)	168(3)
N202 — — H202 ··O1	0.89(2)	1.84(2)	2.708(3)	168(2)
N301 — — H301 ··O2	0.88(3)	1.87(3)	2.732(3)	168(3)
N302 — — H302 ··O1	0.87(2)	1.80(2)	2.659(3)	167(3)

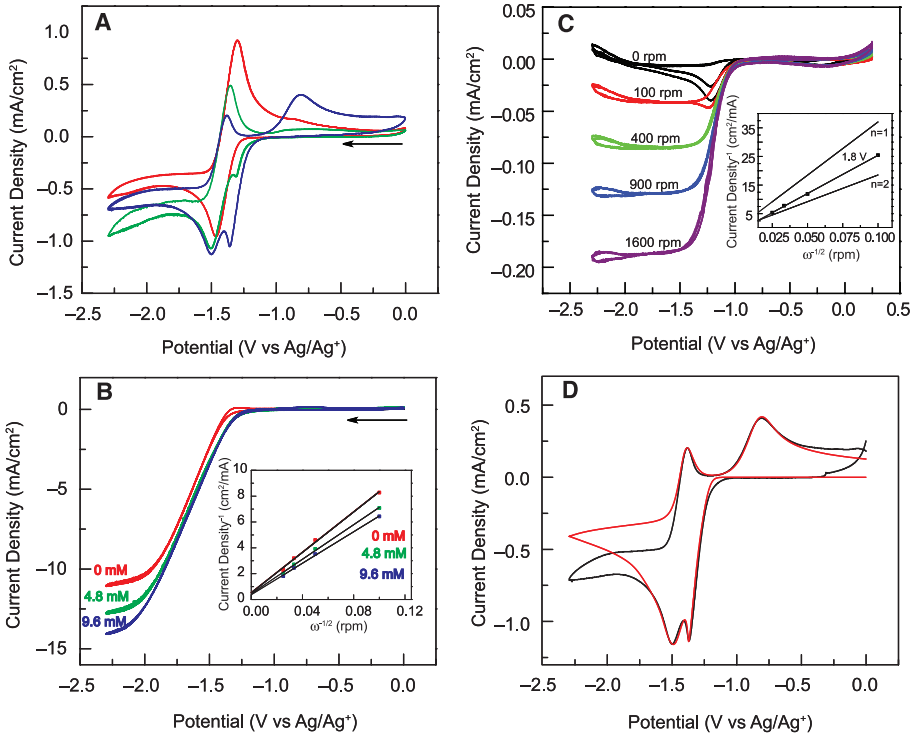


Fig. 3. (**A**) Cyclic voltammograms measured at a glassy carbon electrode in O_2-saturated DMF containing 0.1 M [TBA][ClO_4] in the presence of 0.0 mM *m*BDCA-5t-H_6 (red), 4.8 mM *m*BDCA-5t-H_6 (green), and 9.6 mM *m*BDCA-5t-H_6 (blue) (scan rate of 10 mV/s). (**B**) Rotating-disk electrode measurements using a glassy carbon electrode in O_2-saturated DMF containing 0.1 M [TBA][ClO_4] in the presence of 0.0 mM *m*BDCA-5t-H_6 (red), 4.8 mM *m*BDCA-5t-H_6 (green), and 9.6 mM *m*BDCA-5t-H_6 (blue) at 1600 revolutions per minute (rpm) (scan rate 100 mV/s). (Inset) K-L analysis of rotating-disk electrode data at 2.25 V for 0.0 mM *m*BDCA-5t-H_6 (red), 4.8 mM *m*BDCA-5t-H_6 (green), and 9.6 mM *m*BDCA-5t-H_6 (blue). (**C**) Rotating-disk electrode measurements using a glassy carbon electrode in DMF containing 0.1 M [TBA][ClO_4] saturated with 1% O_2 in argon in the presence of 4.8 mM *m*BDCA-5t-H_6 at 0 rpm (black), 100 rpm (red), 400 rpm (green), 900 rpm (blue), or 1600 rpm (purple) (scan rate 100 mV/s). (Inset) K-L analysis of rotating-disk electrode data at 1.8 V and the expected slopes for n = 1 and n = 2. (**D**) Cyclic voltammogram of 9.6 mM *m*BDCA-5t-H_6 (black) and simulated cyclic voltammogram (red) using the mechanistic steps described in Fig. 4.

On the basis of the reaction chemistry depicted in Fig. 1, we propose that the new reduction wave results from the ability of the cryptand to rapidly sequester O_2^- formed at the cathode and facilitate subsequent transfer of a second electron from either the electrode or another molecule of O_2^-. The sharp decrease in current responsible for the shape of the peak is indicative of the rapid depletion of free cryptand near the electrode, a phenomenon that is due to the ease with which the cryptand reacts with O_2^- and the sluggish diffusion of free cryptand to the electrode relative to free O_2. As the working electrode potential decreases further, one-electron reduction of O_2 produces a steady supply of O_2^-, which can react with free cryptand as it diffuses away from the electrode. Measurements of independently prepared [K_2(DMF)$_5$][(O_2)⊂*m*BDCA-5t-H_6] in argon-saturated solution show predominant oxidation at ~–0.7 V and subsequent reduction at ~–1.4 V, which support observations indicating that these two features correspond to the oxidation of the cryptand peroxide with concomitant release of O_2 and the reformation of [(O_2)⊂*m*BDCA-5t-H_6]$^{2-}$, respectively (fig. S21). Measurements of oxygen reduction in the presence of tris(2-aminoethyl) amine (TREN) or 5-*tert*-butylisophthalic acid (figs. S22 and S23) show negligible oxidation currents from ~–1.5 to ~–0.5 V, indicating that the oxidation process at ~–0.7 V is not cryptand-based and that the cryptand remains intact during the oxygen redox measurements. Overall, the process is electrochemically irreversible under saturated oxygen.

Rotating-disk electrode measurements further confirm that the cryptand drives the O_2 reduction to a two-electron process. Figure 3B and figs. S24 to S26 show the rotating-disk electrode results for increasing concentration of *m*BDCA-5t-

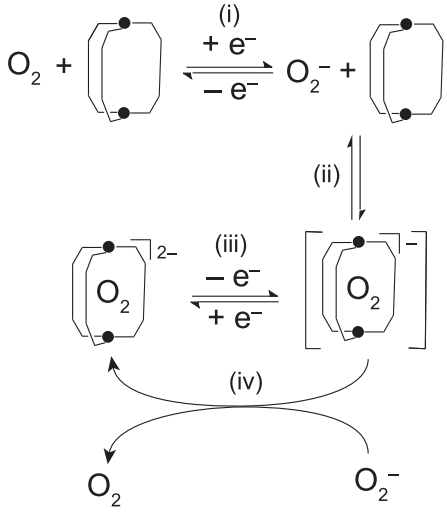


Fig. 4. Proposed mechanism of the reversible cryptand-facilitated O_2 reduction to encapsulated O_2^{2-}. Simulated standard potentials, rate constants, and equilibrium constants for the elementary steps labeled i to iv were derived from fits to the cyclic voltammetry data and are given in table S5a.

Downloaded from www.sciencemag.org on January 27, 2012

H_6 and *m*BDCA-5p-H_6 in oxygen-saturated DMF solution. An increase in the limiting current as well as decreasing slope of the Koutecký-Levich (K-L) analysis of diffusion-limited currents (Fig. 3B, inset) is consistent with a greater number of electrons transferred during reduction of oxygen in the presence of *m*BDCA-5t-H_6 than the one-electron reduction process without *m*BDCA-5t-H_6 (*20*). A large excess of cryptand is needed in order to drive the electrochemical process completely to peroxide encapsulation during rotating-disk electrode experiments. K-L analysis of diffusion-limiting currents as a function of the inverse square root of rotation speed, collected in 0.1 M [TBA][ClO_4] DMF solution saturated with 1% O_2 in argon with 4.8 mM *m*BDCA-5t-H_6 (Fig. 3C), indicates that the number of transferred electrons increases toward an overall two-electron process, which is expected if every oxygen molecule was reduced and encapsulated by the cryptand.

Figure 3D shows a simulation of the cyclic voltammogram using the reaction sequence illustrated in Fig. 4. The reaction sequence used to model the electrochemistry concurs with the established chemical reactivity of O_2 and cryptand described by Fig. 1. Parameters obtained from the simulation are collected in table S5, a and b. Our model suggests that rapid encapsulation of O_2^- by free cryptand drives further one-electron reduction, either directly by the working electrode or through a disproportionation reaction with another equiv of O_2^-, resulting in the formation of $[(O_2)\subset m\text{BDCA-5t-}H_6]^{2-}$. The assumption that the diffusion coefficient of O_2 is much greater than that of the cryptand species (table S5b) in DMF containing 0.1 M [TBA][ClO_4] reproduces the sharp feature observed before the wave attributed to one-electron reduction of O_2. An appropriate fit for the anodic sweep could only be accomplished by modeling the oxidation of $[(O_2)\subset m\text{BDCA-5t-}H_6]^{2-}$ as a series of two, one-electron oxidations.

The reversible one-electron reduction of oxygen in DMF is altered by addition of both strong and weak acids (*21*). In the case of *m*BDCA-5t-H_6, the cryptand could serve as a source of protons. However, figs. S27 and S28 illustrate that the reduction of oxygen in the presence of strong and weak acids, respectively, differs from oxygen reduction in the presence of *m*BDCA-5t-H_6 at equal concentration. These data suggest that the cryptand does not serve as a Brønsted acid in the overall oxygen reduction process.

The electrochemistry of *m*BDCA-5t-H_6 and *m*BDCA-5p-H_6 in the presence of oxygen is consistent with reduction of oxygen by one electron to superoxide followed by incorporation into the cryptand cavity, in turn driving disproportionation to give the cryptand-encapsulated peroxide adduct. Oxidation of peroxide dianion within the cavity restores oxygen and the free cryptand ligand. The proposed electrochemical mechanism in Fig. 4 maps on to the observed chemical reactivity of Fig. 1; the combined chemical and electrochemical studies demonstrate encapsulation-driven chemically reversible two-electron reduction of O_2 to peroxide dianion.

We have synthesized a molecular peroxide dianion adduct by the use of the cavity of hexacarboxamide cryptands as a molecular recognition site. Reduction of oxygen in situ and stabilization of peroxide dianion is facilitated by hydrogen bonding within the cavity of the cryptand, and this process mimics the structural characteristics of biological systems that use peroxide as an oxidant. The use of molecular recognition of an in situ–generated reactive oxygen species has the potential to be incorporated into several technologies, including Li-air batteries, because it is chemically reversible, prevents overreduction to lithium oxide, and imparts substantial solubility in aprotic media (*22*). In addition, because the present peroxide adducts can be obtained in high yield in a one-pot reaction and are stable in solution, they could be used as a soluble source of peroxide dianion for a variety of reactions.

References and Notes

1. B. Meunier, Ed., *Metal-Oxo and Metal-Peroxo Species in Catalytic Oxidations* (Springer, Berlin, 2000).
2. B. Meunier, Ed., *Biomimetic Oxidations Catalyzed by Transition Metal Complexes* (Imperial College Press, London, 2000).
3. B. Meunier, S. P. de Visser, S. Shaik, *Chem. Rev.* **104**, 3947 (2004).
4. A. Butler, M. J. Clague, G. E. Meister, *Chem. Rev.* **94**, 625 (1994).
5. M. V. George, K. S. Balachandran, *Chem. Rev.* **75**, 491 (1975).
6. T. Kato *et al.*, *Chem. Lett.* **39**, 136 (2010).
7. M. Grehl, R. Fröhlich, S. Thiele, *Acta Crystallogr. C* **51**, 1038 (1995).
8. S. O. Kang, J. M. Llinares, D. Powell, D. VanderVelde, K. Bowman-James, *J. Am. Chem. Soc.* **125**, 10152 (2003).
9. S. O. Kang, V. W. Day, K. Bowman-James, *J. Org. Chem.* **75**, 277 (2010).
10. G. E. Alliger, P. Müller, C. C. Cummins, D. G. Nocera, *Inorg. Chem.* **49**, 3697 (2010).
11. G. E. Alliger, P. Müller, L. H. Do, C. C. Cummins, D. G. Nocera, *Inorg. Chem.* **50**, 4107 (2011).
12. J. L. Sessler, P. A. Gale, W.-S. Cho, *Anion Receptor Chemistry* (Royal Society of Chemistry, London, ed. 1, 2006).
13. M. Garcia-Viloca, A. González-Lafont, J. M. Lluch, *J. Am. Chem. Soc.* **119**, 1081 (1997).
14. A. K. Boal, J. A. Cotruvo Jr., J. Stubbe, A. C. Rosenzweig, *Science* **329**, 1526 (2010).
15. R. D. Jones, D. A. Summerville, F. Basolo, *Chem. Rev.* **79**, 139 (1979).
16. G. R. Desiraju, T. Steiner, in *The Weak Hydrogen Bond in Structural Chemistry and Biology* (Oxford Univ. Press, Oxford, 1999), p. 13.
17. The residual electron density of refinements without assignment of the electron density of N-H hydrogen atoms surrounding the peroxide moiety suggests that the protons reside at the carboxamide nitrogens of the cryptand, even though the exact position cannot be obtained from x-ray data. Thus, hydroperoxide anion HO_2^- is unlikely to be the species trapped, and the best model obtained was of peroxide dianion (figs. S29 to S32).
18. N. Bartlett, F. O. Sladky, *Chem. Commun.* **1968**, 1046 (1968).
19. D. L. Maricle, W. G. Hodgson, *Anal. Chem.* **37**, 1562 (1965).
20. A. J. Bard, L. R. Faulkner, in *Electrochemical Methods: Fundamentals and Applications* (Wiley, New York, ed. 2, 2000), p. 341.
21. D. T. Sawyer, G. Chiericato Jr., C. T. Angelis, E. J. Nanni Jr., T. Tsuchiya, *Anal. Chem.* **54**, 1720 (1982).
22. G. Girishkumar, B. McCloskey, A. C. Luntz, S. Swanson, W. Wilcke, *J. Phys. Chem. Lett.* **1**, 2193 (2010).

Acknowledgments: This research was supported by the NSF–Centers for Chemical Innovation (CHE-0802907). Grants from the NSF also provided instrument support to the Department of Chemistry Instrument Facility at MIT (grants CHE-9808061 and DBI-9729592). D.J.G. thanks the NSF Graduate Research Fellowship Program for support. We thank Y. Surendranath for productive discussions and collecting mass spectrometry data, A. F. Cozzolino and P. Müller for structure refinement discussions, and F. A. Armstrong for helpful discussions. Complete crystallographic data were deposited in the Cambridge Crystallographic Database Centre (CCDC 831953 to 831955 and 831962).

Supporting Online Material

www.sciencemag.org/cgi/content/full/335/6067/450/DC1
Materials and Methods
Figs. S1 to S32
Tables S1 to S5
References (*23*–*27*)

15 August 2011; accepted 13 December 2011
10.1126/science.1212678

A Long-Lived Lunar Core Dynamo

Erin K. Shea,[1]* Benjamin P. Weiss,[1] William S. Cassata,[2] David L. Shuster,[2,3] Sonia M. Tikoo,[1] Jérôme Gattacceca,[4] Timothy L. Grove,[1] Michael D. Fuller[5]

Paleomagnetic measurements indicate that a core dynamo probably existed on the Moon 4.2 billion years ago. However, the subsequent history of the lunar core dynamo is unknown. Here we report paleomagnetic, petrologic, and $^{40}Ar/^{39}Ar$ thermochronometry measurements on the 3.7-billion-year-old mare basalt sample 10020. This sample contains a high-coercivity magnetization acquired in a stable field of at least ~12 microteslas. These data extend the known lifetime of the lunar dynamo by 500 million years. Such a long-lived lunar dynamo probably required a power source other than thermochemical convection from secular cooling of the lunar interior. The inferred strong intensity of the lunar paleofield presents a challenge to current dynamo theory.

The discovery of remanent magnetization in samples taken by the Apollo lunar missions and by spacecraft observations of the lunar crust has long suggested that the Moon formed a metallic core and a dynamo-generated magnetic field (*1*). However, the association of magnetization with the antipodes of impact basins and laboratory studies of transient plasma-generated magnetic fields suggest that meteoroid impacts could also be a source of lunar magnetization (*2, 3*).

Downloaded from www.sciencemag.org on January 27, 2012

Because impact fields from the largest basin-forming events are expected to last less than 1 day (*2*), they should only be recorded by shocked or quickly cooled rocks. Therefore, to identify records of a core dynamo field, it is important to study slowly cooled samples with high magnetic recording fidelity that show no petrographic evidence of shock. Unfortunately, few lunar rocks have all of these properties (*1*). An exception is lunar troctolite sample 76535, which was observed to have a stable natural remanent magnetization (NRM) formed in a field of ~1 to 50 μT that is stable up to coercivities >200 mT (*4*). The magnetic history of this sample, coupled with its slow (millions of years) cooling time scale, suggests that the Moon had a core dynamo at 4.2 billion years ago (Ga). This result is consistent with recent analyses of Apollo-era seismic data (*5*) and lunar laser ranging (*6*) that indicate that even today the Moon has a small (~330 km in diameter) partially molten metallic core.

The lifetime of the early lunar dynamo remains uncertain. Thermochemical core convection owing to secular planetary cooling, which is widely thought to power most, if not all, dynamos in the present-day solar system (*7*), is not expected to have persisted beyond ~4.2 Ga (*8, 9*). Therefore, evidence that the dynamo continued after this time would probably indicate that it was powered by an alternative energy source (*10, 11*). Here we report a paleomagnetic study of another lunar sample with high magnetic recording fidelity, mare basalt 10020. This sample has the potential to contain a record of lunar magnetism 500 million years (My) after troctolite 76535 and has a much simpler thermal history. Furthermore, 10020 formed during a putative high-field epoch of the Moon, when paleofields may have exceeded even that of Earth today (*1*).

10020 was collected on 20 July 1969 as unoriented regolith float from the southwestern edge of Mare Tranquillitatis. Along with the other Apollo 11 basalt samples, 10020 is thought to have been excavated from mostly intact bedrock by the impact that created West Crater at ~102 million years ago (Ma) [see supporting online material section 5 (SOM 5) and (*12*)]. 10020 is a fine-grained, vesicular, low-potassium ilmenite basalt of petrologic group B3 (*13*), with primary igneous glass (*14, 15*) and no apparent shock features [SOM 5 and (*16*)]. Its primary ferromagnetic mineral is kamacite (α-$Fe_{1-x}Ni_x$ with $x < 0.02$) [SOM 5 and (*16*)]. Our petrologic observations (SOM 5) found that plagioclase shows no fracturing, mechanical twinning, or alteration to maskelynite, and olivine shows no undulatory extinction, indicating peak shock pressures <5 GPa. 10020 has an $^{40}Ar/^{39}Ar$ age of 3.72 ± 0.04 Ga (*17, 18*) [recalculated using modern decay constants (*19*)], which is within error of Rb/Sr crystallization ages of other group B3 Apollo 11 basalts (*17, 18*). A previous paleomagnetic investigation observed that two unoriented chips of 10020 displayed some of the most stable NRM of any studied lunar sample (blocked up to at least 50 to 65 mT) [(*20*) and fig. 30 in (*1*)], possibly a reflection of its relatively high glass content (SOM 5). The late-stage (≲1100°C) primary igneous cooling rate of 10020

[1]Department of Earth, Atmospheric, and Planetary Sciences, Massachusetts Institute of Technology (MIT), 77 Massachusetts Avenue, Cambridge, MA 02139, USA. [2]Department of Earth and Planetary Science, University of California, Berkeley, CA 94720, USA. [3]Berkeley Geochronology Center, 2455 Ridge Road, Berkeley, CA 94709, USA. [4]Centre Européen de Recherche et d'Enseignement, CNRS/Université Aix-Marseille 3, France. [5]University of Hawaii at Manoa, Honolulu, HI, USA.

*To whom correspondence should be addressed. E-mail: nuptse@mit.edu

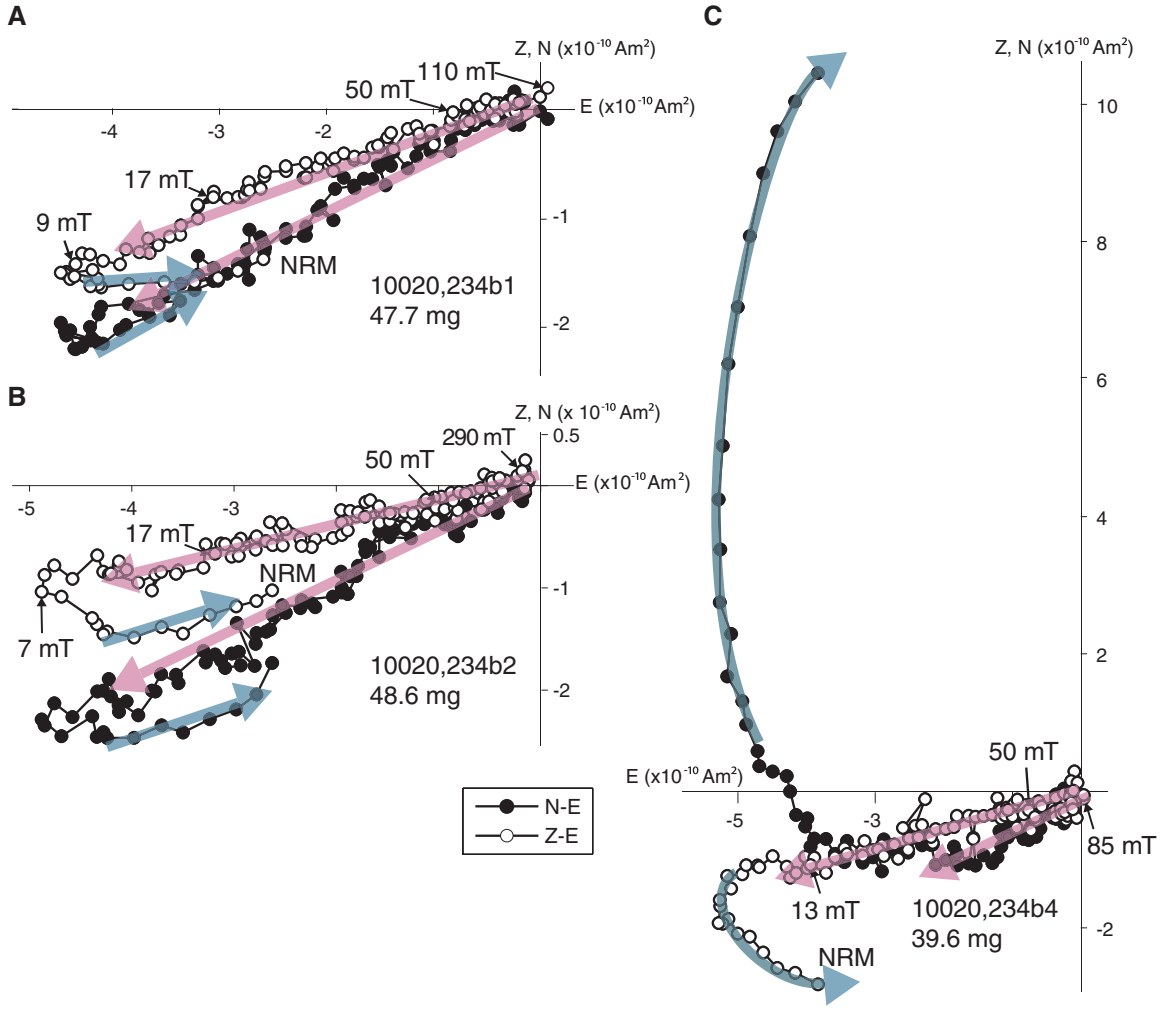


Fig. 1. NRM in mare basalt 10020. Shown is a two-dimensional projection of the NRM vectors of subsamples 234b1, 234b2, and 234b4 during AF demagnetization. Solid symbols represent the end points of magnetization projected onto the horizontal N-E planes, and open symbols represent those projected onto the vertical Z-E planes. Peak fields for selected AF steps are labeled in microteslas. Arrows denote HC component directions determined from principal components analyses (PCA). The mass of each subsample is listed below the sample name. (**A**) Subsample 234b1. (**B**) Subsample 234b2. (**C**) Subsample 234b4.

Downloaded from www.sciencemag.org on January 27, 2012

is estimated to have been 3°C hour^{-1} (*13*), using the maximum plagioclase width cooling indicator [SOM 5 and (*21*)]. Given that cooling rates are often slower at lower temperatures, this indicates that cooling and the acquisition of magnetization from the 780°C Curie temperature of kamacite to ambient lunar temperatures occurred over at least ~300 hours, far longer than the lifetime of modeled impact-generated fields.

These features make 10020 an ideal sample for testing the lunar dynamo hypothesis at 3.7 Ga. However, previous paleomagnetic analyses of 10020 (*1, 20*) did not demonstrate conclusively that the NRM originated on the Moon as a primary thermoremanence (TRM) (SOM 2). More importantly, these studies did not establish whether this field originated from a lunar dynamo or from transient impact-generated fields (SOM 2). We used nondestructive three-axis alternating field (AF) demagnetization to characterize the NRM component in two discrete sets of mutually oriented subsamples, one of which is discussed here and the other in SOM 2.

We identified a low-coercivity (LC) and high-coercivity (HC) component in each subsample (Figs. 1 and 2 and figs. S1 and S3). The LC component, blocked below ~17 mT, is approximately unidirectional at the scale of several millimeters but nonunidirectional at larger scales and has a relatively high ratio of NRM to isothermal remanent magnetization (IRM) (ranging up to 8%). These features suggest that the LC component is a secondary IRM resembling that observed in

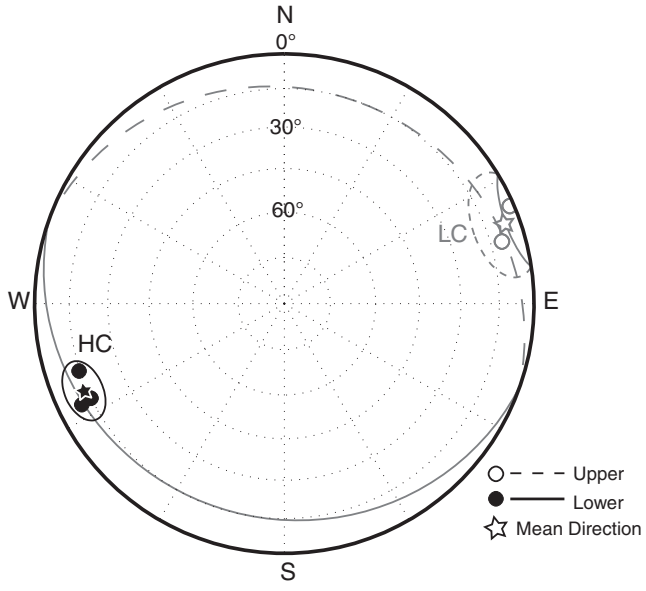
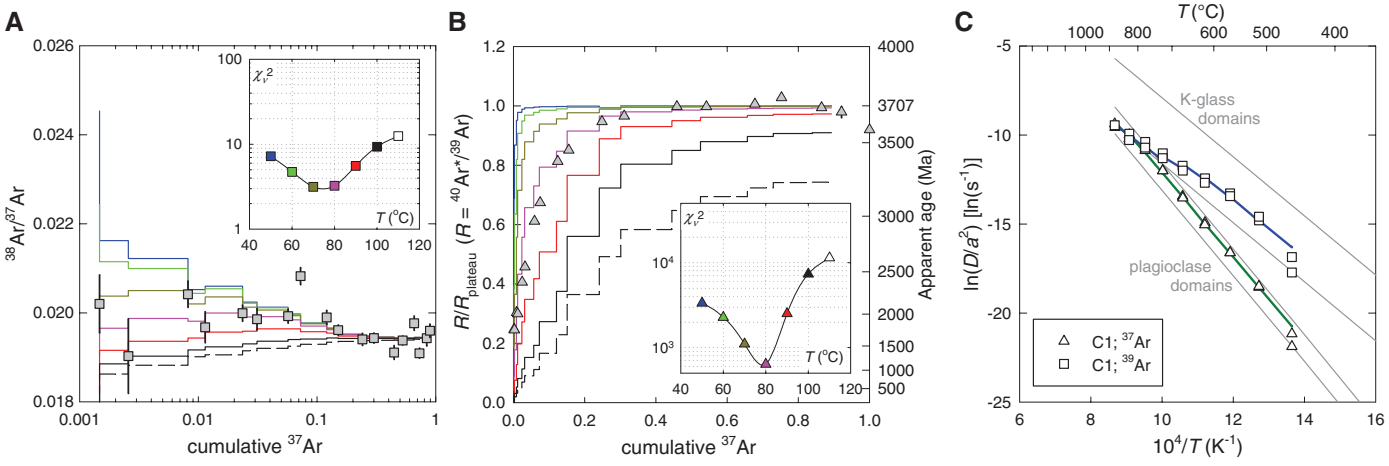


Fig. 2. Equal area stereographic projection of NRM component fits to 10020 subsamples 234b1, 234b2, and 232b4. Black circles denote HC directions for each subsample and light gray circles denote LC directions for samples 234b1 and 234b2. The LC component for sample 234b4 is less well constrained and lies somewhere on the gray great circle. Stars give mean directions for HC and LC components for the three subsamples, with surrounding ellipses indicating 95% formal confidence intervals on mean directions from PCA (not accounting for an additional ~3° to 5° of mutual orientation uncertainty). Solid and open symbols indicate the lower and upper hemisphere, respectively.



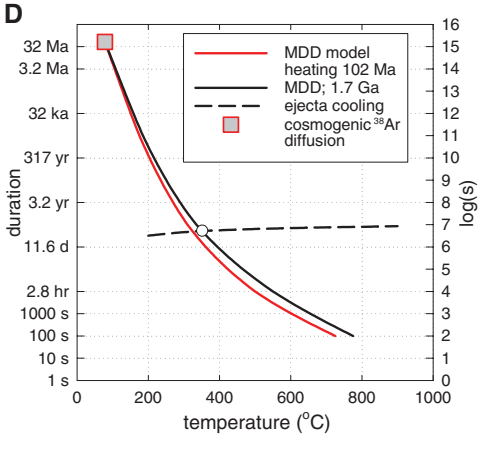


Fig. 3. Thermal constraints on 10020 from the production and diffusion of cosmogenic ^{38}Ar and radiogenic ^{40}Ar. (**A**) Cosmogenic ^{38}Ar constraints. Squares are observed ^{38}Ar/^{37}Ar ratios ± 1 SD as a function of the release fraction of ^{37}Ar and normalized to the first 20 release steps (note log scale). Colored steps are predicted release spectra using the multiple-phase multiple-diffusion domain (MP-MDD) model parameters in (C) and for solar heating to temperatures (T) ranging from 50° to 110°C since the surface exposure age of 102 Ma (SOM 6). The inset shows reduced χ_ν^2 statistics of each fit, identifying ~75°C as the best-fit temperature. (**B**) Diffusion of ^{40}Ar* due to solar heating. Triangles are measured ^{40}Ar*/^{39}Ar ratios (R) normalized to the mean ratio of the apparent plateau ($R_{plateau}$; corresponding to 3707 Ma) versus the cumulative ^{37}Ar release fractions normalized to the first 20 release steps (SOM 6). Colored steps are model release spectra for solar heating conditions, as in (A); the inset identifies ~80°C as the best-fit temperature. (**C**) Diffusivity as a function of temperature calculated from ^{37}Ar and ^{39}Ar released during the first 20 heating steps (*29*); the points are diffusion coefficients (D) divided by the square of the effective diffusive length scale (a). The blue and green curves represent the MDD model fit to the data (SOM 6); the gray lines are diffusion kinetics of the model domains. The gray lines indicate the input diffusion kinetics of each of the four model domains. (**D**) Duration and temperature constraints on possible thermal excursions experienced by sample 10020. Solid curves are conditions at 1.7 Ga (black) and 102 Ma (red) that would best predict the observed ^{40}Ar*/^{39}Ar spectrum shown in (B) using the MP-MDD model in (C); the square is the best-fit solution from (A). The dashed curve predicts the time required to diffusively cool from an initial temperature T to <100°C in a 6-m-thick ejecta blanket (SOM 6). The intersection of this curve with the solid curve (open circle) gives the peak temperature that would explain the Ar data under this scenario.

Downloaded from www.sciencemag.org on January 27, 2012

many other Apollo samples (*4, 22, 23*) and which is inferred to originate from handling after sampling on the Moon.

Depending on the subsample, the HC component is blocked from 8.5 to 17.5 mT up to >66 to 290 mT and decays linearly to the origin, suggesting that it is the final, primary component. Although the LC and HC components in the three 234b subsamples are antipodal (Fig. 2), other subsamples (SOM 2) do not show this relationship, making it unlikely that this has a rock magnetic source in general. The rate of decay of the HC component during AF demagnetization differs from that of a strong-field IRM or a weak-field pressure remanent magnetization (PRM) acquired at 1.8 GPa (the upper limit of our experimental setup), but is very similar to that of an anhysteretic remanent magnetization (ARM), an analog for TRM (SOM 3 and 4). Furthermore, our PRM acquisition experiments indicate that a very strong field (~700 μT) would have been necessary to produce the HC component if it were a shock remanent magnetization (SRM) (SOM 4). Our viscous remanent magnetization (VRM) acquisition experiments suggest that no more than 0.1% of the NRM could be a VRM acquired since the sample's arrival on Earth (SOM 4). These data collectively indicate that the HC component is very likely a TRM acquired during primary cooling in a field on the Moon.

The inferred paleointensities (SOM 3) for the HC components for our five subsamples, using anisotropy-corrected IRM and ARM methods, are 66 ± 37 μT and 55 ± 19 μT (uncertainty ranges are observed from multiple samples with 1 SD) with an overall mean value of 60 μT and estimated minimum value of ~12 μT (for comparison, Earth's surface field intensity is ~50 μT) (SOM 4). Such paleointensities are several orders of magnitude larger than that expected from external sources such as Earth, the Sun, the protoplanetary disk, or the Galaxy at 3.7 Ga (*4, 24*) and are nearly two orders of magnitude stronger than the strongest crustal remanent fields measured at the Apollo landing sites (*1*). The very slow cooling rate and lack of shock effects in 10020 suggest that the recorded field was temporally stable, like that expected from a core dynamo.

Although the crystallization age of 10020 is 3.7 Ga, its magnetization could have been acquired during subsequent thermal events. The lack of shock features precludes any brief, high-temperature shock-heating events associated with impacts, but temperature excursions such as those associated with low-grade metamorphism or burial in a hot ejecta blanket are possible. To assess this possibility, we conducted $^{40}Ar/^{39}Ar$ and $^{38}Ar/^{37}Ar$ thermochronometry on two whole-rock subsamples (SOM 6). We found that 10020 has a weighted average $^{40}Ar/^{39}Ar$ plateau age of 3705.6 ± 13.5 Ma [uncertainty 1 SD; includes uncertainty in the decay constant and the age of the fluence monitor (*25*)], which is indistinguishable from a previous study of this rock as well as the mean crystallization age of other Apollo 11 group B3 basalts (*19*). The apparent spatial distributions of radiogenic ^{40}Ar ($^{40}Ar^*$) and cosmogenic ^{38}Ar ($^{38}Ar_{cos}$) within plagioclase and glass (Fig. 3, A and B, and SOM 6) are consistent with diffusive loss of Ar due to heating to a constant temperature of ~80°C since the rock was exposed near the lunar surface at ~102 Ma [as indicated by cosmic ray exposure ages from (*17, 18*) and our measurements (SOM 6)]. This temperature is essentially the effective temperature equivalent to the expected Ar degassing solely due to solar heating integrated over the exposure age of 10020 (*26*). As has been concluded for many other Apollo 11 basalts (*26*), the only apparent thermal disturbance to 10020 since its formation at 3.70 Ga was from solar heating over the past 100 My (*27*).

Our data thus indicate that a dynamo field, and therefore an advecting metallic core, persisted on the Moon until at least as recently as ~3.70 Ga. It is not yet clear when the dynamo ceased activity. Combined with the paleomagnetic study of the 4.2-billion-year-old troctolite 76535 (*4*), our data imply a minimum lifetime of 500 My for the lunar dynamo, although it need not have been continuously active throughout the period spanned by these two samples. The lunar dynamo persisted until at least ~130 My after the estimated end of the late heavy bombardment [3.90 to 3.85 Ga (*28*)] and long after monotonic secular cooling models (*9*) predict that a core dynamo should have been active. Even non-monotonic models involving the removal of thermal blankets from the core/mantle boundary do not unambiguously generate a dynamo after ~4.4 Ga (*8*). Potential alternative mechanisms for generating a late lunar dynamo are mechanical stirring of the core by precession (*11*) or by the impact of large bolides (*10*). These models predict surface fields at 3.7 Ga of ~0.2 to 15 μT, although this range is uncertain given that it is derived from scaling laws estimated for convection-driven dynamos. Nevertheless, these values are well below our mean 60 μT paleointensity estimate and barely overlap our minimum 12 μT estimate from 10020. Therefore, the late, intense paleomagnetic record from 10020 presents a challenge to current dynamo theory.

References and Notes

1. M. Fuller, S. M. Cisowski, in *Geomagnetism,* J. A. Jacobs, Ed. (Academic Press, Orlando, FL, 1987), vol. 2, pp. 307–455.
2. L. L. Hood, N. A. Artemieva, *Icarus* **193**, 485 (2008).
3. D. A. Crawford, P. H. Schultz, *Int. J. Impact Eng.* **23**, 169 (1999).
4. I. Garrick-Bethell, B. P. Weiss, D. L. Shuster, J. Buz, *Science* **323**, 356 (2009).
5. R. C. Weber, P.-Y. Lin, E. J. Garnero, Q. Williams, P. Lognonné, *Science* **331**, 309 (2011).
6. J. R. Williams, D. H. Boggs, C. F. Yoder, J. T. Ratcliff, J. O. Dickey, *J. Geophys. Res.* **106**, 27933 (2001).
7. D. J. Stevenson, *Space Sci. Rev.* **152**, 651 (2010).
8. D. R. Stegman, A. M. Jellinek, S. A. Zatman, J. R. Baumgardner, M. A. Richards, *Nature* **421**, 143 (2003).
9. W. Konrad, T. Spohn, *Adv. Space Res.* **19**, 1511 (1997).
10. M. Le Bars, M. A. Wieczorek, Ö. Karatekin, D. Cébron, M. Laneuville, *Nature* **479**, 215 (2011).
11. C. A. Dwyer, D. J. Stevenson, F. Nimmo, *Nature* **479**, 212 (2011).
12. D. W. Beaty, A. L. Albee, *Proc. Lunar Planet. Sci. Conf. 11th*, 23 (1980).
13. D. W. Beaty, A. L. Albee, *Proc. Lunar Planet Sci. Conf. 9th*, 359 (1978).
14. E. Roedder, P. W. Weiblen, *Proc. Apollo 11 Lunar Sci. Conf.*, 801 (1970).
15. M. R. Dence, J. A. V. Douglas, A. G. Plant, R. J. Traill, *Proc. Apollo 11 Lunar Sci. Conf.*, 315 (1970).
16. S. E. Haggerty, F. R. Boyd, P. M. Bell, L. W. Finger, W. B. Bryan, *Proc. Apollo 11 Lunar Sci. Conf.*, 513 (1970).
17. J. Geiss *et al.*, *Philos. Trans. R. Soc. London Ser. A* **285**, 151 (1977).
18. S. Guggisberg *et al.*, *Proc. Lunar Planet. Sci. Conf. 10th*, 1 (1979).
19. G. A. Snyder, D.-C. Lee, L. A. Taylor, A. N. Halliday, E. A. Jerde, *Geochim. Cosmochim. Acta* **58**, 4795 (1994).
20. D. W. Collinson, S. K. Runcorn, A. Stephenson, A. J. Manson, *Proc. Lunar Sci. Conf. 3rd*, 2343 (1972).
21. T. L. Grove, D. Walker, *Proc. Lunar Sci. Conf. 8th*, 1501 (1977).
22. K. P. Lawrence, C. L. Johnson, L. Tauxe, J. Gee, *Phys. Earth Planet. Inter.* **168**, 71 (2008).
23. G. W. Pearce, D. W. Strangway, *Apollo 16 Preliminary Science Report. NASA SP-315* (NASA, Washington, DC, 1972), pp. 7–55 to 7–58.
24. B. P. Weiss *et al.*, *Science* **322**, 713 (2008).
25. P. R. Renne, G. Balco, K. Ludwig, R. Mundil, K. Min, *Geochim. Cosmochim. Acta* **75**, 5097 (2011).
26. G. Turner, *Earth Planet. Sci. Lett.* **11**, 169 (1971).
27. Some other thermal histories cannot be excluded by the Ar data alone. However, the combination of Ar data with geologic constraints strongly favors solar heating as the only major thermal disturbance after primary cooling (SOM 6).
28. C. R. Chapman, B. A. Cohen, D. H. Grinspoon, *Icarus* **189**, 233 (2007).
29. H. Fechtig, S. T. Kalbitzer, in *Potassium Argon Dating,* O. A. Schaeffer, J. Zahringer, Eds. (Springer-Verlag, New York, 1966), pp. 68–107.

Acknowledgments: We thank the Johnson Space Center staff and the Curation and Analysis Planning Team for Extraterrestrial Materials for allocating 10020; N. Chatterjee for help with the microprobe analyses; C. Ross for use of her vibrating sample magnetometer; B. Carbone for administrative help; and C. Dwyer, F. Nimmo, M. Wieczorek, and J. Wisdom for helpful discussions. B.P.W., M.D.F., and D.L.S. thank the NASA Lunar Advanced Science and Exploration Research Program; B.P.W. thanks the NASA Lunar Science Institute; B.P.W. and J.G. thank the MIT-France Seed Funds Program, the PICS Program (CNRS), and the Programme National de Planetologie (INSU/CNES); E.K.S. and S.M.T. thank the NASA Graduate Student Researchers Program; and D.L.S. thanks the Ann and Gordon Getty Foundation for support. D.L.S acknowledges the support of NSF grants EAR-0618219 and EAR-0838572. W.S.C. was supported by an NSF Graduate Research Fellowship. Paleomagnetic data have been included in the SOM.

Supporting Online Material

www.sciencemag.org/cgi/content/full/335/6067/453/DC1
SOM Text
Figs. S1 to S24
Tables S1 to S8
References (*30–102*)
Database S1
Caption for Database S1

17 October 2011; accepted 23 December 2011
10.1126/science.1215359

Downloaded from www.sciencemag.org on January 27, 2012

The Molecular Diversity of Adaptive Convergence

Olivier Tenaillon,[1,2,3]† Alejandra Rodríguez-Verdugo,[1] Rebecca L. Gaut,[1] Pamela McDonald,[1] Albert F. Bennett,[1] Anthony D. Long,[1]* Brandon S. Gaut[1]*†

To estimate the number and diversity of beneficial mutations, we experimentally evolved 115 populations of *Escherichia coli* to 42.2°C for 2000 generations and sequenced one genome from each population. We identified 1331 total mutations, affecting more than 600 different sites. Few mutations were shared among replicates, but a strong pattern of convergence emerged at the level of genes, operons, and functional complexes. Our experiment uncovered a set of primary functional targets of high temperature, but we estimate that many other beneficial mutations could contribute to similar adaptive outcomes. We inferred the pervasive presence of epistasis among beneficial mutations, which shaped adaptive trajectories into at least two distinct pathways involving mutations either in the RNA polymerase complex or the termination factor *rho*.

Beneficial mutations fuel adaptation, yet little is known about their potential diversity. If identical populations adapted to a fixed environment, would adaptation occur via identical convergent mutations or via numerous alternative pathways? How might such pathways be shaped by interactions among beneficial mutations? Studies have shown that both the rate and effect of beneficial mutations varies during the course of adaptation because of epistatic interactions that modify the amplitude of fitness effects. However, these studies have been either statistical, without knowledge of affected sites and functions (*1*), or based on interactions between only a handful of beneficial mutations (*2*–*5*).

The potential number and diversity of beneficial mutations can be assessed experimentally under tight control and replication, but assessment requires a large number of replicates for statistical power; complete genome sequencing, so that mutations are identified unambiguously; and a complex biological system, to ensure that the number of potential adaptive solutions is not trivial. Thus far, no studies have fulfilled all three criteria. Experimental evolution of *Drosophila*, yeast, and *Escherichia coli* has been particularly limited by the level of replication. The most prominent long-term studies consist of only 5 (*6*) and 12 (*7*) lines per treatment, and only a subset of lines has been sequenced (*8*, *9*).

We coupled whole-genome sequencing with 115 replicate populations to characterize the genetic response of *E. coli* to high temperature (42.2°C). Temperature is a complex environmental variable because it governs the rates of biological reactions that underlie activities such as respiration, growth, and reproduction. Adaptation to temperature is also pertinent for understanding the biological consequences of ongoing global climate change. Finally, previous experiments have documented a rapid adaptive response of *E. coli* to high temperature (*10*), with hints that the genetic response may be diverse (*11*, *12*). However, these studies lacked sufficient replication or genetic characterization to assess fully the diversity of genetic changes underlying adaptation.

We serially propagated more than 100 *E. coli* asexual lines for 2000 generations in Davis minimal medium, supplemented with 25 mg/l glucose, at a constant temperature of 42.2°C. These lines originated from a common *E. coli* B REL1206 ancestral clone that had been adapted to the same medium for 2000 generations at 37°C (*7*). Selection was strong, because the temperature was the maximum for population persistence in the experimental environment. The duration of the experiment was chosen to encompass most of the expected fitness gain (*13*), but adaptation was likely not complete. At the end of the experiment, a single clone of each population was sequenced and analyzed for relative fitness and yield at 42.2°C (table S1). Fitness was estimated by competition with the ancestor (*14*) and increased markedly in all lines to a mean of 1.42 (±0.024 95% confidence level). Yield, a measure of absolute fitness, was on average 1.94-fold that of the ancestor (paired *t* test, $P < 0.001$).

To investigate the genetic changes underlying adaptation, we sequenced all 115 clones to an average of 90× coverage, for a total data set of 50 gigabase pairs (Gbp) (*14*). We developed a computational pipeline to identify all de novo mutations relative to the *E. coli* B reference genome (*14*, *15*). On the basis of both phenotypic and genotypic analysis, one of the lines had an increased mutation rate, because of a nonfunctional *mut*L gene. This line had higher fitness but many more mutations (73) than the other lines and was excluded from additional analyses. For the remaining 114 lines, we detected a total of 1258 molecular changes (Fig. 1), with an average of 11.0 events per clone: 6.9 point mutations, 2.3 short insertions and deletions, 1.0 large deletions (>30 bp), 0.6 insertional sequence (IS) element integrations, and 0.2 large duplications. There was no detectable correlation with a clone's fitness and its number of mutations ($r = -0.11$; $P = 0.63$), but the point mutations emitted a strong signal of adaptive evolution. Over 114 genomes, the ratio of nonsynonymous to synonymous mutations per site was 5.75, as was the ratio of intergenic to synonymous mutations. We thus estimate that ~80% of intergenic and nonsynonymous mutations were beneficial (*14*).

Convergent mutations provide additional evidence of adaptive events (*16*), but convergence varied by mutational type. Among point mutations, none of the 36 synonymous and 157 of the 634 nonsynonymous mutations were shared among two or more lines, but some were shared extensively. Eighteen lines contained a nonsynonymous mutation in codon 966 of the RNA polymerase (RNApol) β subunit (*rpoB*), and 17 lines contained a nonsynonymous mutation in codon 15 of the *rho* gene.

In contrast to point mutations, 69% (82 of 119) of large (>30-bp) deletions were identical between at least two lines. Of these deletions, 43% had end points overlapping IS elements, consistent with deletion mediated by homologous recombination between elements. These results demonstrate that IS elements can be the basis for adaptive mutation events (*17*), even if the insertions themselves are selectively neutral or even deleterious. Duplications, indels, and IS element integrations were shared among lines at proportions intermediate to those of point mutations and large deletions (Fig. 1, C and D).

Previous *E. coli* studies suggested that the gene level is more appropriate to assess convergence (*18*). In some cases, this was obviously true. For example, the gene *yba*L, a predicted potassium promoter, was mutated in 65 lines because of 38 nonsynonymous mutations, 6 in-frame indels, 17 frameshift mutations, 3 large deletions, and one IS integration. The targeting of 65 different mutations to one gene is highly nonrandom ($P < 10^{-100}$). *yba*L inactivation may be advantageous in our experimental setting (*14*) and also occurred in an independent high-temperature study (*12*). Overall, convergence is much higher among genes than among sites: On average, two strains shared 2.6% of mutations (excluding synonymous mutations) but shared 20.2% of modified genes and 24.5% of affected operons (Fig. 2A).

Selection may ultimately target multigenic functional groups, such as protein complexes. Focusing on genes with >5 mutations, we clustered them into 10 functional units containing 35.7% of the mutations (*14*) (Table 1 and table S2). Among these, the RNApol complex was an obvious target, with 205 mutations and the most-mutated gene (*rpo*B). The other functional units accrued mutations more frequently than expected (Table 1) including proteins that regulate the *rpo*S stress response (RSS), which had been identified previously as a target of selection under high temperature (*11*). At this functional level, two lines shared an average of 31.5% of affected units (Fig. 2A).

[1]Department of Ecology and Evolutionary Biology, University of California, Irvine, 321 Steinhaus Hall, Irvine, CA 92697, USA. [2]INSERM, UMR-S 722, 75018 Paris, France. [3]Université Paris Diderot, Sorbonne Paris Cité, UMR-S 722, Site Xavier Bichat, 75018 Paris, France.

*These authors contributed equally to the manuscript.
†To whom correspondence should be addressed. E-mail: olivier.tenaillon@inserm.fr (O.T.); bgaut@uci.edu (B.S.G.)

Downloaded from www.sciencemag.org on January 27, 2012

The difference in convergence between point mutations (2.6%) and functional units (31.5%) suggests that we have not explored the diversity of possible adaptive mutations. To illustrate this result qualitatively, we plotted the number of different beneficial mutations at various levels (i.e., mutation, gene, operon, or functional unit) as a function of the number of sequenced lines (*14*). This exercise indicates that we are far from detecting all possible beneficial mutations (Fig. 2B). However, the discovery of affected genes, operons, and functional units was nearly saturated, which suggested that fewer replicates may have recovered the major targets of selection.

To estimate the number of sites that contribute to an adaptive response, we developed a simple model of mutation sampling analogous to the coupon collector's problem (*19*). Assuming that beneficial mutations are sampled from a set of L mutations, all with an equal mutation rate (μ) and selective coefficient (s), we fit the model to the saturation curves in Fig. 2B (*14*). For genes with >3 point mutations, we estimate that $L = 850$ possible sites of beneficial mutations are required to yield our 400 observed point mutations (Fig. 2C). $L = 850$ is a minimum, because our approach assumes no variance in μ and s among sites. With the addition of variance (*20*), the estimated number of sites increases, potentially reaching several thousand sites (Fig. 2C). We conclude that a large number of potentially beneficial sites are clustered within a few operational units. This was expected for the case of gene inactivation, for which different mutations lead to the same phenotype, but the diversity of possible solutions in essential functions, like RNApol, is more surprising (table S2).

Do interactions among beneficial mutations shape the adaptive trajectory? By examining all combinations of a small number of beneficial mutations, recent studies have demonstrated negative epistasis between beneficial mutations in different genes (*3*–*5*) and sign epistasis—in which a

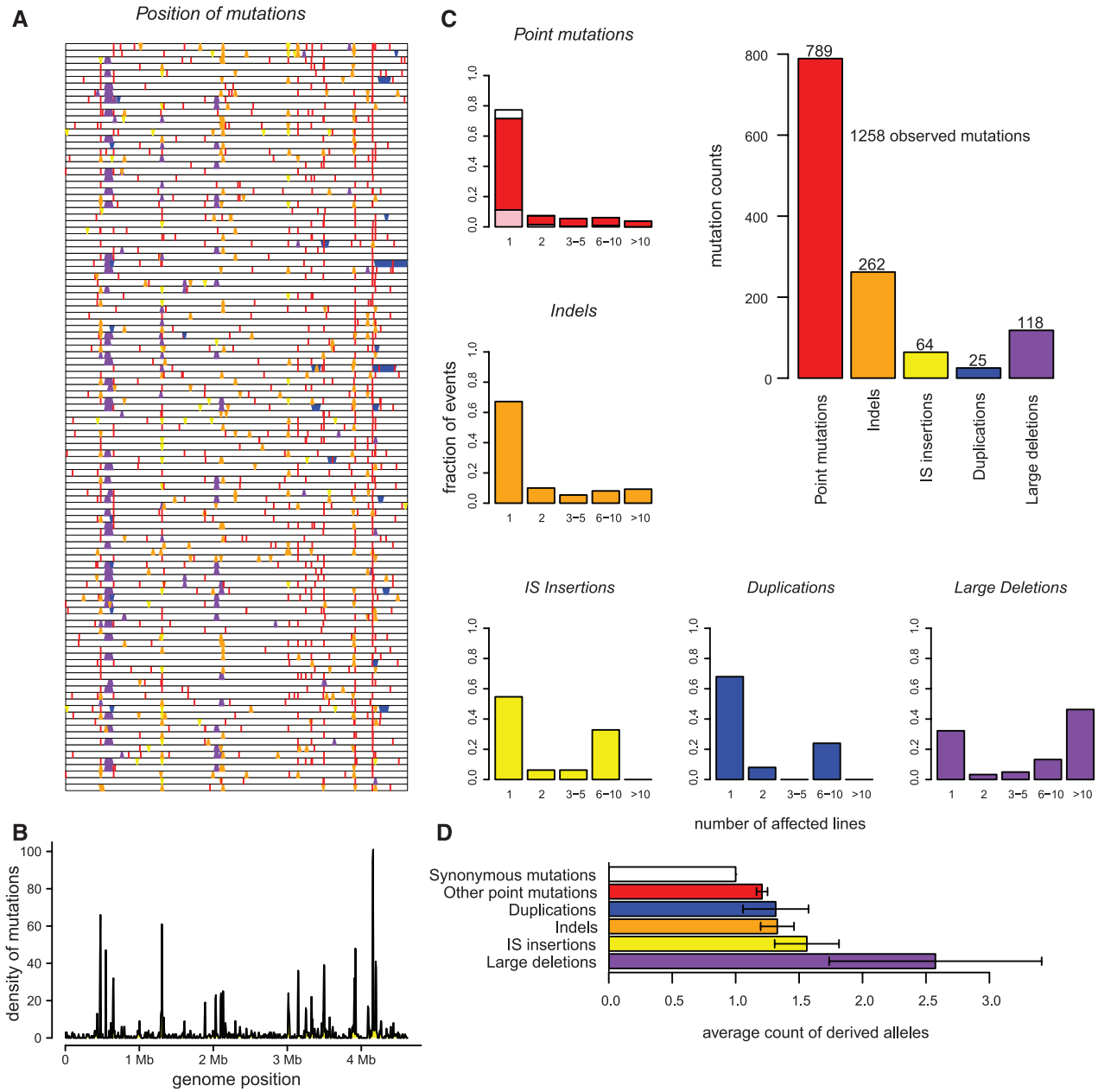


Fig. 1. (**A**) Mutations in 114 independently evolved clones represented along the *E. coli* B chromosome (*15*). Downward and upward triangles are insertions and deletions, respectively. Mutational types are colored as in (**C**). (**B**) The density of mutations along the genome in 5-kb sliding windows. (**C**) The distribution of events according to mutational type. Point mutations are split into nonsynonymous mutations (red), synonymous (white), and intergenic (orange). (**D**) The number of lines sharing mutational types (means ± SEM). All synonymous mutations were singletons.

Downloaded from www.sciencemag.org on January 27, 2012

mutation becomes either deleterious or beneficial depending on the genetic background—within a gene (*2*). We examined epistasis statistically using a resampling procedure (*14*) and also measured associations among mutations using D' (*21*) and the correlation coefficient (r). We focused analyses on operational units with >25 mutations to have reasonable statistical power (Table 1).

Our data contain striking signals of associations. Within units, strains harbored dramatically fewer multiple hits than expected ($P < 1e^{-23}$ within genes and $P < 1e^{-14}$ within functional units); for

Table 1. Operational units with >25 mutational events. Class: Categories correspond to levels, where 1 is a mutation; 2 is the gene; 3 is the operon; 4 is a functional unit. Genes involved are separated by a line when physically separated on the chromosome. Mutations per gene are in parentheses. *P* value testing of whether the number of accumulations in the unit is random. Mutational types: NS, nonsynonymous mutations and short in-frame indels; inactivation, gene inactivations; Reg, mutations in putative regulatory regions or genes.

Unit	Class	Function	Mutations (no.)	Genes involved (no.)	Log (*P* value)	Mutational type
RNApol	4: Protein complex	Extended RNApol complex	205	*rpo*B (87) *rpo*C (21)	−267	NS and Reg
				*rpo*A (4)		
				*rpo*D (36)		
				*nus*A (12)		
				rho (45)		
YBAL	2	Putative CPA-2 proton antiporter	65	*yba*L (65)	−113	Inactivation
CLS	2	Cardiolipin synthetase	64	*cls* (64)	−114	Inactivation
ROD	4: Protein structure	Protein complex involved in the rod shape of the cell	54	*mrd*A (22) *mrd*B (8)	−57	NS
				*mre*B (12) *mre*C (5) *mre*D(5)		
				*yfg*A (2)		
DEL_1	1: Large deletion	Deletion of the region including fep, ent, and cus operons	45	From 547 to 619 kbp	NA	Large deletion bounded by IS elements
ICLR	2	Transcriptional repressor of the glyoxylate bypass operon	39	*icl*R	−68	Inactivation
GLG	3	Glycogen synthesis and degradation	36	*glg*A (2) *glg*C (6) *glg*P (28)	−36	NS
GLP	4: Metabolic and regulatory connection	Uptake of glycerol and *sn*-glycerol 3-phosphate from periplasm to cytoplasm and its regulation	36	*glp*E (2) *glp*G (2) *glp*R (9)	−34	Inactivation
				*glp*F (13) *glp*K (2)		
				*glp*T (8)		
FRU	4: Metabolic proximity	Fructose 1,6-bisphosphate synthesis and degradation	35	*fba*B (25)	−47	NS and Reg
				fbp (7)		
				*fru*K (3)		
KPS	4: Protein complex	Secretion complex of capsule	33	*kps*D (13) *kps*E (11)	−31	Inactivation
				*kps*M (7) *kps*T (2)		
ILVL	2	Leader peptide regulating isoleucine and valine biosynthesis operons	29	*ilv*L (29)	−58	Reg
RSS	4: Regulatory connection	General stress response regulation	27	*csp*C (13)	−34	NS and Reg
				*rss*B (11)		
				*rpo*S (3)		

Downloaded from www.sciencemag.org on January 27, 2012

example, ICLR, CLS, *rho*, *rpo*D, KPS, YBAL, and GLP (defined in Table 1) never had >1 mutation within a single line (Fig. 3A). This pattern is explained by negative epistasis, for which the fixation of a single beneficial mutation transforms tens to hundreds of potentially adaptive mutations to be either neutral or deleterious (*3*). The cause is clear for gene inactivation: Once a gene like *yba*L is inactivated, little fitness benefit can be achieved by further mutations. However, we observed similar patterns for genes that retained function. For example, none of the six ROD genes were inactivated, but no genome harbored more than one mutation in this gene set ($P < 1e^{-3}$), even though ROD was a repeated target of mutation (Table 1).

The exception was RNApol, which accumulated >1 mutation within a single line (Fig. 3A). In fact, *rpo*B differed from all other genes in having two or more mutations in a single genome, occurring in 11 lines. Because the *rpo*BC operon is pleiotropic (*22*), the occurrence of multiple mutations is compatible with selection for compensatory mutations or for multiple phenotypes. Although a different set of mutations in RNApol were recovered after adaptation to 37°C in slightly different conditions (*22*), none were observed over >20,000 generations in the population from which our ancestor was derived (*8*), which suggested that our RNApol mutations are temperature-specific adaptations.

We also detected epistasis between units, including negative associations. For example, all 114 lines had at least one mutation in the *rpo*BC operon or one mutation in *rho* but these tended to be in repulsion (Fisher's exact test: $P < 3e^{-6}$; Fig. 3B). In fact, the two codons with the most mutations in the data set (17 mutations in *rho* codon 15 and 18 mutations in *rpo*B codon 966) were in complete repulsion (Fisher's exact test: $P < 0.01$ for *rpo*B Ile^{966}, and $P < 2e^{-}7$ for *rho* Ile^{15}). Similarly, a previous thermal adaptation experiment detected an early mutation in *rho* without ensuing *rpo*BC mutations (*12*). Other associations between units were consistent with positive epistasis. For example, mutations in *rpo*D (Fisher's exact test: $P < 1e^{-4}$), ILV ($P < 0.0004$), KPS ($P < 0.0001$), and RSS ($P < 0.002$) occurred only in an *rpo*BC mutant background, which suggested that the sign or amplitude of effects depends on the *rpo*BC background.

The overall pattern of associations suggests at least two competing evolutionary trajectories (Fig. 3B). In the first, mutations in *rpoBC* are in positive epistasis with changes in *rpo*D, ILV, KPS, RSS, and ROD. In the second, a mutation in *rho* deters the acquisition of mutations in *rpoBC* and favors selection for mutations in *cls* and *icl*R. There is no difference in average fitness between clones that traversed the different pathways (*t* test; $P = 0.96$), but the two trajectories suggest physiological interactions that have yet to be deciphered functionally. Moreover, these pathways suggest dynamic interactions between

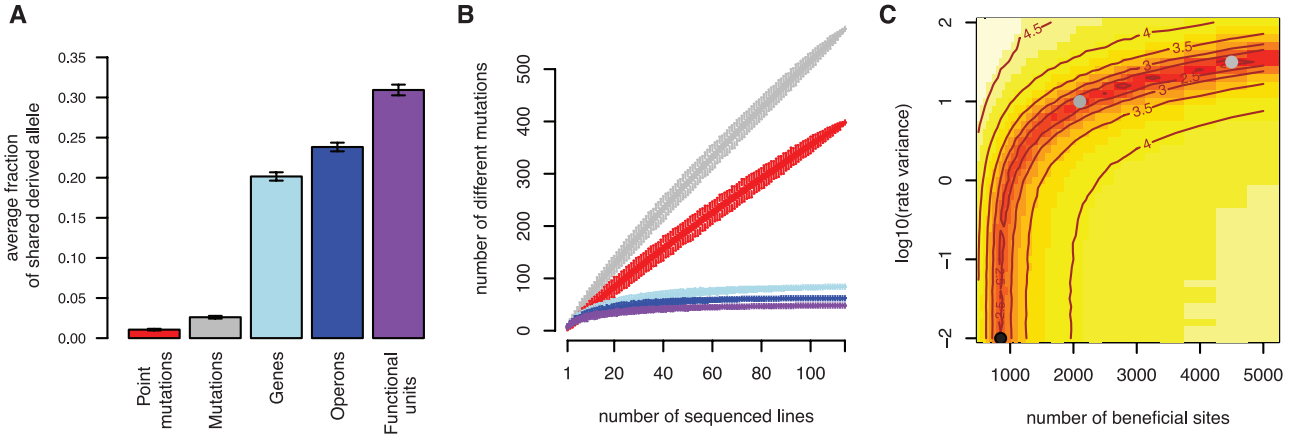


Fig. 2. (**A**) The pairwise fraction of shared events as a function of organizational level (means ± SEM). (**B**) The number of different mutations for subsamples of lines. The colors represent the levels of organization, as defined in (A). (**C**) The fit of the model used to estimate the number of potential beneficial sites *L* for point mutations; hotter colors represent a better fit to the data. The black dot represents the estimate ($L = 850$) under the coupon collector model; the gray dots represent solutions when the sampling probability of beneficial mutations varies among sites.

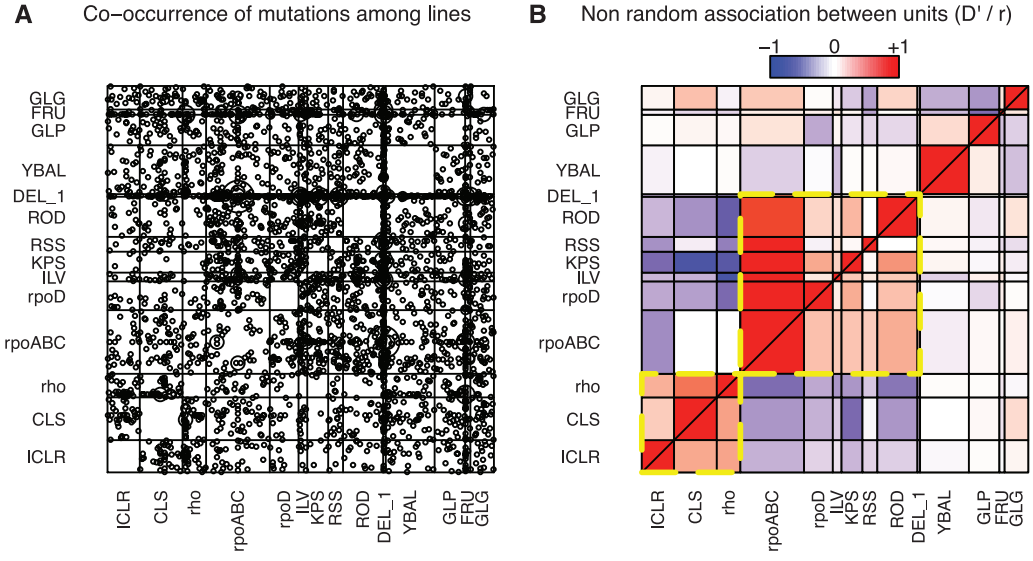


Fig. 3. (**A**) A plot of the co-occurrence of mutations among lines. The labels represent units defined in Table 1, except RNApol, which was split to emphasize unique patterns of accumulation. Each circle represents an instance of a mutation in the units on both the *y* and *x* axes; the size of the circle represents the number of lines sharing both mutations. Most diagonal units had no more than one mutation in a line, and so have no corresponding circles (e.g., YBAL). (**B**) Both *D*′ (top left) and the correlation coefficient, *r* (bottom right), measure associations between mutations. The color of the boxes corresponds to the scale, with hot colors representing positive associations and cooler colors negative associations. The broken yellow lines encompass two alternative evolutionary strategies.

Downloaded from www.sciencemag.org on January 27, 2012

a single beneficial mutation and entire "blocks" of potential beneficial mutations. In this model, one mutation affects its own block, so that potentially beneficial mutations usually become neutral or deleterious, and also opens new blocks to selection, which affects the amplitude and sign of mutational effects within the new block.

References and Notes

1. O. K. Silander, O. Tenaillon, L. Chao, *PLoS Biol.* **5**, e94 (2007).
2. D. M. Weinreich, N. F. Delaney, M. A. Depristo, D. L. Hartl, *Science* **312**, 111 (2006).
3. D. R. Rokyta *et al.*, *PLoS Genet.* **7**, e1002075 (2011).
4. A. I. Khan, D. M. Dinh, D. Schneider, R. E. Lenski, T. F. Cooper, *Science* **332**, 1193 (2011).
5. H. H. Chou, H. C. Chiu, N. F. Delaney, D. Segrè, C. J. Marx, *Science* **332**, 1190 (2011).
6. H. Teotónio, I. M. Chelo, M. Bradić, M. R. Rose, A. D. Long, *Nat. Genet.* **41**, 251 (2009).
7. R. E. Lenski, M. Rose, S. Simpson, S. Tadler, *Am. Nat.* **138**, 1315 (1991).
8. J. E. Barrick *et al.*, *Nature* **461**, 1243 (2009).
9. M. K. Burke *et al.*, *Nature* **467**, 587 (2010).
10. A. F. Bennett, K. M. Dao, R. E. Lenski, *Nature* **346**, 79 (1990).
11. M. M. Riehle, A. F. Bennett, A. D. Long, *Proc. Natl. Acad. Sci. U.S.A.* **98**, 525 (2001).
12. T. Kishimoto *et al.*, *PLoS Genet.* **6**, e1001164 (2010).
13. A. Bennett, R. Lenski, J. Mittler, *Evolution* **46**, 16 (1992).
14. Materials and methods are available as supporting material on *Science* Online.
15. H. Jeong *et al.*, *J. Mol. Biol.* **394**, 644 (2009).
16. P. A. Christin, D. M. Weinreich, G. Besnard, *Trends Genet.* **26**, 400 (2010).
17. L. Chao, C. Vargas, B. B. Spear, E. C. Cox, *Nature* **303**, 633 (1983).
18. R. Woods, D. Schneider, C. L. Winkworth, M. A. Riley, R. E. Lenski, *Proc. Natl. Acad. Sci. U.S.A.* **103**, 9107 (2006).
19. K. Read, *Am. Stat.* **52**, 175 (1998).
20. A. Poon, B. H. Davis, L. Chao, *Genetics* **170**, 1323 (2005).
21. R. C. Lewontin, *Genetics* **49**, 49 (1964).
22. T. M. Conrad *et al.*, *Proc. Natl. Acad. Sci. U.S.A.* **107**, 20500 (2010).

Acknowledgments: We thank L. Chao, C. Herman, and D. Schneider for discussion. This work was supported by NSF grant DEB-0748903 to A.F.B., A.D.L., and B.S.G. and by Agence Nationale de la Recherche, Programme Génomique, grant ANR-08-GENM-023-001 to O.T. Raw sequence data are available for download at http://wfitch.bio.uci.edu/~tdlong/Coli_EE_RawData.tgz.

Supporting Online Material

www.sciencemag.org/cgi/content/full/335/6067/457/DC1
Materials and Methods
Tables S1 to S3
References (*23*–*45*)

22 August 2011; accepted 2 November 2011
10.1126/science.1212986

Centrosome Loss in the Evolution of Planarians

Juliette Azimzadeh,[1]* Mei Lie Wong,[1] Diane Miller Downhour,[2] Alejandro Sánchez Alvarado,[3] Wallace F. Marshall[1]*

The centrosome, a cytoplasmic organelle formed by cylinder-shaped centrioles surrounded by a microtubule-organizing matrix, is a hallmark of animal cells. The centrosome is conserved and essential for the development of all animal species described so far. Here, we show that planarians, and possibly other flatworms, lack centrosomes. In planarians, centrioles are only assembled in terminally differentiating ciliated cells through the acentriolar pathway to trigger the assembly of cilia. We identified a large set of conserved proteins required for centriole assembly in animals and note centrosome protein families that are missing from the planarian genome. Our study uncovers the molecular architecture and evolution of the animal centrosome and emphasizes the plasticity of animal cell biology and development.

The centrosome controls essential cellular processes such as cell division, migration, and polarity by anchoring microtubule-nucleating factors and cell cycle regulators. In animals, it also plays a crucial role during development (including organogenesis) through its ability to control nucleus positioning and cell division orientation, and by nucleating primary cilia. The centrosome is found in all animals examined and is essential to the development of all animal species studied so far. However, centrosomes are dispensable for cell division in some instances, in particular during mouse early embryogenesis and the later stages of *Drosophila* development, raising the question of how central the centrosome really is to fundamental cell biology and development (*1*, *2*).

Animal centrosome duplication relies on duplication of its core components, the centrioles, once per cell cycle. A second pathway, called acentriolar pathway, allows assembly of large numbers of centrioles in multiciliated cells undergoing terminal differentiation (*3*). In vertebrates,

[1]Department of Biochemistry and Biophysics, University of California, San Francisco, CA 94143, USA. [2]University of Utah School of Medicine, Department of Genetics, Salt Lake City, UT 84132–3401, USA. [3]Stowers Institute for Medical Research and Howard Hughes Medical Institute, Kansas City, MO 64110, USA.

*To whom correspondence should be addressed. E-mail: juliette.azimzadeh@ucsf.edu (J.A.); wallace.marshall@ucsf.edu (W.F.M.)

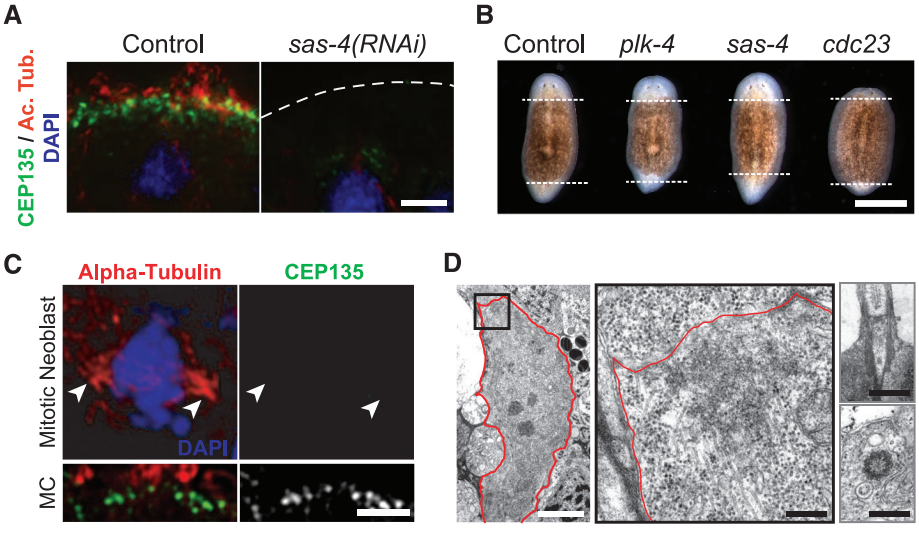


Fig. 1. Centrioles in planarians are present in multiciliated cells but not proliferating cells. (**A**) Immunofluorescence staining of ventral epidermis in control or *sas-4(RNAi)* animals; centrioles (green, anti–SMED-CEP135), cilia (red, anti–acetylated tubulin), nuclei [blue, DAPI (4′,6-diamidino-2-phenylindole)]. Dashed line: apical cell boundary. (**B**) Regenerating trunk fragments. Dashed lines: boundary between newly formed and preexisting tissues. (**C**) Immunofluorescence staining of control mitotic neoblast; centrioles (green, anti–SMED-CEP135), mitotic spindle (red, anti–alpha-tubulin), chromosomes (blue, DAPI). Arrowheads: spindle poles. Lower panel: centrioles in a multiciliated cell (MC) from the same section. (**D**) Left: TEM view of control mitotic neoblast (3200×). Red line: plasma membrane. Middle: high-magnification view (15,000×) of boxed area. Right: High-magnification views (21,000×) of centrioles from the ventral multiciliated epidermis are shown for comparison. Top: longitudinal section through a centriole and the base of the corresponding cilium; bottom: cross section. Bar: 5 μm in (A), (C), and (D) (left panel); 1 mm in (B); and 0.25 μm in (D) (middle and right panels).

Downloaded from www.sciencemag.org on January 27, 2012

multiciliated cells drive mucus clearance, cerebrospinal fluid circulation, and egg transportation along the oviduct. However, the molecular pathway underlying centriole assembly in multiciliated cells is poorly characterized. Flatworms like the freshwater planarian *Schmidtea mediterranea* use multiciliated cells for locomotion, suggesting they can serve as model systems for studying centriole assembly in multiciliated cells. Furthermore, the role played by centrioles in the regeneration of planarians remains unexplored thus far.

To characterize the phenotypes associated with the inhibition of centriole assembly in planarians, we used RNA interference (RNAi) technology to eliminate the products of genes encoding planarian homologs of the conserved centriolar components SAS-4/CPAP and Plk4/SAK in asexual planarians (*2*, *4*, *5*). In contrast to untreated animals that glide smoothly on their ciliated epithelium, 100% of the *plk4(RNAi)* or *sas-4(RNAi)* animals exhibited inchworming locomotion ($n = 100$, 5 independent experiments; movies S1 and S2), a phenotype known to result from impaired ciliary function (*6*, *7*). Using an antibody raised against SMED-CEP135, the planarian homolog of a conserved component of centrioles (*5*), we found that the ventral surface of *plk4(RNAi)* or *sas-4(RNAi)* animals was almost entirely devoid of centrioles and cilia (Fig. 1A and figs. S1 and S2). Thus, depleting the planarian homologs of proteins essential for centriole duplication within the centrosome abolished centriole assembly in planarian multiciliated cells. The remarkable ability of planarians to regenerate whole animals from almost any part of their body requires division of the neoblasts, a population of totipotent stem cells and the only cells to undergo mitosis in asexual planarians (*8*). Blocking cell division by depleting the planarian homolog of CDC23, a component of the anaphase-promoting complex, resulted in regression of the regeneration blastemata as previously described (*9*). In contrast, animals depleted of centriole components regenerated missing tissues to a similar extent as control animals (Fig. 1B and fig. S3). These results suggested that centrioles are dispensable for cell division and tissue formation in planarians. Whereas centrioles were observed in the different ciliated tissues, they were not detected at all in nonciliated cells as assessed by immunofluorescence costaining of centrioles and cilia in 10-μm tissue sections from wild-type planarians ($n = 8$ planarians, 10 to 15 sections per animal; Fig. 1A and figs. S2 and S4). In particular, we did not observe centrioles in control neoblasts, either by immunofluorescence or by transmission electron microscopy (TEM) (Fig. 1, C and D, and figs. S4 to S6), as also suggested by earlier ultrastructural studies (*10*, *11*). We obtained the same result when analyzing *S. mediterranea* embryos by immunofluorescence, indicating that dividing embryonic cells also lack centrioles (fig. S4). Thus, centrioles are missing from the only two cell types that can proliferate in planarians, and appear to be missing from all nonciliated terminally differentiated cells that we have observed as well. This result might at first seem reminiscent of the case in *Drosophila* in which later stages of development can take place in mutants deficient for centriole duplication (*2*, *4*). However, early *Drosophila* development is absolutely dependent on the presence of centrioles (*12*, *13*). In contrast, our results show that planarians do not require centrioles at any stage of development. In animal cells, centrioles are essential for the duplication and stability of the centrosome (*2*, *4*, *14*). Our results thus indicate that planarians do not assemble centrosomes, but only assemble centrioles de novo during the differentiation of ciliated cells.

A first prediction based on this model is that proteins specifically required for centrosome

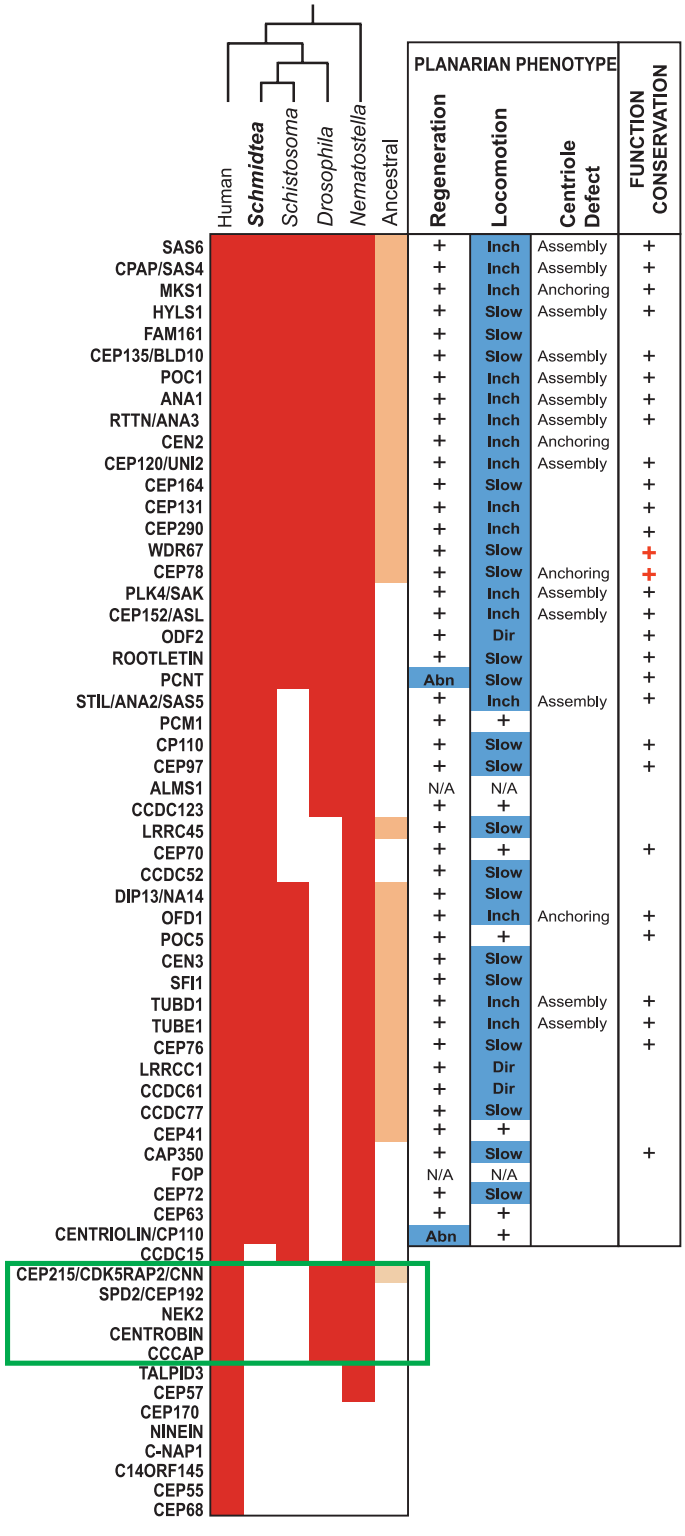


Fig. 2. Planarian homologs of human centrosome components are required for centriole assembly in multiciliated cells. Left: conservation of centrosome components in animals (red). Ancestral eukaryotic genes are in orange. Green box: centrosome signature genes lost in the planarian *Schmidtea mediterranea* and the parasite flatworm *Schistosoma mansoni* but present in *Drosophila*. Middle: regeneration and locomotion phenotypes in planarians (+: no defect; Abn: abnormal; Inch: inchworming; Dir: abnormal direction of locomotion; N/A: not applicable.). Right: +: genes implicated in centriole duplication or ciliogenesis in other systems (red +: this study; supporting online material).

Downloaded from www.sciencemag.org on January 27, 2012

assembly or function should have been eliminated from the planarian genome during evolution. To test this, we used a list of core centrosome components (table S1) derived from the human centrosome proteome (*15*) and searched for potential homologs in the planarian genome. We found planarian homologs for a majority (47/55) of the centrosome components that were unequivocally present in the last common ancestor of humans and planarians (Fig. 2). Five protein families were conserved among human, *Nematostella*, and *Drosophila* but missing not only in *Schmidtea* but also in the parasitic flatworm *Schistosoma mansoni*. The missing subset included three protein families required for assembly or reproduction of the centrosome: SPD-2/Cep192, CNN/CDK5RAP2, and Nek2 (*5*, *16*, *17*). Thus, a key set of centrosome components essential to centrosome function is missing from the planarian genome. Because planarians evolved from a metazoan ancestor that contained these proteins families, we infer that they were eliminated from the planarian genome together with the centrosome itself during evolution, whereas an acentriolar pathway was retained to assemble centrioles during differentiation of multiciliated cells (Fig. 3A).

A second prediction is that components of the human centrosome for which homologs are still present in planarians should be required for ciliogenesis through the acentriolar pathway. We targeted the homologs of centrosome components conserved in the planarian genome by RNAi and indeed we observed a locomotion defect in a majority of the knockdowns (38/45 genes tested) (Fig. 2). We identified a large set of conserved proteins required for ciliogenesis or optimal ciliary function in multiciliated cells, revealing functions for the homologs of centrin 2 (*Smed-cen2*) and the uncharacterized protein Cep78 in centriole anchoring and ciliogenesis (Fig. 2 and figs. S7 to S11). Only two genes coding for pericentrin and centriolin homologs were found to affect regeneration via a cell proliferation–independent mechanism (Fig. 2 and figs. S12 and S13), likely reflecting the centrosome-independent functions of these proteins (*18*, *19*). Thus, most centrosome components conserved in planarians are required for centriole assembly or ciliogenesis in multiciliated cells, which demonstrates that centrosome duplication in proliferating cells, and centriole assembly through the acentriolar pathway in multiciliated cells, rely on essentially the same mechanisms (fig. S14). A key difference between the two pathways appears to be the involvement of SPD-2/Cep192 in centrosome duplication (*5*) but not in the acentriolar pathway, as supported by the loss of this protein family from the planarian genome.

The loss of the centrosome in planarians and possibly also in schistosomes is a remarkable event in the evolutionary history of animals. To determine when in evolution this event took place, we searched for homologs of the centrosome signature proteins in the genomes of species closely related to the planarian, in particular the basal flatworm *Macrostomum lignano*. We found *Macrostomum* homologs for SPD-2/Cep192 and Nek2 (fig. S15), which supports the notion that the centrosome was still present during early stages of flatworm evolution and was subsequently lost in the lineage leading to planarians and parasitic flatworms. In agreement with this hypothesis, centrioles are found at the poles of mitotic cells in *Macrostomum* embryos (*20*), in contrast to what we observed in planarians.

It is notable that the loss of such a conserved organelle as the centrosome occurred within nonparasitic flatworms, as cellular and developmental processes appear largely conserved between these species (*21*). A difference can be found in the mode of embryonic cleavage, however. *Macrostomum* retained the ancestral spiral cleavage, also found in annelids and mollusks, which relies on a stereotypical pattern of cell division orientation (Fig. 3B). In contrast, planarian and *Schistosoma* embryos undergo divergent modes of embryonic cleavage, which apparently do not involve oriented cell divisions (*22*, *23*). We hypothesize that centrosome loss occurred concomitantly with the loss of the spiral cleavage and oriented cell divisions in the ancestor of planarians and schistosomes (Fig. 3B). Our results suggest that selective pressure to maintain the centrosome in animals comes from the need to coordinate specific developmental processes rather than a fundamental cellular requirement for the organelle.

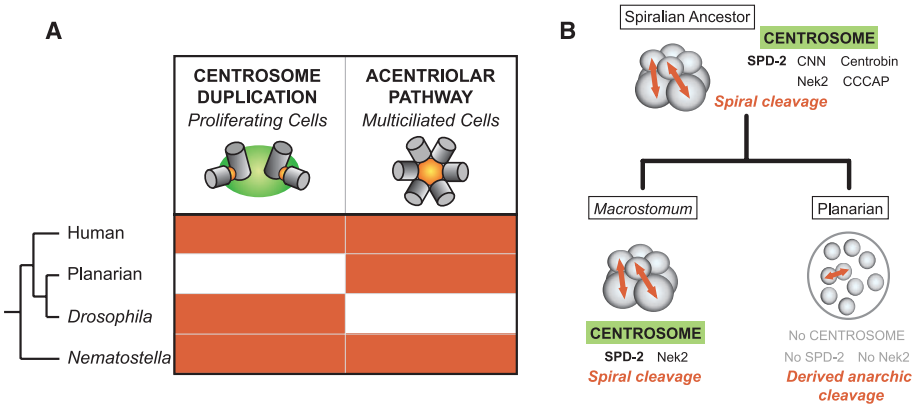


Fig. 3. (**A**) Conservation of the two main pathways for centriole assembly in animals. Centrosome duplication and the acentriolar pathway are highlighted in red when present. Planarians lost the centrosome duplication pathway and *Drosophila* lost the acentriolar pathway together with multiciliated epithelia during evolution. (**B**) Model of the correlation between loss of the centrosome and loss of the spiral cleavage pattern.

References and Notes

1. P. D. Calarco-Gillam, M. C. Siebert, R. Hubble, T. Mitchison, M. Kirschner, *Cell* **35**, 621 (1983).
2. R. Basto *et al.*, *Cell* **125**, 1375 (2006).
3. H. R. Dawe, H. Farr, K. Gull, *J. Cell Sci.* **120**, 7 (2007).
4. M. Bettencourt-Dias *et al.*, *Curr. Biol.* **15**, 2199 (2005).
5. J. Azimzadeh, W. F. Marshall, *Curr. Biol.* **20**, R816 (2010).
6. J. C. Rink, K. A. Gurley, S. A. Elliott, A. Sánchez Alvarado, *Science* **326**, 1406 (2009).
7. P. Rompolas, R. S. Patel-King, S. M. King, *Mol. Biol. Cell* **21**, 3669 (2010).
8. D. E. Wagner, I. E. Wang, P. W. Reddien, *Science* **332**, 811 (2011).
9. P. W. Reddien, A. L. Bermange, K. J. Murfitt, J. R. Jennings, A. Sánchez Alvarado, *Dev. Cell* **8**, 635 (2005).
10. M. Morita, J. B. Best, *J. Exp. Zool.* **187**, 345 (1974).
11. A. Sakai-Wada, C. Mukaidani, *Chromosoma* **93**, 43 (1985).
12. N. R. Stevens, A. A. Raposo, R. Basto, D. St Johnston, J. W. Raff, *Curr. Biol.* **17**, 1498 (2007).
13. A. Rodrigues-Martins, M. Riparbelli, G. Callaini, D. M. Glover, M. Bettencourt-Dias, *Cell Cycle* **7**, 11 (2008).
14. Y. Bobinnec *et al.*, *J. Cell Biol.* **143**, 1575 (1998).
15. J. S. Andersen *et al.*, *Nature* **426**, 570 (2003).
16. N. Kraemer *et al.*, *Cell. Mol. Life Sci.* **68**, 1719 (2011).
17. T. Mayor, U. Hacker, Y. D. Stierhof, E. A. Nigg, *J. Cell Sci.* **115**, 3275 (2002).
18. A. Gromley *et al.*, *Cell* **123**, 75 (2005).
19. B. Delaval, S. J. Doxsey, *J. Cell Biol.* **188**, 181 (2010).
20. S. Tyler, *Hydrobiologia* **84**, 231 (1981).
21. B. Egger, R. Gschwentner, R. Rieger, *Dev. Genes Evol.* **217**, 89 (2007).
22. A. Cardona, V. Hartenstein, R. Romero, *Dev. Genes Evol.* **216**, 667 (2006).
23. A. D. Jurberg *et al.*, *Dev. Genes Evol.* **219**, 219 (2009).

Acknowledgments: We thank J. Rink for sharing reagents and helping with planarian embryo analysis; R. Zalpuri and K. McDonald for help with TEM sample preparation; N. Tang for help with cryostat sectioning; K. Thorn and the Nikon Imaging Center for help with confocal imaging; Y. Chen and M. Braunfeld for help with TEM acquisition; L. Holt, D. David, M. Bettencourt-Dias, and M. Bornens for critical reading of the manuscript; and the Marshall lab and the Sánchez lab for insightful comments. This work was supported by the W. M. Keck Foundation (W.F.M.) and NIH grants GM077004 (W.F.M.) and GM57260 (A.S.A.). A.S.A. is a Howard Hughes Medical Institute investigator. All accession numbers for sequences associated with this study are provided in table S1.

Supporting Online Material

www.sciencemag.org/cgi/content/full/science.1214457/DC1
Materials and Methods
Figs. S1 to S15
Tables S1 and S2
References
Movies S1 and S2

8 June 2011; accepted 21 November 2011
Published online 5 January 2012;
10.1126/science.1214457

Downloaded from www.sciencemag.org on January 27, 2012

Global Correlations in Tropical Tree Species Richness and Abundance Reject Neutrality

Robert E. Ricklefs[1]* and Susanne S. Renner[2]

Patterns of species richness and relative abundance at some scales cannot be distinguished from predictions of null models, including zero-sum neutral models of population change and random speciation-extinction models of evolutionary diversification. Both models predict that species richness or population abundance produced by independent iterations of the same processes in different regions should be uncorrelated. We find instead that the number of species and individuals in families of trees in forest plots are strongly correlated across Southeast Asia, Africa, and tropical America. These correlations imply that deterministic processes influenced by evolutionarily conservative family-level traits constrain the number of confamilial tree species and individuals that can be supported in regional species pools and local assemblages in humid tropical forests.

Discussion of patterns in biodiversity and population size has been heightened during the past two decades by insights gained from the properties of random birth-death processes. Applied to species diversification within evolutionary clades, a particular random speciation and extinction process can produce a wide range in species richness, with a preponderance of small clades and a few large ones (*1*). Random births and deaths of individuals (ecological drift) result in a similar distribution of the sizes of species populations (*2*), mimicking the effect of genetic drift on the frequency of neutral alleles within populations. In random birth-death models, each replication of the process over time is independent, and so the outcomes of separate iterations are uncorrelated. Pitman *et al*. (*3*, *4*) used this logic to test for any correspondence in the number of species and individuals in tree families between terre firma tropical forests in Peru and Ecuador, following the earlier insight of Alwyn Gentry concerning what he called "family-level niches" (*5*). Although the two sites exhibited strong positive correlations, seemingly rejecting random models of diversification and population growth, shared history and ongoing migration might have substantially homogenized these floras over the 1400 km separating the sites across the upper Amazon basin (SOM text).

Although floras within continents may lack independence, global comparisons between areas separated by tens of millions of years of independent evolutionary diversification allow valid tests of neutral theory, which assumes that random processes predominate in ecology and evolution (*5*). In one such comparison, regional floras in Ecuador, Madagascar, and Malaysia exhibited strong correlations (correlation coefficient $r = 0.65$ to 0.81) between the number of genera per order of flowering plants (Angiospermae) (*6*). Parallel correlations between temperate regional floras in eastern North America and eastern Asia were equally compelling. This result implies taxon-specific variation in either the propensity of these clades to diversify or in the capacity of the environment to support genera within each order.

The 25- to 52-ha plots established at several sites around the world and associated with the Center for Tropical Forest Science (CTFS) (www.ctfs.si.edu) now provide detailed information on species richness and local relative abundance of trees within family-level taxa (*7*). We compared the number of species and individuals in shared families between seven plots in three regions (Fig. 1 and Table 1) to test the prediction from neutral theory of random diversification and population change that diversity and abundance should be uncorrelated between independently evolved floras (*8*).

The number of families currently recognized by the Angiosperm Phylogeny Group (APG III) (*9*, *10*) and represented by tree-sized species [>10-cm diameter at breast height (dbh)] on the CTFS forest plots varied from 47 (Korup, Cameroon)

[1]Department of Biology, University of Missouri–St. Louis, St. Louis, MO 63121–4499, USA. [2]Department of Biology, University of Munich, 80638 Munich, Germany.

*To whom correspondence should be addressed. E-mail: ricklefs@umsl.edu

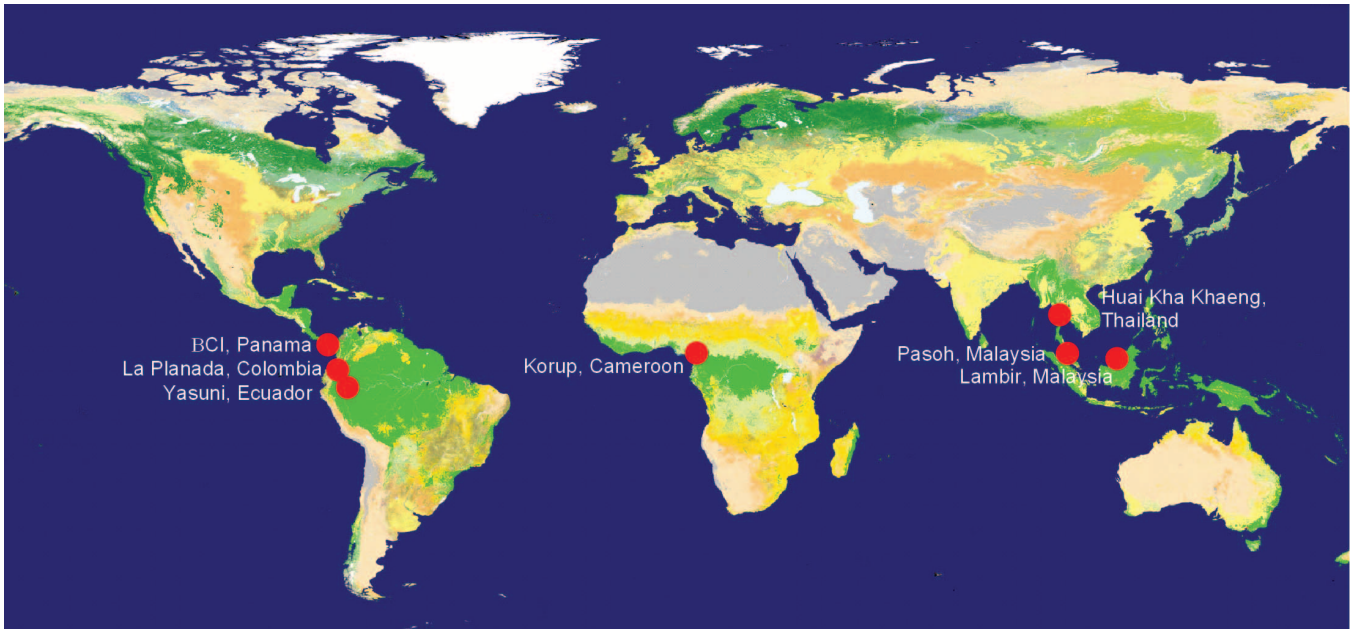


Fig. 1. Location of seven CTFS forest plots. The distribution of tropical rainforest is indicated in bright green within tropical latitudes. BCI, Barro Colorado Island. Base map from http://eoimages.gsfc.nasa.gov/images/news/NasaNews/ReleaseImages/LCC/Images/lcc_global_2048.jpg.

Downloaded from www.sciencemag.org on January 27, 2012

to 76 (Lambir, Malaysia). The number of families shared between plots varied from 29 to 59 (27 to 44 in between-region comparisons; i.e., South America, Africa, Southeast Asia). Few genera are shared between plots in different regions, consistent with the independence of species diversification between regions (SOM text). For example, the plots at Yasuni, Ecuador, and Pasoh, Malaysia, share 44 of their 65 (68%) and 76 (58%) families, respectively, but only 35 of their 296 (11.8%) and 259 (13.5%) genera.

Time-calibrated molecular phylogenetic reconstructions available for some families emphasize the distant connections between and the general independence of the tree floras of the three floristic regions included in this study. For example, species in the families Annonaceae, Lauraceae, Meliaceae, and Myrtaceae occurring at Yasuni, Ecuador, and Pasoh, Malaysia, have most recent common ancestors no younger than the early Oligocene, ~30 million years ago, and mostly older (SOM text). Because the ancestors of the species in Malaysia and Ecuador mostly coalesce within each of the regions, with connections within families between the regions being older, the predicted correlation in the species richness of families between the regions under neutral theory is essentially zero.

Table 1. Attributes of the seven CTFS forest plots. Data are from www.ctfs.si.edu. Negative latitudes are south of the equator; negative longitudes are west of the Greenwich Meridian. Lat, latitude; Long, longitude; Fam, number of families; Spp, number of species; Inds, number of individuals.

Location	Lat (°)	Long (°)	Elevation (m)	Plot size (ha)	Fam	Spp	Inds (>10-cm dbh)
Yasuni, Ecuador	–0.69	–76.40	215–245	50	65	846	17017
La Planada, Colombia	1.16	–77.99	1796–1891	25	50	179	14620
Barro Colorado Island, Panama	9.15	–79.85	120–160	50	53	251	21051
Korup, Cameroon	5.07	8.85	700–850	40*	47	281	24188
Pasoh, Malaysia	2.98	102.31	70–90	50	73	700	27955
Lambir, Malaysia	4.19	114.02	104–244	52	76	1009	31465
Huai Kha Khaeng, Thailand	15.63	99.22	549–638	50	55	247	21524

*Four 10-ha plots.

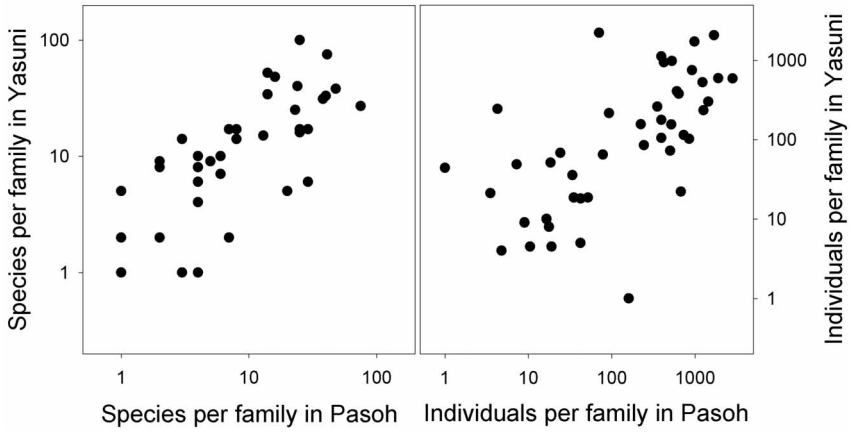


Fig. 2. Relation between the number of species per family and the number of individuals per family in Pasoh, Malaysia, and Yasuni, Ecuador. Correlation coefficients are Spearman (rank) values.

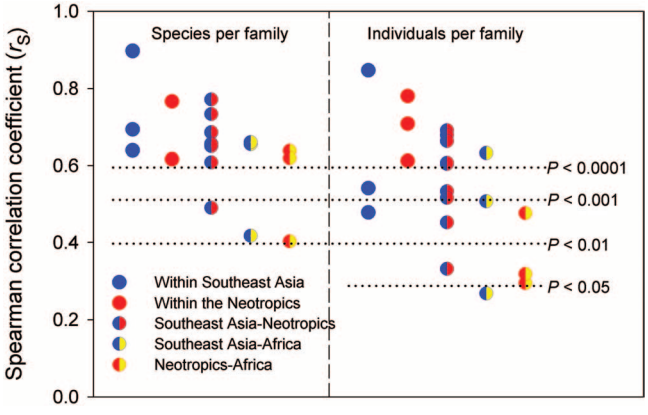


Fig. 3. Correlations of the number of species and the number of individuals per family between forest plots. Regions are color-coded: Southeast Asia (blue), Neotropics (red), and Africa (yellow). The average number of shared families is as follows (number of comparisons shown in parentheses): within Asia, 50.7 (3); within the Neotropics, 40.0 (3); between Asia and the Neotropics, 37.6 (9); between Africa and Asia, 36.0 (3); and between Africa and the Neotropics, 33.7 (3). Levels of statistical significance are based on the minimum sample of $n = 34$ shared families and are, therefore, conservative for most of the comparisons.

Spearman rank correlation coefficients (r_S) between the number of species per family recorded in the seven ~50-ha plots are all significant, and many of them are quite high ($r_S > 0.60$, $P < 0.0001$) (Figs. 2 and 3 and table S1). Correlations between sites in the Neotropics and Southeast Asia (all but one $r_S > 0.60$) even approach those within floristic regions, where dispersal tends to homogenize local floras, and many more genera are shared between sites [for instance, 177 genera out of 259 (68%) and 261 (68%), respectively, and many species, between Pasoh and Lambir, Malaysia]. With respect to the numbers of individuals per family, the correlations within Southeast Asia and within the Neotropics are significant (r_S, $P < 0.01$); the correlations between Southeast Asia and the Neotropics also are significant (r_S, $P < 0.05$); and the correlations between these two regions and the African site are weaker, although most are significant. All are positive; none remotely approach zero.

Correlations of number of species per taxon also are strong above the family level within angiosperm orders, but not below the family level within genera. For example, between Yasuni, Ecuador, and Pasoh, Malaysia, the numbers of species are highly correlated among the 19 shared orders ($r_S = 0.86$), but not among the 35 shared genera ($r_S = 0.037$). In general, the number of species per genus is correlated within regions (six comparisons, all $r_S > 0.39$, $n > 44$ genera, $P < 0.001$), but not between regions (15 comparisons, all $r_S < 0.31$, $n < 35$ genera, $P > 0.05$), which is suggestive of the homogenizing effect of shared ancestry and dispersal within regions and further emphasizes the independence of floras between regions.

Representation of families within regions over time appears to be conservative, also contradicting the predictions of neutral theory (*11*). The most abundant families identified from the Paleocene Cerrejón megafossil flora of northern Colombia (*12*) are among the most abundant families in present-day Neotropical rainforests, a point also emphasized by Wing *et al.* (*12*). For example, 25 of 33 Cerrejón macrofossils assignable to modern families are referable to the 15 most species-rich of 76 families in the contemporary Yasuni flora (likelihood ratio $G = 30.7$, $P < 10^{-6}$); the numbers of species per family in the Paleocene and modern floras, separated by ~58 million years, are significantly correlated ($r_S = 0.45$, $P < 0.0001$) (Fig. 4).

Our analyses show that the number of species, as well as the total number of individuals, per family of trees in tropical forests is conserved across floristic regions widely separated in space and time on the globe and across tens of millions of years within the same region. This

Downloaded from www.sciencemag.org on January 27, 2012

conservation of species richness within monophyletic (APG III) families, in spite of independent evolutionary diversification between floristic regions and complete turnover of species several times within regions (*13*), firmly rejects the hypotheses that individuals are replaced at random within forests irrespective of species identity (zero-sum ecological drift) (*2*) and that species formation and extinction occur randomly among extant lineages (*14*, *15*). This result supports other evidence for deterministic community assembly on the basis of convergent forest succession (*16*) and the consistent relationship of species richness to physical conditions of the environment (*17*). Although nature is stochastic and unpredictable at some scales of time and space, deterministic regional processes responsible for patterns of tree species diversity, abundance, and distribution override the relatively weak influence of randomness in large systems.

Because the number of species per genus is not significantly correlated between regions, we cannot reject zero-sum random drift (that is, neutrality) within families. However, neutral theory implies that time (in generations) to complete species turnover within a family is on the order of the number of confamilial individuals in the metacommunity (*18*). Significant correlations in the number of species per genus within regions suggest homogenization of these floras by dispersal, resulting in extremely large metacommunities within individual families (averaging perhaps 10^8 individuals per family in Neotropical forests) (*19*) that are simply too large to match the observed turnover of species during the Tertiary. Thus, deterministic processes would appear to be responsible for patterns of abundance within families, as well as among families.

Conservation of species richness within families suggests diversity-dependent controls on either the rate of diversification of species or the number of species supported within a region at a speciation-extinction equilibrium. At high taxonomic levels (e.g., families of flowering plants), the frequently noted absence of a relation between clade age and number of species suggests that observed species richness is constrained at clade-specific speciation-extinction equilibria (*6*, *20*), although variation in family-specific rates during the initial phase of diversification are not precluded by the data. But eventually, each family tends to reach a characteristic number of species within a region or locally within a plot.

The relative success of families indicated by their high or low numbers of species does not, however, carry over to the abundance of individual species. Although the total numbers of individuals per family are correlated across independent floristic regions, the average number of individuals per species varies little among families and is uncorrelated across regions; for example, between the Pasoh and Yasuni plots, $r_S = -0.03$ ($n = 44$, $P > 0.05$). That is, particular families do not tend to produce species with individually high or low densities across regions, and average local abundance of species within plots is unrelated to the number of species per family (*6*, *21*). The total number of individuals within families simply varies in parallel with the number of species per family (e.g., Pasoh $r_S = 0.81$; Yasuni $r_S = 0.88$) (table S1). Moreover, because most of the variance in abundance reflects differences between closely related (that is, congeneric) species (*6*, *22*), population size does not exhibit long-term evolutionary conservatism, unlike the situation for larger taxa identified here (*5*, *23*). The picture is one of variable species populations within a comparatively stable larger taxon. The processes underlying these patterns are, as yet, poorly understood.

The abundance of species in tropical forests may be partly determined by self-limitation that is mediated by pathogens and dependent on density, the so-called Janzen-Connell effect (*24*, *25*). In the 50-ha plot on Barro Colorado Island, Panama, the abundance of species is inversely related to the strength of inhibition of neighboring seedlings and adults of the same species (*26*, *27*). Adults or seedlings of other species had negligible effects on seedling survival. This result strongly suggests that self-limitation is mediated through species-specific pathogens. Species-specificity would also explain why the average abundance of species is independent of the number of closely related species; that is, species in the same family.

When pathogens are shared among confamilial species, new species might be limited by existing related species and effectively excluded from a local assemblage or a regional species pool (*28*). Thus, under the Janzen-Connell model, the species richness of families could depend on the degree of host specialization of their pathogens (*23*). Facilitation resulting from sharing pollinators or other mutualistic species might also promote the coexistence of more species within a family. In this case, species richness itself could generate ecological opportunities for new species within a larger taxon (*29*). For example, species of legumes (Fabaceae) might acquire *Rhizobium* symbionts more readily in the presence of related species. Figs and their pollinating wasps are extremely diverse in tropical forests throughout the world, involving an estimated 750 interdependent species pairs, and provide another example of how the presence of congeners might facilitate further speciation (*30*).

A noteworthy implication of global and long-term correlations in species richness among families of tropical forest trees is the existence of clade-specific properties that constrain the number of species-level taxa in spite of their continual turnover through time; within this constraint, the distribution and abundance of individual species are, by comparison, highly dynamic. We have not identified specific causes of the turnover of species or the stability of larger taxa, although we believe that biological interactions, particularly with pathogens and mutualists, may hold the key (*21*, *31*). Clearly, regional and local patterns of species richness are shaped by evolutionarily conservative traits of higher taxa (*32*, *33*); in comparison, the distribution and abundance of individual species are highly dynamic within this constraint.

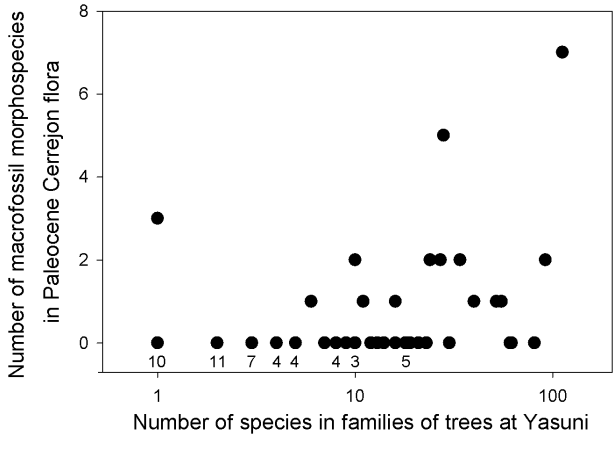


Fig. 4. Correlation of family-level diversity over time. Relation between the number of morphospecies in the Paleocene Cerrejón Flora assignable to contemporary families and the number of species per family in the Yasuni forest plot ($r_S = 0.45$, $P < 0.0001$) is shown. The Cerrejón data are from table S10 in Wing *et al.* (*12*), who reported correlations averaging $r_S = 0.30$ in species per family between the Cerrejón Flora and 72 0.1-ha Neotropical forest plots. Numbers under the black circles indicate the number of families represented by the individual symbols.

References and Notes

1. S. Nee, *Annu. Rev. Ecol. Evol. Syst.* **37**, 1 (2006).
2. S. P. Hubbell, *The Unified Neutral Theory of Biodiversity and Biogeography*, Monographs in Population Biology 32 (Princeton Univ. Press, Princeton, NJ, 2001).
3. N. C. A. Pitman *et al.*, *Ecology* **82**, 2101 (2001).
4. N. C. A. Pitman *et al.*, *Ecology* **83**, 3210 (2002).
5. A. H. Gentry, *Ann. Mo. Bot. Gard.* **75**, 1 (1988).
6. R. E. Ricklefs, in *Speciation and Patterns of Diversity*, R. Butlin, J. Bridle, D. Schluter, Eds. (Cambridge Univ. Press, Cambridge, 2009), pp. 257–277.
7. R. Condit, *Trends Ecol. Evol.* **10**, 18 (1995).
8. Materials and methods are available as supporting material on *Science* Online.
9. P. F. Stevens, Angiosperm Phylogeny Web site, www.mobot.org/mobot/research/apweb (Missouri Botanical Garden, St. Louis, MO, 2001 onward).
10. The Angiosperm Phylogeny Group, *Bot. J. Linn. Soc.* **161**, 105 (2009).
11. B. J. McGill, E. A. Hadly, B. A. Maurer, *Proc. Natl. Acad. Sci. U.S.A.* **102**, 16701 (2005).
12. S. L. Wing *et al.*, *Proc. Natl. Acad. Sci. U.S.A.* **106**, 18627 (2009).
13. C. Jaramillo, M. J. Rueda, G. Mora, *Science* **311**, 1893 (2006).
14. J. Hey, *Evolution* **46**, 627 (1992).

Downloaded from www.sciencemag.org on January 27, 2012

15. S. Nee, R. M. May, P. H. Harvey, *Philos. Trans. R. Soc. London Ser. B Biol. Sci.* **344**, 305 (1994).
16. J. Terborgh, R. B. Foster, P. Nuñez, *Ecology* **77**, 561 (1996).
17. H. Kreft, W. Jetz, *Proc. Natl. Acad. Sci. U.S.A.* **104**, 5925 (2007).
18. E. G. Leigh Jr., *J. Theor. Biol.* **90**, 213 (1981).
19. R. E. Ricklefs, *Ecology* **87**, 1424 (2006).
20. D. L. Rabosky, *Ecol. Lett.* **12**, 735 (2009).
21. R. E. Ricklefs, *Proc. Natl. Acad. Sci. U.S.A.* **107**, 1265 (2010).
22. K. J. Gaston, *Philos. Trans. R. Soc. London Ser. B Biol. Sci.* **353**, 219 (1998).
23. T. J. Givnish, *J. Ecol.* **87**, 193 (1999).
24. J. H. Connell, *Science* **199**, 1302 (1978).
25. D. H. Janzen, *Am. Nat.* **104**, 501 (1970).
26. L. S. Comita, H. C. Muller-Landau, S. Aguilar, S. P. Hubbell, *Science* **329**, 330 (2010).
27. S. A. Mangan *et al.*, *Nature* **466**, 752 (2010).
28. X. Liu *et al.*, *Ecol. Lett.* 10.1111/j.1461-0248.2011.01715.x (2011).
29. S. Nee, A. O. Mooers, P. H. Harvey, *Proc. Natl. Acad. Sci. U.S.A.* **89**, 8322 (1992).
30. N. Rønsted *et al.*, *Proc. Biol. Sci.* **272**, 2593 (2005).
31. R. E. Ricklefs, *Philos. Trans. R. Soc. London Ser. B Biol. Sci.* **365**, 1139 (2010).
32. T. J. Givnish, *Taxon* **59**, 1326 (2010).
33. R. E. Ricklefs, S. S. Renner, *Evolution* **48**, 1619 (1994).

Acknowledgments: We are grateful to the principal investigators of the CTFS forest plots used in this analysis for the assembly and sharing of unique data on the structure and dynamics of tropical forests: R. Condit, S. Hubbell, R. Foster (Barro Colorado Island, Panama); S. Bunyavejchewin (Huai Kha Khaeng, Thailand); D. Thomas, D. Kenfack, G. Chuyong (Korup, Cameroon); M. Alvarez (La Planada, Colombia); S. Tan, L. H. Seng, S. Davies, T. Yamakura (Lambir, Malaysia); S. Noor, R. Kassim (Pasoh, Malaysia); and R. Valencia (Yasuni, Ecuador). The manuscript benefitted from the insightful and constructive comments of two reviewers. R.E.R. thanks the Alexander von Humboldt Foundation and the Curators of the University of Missouri for financial support. Original data are available at www.ctfs.si.edu.

Supporting Online Material

www.sciencemag.org/cgi/content/full/335/6067/464/DC1
Materials and Methods
SOM Text
Table S1
References (*34*–*40*)

12 October 2011; accepted 5 December 2011
10.1126/science.1215182

Heavy Livestock Grazing Promotes Locust Outbreaks by Lowering Plant Nitrogen Content

Arianne J. Cease,[1]* James J. Elser,[1]* Colleen F. Ford,[1] Shuguang Hao,[2] Le Kang,[2]* Jon F. Harrison[1]*

Current paradigms generally assume that increased plant nitrogen (N) should enhance herbivore performance by relieving protein limitation, increasing herbivorous insect populations. We show, in contrast to this scenario, that host plant N enrichment and high-protein artificial diets decreased the size and viability of *Oedaleus asiaticus*, a dominant locust of north Asian grasslands. This locust preferred plants with low N content and artificial diets with low protein and high carbohydrate content. Plant N content was lowest and locust abundance highest in heavily livestock-grazed fields where soils were N-depleted, likely due to enhanced erosion. These results suggest that heavy livestock grazing and consequent steppe degradation in the Eurasian grassland promote outbreaks of this locust by reducing plant protein content.

Plant nitrogen (N) content has long been linked to the performance and dynamics of herbivorous insects (*1*). Most nitrogen in plants is in the form of protein, and current paradigms generally assume that increased plant N content will enhance herbivore performance by relieving any constraints on growth and reproduction due to limitations of available protein (*2*). Because plants in many terrestrial ecosystems are N-limited (*3*), it is often assumed that primary consumers would be as well (*2*). However, studies performed on the basis of the geometric framework (*4*) have shown that many animals have specific dietary intake targets for protein, carbohydrates, and other nutrients. Interestingly, such studies have found that excess protein decreased life span in fruit flies (*5*) and that herbivores and omnivores (including humans) will overeat carbohydrates but are unlikely to overeat protein (*6*). Thus, animals may sometimes be impaired by ingesting excess protein (*7*). Indeed, the Australian plague locust, *Chortoicetes terminifera* (Acrididae: *Oedipodinae*), grew slowly on one host plant because it obtained excess protein relative to carbohydrate (*8*). Given that humans have substantially altered ecosystem N cycling through fossil fuel combustion, agricultural fertilizer application (*9*), and domesticated animal production (*10*), they may also affect insect dynamics in unexpected ways by altering plant nitrogen supplies. Understanding these anthropogenic impacts is critical to developing sustainable land management practices that minimize economically damaging insect outbreaks.

Oedaleus asiaticus (Acrididae: *Oedipodinae*) is a nonmodel [e.g., (*11*)], economically damaging locust of the north Asian steppe (*12*, *13*), part of the largest grasslands in the world (Fig. 1A). We examined the effects of increases in the N content of host plants due to fertilization inputs of 175 kg N ha^{-1} $year^{-1}$ on growth and viability of this locust in both laboratory and field cage experiments (*14*). This level of N addition is similar to the fertilization rates of most crops (*15*). We then used artificial diets varying in their protein:carbohydrate ratio to assess effects on dietary preference and growth rates.

In contrast to the existing paradigm of limitation of insects by low content of plant protein, our results show that N fertilization and high-protein artificial diets can have consistent negative effects on the performance of the locust. Survival decreased strongly with N fertilization in the field (Fig. 1B). The decreased survival of *O. asiaticus* in N-fertilized field plots could have been due to many possible consequences of fertilization, such as changes in plant structure or chemical content, species composition, predators, or microclimate. However, results from lab experiments that controlled for these factors indicated that growth rate, size, and development rate were all reduced when locusts were fed N-fertilized plants (Fig. 1C), indicating that the field survival results were due to effects associated with plant N status. Furthermore, when offered complementary artificial diets [e.g., (*16*)], locusts selectively consumed a protein:carbohydrate ratio of 0.5, which most correlated with maximal survival (Fig. 1, D and E). Performance (growth rate × survival) was significantly reduced when locusts were confined to artificial diets with a protein:carbohydrate ratio above 1:1 (Fig. 1E), consistent with the hypothesis that the mechanism by which N fertilization reduces survival of this locust in the field is elevation of plant protein content.

In addition, plant N content was closely associated with the relative amounts of different food plants consumed when locusts were offered a palette of the six most common local plants collected from unfertilized plots (five grasses and one sedge) (Fig. 2A). Indeed, contrary to expectations from protein-limitation paradigms, *Stipa grandis*, the grass with the lowest N content, was the most highly consumed over 36 hours [a period long enough for locusts to take multiple meals and regulate nutrient intake on the basis of internal conditions (*17*)]. Direct behavioral observations confirm that low-N *S. grandis* was the most highly consumed plant under field conditions (*18*).

We compared food selection over 8 hours between N-fertilized and unfertilized *S. grandis*, using dried, ground leaves to control for toughness and water content (*8*, *19*). Locusts strongly favored unfertilized *S. grandis* leaves over *S. grandis*

[1]School of Life Sciences, Arizona State University, Tempe, AZ 85287, USA. [2]State Key Laboratory of Integrated Pest Management, Institute of Zoology, Chinese Academy of Sciences, Beijing, China.

*To whom correspondence should be addressed. E-mail: arianne.cease@asu.edu (A.J.C); jon.harrison@asu.edu (J.F.H); james.elser@asu.edu (J.J.E.); lkang@ioz.ac.cn (L.K.)

Downloaded from www.sciencemag.org on January 27, 2012

collected from N-fertilized plots (Table 1). N fertilization increased the protein content of *S. grandis* (Table 2), suggesting that the negative effects of N fertilization are due to changes in the protein:carbohydrate ratio away from the intake target of *O. asiaticus (20)*, although it is also possible that N fertilization increased the concentration of N-rich alkaloids or other allelochemicals (*21*).

In Inner Mongolia, a primary outcome of heavy livestock grazing is the loss of topsoil and organic N due to erosion, resulting in plants with a low N content (*10*). Grazing also results in a shift in the balance between *S. grandis* and *Leymus chinensis*, with *S. grandis* becoming more prevalent in heavily grazed fields (*13*). [Note, however, that there was always a substantial biomass of each species available across our study sites and field cages (table S1).] Together, these grasses comprise roughly 80% of the above-ground biomass in the Inner Mongolian grasslands (*22*); thus, a large locust outbreak must depend on one or, more likely, both of these grasses during its development.

Consistent with a population-level impact of sheep grazing on locust abundance via effects on plant N content, locust density was highest in heavily grazed pastures dominated by plants with the lowest N content (Fig. 2B). Furthermore, locusts preferred low-N *S. grandis* collected from heavily grazed pastures over *S. grandis* from ungrazed plots (on the basis of paired-choice comparisons involving either fresh leaves or dried, ground leaves, to control for toughness and water content) (Table 1). Although the field measurements of locust abundance did not control for other possible effects of livestock grazing [e.g., shifts in predator communities, microclimate, sward structure, plant secondary chemicals, and landscape patchiness (*23*)], these data are consistent with the hypothesis that the high densities of *O. asiaticus* on the heavily grazed plots are due to this locust's preference for low-N plants and its improved growth and survival on such plants.

The hypothesis that low plant N can stimulate locust outbreaks is also supported by observations that *O. asiaticus* population explosions occur exclusively in pastures heavily grazed by livestock (*24*). Our data are in accordance with work showing that some North American Acrididae species (grasshoppers and locusts) also prefer low-N plants, likely due to their long-term adaptation to N-limited grassland environments (*25*). There is mounting evidence that N excess, rather than N limitation, is a critical nutritional factor regulating plant-insect interactions, especially for grasshoppers (*8*, *26*) and other herbivores that have evolved to exploit a relatively poor autotroph nutrient base in nature.

Our results fit well with the emerging paradigm that related animal species can vary dramatically in intake targets and performance responses to dietary variation. Seven cogeneric grasshopper species from one community were tested and all but two had unique target intake ratios, which suggests that each species may fill a unique nutritional niche and that species with extreme intake targets might be most sensitive to environmental variation (*27*). The lowest protein:carbohydrate intake target observed was 0.7, similar to what has been reported for the migratory locust (*L. migratoria*), which shares a subfamily with *Oedaleus* (*28*). We found that *O. asiaticus* had a protein:carbohydrate intake target of 0.5 (Fig. 1D), lower than any grasshopper previously studied (*21*). This finding may explain why dramatic, damaging population outbreaks of *O. asiaticus* occur in association with changes in land management (in this case, grazing intensity).

Our results strongly suggest that heavy livestock grazing promotes outbreaks of this locust by shifting plant nutrient content toward lower N conditions favorable to *O. asiaticus*. Although the precise physiological mechanisms by which high plant N exerts negative effects on this locust in the field remain to be elucidated, data from our artificial diet studies strongly suggest that protein

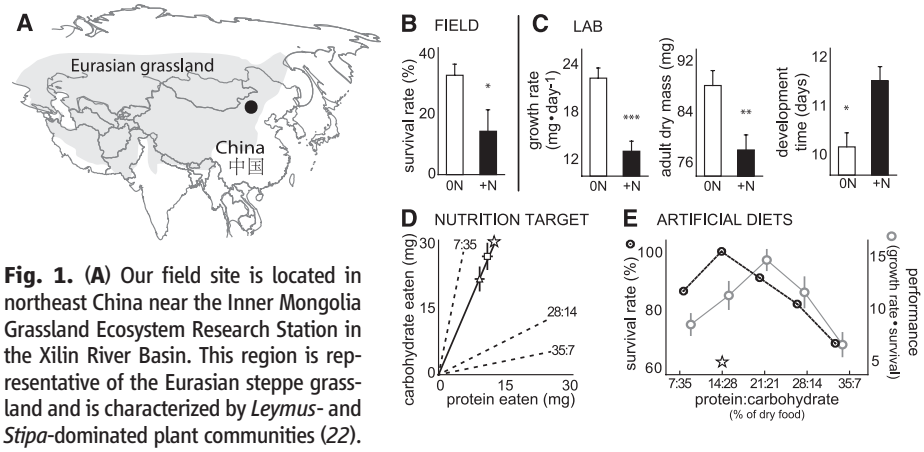


Fig. 1. (**A**) Our field site is located in northeast China near the Inner Mongolia Grassland Ecosystem Research Station in the Xilin River Basin. This region is representative of the Eurasian steppe grassland and is characterized by *Leymus*- and *Stipa*-dominated plant communities (*22*). Rapid steppe degradation (*29*) has led to reduced biodiversity, decreased productivity and, in some cases, desertification (*30*), likely due to anthropogenic factors, especially livestock grazing (*31*). N fertilization of field plots negatively affected *O. asiaticus*, (**B**) reducing survival in field cages and (**C**) growth, size, and development rates when reared in the laboratory (on *L. chinensis* from these plots). All comparisons were made using Student's *t* tests; data for proportion surviving in field cages were arcsine transformed before analysis (*$P < 0.05$, **$P \leq 0.01$, ***$P \leq 0.001$). In artificial diet studies of field-collected animals, (**D**) locusts given pairs of diets complementary in their protein:carbohydrate ratios—7:35 and 35:7 (square) or 7:35 and 28:14 (triangle)—ate similar amounts of carbohydrate and protein (multivariate analysis of covariance: Wilks' lambda = 0.95, $F_{2,29} = 0.72$, $P = 0.50$; initial locust mass covariate means, 244 mg). Locusts fed nonrandomly to achieve a target protein:carbohydrate intake of ~0.5. (**E**) Locusts had 100% survival when fed artificial diets with a 0.5 protein:carbohydrate ratio, the same ratio they selected when given a choice. Survival rate was lowest (68%) in the highest protein diet. Overall performance (i.e., growth rate × survival) decreased above and below a protein:carbohydrate ratio of 1:1 (analysis of covariance: $F_{4,68} = 8.85$, $P < 0.001$; initial locust mass covariate means, 136 mg).

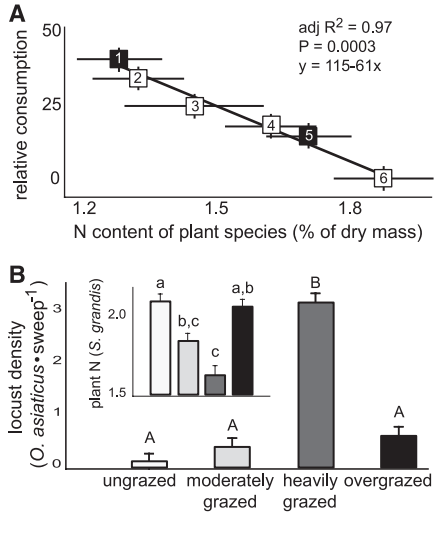


Fig. 2. (**A**) The percentage of consumption of each plant species (see SOM for how this was calculated) was negatively related to the percentage of N of that species (N was measured in leaf blades). Locusts were concurrently offered leaf blades from each of the six most common plants for 36 hours. 1, *S. grandis*; 2, *Carex korshinskyi*; 3, *Agropyron cristatum*; 4, *Cleistogenes squarrosa*; 5, *L. chinensis*; 6, *Achnatherum sibiricum.* Darkened squares are the two most common plants, each responsible for ~40% of aboveground biomass. Remaining species make up <5% each of aboveground biomass. (**B**) *O. asiaticus* was most abundant in heavily grazed fields where the N content of *S. grandis* was lowest during an outbreak year (2009); collected from large (>20 ha) and adjacent pastures [analysis of variance (ANOVA): $F_{3,16} = 64.95$, $P < 0.001$]. The ungrazed field has been fenced and protected since 1979; adjacent fields have been grazed at relatively constant levels for >5 years. Grazing level was determined by differences in ground cover and aboveground biomass [e.g., (*12*)]. Each observation represents the number of *O. asiaticus* collected in sweep-net samples from a given pasture and the percentage of N of a concurrently collected composite of above ground *S. grandis* leaves from a 1-m^2 quadrat (inset) (ANOVA: $F_{3,12} = 14.81$, $P < 0.001$). Letters indicate differences using Scheffe's post hoc comparison tests.

Downloaded from www.sciencemag.org on January 27, 2012

Table 1. Nitrogen enrichment of field plots decreased the palatability of *S. grandis* (the preferred host plant), and heavy grazing increased palatability in paired-choice tests using either dried/ground (8-hour assay) or fresh leaves (single-meal assay, average percentage of leaf area consumed).

Treatment (*S. grandis*)	Number of wins	Amount consumed	Chi- squared *P*
		Ground leaf	
Unfertilized	18	13.8 ± 2*	<0.01
Fertilized	7	8.6 ± 2*	
Heavily grazed	9	4.1 ± 1*	0.01
Ungrazed	3	2.9 ± 1*	
		Fresh leaf	
Heavily grazed	8	28 ± 7†	0.03
Ungrazed	3	15 ± 5†	

Table 2. Nitrogen enrichment of field plots increased the N content (percentage of dry mass) and protein content (percentage of dry mass) of *S. grandis* and *L. chinensis*. All comparisons were analyzed using Student's *t* tests after arcsine transformation of proportional data.

Nutrient	Unfertilized	N-fertilized	*P*	N	Heavily grazed	Ungrazed	*P*	N
			S. grandis					
% C	46 ± 0.8	46 ± 0.8	0.77	24	47 ± 0.2	44 ± 2	0.12	9
% N	1.4 ± 0.05	2.4 ± 0.06	<0.001	24	1.7 ± 0.05	2.1 ± 0.04	<0.001	9
% protein	4.3 ± 0.5	11.1 ± 1.8	<0.01	24				
Protein/N ratio	3.1 ± 0.4	4.6 ± 0.7	0.10	24				
			L. chinensis					
% C	46 ± 1	46 ± 0.8	0.99	24	46 ± 0.3	46 ± 0.3	0.18	8
% N	1.8 ± 0.08	2.9 ± 0.1	<0.001	24	2.4 ± 0.09	2.7 ± 0.03	0.12	8
% protein	8.7 ± 1	11.9 ± 1	0.03	23				
Protein/N ratio	4.9 ± 0.5	4.2 ± 0.4	0.37	23				

excess is playing a role. Furthermore, these findings reinforce the realization that differential responses of herbivore species to plant nutrient content can structure herbivore communities (*27*), providing new insights that may improve livestock and fertilization management strategies to limit the occurrence of economically damaging locust outbreaks.

References and Notes

1. W. J. Mattson Jr., *Annu. Rev. Ecol. Syst.* **11**, 119 (1980).
2. T. White, *The Inadequate Environment: Nitrogen and the Abundance of Animals* (Springer-Verlag Berlin, 1993).
3. J. J. Elser *et al.*, *Ecol. Lett.* **10**, 1135 (2007).
4. D. Raubenheimer, S. J. Simpson, *Anim. Behav.* **45**, 953 (1993).
5. K. P. Lee *et al.*, *Proc. Natl. Acad. Sci. U.S.A.* **105**, 2498 (2008).
6. S. J. Simpson, D. Raubenheimer, *Aging* **1**, 875 (2009).
7. E. A. Bernays, in *Nitrogen as an Ecological Factor*, J. A. Lee, S. McNeill, I. H. Ronson, Eds. (Blackwell, Oxford, 1983), pp. 321–344.
8. F. J. Clissold, G. D. Sanson, J. Read, *J. Anim. Ecol.* **75**, 1000 (2006).
9. J. Galloway *et al.*, *Biogeochemistry* **70**, 153 (2004).
10. L. Wu, N. He, Y. Wang, X. Han, *J. Environ. Qual.* **37**, 663 (2008).
11. H. Song, *Psyche* **2011**, 1 (2011).
12. A. J. Cease, S. Hao, L. Kang, J. J. Elser, J. F. Harrison, *J. Insect Physiol.* **56**, 926 (2010).
13. L. Kang, X. G. Han, Z. B. Zhang, O. J. Sun, *Philos. Trans. R. Soc. London Ser. B* **362**, 997 (2007).
14. Materials and methods are available as supporting material on *Science* Online.
15. IFA/IFDC/FAO, *Fertilizer Use by Crop*. (Food and Agriculture Organization of the United Nations, Rome, ed. 5, 2006).
16. D. Raubenheimer, S. Simpson, *Entomol. Exp. Appl.* **91**, 67 (1999).
17. D. Raubenheimer, S. Jones, *Anim. Behav.* **71**, 1253 (2006).
18. D. F. B. Flynn, thesis, Columbia University, New York, (2011).
19. F. J. Clissold, G. D. Sanson, J. Read, S. J. Simpson, *Ecology* **90**, 3393 (2009).
20. D. Raubenheimer, S. J. Simpson, *J. Exp. Biol.* **206**, 1669 (2003).
21. S. T. Behmer, *Annu. Rev. Entomol.* **54**, 165 (2009).
22. Z. Chen, S. Wang, *Typical Steppe Ecosystems of China* (Science Press, Beijing, 2000).
23. D. H. Branson, A. Joern, G. A. Sword, *Bioscience* **56**, 743 (2006).
24. L. Kang, Y. L. Chen, *Insect Sci.* **2**, 265 (1995).
25. A. Joern, S. T. Behmer, *Oecologia* **112**, 201 (1997).
26. D. Berner, W. U. Blanckenhorn, C. Korner, *Oikos* **111**, 525 (2005).
27. S. T. Behmer, A. Joern, *Proc. Natl. Acad. Sci. U.S.A.* **105**, 1977 (2008).
28. S. Simpson, D. Raubenheimer, *Philos. Trans. R. Soc. London Ser. B* **342**, 381 (1993).
29. C. Tong, J. Wu, S. Yong, J. Yang, W. Yong, *J. Arid Environ.* **59**, 133 (2004).
30. J. Wu, C. Overton, *Bull. Ecol. Soc. Am.* **83**, 189 (2002).
31. J. Han *et al.*, *Rangeland J.* **30**, 233 (2008).

Acknowledgments: The authors thank F. Jin, D. Niren, D. Flynn, Y. Kong, Z. Fan, J. Esman, Q. Chen, and G. Zhang for field and laboratory assistance; M. Quinlan, D. Denardo, J. VandenBrooks, C. Klok, S. Behmer, and J. Sabo for helpful discussion of experimental design; J. Wu for funding and scientific support; and M. McCrackin, F. Clissold, and three anonymous reviewers for valuable comments on the manuscript. This work was supported by the National Science Foundation (EAPSI, DDEP to A.J.C., DEB-0925017 to J.J.E., and EAR-0746352 to J.F.H.), Sigma Xi, Achievement Rewards for College Scientists (Marley-Webb and Johnston Foundations), P.E.O. Scholar Award to A.J.C., the Chinese Research Grants of Public Welfare Fund for Agriculture (Project 200903021), and the Foundation of Chinese Academy of Sciences (Project Kscx2-yw-z-1021). A.J.C. designed and performed experiments, analyzed data, and wrote the paper. J.J.E. and J.F.H. designed experiments and wrote the paper. C.F.F. and S.H. designed and performed experiments. L.K. gave scientific support and guidance. Data used in the analyses are available in the Supporting Online Material.

Supporting Online Material

www.sciencemag.org/cgi/content/full/335/6067/467/DC1
Materials and Methods
Fig. S1
Table S1
References (*32*–*36*)

26 September 2011; accepted 15 November 2011
10.1126/science.1214433

Depth Perception from Image Defocus in a Jumping Spider

Takashi Nagata,[1]* Mitsumasa Koyanagi,[1]† Hisao Tsukamoto,[1] Shinjiro Saeki,[2] Kunio Isono,[2] Yoshinori Shichida,[3] Fumio Tokunaga,[4] Michiyo Kinoshita,[5] Kentaro Arikawa,[5] Akihisa Terakita[1]†

The principal eyes of jumping spiders have a unique retina with four tiered photoreceptor layers, on each of which light of different wavelengths is focused by a lens with appreciable chromatic aberration. We found that all photoreceptors in both the deepest and second-deepest layers contain a green-sensitive visual pigment, although green light is only focused on the deepest layer. This mismatch indicates that the second-deepest layer always receives defocused images, which contain depth information of the scene in optical theory. Behavioral experiments revealed that depth perception in the spider was affected by the wavelength of the illuminating light, which affects the amount of defocus in the images resulting from chromatic aberration. Therefore, we propose a depth perception mechanism based on how much the retinal image is defocused.

Visual systems that accurately and reliably judge distance or depth are valuable. A wide variety of animals, including humans, perform this task with binocular stereoscopic depth perception (*1*). Two types of monocular depth cues also provide absolute depth perception in some animals: accommodation (i.e., focal adjustment) in chameleons and other vertebrates (*2*, *3*)

Downloaded from www.sciencemag.org on January 27, 2012

and motion parallax (i.e., image motion on the retina, the amount of which depends on the distance to an object) in some insects (*4*). The insects obtain motion parallax information by typical side-to-side translational movements of the head. Theoretically, however, the amount of image defocus (i.e., how much an image defocused) can be used as an absolute depth cue by comparing a defocused image with one or more additional images in which the same object is sharply focused or differently defocused (*5*). Humans use image defocus for a rough estimation of the relative depth positions of objects (*6*), but until now no animals have been known to use image defocus as an absolute depth cue. We show here that jumping spiders (*Hasarius adansoni*) perceive absolute depth by using image defocus.

Jumping spiders approach their prey and jump accurately by using two pairs of forward-facing eyes, the principal eyes (PEs) and the anterior lateral eyes (ALEs) (*7*, *8*) (Fig. 1A). If both ALEs are occluded, spiders can make accurate jumps, demonstrating that PEs provide absolute depth perception (*7*). Interestingly, however, PEs have neither overlapping fields of view nor a focal adjustment mechanism (*9*). Furthermore, no kind of motion that could generate motion parallax during the hunting behavior has been reported. To check whether jumping spiders use motion parallax cues, we investigated hunting behavior by using the apparatus shown in fig. S1 and compared the distance of jumps to the actual distance from the spider to a target fly. Spiders whose bilateral ALEs and a PE were occluded, with a single PE left untouched, made accurate jumps and caught the fly without any motion that could generate motion parallax (movie S1 and Fig. 1B). This indicates that the spiders accurately measured the distance without the use of any of the three kinds of cues known in animals.

A clue to the depth perception mechanism is found in the unique structure of the PE retina, which has four layers consisting of rhabdomeres, the photoreceptive portions of photoreceptor cells (*10*, *11*) (Fig. 1C). In the retina, the position of an image focused by the lens is determined by the distance to the object and the wavelength of light because of the chromatic aberration of the lens. Blest *et al*. electrophysiologically found some green-sensitive photoreceptor cells in the second-deepest layer, L2, but green light is not focused on L2 but rather on the deepest layer, L1, in jumping spiders of genus *Plexippus* (*12*). Therefore, these authors suggested that the green-sensitive photoreceptor cells in L2 receive defocused images. This appears to be true for the species used in this study, *H. adansoni*, because the chromatic aberration of PE lens of *H. adansoni* is similar to that of *Plexippus* (*12*) (fig. S2). We hypothesized that jumping spiders perceive depth on the basis of the amount of defocus in images received by L2 because, in principle, the distance to objects can be uniquely determined from the amount of defocus in L2 (Fig. 1D).

We then investigated the visual pigments in the PE retina. A basic premise of our hypothesis is that green-sensitive photoreceptors are widely and densely distributed in L2, but the spectral sensitivity of most of the photoreceptors in L2 remains unknown. We found two visual pigments, Rh1 and Rh3, in the PE (Fig. 2A) among four visual pigments, Rh1 to 4 (fig. S3). Rh1 is a green-sensitive pigment (Fig. 2B) and localized in all rhabdomeres of L2 and L1, whereas Rh3 is an ultraviolet (UV)-sensitive pigment (fig. S4) and localized only in L3 and L4 (Fig. 2C and fig. S5), demonstrating that the photoreceptors in L2 and L1 are all green-sensitive whereas those in L3 and L4 are all UV-sensitive. This is consistent with the electroretinographically determined sensitivity spectrum of PEs (fig. S6) as well as the reported intracellular recordings (*12*–*14*) and supports our hypothesis.

Rh2, a blue-sensitive pigment (fig. S7), was never detected in PEs (fig. S8). This strongly suggests that the green-sensitive Rh1 is more suitable for the function of L2, although Rh2 seems more appropriate to receive focused images because blue light should be focused in L2 (*12*). This supports the idea that the defocus of images received by L2 is physiologically important.

To test our hypothesis, we investigated jumps under monochromatic green (≈520 nm) and red (≈630 nm) light (fig. S9), to which only L2 and

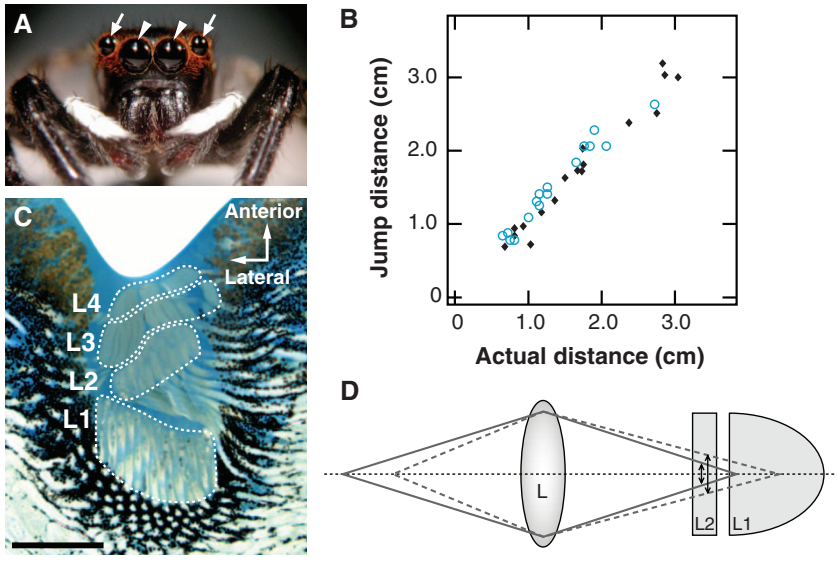


Fig. 1. Depth perception of jumping spiders with the principal eyes and its hypothetical mechanism. (**A**) Anterior view of the jumping spider, *H. adansoni*. PEs (arrowheads) and ALEs (arrows) are indicated. (**B**) Jump distance versus the actual distance of intact jumping spiders (black diamonds; $n = 4$) and spiders with one PE and both ALEs occluded (blue open circles; $n = 3$). (**C**) Horizontal section of PE retina stained with toluidine blue. The photoreceptor layers are traced. Incoming light comes from above. Scale bar, 50 μm. (**D**) Schematic drawing of the paths of green light passing through the lens (L) and received by L1 and L2 (solid and broken lines). The amount of defocus on L2 (arrows) depends on the distance between the lens and the object.

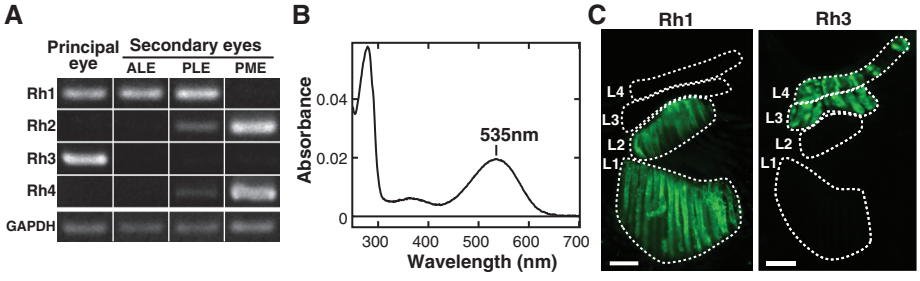


Fig. 2. Distribution and absorption spectrum of visual pigments expressed in the principal eye. (**A**) Reverse-transcription polymerase chain reaction analyses of visual pigment gene expression in PE, ALE, posterior lateral eye (PLE), and posterior median eye (PME). GAPDH (glyceraldehyde-3-phosphate dehydrogenase) serves as an internal standard. (**B**) Absorption spectrum of purified Rh1 with 11-*cis*-retinal (fig. S12). (**C**) Immunofluorescence labeling of Rh1 and Rh3 in PE retina. Scale bars, 10 μm.

[1]Department of Biology and Geosciences, Graduate School of Science, Osaka City University, Osaka 558-8585, Japan. [2]Graduate School of Information Sciences, Tohoku University, Sendai 980-8579, Japan. [3]Department of Biophysics, Graduate School of Science, Kyoto University, Kyoto 606-8502, Japan. [4]Department of Earth and Space Science, Graduate School of Science, Osaka University, Toyonaka 560-0043, Japan. [5]Laboratory of Neuroethology, The Graduate University for Advanced Studies (Sokendai), Hayama 240-0193, Japan.

*Present address: Laboratory of Neuroethology, The Graduate University for Advanced Studies (Sokendai), Hayama 240-0193, Japan.

†To whom correspondence should be addressed. E-mail: koyanagi@sci.osaka-cu.ac.jp (Mitsumasa K.); terakita@sci.osaka-cu.ac.jp (A.T.)

Downloaded from www.sciencemag.org on January 27, 2012

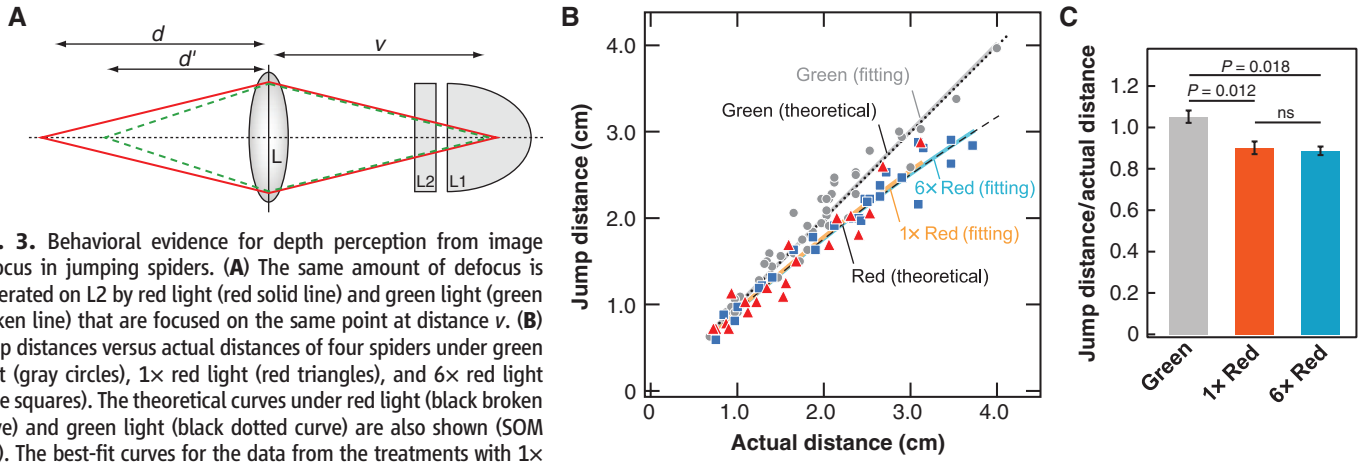


Fig. 3. Behavioral evidence for depth perception from image defocus in jumping spiders. (**A**) The same amount of defocus is generated on L2 by red light (red solid line) and green light (green broken line) that are focused on the same point at distance *v*. (**B**) Jump distances versus actual distances of four spiders under green light (gray circles), 1× red light (red triangles), and 6× red light (blue squares). The theoretical curves under red light (black broken curve) and green light (black dotted curve) are also shown (SOM text). The best-fit curves for the data from the treatments with 1× red light (orange curve), 6× red light (blue curve), and green light (gray curve) were obtained by using Eq. 1. (**C**) Ratios of the jump distance to the actual distance. Data are presented as the mean ± SEM (n = 4). ns, not significant. Statistical analysis was performed by ANOVA.

L1 are sensitive. The focal length of red light is greater than that of green light (fig. S2), and the defocus amount under red light is equal to that generated by a closer object under green light (Fig. 3A). Accordingly, if jumping spiders estimate distance by using the amount of defocus, they are expected to underestimate the distance and make shorter jumps under red light because they would basically judge the distance by basing distance-defocus relationship in green light, which Rh1 absorbs most effectively under natural light conditions (fig. S10). We occluded bilateral ALEs of spiders and measured the jump distances under green light and under two intensities (1× and 6×) of red light and compared them with the actual distances. The spiders jumped accurately onto the targets under green light, whereas they exhibited shorter jumps under red light (n = 4) (Fig. 3B). In fact, the spiders sometimes failed to capture targets in a single jump under red light because their jumps were too short (movie S2). The mean ratio of the jump distance to the actual distance under 1× red light (≈0.90, n = 4) was significantly lower than the ratio under green light (≈1.0, n = 4) [P = 0.012, analysis of variance (ANOVA) with Bonferroni correction] (Fig. 3C), showing that jump distances were shorter than actual distances under red light.

In the above experiment, the intensities of the green and 1× red lights were adjusted by using purified Rh1 pigment so that the two types of light activated Rh1 with the same efficiency (fig. S11); that is, the subjective brightness of the two lights for the spider appeared to be identical. Additionally, the ratio of the jump distance to the actual distance under a sixfold brighter red light (6× red light) was ≈0.89 (n = 4), which was similar to the ratio under the 1× red light and also significantly lower than the ratio under the green light (P = 0.018, ANOVA with Bonferroni correction) (Fig. 3C). Therefore, the shorter jump distances observed under red light can be attributed to the wavelength rather than the intensity.

To evaluate these results, we compared jump distances with theoretically predicted distances based on our hypothesis. Figure 3A shows paths of red light from a point at distance d and green light from another point at distance d', both causing the same amount of defocus. If the hypothesis is correct, d' corresponds to the distance estimated by the spiders and therefore would correspond to the jump distance. From the lens equation,

$$d' = \frac{1}{f}\left(1 - \frac{1}{1 + fd}\right), \quad f = \frac{1}{F_g} - \frac{1}{F_r}, \quad (1)$$

where F_r and F_g are focal lengths of the lens under red and green light, respectively [supporting online material (SOM) text]. We determined the focal lengths of the lens (table S1) and obtained the theoretical curves of d' (black broken and dotted curves in Fig. 3B). These theoretical curves correspond well with the experimental data on jump distances, and this result is supported by the agreement of these curves with fitting curves of the experimental data (solid curves in Fig. 3B, see SOM text). These results show that the model based on the amount of defocus (Figs. 1D and 3A) could account for the shorter jump distances under the red light, which strongly supports the hypothesis that depth perception in jumping spiders has its basis in the amount of defocus in images received by L2.

Blest *et al.* (*12*) reported that the staircase-like organization of the distal ends of L1 (Fig. 1C) enables a wide focus range because different parts of L1 receive focused images from objects at different distances. Because jumping spiders jumped accurately under green light to which only L1 and L2 are sensitive, depth perception might be achieved by comparison of defocused images received by L2 with focused images received by L1, although at present there is no evidence for an underlying neuronal mechanism. In addition, the staircase-like organization of L1 suggests that during lateral scanning (*9*) the location on L1 of the best-focused image could provide distance information, although Blest *et al.* (*12*) considered this unlikely. Similarly, the changing separation of L1 and L2 across the retina might provide a changing defocus signal that could be used in a similar way. Whether and how such mechanisms are used in depth perception remains an open question.

PEs of jumping spiders may be a real-life example of "depth from defocus," a notable depth measurement technique that is being developed for computer vision. Further investigation of the optics, retinal structure, and neural basis of depth perception in jumping spiders may provide biological inspiration for computer vision as well.

References and Notes

1. J. M. Harris, *Philos. Trans. R. Soc. London Ser. A* **362**, 2721 (2004).
2. L. Harkness, *Nature* **267**, 346 (1977).
3. H. Wagner, F. Schaeffel, *J. Comp. Physiol. A* **169**, 515 (1991).
4. K. Kral, *Behav. Processes* **64**, 1 (2003).
5. S. Chaudhuri, A. N. Rajagopalan, *Depth from Defocus: A Real Aperture Imaging Approach* (Springer-Verlag, New York, 1999).
6. A. P. Pentland, *IEEE Trans. Pattern Anal. Mach. Intell.* **9**, 523 (1987).
7. L. M. Forster, *N. Z. J. Zool.* **6**, 79 (1979).
8. D. B. Zurek, A. J. Taylor, C. S. Evans, X. J. Nelson, *J. Exp. Biol.* **213**, 2372 (2010).
9. M. F. Land, *J. Exp. Biol.* **51**, 471 (1969).
10. M. F. Land, *J. Exp. Biol.* **51**, 443 (1969).
11. R. M. Eakin, J. L. Brandenburger, *J. Ultrastruct. Res.* **37**, 618 (1971).
12. A. D. Blest, R. C. Hardie, P. McIntyre, D. S. Williams, *J. Comp. Physiol. A* **145**, 227 (1981).
13. R. D. DeVoe, *J. Gen. Physiol.* **66**, 193 (1975).
14. S. Yamashita, H. Tateda, *J. Comp. Physiol. A* **105**, 29 (1976).

Acknowledgments: We thank R. S. Molday for supplying the rho 1D4–producing hybridoma, T. Suzuki for supplying the antibody against $G\alpha_q$, R. J. Lucas for his comments on the manuscript and T. Matsuyama for building the light-emitting diode (LED) lighting equipment. This work was supported by Grants-in-Aid for Scientific Research (K.A., Mitsumasa K., Y.S., and A.T.) and Grant-in-Aid for Japan Society for the Promotion of Science Fellows (T.N.). Sequences are available from the DNA Data Bank of Japan (AB506462 and AB506463).

Supporting Online Material

www.sciencemag.org/cgi/content/full/335/6067/469/DC1
Materials and Methods
SOM Text
Figs. S1 to S12
Table S1
References (*15*–*23*)
Movies S1 and S2

25 July 2011; accepted 7 December 2011
10.1126/science.1211667

Downloaded from www.sciencemag.org on January 27, 2012

Facilitated Cross-Species Transmission of Prions in Extraneural Tissue

Vincent Béringue,[1]* Laëtitia Herzog,[1]† Emilie Jaumain,[1]† Fabienne Reine,[1]† Pierre Sibille,[1] Annick Le Dur,[1] Jean-Luc Vilotte,[2] Hubert Laude[1]*

Prions are infectious pathogens essentially composed of PrP^{Sc}, an abnormally folded form of the host-encoded prion protein PrP^{C}. Constrained steric interactions between PrP^{Sc} and PrP^{C} are thought to provide prions with species specificity and to control cross-species transmission into other host populations, including humans. We compared the ability of brain and lymphoid tissues from ovine and human PrP transgenic mice to replicate foreign, inefficiently transmitted prions. Lymphoid tissue was consistently more permissive than the brain to prions such as those causing chronic wasting disease and bovine spongiform encephalopathy. Furthermore, when the transmission barrier was overcome through strain shifting in the brain, a distinct agent propagated in the spleen, which retained the ability to infect the original host. Thus, prion cross-species transmission efficacy can exhibit a marked tissue dependence.

Mammalian prions are proteinaceous infectious agents responsible for fatal neurodegenerative disorders in farmed animals and humans. They are primarily composed of macromolecular assemblies of PrP^{Sc}, a misfolded form of the ubiquitously expressed, host-encoded prion protein PrP^{C}. Upon infection, PrP^{Sc} assemblies are thought to self-perpetuate the conformational conversion from PrP^{C} to PrP^{Sc}, leading to PrP^{Sc} deposition in the brain and sometimes in the lymphoid tissue (*1*, *2*). Multiple prion strains can self-propagate in the same host and exhibit distinct, heritable phenotypic traits, presumably through the existence of stable, structurally distinct PrP^{Sc} conformers (*3*, *4*).

Prions can transmit between species presenting a zoonotic risk, as exemplified by the emergence of variant Creutzfeldt-Jakob disease (vCJD) in the human population after exposure to bovine spongiform encephalopathy (BSE) prions (*2*). However, such events are restricted by the so-called transmission barrier (*5*, *6*), the strength of which depends on interactions between host PrP^{C} and the infecting prion strain type(s). The transmission barrier is routinely gauged by the appearance of disease-specific, clinical signs and/or PrP^{Sc} in the brain of the new host. Their concomitant absence (*7*–*9*) would usually suggest a resistance to infection or a disease incubation time exceeding the exposed host life span. Prion interspecies transmission can be associated with the acquisition of new biological strain properties (*10*–*14*). To accommodate these observations, the conformational-selection model proposes that prion interspecies transmission is essentially constrained by the degree of steric compatibility between the incoming PrP^{Sc} and the spectrum of conformations the exposed host PrP^{C} primary structure can adopt in the PrP^{Sc} state (*6*). It is not clear whether different cellular environments or PrP^{C} isoform variation among brain and extraneural tissues is involved in prion cross-species transmission. A number of prion strains can replicate in the lymphoid tissue, which can be targeted after infection, whatever the entry route (*5*, *15*).

We examined the tissue-dependence of prion cross-species transmission efficacy in three different mouse models in which primary transmission seemed to be particularly inefficient, based on the absence of clear neurological signs and of proteinase K–resistant PrP^{Sc} (PrP^{res}) in the brains of most inoculated animals at end of life. In each model, mice were inoculated intracerebrally and euthanized at end of their life span or in triplicate at regular intervals postexposure, so as to consider any age-related immune system dysfunction (*16*). Mice culled because of intercurrent disease were also analyzed whenever possible. The presence of PrP^{res} in brain and spleen tissues was assessed by immunoblotting (*17*).

The first model consisted of ovine PrP transgenic mice (VRQ allele, *tg338* line) (*18*) inoculated with prions responsible for chronic wasting disease (CWD) in cervids, an expanding epidemic in northern America. As expected (*19*), no clinical disease was observed upon inoculation with one elk CWD field isolate, despite efficient transmission to murine PrP transgenic mice (*tga20*) (fig. S1). PrP^{res} was observed in only 2 of 29 (2/29) *tg338* brains at the end of life (507 and 793 days). In marked contrast, significant levels of PrP^{res} were detected in the spleens of all but one mouse analyzed from ~380 days onward (n = 18 mice) (Fig. 1, A and B, and fig. S2). Quantifying the leakiness of the transmission barrier as the proportion of PrP^{res}-positive mice in the brain and spleen yielded large differences from 9% in the brain to 94% in the spleen (Table 1). Because interspecies transmission of prions can occur in the absence of detectable PrP^{res} in the brain (*20*), a second passage was performed with PrP^{res}-negative brain and PrP^{res}-positive spleen material from an asymptomatic mouse euthanized at 545 days postinfection. None of the six mice inoculated with the brain material demonstrated neurological signs or accumulated PrP^{res} in brain and spleen, even at a very late stage (range of survival time: 616 to 973 days), whereas three out of five mice inoculated with spleen material accumulated PrP^{res} in brain and spleen tissue (749, 836, and 947 days) (Fig. 1B and fig. S3). Thus CWD prions propagate much more easily in the spleen than in the brain on primary passage in "ovinized" mice.

We next examined whether a similarly facilitated lymphoid replication might also occur upon interspecies transmission of prions known to be essentially neurotropic. Hamster prion (*15*, *21*) from three different sources [cloned Sc237 and 263K propagated in hamster and Sc237 serially passaged and recloned in hamster PrP transgenic *tg7* mouse (*22*)] was inoculated into *tg338* mice. None of the mice developed clinical signs. Only 8/40 brains analyzed were PrP^{res}-positive, all at the end of the mouse life span (from ~570 to 875 days). However, the proportion of PrP^{res}-positive spleens was substantially higher overall (18/30),

Table 1. Leakiness of the transmission barrier, depending on whether PrP^{res} detection is performed on brain or spleen tissue. exp, experiment; Fr, French, It, Italy. *tgHa* and *tgBov* are prions passaged in hamster (Ha) or bovine (Bov) PrP transgenic (tg) mice.

Mice transgenic for	Infecting source	Proportion of PrP^{res} positive mice*			
		Brain		Spleen	
		n/n_0†	Rate (%)	n/n_0†	Rate (%)
Ovine PrP	Elk CWD (exp1)	0/9	9	4/4	94
	Elk CWD (exp2)	2/14		13/14	
Ovine PrP	Hamster 263K	2/6	24	2/2	75
	Hamster Sc237	3/5		2/2	
	Hamster Sc237 (*tgHa*)	3/23		14/20	
Human PrP	Cattle BSE (Fr3)	2/22	7	14/22	65
	Cattle BSE (*tgBov*)	1/4		2/3	
	Cattle BSE (It)	0/4		1/4	
	Goat BSE (*tgBov*)	0/13		9/11	

*The time points included for calculation start from the first PrP^{res} positive tissue sample. †n/n_0: number of PrP^{res}-positive tissue samples per number of analyzed tissue samples.

[1]Institut National de la Recherche Agronomique (INRA), UR892, Virologie Immunologie Moléculaires, Bâtiment 440, F-78350 Jouy-en-Josas, France. [2]INRA, UMR1313, Génétique Animale et Biologie Intégrative, F-78350 Jouy-en-Josas, France.

*To whom correspondence should be addressed. E-mail: vincent.beringue@jouy.inra.fr (V.B.); hubert.laude@jouy.inra.fr (H.L.)

†These authors contributed equally to this work.

Downloaded from www.sciencemag.org on January 27, 2012

and the protein was detected earlier, inconsistently from 380 days onward but in every mouse after 500 days (Fig. 1C, fig. S2, and Table 1). Spleen and brain also differed in the PrP^{res} electrophoretic type, which was stably maintained on serial passage (Figs. 1D and 2B). In the spleen, the unglycosylated PrP^{res} core consistently retained an apparent molecular mass of ~21 kD (n = 29), as in the original inocula, whereas a shift to 19 kD was observed in all PrP^{res}-positive *tg338* brains (n = 20). The possibility that distinct agents were preferentially amplified in brain and spleen tissues was formally examined by transmitting collected tissue materials from the same *tg338* mice (at third and fourth passage) to reporter *tg338* and *tg7* mice (Fig. 2A). In *tg338 mice*, the prion phenotypic features largely overlapped, whether spleen or brain extract was inoculated. Yet the presence of an additional 21-kD PrP^{res} pattern (Fig. 2B) and of numerous plaque-like PrP^{res} deposits (Fig. 2C), specifically after spleen extract inoculation, suggested that the 21- and 19-kD components coexisted in this tissue, with the 21-kD component in higher proportion. The tissue-specific differences were even greater upon transmission to *tg7* mice. *Tg338* spleen extracts were able to reinfect all *tg7* mice in ~350 days (Fig. 2A) and to induce PrP^{res} accumulation in their brain (Fig. 2, B and C), whereas the *tg338* brain extracts repeatedly failed to do so (Fig. 2). Thus, the selection and/or mutational constraints imposed onto Sc237 prions by the cross-species barrier differ radically between the brain and spleen, allowing the component preferentially amplified in the spleen to reinfect the donor species efficiently, despite iterated passage in the new host.

To see whether our observations could extend to another mouse model, we compared the susceptibility of lymphoid and brain tissue from human PrP transgenic mice (Met allele, *tg650* line) (*12*) to epizootic BSE prions. The two primary BSE isolates and the bovine PrP mouse-passaged BSE and goat BSE isolates used here have been previously described (*11*, *23*–*25*); they all exhibited similarly high infectivity levels in bovine PrP mice. Their transmission to *tg650* mice appeared inefficient on primary passage, as shown by the absence of clear neurological signs and the detection of PrP^{res} in 3/44 brains analyzed, all beyond 600 days postinfection (Fig. 1E and fig. S2) (*24*, *25*). The pathological protein was not

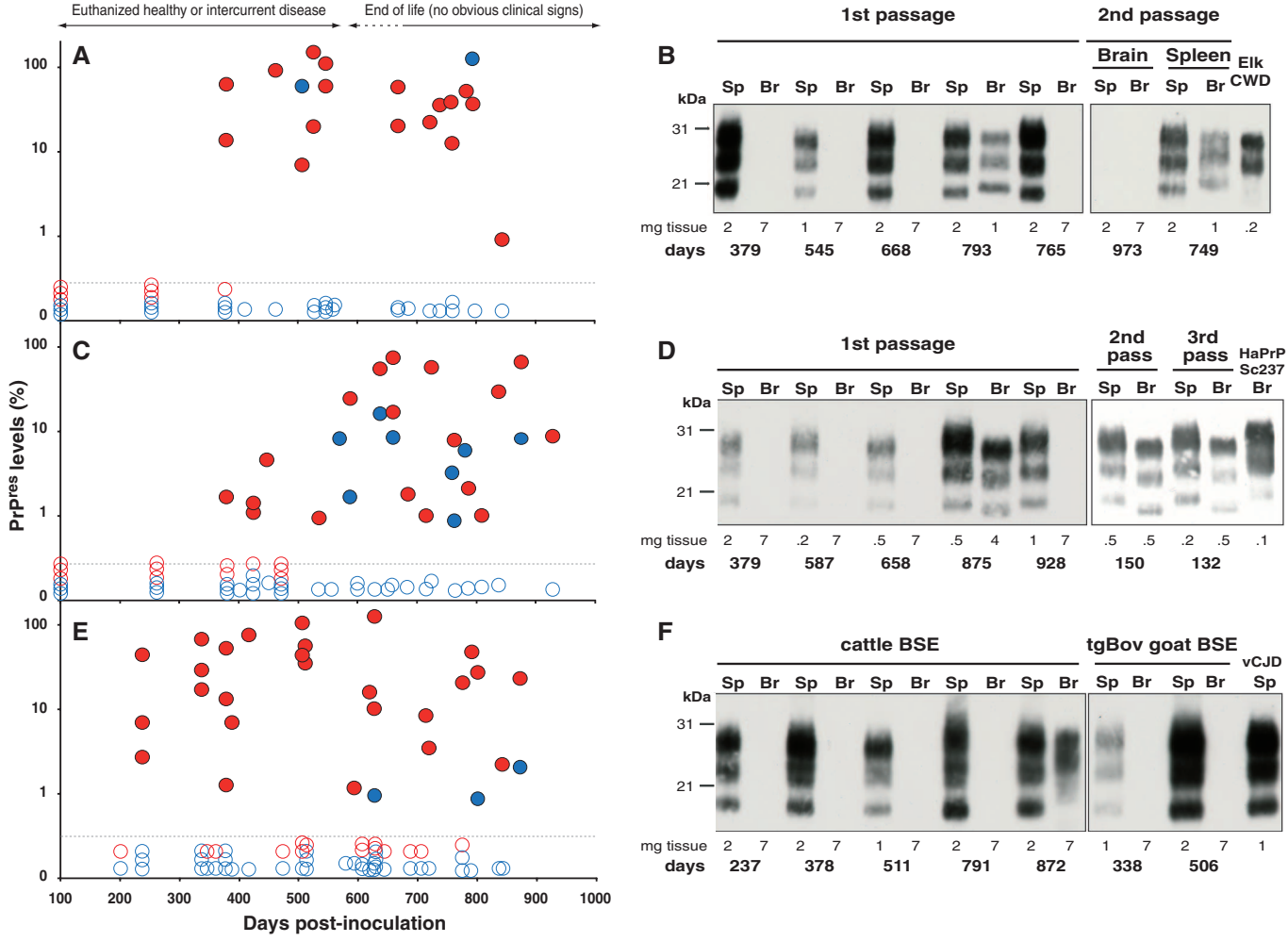


Fig. 1. Time course of PrP^{res} accumulation in the brain and spleen tissue of ovine and human PrP mice inoculated with CWD, Sc237, and BSE prions. PrP^{res} extracted from spleen (Sp, red) and brain (Br, blue) tissues was detected by immunoblot (**B**, **D**, **F**) and quantified (**A**, **C**, **E**) as a percentage of that found at maximum in the spleens (logarithmic scale). The positive threshold is indicated by the horizontal dotted line (*17*). Tissue samples in which no PrP^{res} was detected are symbolized by open circles. (A and B) Ovine PrP *tg338* mice inoculated with elk CWD prions. (A) Data resulting from two independent primary transmission experiments have been pooled (see Table 1 and fig. S2 for more detailed data). (B) Secondary passage was made using either brain or spleen homogenates (fig. S3), as indicated. (C and D) *tg338* mice inoculated with different infectious sources of closely related hamster (Ha) prions (Sc237 and 263K; see text) (see Table 1 and fig. S2 for more detailed data). (D) The second and third passages were made with brain homogenates from *tg338* mice inoculated with hamster Sc237 prions. (E and F) Human PrP *tg650* mice inoculated with various cattle BSE isolates or with BSE prions serially passaged in bovine PrP transgenic mice (tgBov) (see Table 1 and fig. S2 for more detailed results). (F) The electrophoretic pattern of variant CJD in *tg650* mouse spleen is shown for comparison. Variant CJD PrP^{res} levels in spleen would attain ~100% on (E) at terminal stage of disease.

Downloaded from www.sciencemag.org on January 27, 2012

detectable in the brains of healthy mice euthanized before that time point ($n = 24$) (Fig. 1E and fig. S2). PrP^{res}-negative brains appeared 250- to 1000-fold less infectious than PrP^{res}-positive brains (table S1). Out of 41 spleens analyzed, 26 were PrP^{res}-positive, the first as early as at 230 days postinfection (detection not assayed before) (Fig. 1, E and F). This provides a transmission barrier that is more than sevenfold leakier in the spleen than in the brain (Table 1). The spleen PrP^{res} electrophoretic signature was identical to that found after vCJD transmission to *tg650* mice (*12*), and most positive spleens had PrP^{res} levels that did not differ by more than threefold (Fig. 1, E and F). In contrast, vCJD inoculation led to accumulation of PrP^{res} in the brain of all infected mice (*12*). Thus, again these data argue for a markedly higher permissiveness of the spleen over the brain tissue to foreign prions.

Here, we have demonstrated that prion cross-species transmission efficacy can exhibit a dramatic tissue-dependence in the same host. In three distinct mouse models, lymphoid tissue appeared markedly more permissive than nervous tissue, despite an intracerebral infection route. This phenomenon was observed with both natural and experimental prions and did not seem to rely on a pronounced, preexisting lymphotropism. The PrP transgenic models used here faithfully reproduce the most relevant disease features in the natural host, including prion strain-dependant (in)ability to replicate in lymphoid tissue (*12*, *18*, *23*). Furthermore, the spleen-to-brain PrP^{C} level ratios

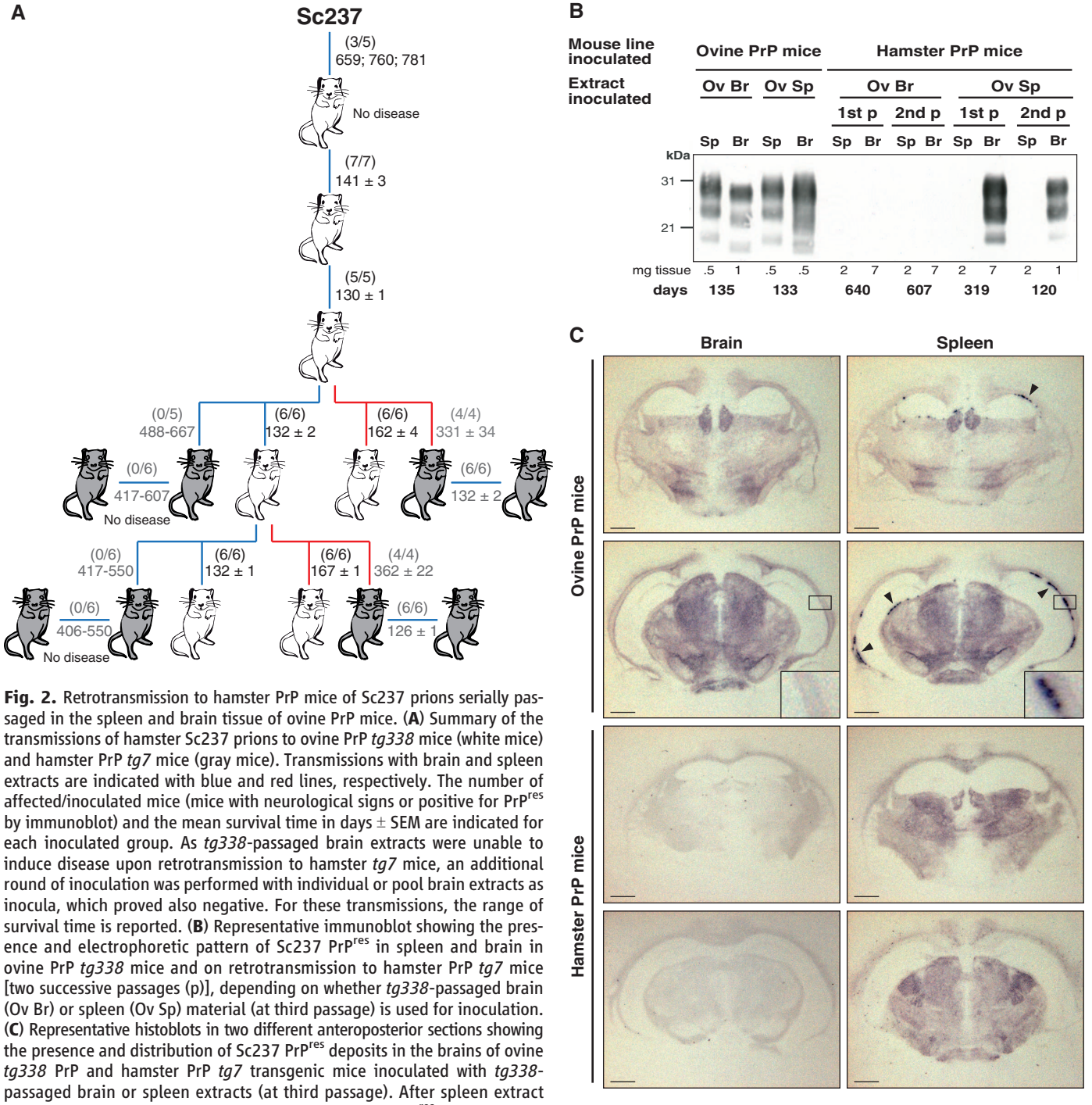


Fig. 2. Retrotransmission to hamster PrP mice of Sc237 prions serially passaged in the spleen and brain tissue of ovine PrP mice. (**A**) Summary of the transmissions of hamster Sc237 prions to ovine PrP *tg338* mice (white mice) and hamster PrP *tg7* mice (gray mice). Transmissions with brain and spleen extracts are indicated with blue and red lines, respectively. The number of affected/inoculated mice (mice with neurological signs or positive for PrP^{res} by immunoblot) and the mean survival time in days ± SEM are indicated for each inoculated group. As *tg338*-passaged brain extracts were unable to induce disease upon retrotransmission to hamster *tg7* mice, an additional round of inoculation was performed with individual or pool brain extracts as inocula, which proved also negative. For these transmissions, the range of survival time is reported. (**B**) Representative immunoblot showing the presence and electrophoretic pattern of Sc237 PrP^{res} in spleen and brain in ovine PrP *tg338* mice and on retrotransmission to hamster PrP *tg7* mice [two successive passages (p)], depending on whether *tg338*-passaged brain (Ov Br) or spleen (Ov Sp) material (at third passage) is used for inoculation. (**C**) Representative histoblots in two different anteroposterior sections showing the presence and distribution of Sc237 PrP^{res} deposits in the brains of ovine *tg338* PrP and hamster PrP *tg7* transgenic mice inoculated with *tg338*-passaged brain or spleen extracts (at third passage). After spleen extract inoculation, note the presence of numerous plaquelike PrP^{res} deposits in the *tg338* brain (arrowheads), particularly in the corpus callosum (inset squares). Scale bars, 1 mm.

Downloaded from www.sciencemag.org on January 27, 2012

(~1:20) in all of the transgenic lines used are comparable to that in conventional models (fig. S4A). The strongest PrP^C staining was associated with the follicular dendritic cells network (fig. S5), as documented in nontransgenic species (*16*, *26*). The PrP^C level in the spleen of the overexpressing lines stayed below its physiological level in the brain (fig. S4B). Thus, our findings are unlikely to be caused by an aberrant qualitative or quantitative expression of the PrP transgene in the spleen. Despite strong selective pressure, active prion replication in a nonneuronal tissue on minimal passage in a foreign host clearly constitutes a possible way to extend prion host range. This questions the long established notion of absolute species barriers (*27*). Chronic inflammation induces the formation of secondary lymphoid follicles, thus expanding extraneural prion replication to otherwise refractory organs (*28*). It has been proposed that prions could exist as quasi-species (*6*, *29*) and may thus be endowed with organ-specific subvariants, as observed repeatedly with viral pathogens (*30*, *31*). Alternatively, or in combination, tissue-specific host factors may differentially regulate prion replication dynamics under selection pressure. This could involve PrP^C itself, due to some isoform variation between the spleen and brain tissues, or ancillary factors that would create a more favorable environment, including, for instance, a prolonged residence of the incoming prions in lymphoid tissues.

Our data call for closer examination of extraneural PrP^{res} in humanized or primate models when assessing any zoonotic potential of animal prions. The human species barrier to BSE prions may be dramatically lower than previously anticipated, according to brain PrP^{res} detection only (*10*, *24*, *25*, *32*). Because the oral route is known to target lymphoid tissue, albeit less well than the intracerebral route used here (*15*), our data reinforce the legitimacy of the current investigations aimed at evaluating the proportion of silent carriers (*26*, *33*, *34*) in the BSE-exposed UK population (*35*). To provide a reliable assessment of people at risk and determining the probability of vCJD onward transmission via surgery or donated blood or organs, it may be necessary to pursue such screening policy on a long-term basis, because, as shown here, prions could persist silently for nearly a third of a host's life span before being detectable extraneurally by conventional diagnostic methods. Finally, including prion detection in the lymphoid tissue whenever possible might be considered for the surveillance of people exposed to CWD-infected tissue.

References and Notes

1. S. B. Prusiner, *Proc. Natl. Acad. Sci. U.S.A.* **95**, 13363 (1998).
2. J. Collinge, *Annu. Rev. Neurosci.* **24**, 519 (2001).
3. A. Aguzzi, M. Heikenwalder, M. Polymenidou, *Nat. Rev. Mol. Cell Biol.* **8**, 552 (2007).
4. G. C. Telling, *Methods Mol. Biol.* **459**, 249 (2008).
5. V. Béringue, J. L. Vilotte, H. Laude, *Vet. Res.* **39**, 47 (2008).
6. J. Collinge, A. R. Clarke, *Science* **318**, 930 (2007).
7. C. J. Gibbs Jr., D. C. Gajdusek, *Science* **182**, 67 (1973).
8. R. Nonno *et al.*, *PLoS Pathog.* **2**, e12 (2006).
9. J. D. F. Wadsworth *et al.*, *Science* **306**, 1793 (2004).
10. E. A. Asante *et al.*, *EMBO J.* **21**, 6358 (2002).
11. V. Béringue *et al.*, *J. Neurosci.* **27**, 6965 (2007).
12. V. Béringue *et al.*, *PLoS ONE* **3**, e1419 (2008).
13. R. Capobianco *et al.*, *PLoS Pathog.* **3**, e31 (2007).
14. M. R. Scott *et al.*, *J. Virol.* **71**, 9032 (1997).
15. R. H. Kimberlin, C. A. Walker, *Ciba Found. Symp.* **135**, 37 (1988).
16. K. L. Brown, G. J. Wathne, J. Sales, M. E. Bruce, N. A. Mabbott, *J. Immunol.* **183**, 5199 (2009).
17. Materials and methods are available as supporting material on *Science* Online.
18. A. Le Dur *et al.*, *Proc. Natl. Acad. Sci. U.S.A.* **102**, 16031 (2005).
19. G. Tamgüney *et al.*, *J. Virol.* **80**, 9104 (2006).
20. C. I. Lasmézas *et al.*, *Science* **275**, 402 (1997).
21. R. H. Kimberlin, C. A. Walker, *J. Gen. Virol.* **67**, 255 (1986).
22. P. Tixador *et al.*, *PLoS Pathog.* **6**, e1000859 (2010).
23. V. Béringue *et al.*, *PLoS Pathog.* **2**, e112 (2006).
24. V. Béringue *et al.*, *Emerg. Infect. Dis.* **14**, 1898 (2008).
25. D. Padilla *et al.*, *PLoS Pathog.* **7**, e1001319 (2011).
26. D. A. Hilton *et al.*, *J. Pathol.* **203**, 733 (2004).
27. A. F. Hill *et al.*, *Proc. Natl. Acad. Sci. U.S.A.* **97**, 10248 (2000).
28. M. Heikenwalder *et al.*, *Science* **307**, 1107 (2005).
29. J. Li, S. Browning, S. P. Mahal, A. M. Oelschlegel, C. Weissmann, *Science* **327**, 869 (2010).
30. L. G. Epstein *et al.*, *Virology* **180**, 583 (1991).
31. R. Ahmed, M. B. Oldstone, *J. Exp. Med.* **167**, 1719 (1988).
32. M. T. Bishop *et al.*, *Lancet Neurol.* **5**, 393 (2006).
33. J. P. Clewley *et al.*, *BMJ* **338**, b1442 (2009).
34. A. Frosh *et al.*, *Lancet* **364**, 1260 (2004).
35. A. C. Ghani, C. A. Donnelly, N. M. Ferguson, R. M. Anderson, *C. R. Biol.* **325**, 37 (2002).

Acknowledgments: We thank the animal facility staff (Infectiologie Expérimentale Rongeurs Poissons, Jouy-en-Josas, France) for excellent animal care; S. Mouillet-Richard, O. Andréoletti, and H. Rezaei for critical reading of the manuscript; R. Young (INRA-Jouy, France) and M. Farrow (University College London, UK) for English style editing; A. Gröner (Commonwealth Serum Laboratories Behring, Marburg, Germany) for *tg7* mice; and C. Laude for mouse drawings in graphics. This work was partly supported by the Alliance Biosecure Foundation and INRA-Transfert.

Supporting Online Material

www.sciencemag.org/cgi/content/full/335/6067/472/DC1
Materials and Methods
Figs. S1 to S5
Table 1
References (*36*–*42*)

24 October 2011; accepted 30 November 2011
10.1126/science.1215659

Asymmetric Segregation of Polarized Antigen on B Cell Division Shapes Presentation Capacity

Olivier Thaunat,[1] Aitor G. Granja,[1] Patricia Barral,[1] Andrew Filby,[2] Beatriz Montaner,[1] Lucy Collinson,[3] Nuria Martinez-Martin,[1] Naomi E. Harwood,[1] Andreas Bruckbauer,[1] Facundo D. Batista[1]*

During the activation of humoral immune responses, B cells acquire antigen for subsequent presentation to cognate T cells. Here we show that after mouse B cells accumulate antigen, it is maintained in a polarized distribution for extended periods in vivo. Using high-throughput imaging flow cytometry, we observed that this polarization is preserved during B cell division, promoting asymmetric antigen segregation among progeny. Antigen inheritance correlates with the ability of progeny to activate T cells: Daughter cells receiving larger antigen stores exhibit a prolonged capacity to present antigen, which renders them more effective in competing for T cell help. The generation of progeny with differential capacities for antigen presentation may have implications for somatic hypermutation and class switching during affinity maturation and as B cells commit to effector cell fates.

The recognition of antigen through the B cell receptor (BCR) triggers B cell proliferation and differentiation that results in the formation of plasma cells capable of antibody production and long-lasting memory cells (*1*). The majority of B cell activation is initiated by antigen on the surface of presenting cells, including follicular dendritic cells [FDCs (*2*)], dendritic cells (*3*), and macrophages (*4*–*6*). The binding of cognate antigen to the BCR initiates intracellular signaling [reviewed in (*7*–*9*)], resulting in antigen extraction from the cell surface (*10*). BCR-driven uptake targets antigen to intracellular endosomal compartments containing major histocompatibility complex [MHC (*11*)], which allows for presentation to cognate T cells that go on to promote maximal B cell activation (*12*, *13*). During the course of a typical humoral immune response, B cells present antigen to T cells in two distinct situations within secondary lymphoid tissues: at the B-T cell border after initial antigen acquisition (*14*, *15*) and within the germinal center (GC) to

[1]Lymphocyte Interaction Laboratory, London Research Institute, Cancer Research UK, 44 Lincoln's Inn Fields, London WC2A 3LY, UK. [2]Flow Cytometry Laboratory, London Research Institute, Cancer Research UK, 44 Lincoln's Inn Fields, London WC2A 3LY, UK. [3]Electron Microscopy Laboratory, London Research Institute, Cancer Research UK, 44 Lincoln's Inn Fields, London WC2A 3LY, UK.

*To whom correspondence should be addressed. E-mail: facundo.batista@cancer.org.uk

Downloaded from www.sciencemag.org on January 27, 2012

generate affinity-matured antibodies (*16*–*19*). The importance of B cell antigen presentation to T cells is highlighted by the observation that disruptions of B-T conjugate stability result in a profound defect in GC formation and humoral immunity (*20*, *21*) and has been associated with X-linked lymphoproliferative disease in humans (*22*).

After BCR-mediated acquisition in vivo, B cells initially concentrate internalized antigen in a single cargo at the uropod as they migrate to search for cognate T cells (*4*). This observation raises the question of whether this polarized distribution of antigen is maintained over time and during subsequent B cell division. To address this question, we used intensely labeled fluorescent particulates equivalent in diameter to a typical pathogen and coated with hen egg lysozyme (HEL; bHEL, beads with HEL conjugated HEL) to monitor antigen over extended periods of time. Transgenic MD4 B cells that express HEL-specific BCR were labeled with the vital dye SNARF-1 and adoptively transferred into C57BL/6 wild-type (WT) mice 1 day before immunization with

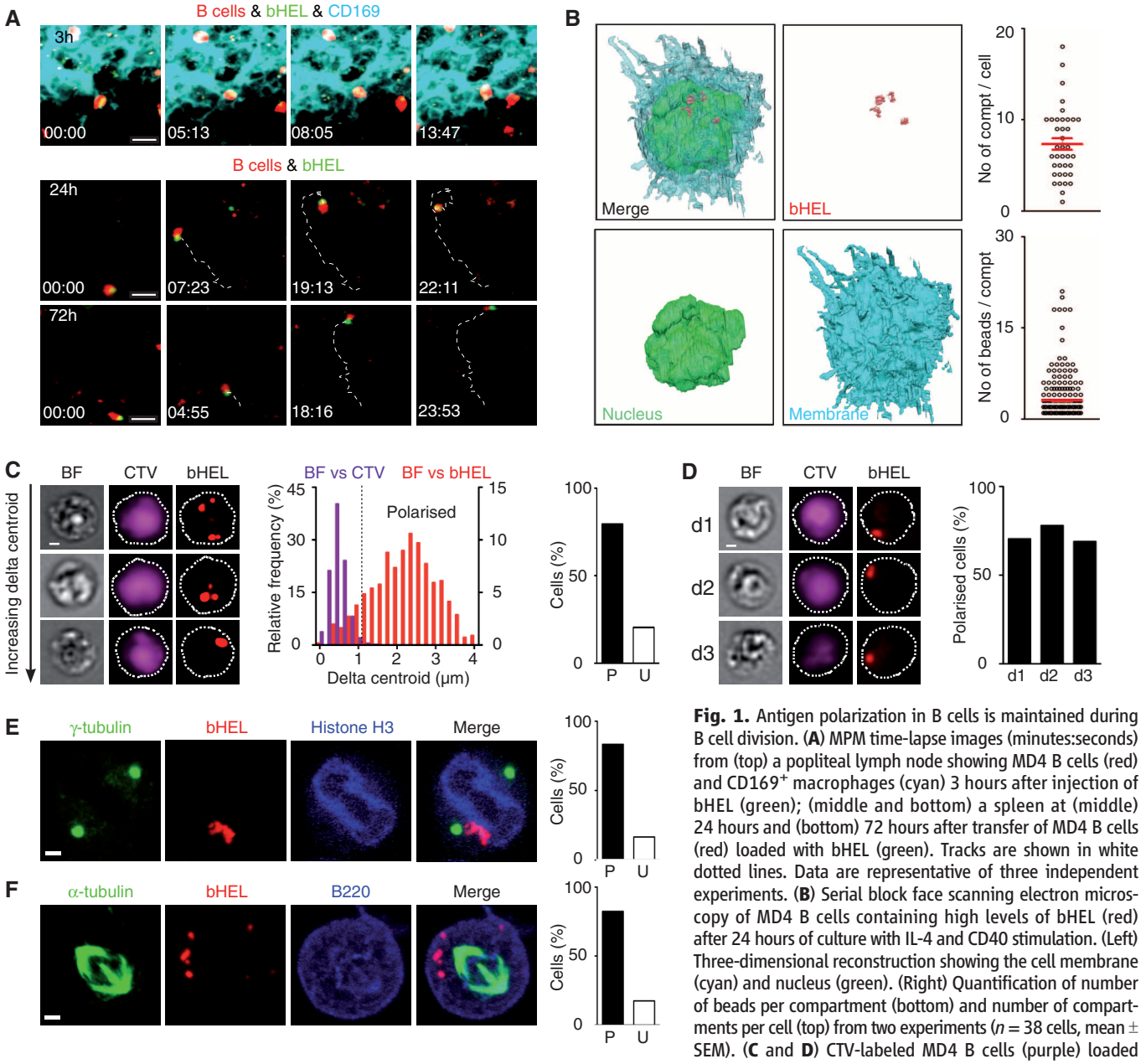


Fig. 1. Antigen polarization in B cells is maintained during B cell division. (**A**) MPM time-lapse images (minutes:seconds) from (top) a popliteal lymph node showing MD4 B cells (red) and CD169$^+$ macrophages (cyan) 3 hours after injection of bHEL (green); (middle and bottom) a spleen at (middle) 24 hours and (bottom) 72 hours after transfer of MD4 B cells (red) loaded with bHEL (green). Tracks are shown in white dotted lines. Data are representative of three independent experiments. (**B**) Serial block face scanning electron microscopy of MD4 B cells containing high levels of bHEL (red) after 24 hours of culture with IL-4 and CD40 stimulation. (Left) Three-dimensional reconstruction showing the cell membrane (cyan) and nucleus (green). (Right) Quantification of number of beads per compartment (bottom) and number of compartments per cell (top) from two experiments ($n = 38$ cells, mean ± SEM). (**C** and **D**) CTV-labeled MD4 B cells (purple) loaded with bHEL (red) analyzed by IS after 72 hours of culture with IL-4 and CD40 stimulation. Polarization is quantified by comparing the centroid positions of the bright-field (BF) images and the particular fluorescent species in two independent experiments (P, polarized; U, unpolarized). (C) Undivided B cells. (Left) Descending images show B cells with increased antigen polarization. (Middle) Distribution of delta centroid values of the bright-field images compared with CTV fluorescence (purple) or bHEL (red). (Right) Quantification of antigen polarization ($n = 557$ cells). (D) Divided B cells. (Left) Descending images show B cells after successive rounds of division (d) and (right) quantification of antigen polarization [division 1 (d1), $n = 3087$; d2, $n = 3792$; d3, $n = 898$]. (**E**) MD4 B cells pre-loaded with bHEL (red) cultured for 48 hours with IL-4 and CD40 stimulation, stained with anti-histone H3 (blue) and γ-tubulin [microtubulin-organizing center (MTOC); green]. (Left) Confocal images. (Right) Quantification of antigen polarization in metaphasic B cells (two MTOCs, $n = 17$ cells) from two independent experiments. (**F**) MD4 B cells loaded with bHEL (red) cultured for 44 hours and treated for 4 hours with cytochalasin B stained with α-tubulin (green) and B220 (B cell membrane; blue). (Left) Confocal images. (Right) Quantification of antigen polarization ($n = 35$ cells) from two independent experiments. Scale bars in (A), 30 μm; in (C) and (D), 2 μm; in (E) and (F), 1 μm.

Downloaded from www.sciencemag.org on January 27, 2012

bHEL. Using multiphoton microscopy (MPM) of explanted lymph nodes, we observed that MD4 B cells acquired antigen in a polarized fashion from CD169$^+$ macrophages (Fig. 1A and movie S1) and maintained this polarization at the uropod as they detached from the subcapsular sinus (fig. S1A and movie S2). Similarly, even up to 3 days after acquisition, the polarized distribution of antigen was maintained in migratory B cells that were pre-loaded with bHEL before being transferred to a WT host (to minimize continued antigen exposure) and visualized in the spleen (Fig. 1A). Moreover, we observed that antigen contained in a small number of endosomal compartments was also distributed toward one pole in B cells pre-incubated with bHEL and cultured with CD40 stimulation and interleukin-4 (IL-4), signals that B cells normally receive by interacting with T cells (Fig. 1B; fig. S1, B to E; and movie S3). Thus, the establishment and preservation of antigen polarity do not appear to require interactions with other cells.

To examine what happens to the polarized distribution of antigen as the B cell undergoes division, we have developed a strategy using an imaging flow cytometer [ImageStream (IS)] to simultaneously visualize the distribution of bHEL antigen and division in B cells (*23*) (fig. S2A). In line with our in vivo observations (Fig. 1A), although some cells contain bHEL that is not polarized, around 75% of undivided cells exhibit a polarized distribution of antigen after 3 days in culture with CD40 stimulation and IL-4 (Fig. 1C). After polarization was established, the distribution of antigen was not altered after treatment with nocodazole, suggesting that the microtubule network is not important for maintaining antigen polarization (fig. S2B). We observed that a similar polarization of bHEL was preserved in cells that had undergone up to three rounds of division (Fig. 1D and fig. S2C). Independent of cell division, the fluorescence corresponding to the bead itself or to the HEL antigen was colocalized, establishing that the bHEL fluorescence represents an accurate readout for the presence of antigen (fig. S2D). These findings indicate that B cells maintain a polarized distribution of antigen even after B cell division.

Because the IS system allows the separation of cells on the basis of multiple parameters, we took advantage of this strategy to investigate

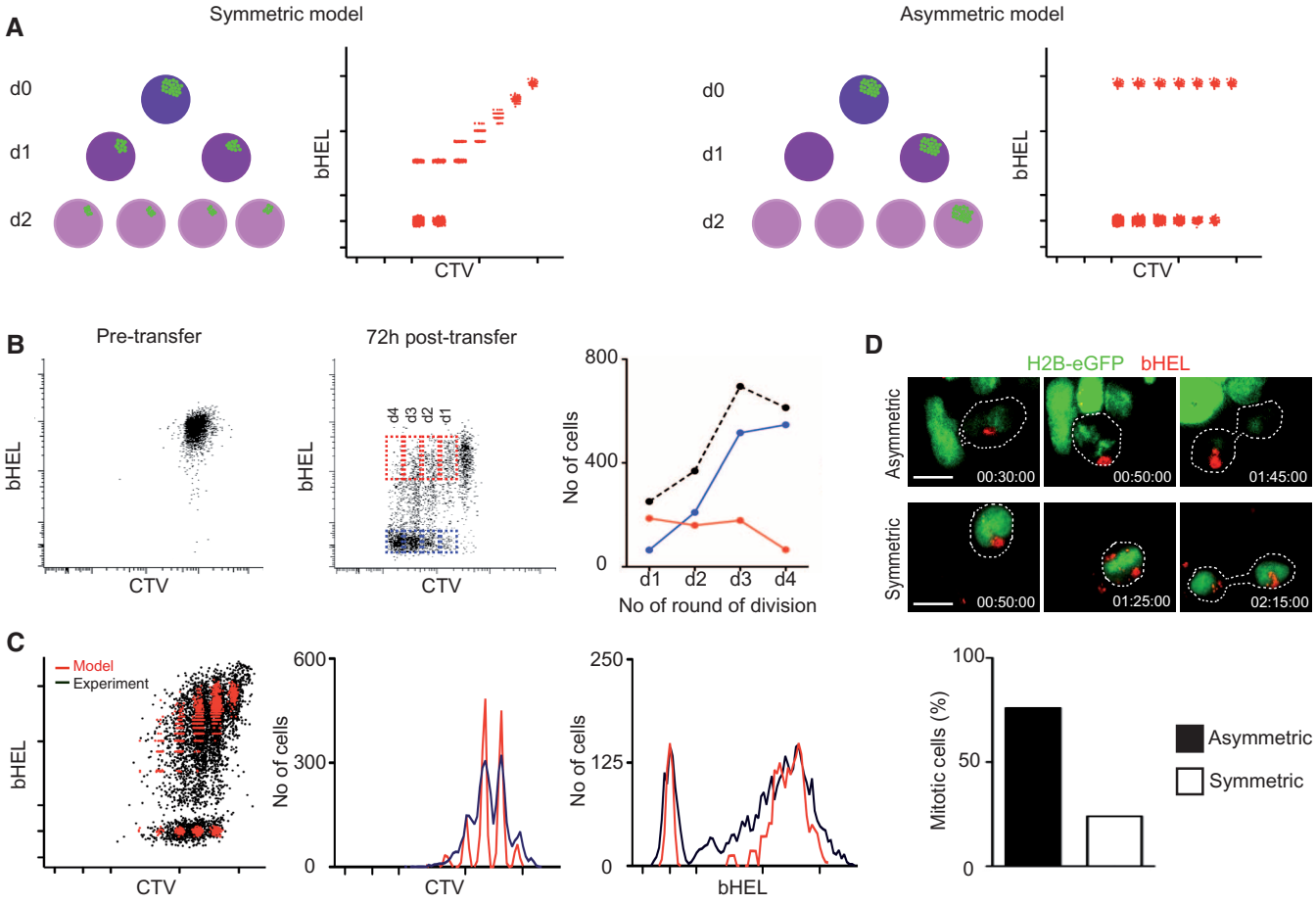


Fig. 2. Antigen can be asymmetrically segregated on B cell division. (**A**) Schematic and fluorescence dot plots for in silico models examining the an-tigen (bHEL) content of dividing B cells relative to an equally divided cell marker such as CTV. (**B**) CTV-labeled CD45.2 MD4 B cells loaded with high levels of green fluorescent bHEL-OVA were (left) sorted before co-transfer with CD4$^+$ OT-II T cells into CD45.1 recipient mice. (Middle) Flow cytometry profile of CTV and bHEL fluorescence of CD45.2 splenic B cells 3 days after transfer. B cells containing high (red) and low (blue) levels of bHEL after successive rounds of division (d1, d2, …) are marked. (Right) Quantification of the total number (black), bHEL-high (red), and bHEL-low (blue) B cells at each round of division. Data are representative of two independent experiments. (**C**) In silico mixed model assuming that 25% of B cells undergo fully asymmetric division, while the remaining cells undergo fully symmetric division. (Left) Fluorescence dot plot generated for the mixed model as compared with the experimental data. Comparison of (middle) CTV and (right) bHEL fluorescence predicted in the mixed model versus collected data in the right panel of fig. S6A. (**D**) A20 B cells expressing HEL-specific D1.3 BCR and histone H2B (H2B)–enhanced green fluorescent protein (eGFP) (green) were loaded with flash red fluorescent bHEL (red) and imaged by low-light microscopy. (Top and middle) Images of B cells at indicated times (hours:minutes:seconds) undergoing (top) asymmetric and (bottom) symmetric segregation of bHEL as they divide. Dashed white lines in the images represent the cell boundary. Scale bars, 10 μm. (Bottom) Quantification of B cells that undergo asymmetric and symmetric division in 21 mitosis events, during four independent experiments.

Downloaded from www.sciencemag.org on January 27, 2012

antigen polarization in B cells as they progressed through mitosis (fig. S3A). We observed that B cells maintain a polarized distribution of accumulated bHEL, but not the ancestral polarity network member protein kinase C–ζ or cell surface proteins such as CD86 and MHCII, as they enter prophase and as they progress through metaphase and anaphase (figs. S3, B to D, and S4, A to D). To verify these findings at high resolution, we visualized the antigen distribution in dividing B cells that were pre-loaded with bHEL, using confocal imaging. In line with the IS data, we observed that antigen was indeed polarized in the majority of B cells, both as they entered mitosis (Fig. 1E and fig. S5A) and if they were trapped in metaphase by incubation with cytochalasin B before fixation (Fig. 1F and fig. S5, B and C). Thus it appears that B cells maintain antigen in a polarized distribution both over time and during division.

The observed polarization raises the possibility that B cell division results in asymmetric antigen segregation and the generation of progeny with unequal antigen inheritance. To investigate this possibility, we constructed two absolute in silico models to predict the impact of cell division on antigen distribution, considering a population initially containing high levels of antigen (*23*) and labeled with a division marker that is equally segregated on division. The first model assumes that antigen is segregated symmetrically on division, giving rise to a linear plot in which the intensities of antigen and division marker are directly correlated (Fig. 2A). On the other hand, the second model assumes that antigen is always segregated asymmetrically, so that one daughter receives all of the accumulated antigen while the other receives none (Fig. 2A). Although the first model predicts that five rounds of division are required to generate cells lacking antigen, that population emerges after one division in the asymmetric model (Fig. 2A). Moreover, the latter model is also characterized by a population retaining high levels of antigen even at later rounds of division. But which of these two division profiles most accurately recapitulates the features of antigen segregation during B cell division in vivo?

To address this question experimentally, a homogeneous population of B cells sorted to contain high levels of both the cell division marker, CellTracker Violet (CTV), and of antigen was transferred into recipient mice; in this case, the antigen also contained ovalbumin (OVA; bHEL-OVA) to allow B cells to receive necessary help for proliferation from cotransferred OVA-specific OT-II T cell receptor transgenic T cells. After 3 days, B cells had undergone up to four rounds of division, and we observed two characteristic features of the asymmetric model: the rapid emergence of a substantial population containing

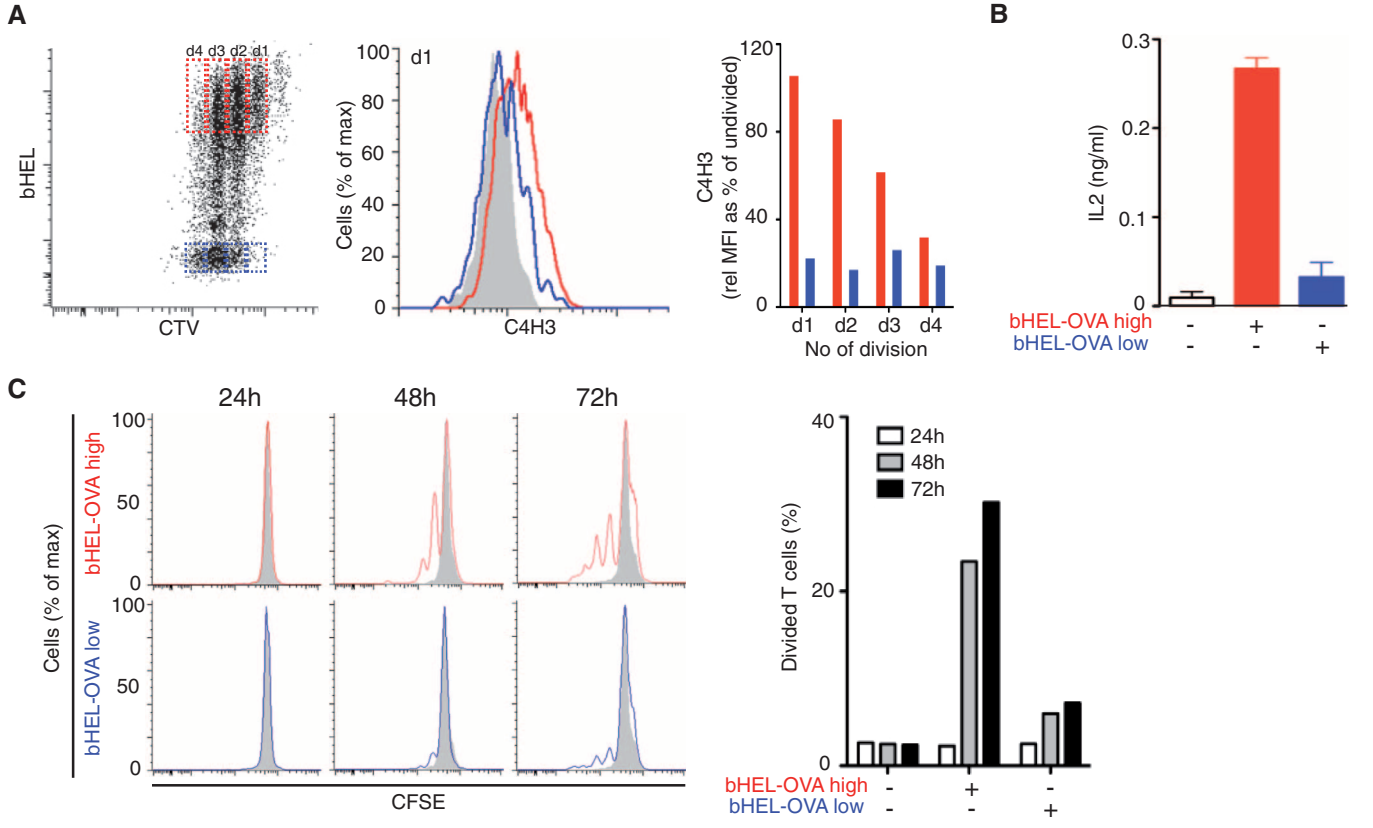


Fig. 3. The amount of antigen stored determines the capacity for B cell presentation to activate cognate T cells. (**A**) CTV-labeled B cells from MD4xB10.BR F_1 mice were loaded with green fluorescent bHEL and cultured with IL-4 and CD40 stimulation for 3 days. B cells containing high (red) and low (blue) levels of bHEL after successive rounds of division (d1, d2, …) are marked. Surface staining for HEL-loaded IA^k complexes using C4H3 antibody is shown. (Left) Flow cytometry profile. (Middle) Staining in B cells from bHEL-high (red) and bHEL-low (blue) B cells from the d1 population. Nonspecific staining was measured after loading of MD4 B cells with microspheres coated with antibody to IgM and is shown in solid gray profile. (Right) Quantification of relative staining across successive rounds of division compared with undivided B cells and corrected for the extent of MHC II expression at each round. Data are representative of three independent experiments. (**B** and **C**) CTV-labeled HyHEL-10 B cells containing high levels (green) of bHEL-OVA were sorted and cultured in medium supplemented with (B) IL-4 and CD40 stimulation or (C) $CD4^+$ OT-II T cells. (B) HyHEL10 B cells were cultured for 3 days before sorting according to levels of bHEL-OVA (high and low) and were cultured for a further day with OVA-specific $CD4^+$ OT-II T cells. IL-2 secretion as a readout of antigen presentation was measured by enzyme-linked immunosorbent assay. Means ± SEM are shown. Data are representative of two independent experiments. (C) CTV-labeled MD4 B cells after 3 days in culture were sorted according to levels of bHEL-OVA (high, red; low, blue). 10^5 divided and sorted B cells were cultured for a further 3 days with carboxyfluorescein diacetate succinimidyl ester (CFSE)–labeled $CD4^+$ OT-II T cells, and T cell proliferation was (left) measured by flow cytometry and (right) quantified at the indicated times. Data are representative of three independent experiments.

Downloaded from www.sciencemag.org on January 27, 2012

no bHEL-OVA and the maintenance of B cells retaining high levels of antigen after several rounds of division (Fig. 2B). However, although CTV was symmetrically divided between progeny, the distribution of antigen did not fully recapitulate either of our in silico models. The asymmetric segregation of antigen appears to be intrinsic to dividing B cells, because similar profiles were obtained for B cells cocultured with OT-II T cells, CD40 stimulation, and IL-4 or lipopolysaccharide for 3 days (fig. S6A).

Our data strongly suggest that although B cell division can occur symmetrically, it often results in the asymmetric segregation of polarized antigen. We tested this hypothesis by comparing our experimental observations (fig. S6A) with a third, combined model, merging the previous two models (Fig. 2C) and incorporating parameters from our in vitro data (*23*) (fig. S6B). We found that to recapitulate the predominant features of antigen segregation in vitro, it was necessary to include at least 25% fully asymmetric division in the combined model (Fig. 2C). In line with this third model, we observed that a population of dividing A20 B cells was capable of segregating loaded bHEL antigen both asymmetrically and symmetrically between daughter B cells (Fig. 2D; movies S4 and S5; and fig. S6, C and D). Because the combined model assumes that the segregation of antigen between daughter cells is either fully symmetric or fully asymmetric, this probably represents an underestimate of the contribution of asymmetric B cell division both in vitro and in vivo. Taken together, our theoretical and experimental approaches establish that the asymmetric segregation of antigen occurs on B cell division.

We moved on to explore the functional significance that the differential stores of antigen confer on progeny. Because BCR-mediated internalization delivers antigen into compartments containing MHC molecules (fig. S7A), we examined the influence that the retention of antigen has on the capacity to present antigen to cognate T cells. B cells containing high levels of bHEL were cultured with CD40 stimulation and IL-4 for 3 days, and the extent of antigen presentation on the surface was detected by staining with C4H3 antibody (*24*). We observed that the amount of HEL-loaded MHC was consistently higher for B cells that contained more bHEL (Fig. 3A), although the extent of antigen presentation decreased on progression through cell division. Moreover, the size of the intracellular antigen store was related to the level of bHEL and to progress through division in a similar manner (fig. S7B). As such, the amount of antigen retained in the cell is indeed related to the capacity to present antigenic peptide in complex with MHC on the B cell surface. To examine the corresponding impact on T cell activation, the extent of IL-2 secretion and proliferation of cocultured T cells was measured. We observed that the amount of bHEL-OVA retained by B cells was related to the extent of IL-2 secretion by cocultured OT-II cells (Fig. 3B). Moreover, the ability of B lymphoma cells expressing HEL-specific D1.3 BCR (*25*) to present antigen to HEL-specific 2G7 T cells was also directly related to the amount of antigen internalized (fig. S8A). In a similar manner, the quantity of antigen stored in B cells was related to the extent of T cell proliferation induced: Whereas B cells containing high levels of bHEL-OVA stimulated almost 60% of T cells to divide, proliferation was severely impaired in T cells cocultured with B cells containing low levels of bHEL-OVA (fig. S8B).

Finally, we wanted to establish that B cells containing differential amounts of stored antigen as a result of asymmetric segregation were capable of inducing T cell activation to different extents. Indeed, whereas B cells containing high levels of bHEL-OVA triggered considerable proliferation in OT-II T cells after 2 days, this was dramatically diminished when low levels of antigenic beads were present in the B cells (Fig. 3C). Although viability issues prevent the monitoring of B cell activation markers directly, before coculture with OT-II cells, the two B cell populations did not express significantly different levels of activation markers, surface MHC, or costimulatory molecules (fig. S9). Thus, the difference in T cell proliferation observed appears to be directly due to the level of antigenic peptide displayed on the B cell surface, and the differential levels of antigen generated by asymmetric segregation directly influence the ability of B cells to induce functional responses in cognate T cells.

Our observation of asymmetry is both interesting and surprising, although perhaps on reflection not unexpected, considering that the partitioning of the endosomal compartment during mitosis occurs in a stochastic manner (*26*). However, because BCR stimulation is associated with the fusion of endosomal vesicles (*27*) and formation of a large autophagosome-like compartment (*28*), we postulate that internalization by this route promotes asymmetric antigen segregation on B cell division. In contrast to the unequal division of proteins in T cells (*29*), the asymmetric segregation of antigen in B cells does not appear to depend on prolonged contact with antigen-presenting cells and the associated formation of the immunological synapse. But what is the functional significance of this asymmetric antigen segregation? We postulate that daughter B cells receiving high amounts of antigen might allow for more effective competition for limited T cell help both at the B-T cell border (*14*, *15*) and in the GC (*30*), facilitating somatic hypermutation and class switch. Asymmetric cell division also allows progeny to be cleansed of accumulated protein (*31*), rapidly generating antigen-negative B cells with a diminished capacity to present antigen. The survival of these cells depends on further accumulation of antigen, allowing "proofreading" of newly mutated BCR and the retention of B cells with higher-affinity BCR for further selection during affinity maturation. Thus, the unequal partitioning of polarized antigen after division generates distinct B cell populations that either retain or rapidly eliminate antigen that together may be critical for the effective induction of humoral immune responses and the production of high-affinity antibodies.

References and Notes

1. K. Rajewsky, *Nature* **381**, 751 (1996).
2. K. Suzuki, I. Grigorova, T. G. Phan, L. M. Kelly, J. G. Cyster, *J. Exp. Med.* **206**, 1485 (2009).
3. H. Qi, J. G. Egen, A. Y. Huang, R. N. Germain, *Science* **312**, 1672 (2006).
4. Y. R. Carrasco, F. D. Batista, *Immunity* **27**, 160 (2007).
5. T. Junt *et al.*, *Nature* **450**, 110 (2007).
6. T. G. Phan, I. Grigorova, T. Okada, J. G. Cyster, *Nat. Immunol.* **8**, 992 (2007).
7. J. M. Dal Porto *et al.*, *Mol. Immunol.* **41**, 599 (2004).
8. A. L. DeFranco, *Curr. Opin. Immunol.* **9**, 296 (1997).
9. T. Kurosaki, *Annu. Rev. Immunol.* **17**, 555 (1999).
10. F. D. Batista, M. S. Neuberger, *EMBO J.* **19**, 513 (2000).
11. S. Amigorena, J. R. Drake, P. Webster, I. Mellman, *Nature* **369**, 113 (1994).
12. A. Lanzavecchia, *Nature* **314**, 537 (1985).
13. K. L. Rock, B. Benacerraf, A. K. Abbas, *J. Exp. Med.* **160**, 1102 (1984).
14. P. Garside *et al.*, *Science* **281**, 96 (1998).
15. T. Okada *et al.*, *PLoS Biol.* **3**, e150 (2005).
16. C. D. Allen, T. Okada, H. L. Tang, J. G. Cyster, *Science* **315**, 528 (2007).
17. A. E. Hauser *et al.*, *Immunity* **26**, 655 (2007).
18. T. A. Schwickert *et al.*, *Nature* **446**, 83 (2007).
19. G. D. Victora *et al.*, *Cell* **143**, 592 (2010).
20. J. L. Cannons *et al.*, *Immunity* **32**, 253 (2010).
21. H. Qi, J. L. Cannons, F. Klauschen, P. L. Schwartzberg, R. N. Germain, *Nature* **455**, 764 (2008).
22. S. Crotty, E. N. Kersh, J. Cannons, P. L. Schwartzberg, R. Ahmed, *Nature* **421**, 282 (2003).
23. Materials and methods are available as supporting material on *Science* Online.
24. G. Zhong, C. Reis e Sousa, R. N. Germain, *Proc. Natl. Acad. Sci. U.S.A.* **94**, 13856 (1997).
25. F. D. Batista, M. S. Neuberger, *Immunity* **8**, 751 (1998).
26. T. Bergeland, J. Widerberg, O. Bakke, T. W. Nordeng, *Curr. Biol.* **11**, 644 (2001).
27. K. Siemasko, B. J. Eisfelder, E. Williamson, S. Kabak, M. R. Clark, *J. Immunol.* **160**, 5203 (1998).
28. A. Chaturvedi, D. Dorward, S. K. Pierce, *Immunity* **28**, 799 (2008).
29. J. T. Chang *et al.*, *Science* **315**, 1687 (2007).
30. I. C. MacLennan, *Annu. Rev. Immunol.* **12**, 117 (1994).
31. A. Singhvi, G. Garriga, *Trends Cell Biol.* **19**, 1 (2009).

Acknowledgments: We thank D. Davies, Biomedical Research Council, Guy's and St Thomas' National Health Service Foundation Trust, and King's College London for assistance with flow cytometry and H. Armer for technical assistance with electron microscopy. We also thank the members of the Lymphocyte Interaction Laboratory for critical reading of the manuscript. This work was funded by Cancer Research UK. F.D.B. also receives support from the Royal Society Wolfson Merit Award, and O.T. receives financial support from Société Française de Transplantation, Société Française de Nephrologie, and Fondation pour la Recherche Medicale. The authors declare that they have no competing financial interests.

Supporting Online Material

www.sciencemag.org/cgi/content/full/335/6067/475/DC1
Materials and Methods
Figs. S1 to S9
References (*32*–*43*)
Movies S1 to S5

16 September 2011; accepted 14 December 2011
10.1126/science.1214100

Downloaded from www.sciencemag.org on January 27, 2012

New Products

LIQUID CHROMATOGRAPHY DETECTOR

Sapphire is a universally compatible, four-channel liquid chromatography detector. Sapphire features a revolutionary sapphire and quartz composite variable path-length flow cell, which allows concurrent measurement of ultraviolet (UV) absorption at 250 and 280 nm, refractive index, and conductivity. Sapphire's innovative design allows an unprecedented 0.001–100 A.U. UV detection range when normalized to a 10 mm path length. Deep UV LED light sources eliminate warm-up associated with traditional lamps and extend lifetime. Data is visualized in real-time on a four color integrated color monitor, and is USB-exportable. Sapphire is designed for purification of proteins and other biological materials as well as for FLASH chromatography.

Reach Devices
For info: 720-979-8940 | www.reachdevices.com



REAL-TIME PCR DETECTION SYSTEM

The CFX Connect real-time polymerase chain reaction (PCR) detection system is an ideal tool for researchers looking for reliable, high performance real-time PCR on a limited budget. The CFX Connect system, which requires a computer for operation, offers the same thermal performance as the CFX96 Touch real-time PCR system. It uses a similar scanning optics shuttle design that reads each well individually with high sensitivity and no cross talk to deliver optimal quantitative results. The CFX Connect detects two fluorophores per well in duplex experiments and detects SYBR Green or EvaGreen in singleplex experiments. Additional key benefits are effortless optimization that saves time and reduces costs by optimizing assays in a single run using the thermal gradient, and accurate data analysis with CFX Manager Software that offers an intuitive user interface and the ability to quickly and accurately validate and analyze data.

Bio-Rad
For info: 800-424-6723 | www.bio-rad.com

MAGNETIC BEADS

MagSi-proteomics beads are magnetic beads that are an ideal tool for the purification, concentration, and desalting of peptides and protein digests. The surface of the beads has been modified with C4-, C8-, and C18-alkyl groups that are optimized for reversed phase applications. Magnetic beads offer a convenient solid support for a variety of assays and procedures based on affinity purification. They are especially well suited for automated procedures because instrumentation is available to easily mix, incubate, and separate the magnetic beads in 96-well plates without columns or centrifugation. Offering higher throughput and cost efficiency compared to tip-based separations, MagSi proteomics beads efficiently bind and elute even tiny sample fractions. The high magnetic strength of MagSi beads makes them applicable for both manual and automated/robotic fractionation, because the beads will typically collect in less than one minute when magnetic force is applied.

AMS Biotechnology
For info: +44-(0)-1235-828200 | www.amsbio.com

GLYCOPROTEINS COUPLING REAGENTS

The new GlycoLink Immobilization and Immunoprecipitation (IP) Kits are designed for protein affinity purification and the study of protein interactions. The GlycoLink Immobilization and IP Kits provide the reagents for coupling glycosylated biological molecules to a beaded resin. The kits contain the Thermo Scientific UltraLink Hydrazide Resin and a reaction catalyst for a fast and efficient method to immobilize carbohydrates and glycoproteins such as antibodies onto a durable polyacrylamide resin. The catalyzed reaction results in greater than 90% coupling in four hours or less, depending on the amount of glycosylation. It also leaves other critical active sites on the molecule such as amines, carboxyls, and sulfhydryls free for other experimental purposes. Several kit configurations are available and contain the complete set of buffers, oxidizing reagent, and resin. The GlycoLink Coupling Catalyst is also available separately.

Thermo Fisher Scientific
For info: 800-874-3723 | www.thermoscientific.com/pierce

DUAL-LINE LIGHT ENGINE

The Cobolt Dual Combiner is a modulated dual-line light engine that is optimized for high-end optogenetics research applications. This version of the Cobolt Dual Combiner offers two attractive emission wavelengths for light-activated proteins: 473 nm (up to 50 mW) + 594 nm (up to 100 mW) from one small box. Through the integrating of a silent SRS shutter, the output beam can be modulated at up to 100 Hz with a very short rise time of <350 µs and with maintained 3% power stability and an RMS noise of <0.3%. Each line can be individually addressed through a software application provided with the lasers, or through RS232/USB communication. The modulated Cobolt Dual Combiner is perfectly suited for optogenetics applications where high level of power stability and control of the delivered energies are required. The modulated Dual Combiner is also available with any other two-line combination of the Cobolt 04-01 series lasers.

Cobolt
For info: +46-8-545-912-30 | www.cobolt.se

Electronically submit your new product description or product literature information! Go to **www.sciencemag.org/products/newproducts.dtl** for more information.

Newly offered instrumentation, apparatus, and laboratory materials of interest to researchers in all disciplines in academic, industrial, and governmental organizations are featured in this space. Emphasis is given to purpose, chief characteristics, and availability of products and materials. Endorsement by *Science* or AAAS of any products or materials mentioned is not implied. Additional information may be obtained from the manufacturer or supplier.

Downloaded from www.sciencemag.org on January 27, 2012

Detection of Apoptosis on the BD FACSVerse™ System

A streamlined approach to application support.



What's Really Exciting Is What's Behind it.

The BD Annexin V FITC assay shown illustrates the detection of camptothecin-induced apoptosis in Jurkat cells using the BD Pharmingen™ Annexin V FITC Apoptosis Detection Kit.

Representative Annexin V FITC-A vs Propidium Iodide-A contour plots using untreated and camptothecin-treated cells show an increase in the Annexin $V^+ PI^-$ population and a decrease in the Annexin $V^- PI^-$ population.

New BD FACSuite™ software makes it easy to convert experiments to reusable assays with setup information, acquisition and analysis templates, gating strategies, and reports you can share with other BD FACSVerse™ systems.

The software also provides BD predefined research assays matched with BD reagent kits for reproducible results. These assays reduce the variability of data between users and among laboratories for the same application.

Download a free application note and learn more about BD FACSuite predefined assays for apoptosis, cell cycle, cell proliferation, and cytokine detection at **bdbiosciences.com/go/verse.**

Simply Brilliant.

BD

Helping all people live healthy lives

Class 1 Laser Product.
For Research Use Only. Not for use in diagnostic or therapeutic procedures.
BD, BD Logo and all other trademarks are property of Becton, Dickinson and Company. © 2011 BD
23-13663-00

BD Biosciences
2350 Qume Drive
San Jose, CA 95131
bdbiosciences.com



Proteins

Antibodies

ELISAs

Assay Services

MultiAnalyte Profiling

Activity Assays

Stem Cells

ELISpot Kits

Flow Cytometry

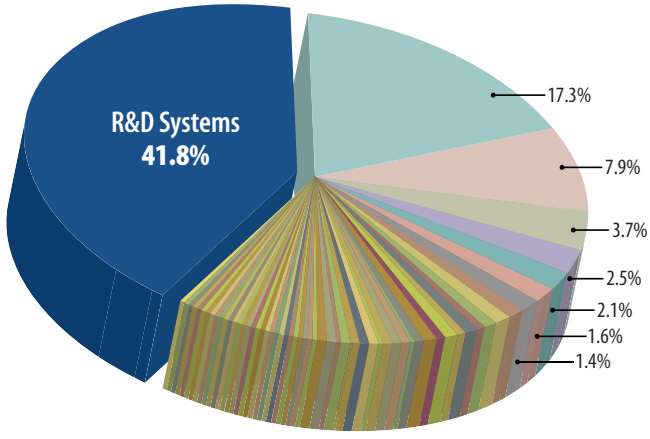
Cell Selection

R&D Systems Quantikine® ELISAs

The Most Referenced Immunoassays

A direct measure of product quality is the frequency of citations in the scientific literature. R&D Systems has more than 20 years of experience designing, testing, and optimizing the most cited ELISA kits in the world. Find out why scientists trust R&D Systems ELISAs more than any other brand.

R&D Systems is the Most Referenced ELISA Manufacturer



Approximately 42% of Referenced Immunoassays are Developed and Manufactured by R&D Systems. A survey of 860 manuscripts from 44 journals was conducted to compare the number of citations specifying the use of R&D Systems ELISAs to the number citing ELISAs from other commercial sources. A total of 433 ELISA citations referencing immunoassays from 66 different vendors were identified in the survey.

NEW Quantikine ELISA Kits

- α1-Acid Glycoprotein
- Angiopoietin-like 3
- Cathepsin V
- Clusterin
- Dkk-1
- EGF R/ErbB1
- EG-VEGF/PK1
- Fetuin A
- FGF-21
- Galectin-3
- Gas 6
- GDF-15
- IL-17A/F Heterodimer
- IL-19
- Lipocalin-2/NGAL
- MBL
- Proprotein Convertase 9/PCSK9
- Periostin/OSF-2
- Progranulin
- ST2/IL-1 R4
- Thrombomodulin/CD141
- Tie-1
- TIM-1/KIM-1

For more information visit our website at www.RnDSystems.com/go/ELISA

For research use only. Not for use in diagnostic procedures.

R&D Systems, Inc. www.RnDSystems.com

R&D Systems Europe, Ltd. www.RnDSystems.co.uk

R&D Systems China Co., Ltd. www.RnDSystemsChina.com.cn

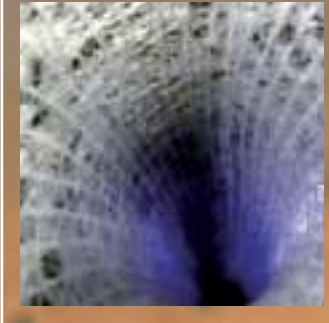
R&D SYSTEMS®

Johannes Gutenberg University Mainz (JGU) is a full university covering a wide range of academic disciplines. With over 37,000 students and more than 500 professors, it is among the ten largest universities in Germany. Materials science, earth system sciences, particle physics and nuclear chemistry are some of JGU's key research strengths where JGU regularly attains top scores. Its institutional strategy fosters structural and individual excellence in research and teaching. Special attention is given to the support of young researchers.
Come and visit us at: **www.uni-mainz.de**

THE GUTENBERG SPIRIT

MOVING MINDS – CROSSING BOUNDARIES







MATERIALS SCIENCE

JGU is an internationally recognized center for materials science, with particular expertise in synthetic methods and the study of non-equilibrium processes from a molecular point of view. Research is complemented by the JGU Graduate School of Excellence MAINZ (Materials Science in Mainz), which crosses disciplinary and institutional boundaries to provide rigorous, high-quality post-graduate education based on an individualized training program. Visit MAINZ at: **www.mainz.uni-mainz.de**

EARTH SYSTEM SCIENCES

Earth system sciences at JGU aim to expand an established expertise in the study of the Anthropocene by investigating the impact of human interference with natural processes. Combining geosciences, atmospheric physics and analytical chemistry with anthropology and archaeology creates an innovative scientific agenda. This concept is unique in Germany and distinguishes JGU´s earth system sciences from other research centers. Visit Geocycles at: **www.geocycles.de**

PARTICLE PHYSICS & NUCLEAR CHEMISTRY

Particle, hadron and atomic physics, as well as nuclear chemistry and mathematics are core elements of JGU's research portfolio. The electron accelerator facility MAMI and the research reactor TRIGA allow for state-of-the-art experimental research. JGU's outstanding capacities are reinforced by new projects in dark matter research and by structured international graduate programs. Learn more at: **www.emg.uni-mainz.de**

JOHANNES GUTENBERG UNIVERSITÄT MAINZ

JG|U

Now available:
Reagent sets for
Ion Torrent™

NEW ENGLAND
BioLabs® Inc.
enabling technologies in the life sciences

Take the next step.



Library Prep Reagents for Next Gen Sequencing

Isn't it time to break away from the constraints of standard workflows for NGS sample prep? With NEBNext® reagents for DNA and RNA, take advantage of multiple product formats and custom options to tailor solutions for your specific needs.

Available for the leading sequencing platforms, NEBNext reagents allow you to take the next step in designing the workflow that works for you.

www.NEBNext.com

Scan this code to learn more about how NEBNext reagents deliver flexibility to your sample prep workflow

Need a code reader? Go to 2dscan.com from your mobile browser, search for 'ScanLife' in your app store or text SCAN to 43588

Ion Torrent™ is a trademark of Life Technologies, Inc.



Confidence comes naturally

Trust Ambion® RNA products for consistent, superior results

Backed by more than 20 years of experience and the industry's most forward-thinking R&D team, Ambion® products provide innovative solutions for specialized RNA applications. Designed for superior performance, **MagMAX™** and ***mir*Vana™ isolation kits** use novel binding methods to recover more RNA, while the **Cells-to-C_T™ kits** enable consistent results through optimized workflows. And all Ambion® kits are subjected to the industry's most rigorous analytical testing and multifaceted QA/QC process to help ensure your success.

Find RNA expertise and tools at **lifetechnologies.com/ambion**

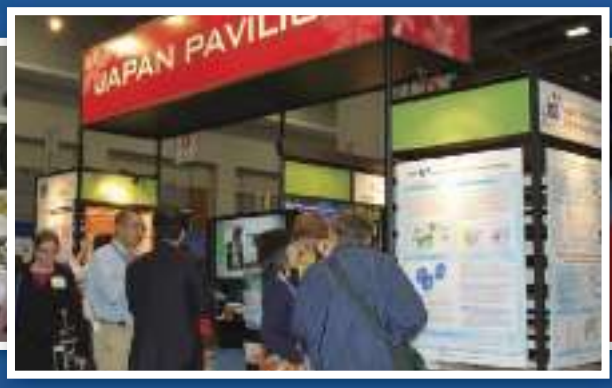
life technologies™

For research use only. Not intended for any animal or human therapeutic or diagnostic use. ©2012 Life Technologies Corporation. All rights reserved. The trademarks mentioned herein are the property of Life Technologies Corporation or their respective owners. CO24551 0112 SCI

AAAS Annual Meeting

Be Part of a Winning Team







Vancouver is a dynamic, multicultural city set in a spectacular natural environment. It was the proud host of the 2010 Olympic and Paralympic Winter Games. In 2012 it hosts the world's annual Olympiad of Science, 16-20 February.

AAAS organizes an international conference annually—4 days of symposia, lectures, seminars, workshops, and poster sessions that cover every area of science, technology, and education. We also organize a unique community science showcase that offers an array of hands-on demonstrations and other family friendly activities.

Attendees constitute a highly educated, global market that promotes the effective use of research and practice.

They represent nearly all U.S. states and territories as well as up to 55 countries. Technologically savvy, our attendees are always looking for new and improved tools and resources.

Take this opportunity to select or design your sponsorship and secure your exhibit space.

For more information about sponsorship opportunities and the exhibition, contact Isabel Patterson, AIM Meetings, (703) 549-9500; ipatterson@aimmeetings.com. For the program, go to www.aaas.org/meetings.

Presenting sponsor

SUBARU

Gold

EUROPEAN COMMISSION
European Research Area

NSF

UBC a place of mind
THE UNIVERSITY OF BRITISH COLUMBIA

Silver

Canada

HELMHOLTZ ASSOCIATION

Bronze

Council of Canadian Academies
Conseil des académies canadiennes

AAAS thanks THE KAVLI FOUNDATION *for its generous support of the Science Journalism Awards.*

AAAS

44

best practices for overcoming skepticism post-Climategate.

One more data point on why you should spend more time at membercentral.aaas.org. There you can enjoy webinars, videos, blogs, discounts, and downloads geared for people who prefer content based on empirical evidence.

membercentral.aaas.org

AAAS MemberCentral

New Products

LIQUID CHROMATOGRAPHY DETECTOR

Sapphire is a universally compatible, four-channel liquid chromatography detector. Sapphire features a revolutionary sapphire and quartz composite variable path-length flow cell, which allows concurrent measurement of ultraviolet (UV) absorption at 250 and 280 nm, refractive index, and conductivity. Sapphire's innovative design allows an unprecedented 0.001–100 A.U. UV detection range when normalized to a 10 mm path length. Deep UV LED light sources eliminate warm-up associated with traditional lamps and extend lifetime. Data is visualized in real-time on a four color integrated color monitor, and is USB-exportable. Sapphire is designed for purification of proteins and other biological materials as well as for FLASH chromatography.

Reach Devices
For info: 720-979-8940 | www.reachdevices.com



REAL-TIME PCR DETECTION SYSTEM

The CFX Connect real-time polymerase chain reaction (PCR) detection system is an ideal tool for researchers looking for reliable, high performance real-time PCR on a limited budget. The CFX Connect system, which requires a computer for operation, offers the same thermal performance as the CFX96 Touch real-time PCR system. It uses a similar scanning optics shuttle design that reads each well individually with high sensitivity and no cross talk to deliver optimal quantitative results. The CFX Connect detects two fluorophores per well in duplex experiments and detects SYBR Green or EvaGreen in singleplex experiments. Additional key benefits are effortless optimization that saves time and reduces costs by optimizing assays in a single run using the thermal gradient, and accurate data analysis with CFX Manager Software that offers an intuitive user interface and the ability to quickly and accurately validate and analyze data.

Bio-Rad
For info: 800-424-6723 | www.bio-rad.com

MAGNETIC BEADS

MagSi-proteomics beads are magnetic beads that are an ideal tool for the purification, concentration, and desalting of peptides and protein digests. The surface of the beads has been modified with C4-, C8-, and C18-alkyl groups that are optimized for reversed phase applications. Magnetic beads offer a convenient solid support for a variety of assays and procedures based on affinity purification. They are especially well suited for automated procedures because instrumentation is available to easily mix, incubate, and separate the magnetic beads in 96-well plates without columns or centrifugation. Offering higher throughput and cost efficiency compared to tip-based separations, MagSi proteomics beads efficiently bind and elute even tiny sample fractions. The high magnetic strength of MagSi beads makes them applicable for both manual and automated/robotic fractionation, because the beads will typically collect in less than one minute when magnetic force is applied.

AMS Biotechnology
For info: +44-(0)-1235-828200 | www.amsbio.com

GLYCOPROTEINS COUPLING REAGENTS

The new GlycoLink Immobilization and Immunoprecipitation (IP) Kits are designed for protein affinity purification and the study of protein interactions. The GlycoLink Immobilization and IP Kits provide the reagents for coupling glycosylated biological molecules to a beaded resin. The kits contain the Thermo Scientific UltraLink Hydrazide Resin and a reaction catalyst for a fast and efficient method to immobilize carbohydrates and glycoproteins such as antibodies onto a durable polyacrylamide resin. The catalyzed reaction results in greater than 90% coupling in four hours or less, depending on the amount of glycosylation. It also leaves other critical active sites on the molecule such as amines, carboxyls, and sulfhydryls free for other experimental purposes. Several kit configurations are available and contain the complete set of buffers, oxidizing reagent, and resin. The GlycoLink Coupling Catalyst is also available separately.

Thermo Fisher Scientific
For info: 800-874-3723 | www.thermoscientific.com/pierce

DUAL-LINE LIGHT ENGINE

The Cobolt Dual Combiner is a modulated dual-line light engine that is optimized for high-end optogenetics research applications. This version of the Cobolt Dual Combiner offers two attractive emission wavelengths for light-activated proteins: 473 nm (up to 50 mW) + 594 nm (up to 100 mW) from one small box. Through the integrating of a silent SRS shutter, the output beam can be modulated at up to 100 Hz with a very short rise time of <350 µs and with maintained 3% power stability and an RMS noise of <0.3%. Each line can be individually addressed through a software application provided with the lasers, or through RS232/USB communication. The modulated Cobolt Dual Combiner is perfectly suited for optogenetics applications where high level of power stability and control of the delivered energies are required. The modulated Dual Combiner is also available with any other two-line combination of the Cobolt 04-01 series lasers.

Cobolt
For info: +46-8-545-912-30 | www.cobolt.se

Electronically submit your new product description or product literature information! Go to **www.sciencemag.org/products/newproducts.dtl** for more information.

Newly offered instrumentation, apparatus, and laboratory materials of interest to researchers in all disciplines in academic, industrial, and governmental organizations are featured in this space. Emphasis is given to purpose, chief characteristics, and availability of products and materials. Endorsement by *Science* or AAAS of any products or materials mentioned is not implied. Additional information may be obtained from the manufacturer or supplier.

WEBINAR
Now available on demand.



FACTS & FICTION

Careers in Industry and Academia

Trying to figure out the next step in your career? Join us for a roundtable discussion that will look at facts and fiction surrounding academic and industry career options for PhD-level scientists. Get some nuts and bolts advice on how to research career options, what questions to ask, and how to best prepare for various careers.

- Do industry and academic careers require different skill sets?
- Do industry jobs have better compensation? Less autonomy?
- Do academic scientists have less work/life balance?

For answers view our roundtable discussion for free at:

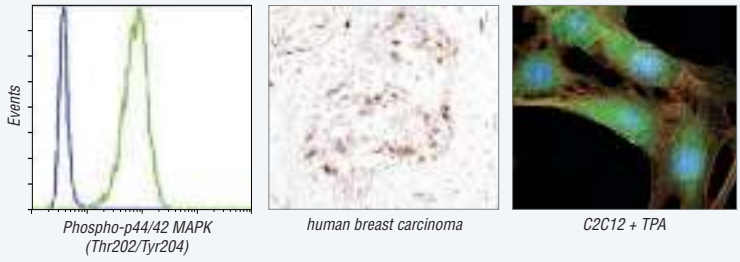
ScienceCareers.org/webinar

Science Careers
From the journal *Science* AAAS

Produced by the *Science*/AAAS Business Office.

© 2012 Cell Signaling Technology, Inc.







Phospho-p44/42 MAPK (Erk1/2) (Thr202/Tyr204) (D13.14.4E) XP® Rabbit mAb #4370 *(top) and* ***p44/42 MAPK (Erk1/2) (137F5) Rabbit mAb #4695*** *(bottom).*

For full validation details see www.cellsignal.com

The Highest Quality MAPK Antibodies *are from Cell Signaling Technology*

Unparalleled product quality, validation, and technical support

Over 30 thoroughly validated MAPK Antibodies available

Cell Signaling Technology (CST™) offers the widest range of phospho and total protein MAPK antibodies. These reagents are the most thoroughly validated, widely used, and highly cited MAPK antibodies available.

- CST™ phospho and total protein MAPK antibodies offer **unsurpassed specificity, sensitivity, and performance**.
- **Extensive in-house validation** in a wide range of applications means that optimization is not left up to you, the user.
- **Technical support is provided by scientists** who produce the products and know them best.

WINNER! Life Science Industry Awards®
Best Antibodies :: *Best Breakthrough Products for Cancer Research*

for quality products you can trust...

www.cellsignal.com

Cell Signaling TECHNOLOGY®

Orders (toll-free) 1-877-616-CELL (2355) orders@cellsignal.com | **Fax ordering** 1-978-867-2488 | **Technical support** (toll-free) 1-877-678-TECH (8324) support@cellsignal.com | **Inquiries** info@cellsignal.com

Cell Signaling Technology®, CST™, and XP® are trademarks of Cell Signaling Technology, Inc. Selected rabbit monoclonal antibodies are produced under license (granting certain rights including those under U.S. Patents No. 5,675,063 and 7,429,487) from Epitomics, Inc.



Science Careers Advertising

For full advertising details, go to ScienceCareers.org and click For Employers, or call one of our representatives.

Tracy Holmes
Worldwide Associate Director
Science Careers
Phone: +44 (0) 1223 326525

UNITED STATES & CANADA
E-mail: advertise@sciencecareers.org
Fax: 202-289-6742

Tina Burks
Midwest/West Coast/
South Central/Canada
Phone: 202-326-6577

Elizabeth Early
East Coast & Corporate
Phone: 202-326-6578

Marci Gallun
Sales Administrator
Phone: 202-326-6582

Online Job Posting Questions
Phone: 202-312-6375

EUROPE & REST OF WORLD
E-mail: ads@science-int.co.uk
Fax: +44 (0) 1223 326532

Simone Jux
Phone: +44 (0)1223 326529

Lucy Nelson
Phone: +44 (0)1223 326527

Kelly Grace
Phone: +44 (0) 1223 326528

JAPAN
Makiko Hara
Phone: +81 (0) 90-9853-9982
E-mail: mhara@aaas.org
Fax: +81 (0) 3-6369-4491

CHINA & TAIWAN
Ruolei Wu
Phone: +86-1367-1015-294
E-mail: rwu@aaas.org

All ads submitted for publication must comply with applicable U.S. and non-U.S. laws. *Science* reserves the right to refuse any advertisement at its sole discretion for any reason, including without limitation for offensive language or inappropriate content, and all advertising is subject to publisher approval. *Science* encourages our readers to alert us to any ads that they feel may be discriminatory or offensive.



MoveAhead

Change your future and become part of Abbott's success in one of the following roles:

Senior Histopathologist – Req # 102754BR

Seeking a Sr. Histopathologist to join the *In Vivo* Tumor Biology team to support the IHC needs of multiple small molecule and biologics programs and drive the strategy for translational biomarker development.

Requirements:
MD and/or DVM (board certification is highly desired) or PhD in a relevant field with 5-8 years experience. Must have 3+ years experience in IHC, antibody selection and optimization of IHC protocols. Strong pathology experience is required; clinical pathology and digital pathology experience with relevant cancer biology research background is highly preferred. Leadership skills, strong research and industry experience, good interpersonal skills, ability to direct or lead technical studies, strong communication (excellent verbal and written skills) and teamwork skills are required.

Senior Scientist/Principal Research Scientist –

(2 positions available: Req # 98284BR/Req # 93371BR)

The incumbent will be responsible for identification and validation of novel cancer targets, developing assay infrastructure and biology strategy toward discovery of compounds for promising targets, and championing such projects toward clinical proof of concept. The individual must have solid and multi-faceted experience in cancer biology (cell cycle, cell death, DNA repair, cancer metabolism, epigenetics, signal transduction, etc). Strong communication and teamwork skills are essential.

Requirements:
Ph.D. in Cell/Mol Biology or related with 2 years post-graduate experience in cancer biology is required. Demonstrated scientific achievements, i.e., strong publication and/or patent record. Proficiency in standard biochemical, cellular and molecular techniques; ability to guide the development of novel target candidates; develop and maintain appropriate *in vitro* assays to guide SAR studies; interact with cross-functional teams to facilitate lead advancement; critically evaluate relevant scientific data and apply this knowledge to research efforts; contribute substantially to the overall research strategies; continually implement and validate novel research approaches to advance project goals; communicate results to multi-disciplinary teams; publish in peer-reviewed journals. The position grade level will be filled commensurate with experience.

Abbott is at the forefront of cancer research in discovering and developing novel treatments that offer a new approach to cancer therapy. Our strong pipeline includes signal transduction inhibitors as well as first in class agents that target angiogenesis, metastasis and resistance to apoptosis. Abbott's oncology franchise extends beyond pharmaceutical research to provide a range of health care products, from supportive care products for pain management, to diagnostic tests for the detection of cancer.

We invite you to apply online at www.abbottcareers.com and search for the desired Req #.

An equal opportunity employer, Abbott welcomes and encourages diversity in our workforce.

Abbott
A Promise for Life

NIMHD
National Institute on Minority Health and Health Disparities

Department of Health and Human Services
National Institutes of Health
National Institute on Minority Health and Health Disparities

The National Institute on Minority Health and Health Disparities of the National Institutes of Health is searching for a Clinical Director/Senior Investigator qualified for tenured appointment to direct its clinical research program. Additionally, the Clinical Director is expected to conduct her/his own independent research as a Senior Investigator. As Clinical Director/Senior Investigator, the incumbent is responsible for the leadership of the intramural NIMHD clinical program located at the NIH Clinical Center in Bethesda, Maryland. The Director of the clinical research program/Senior Investigator position is administratively within the Office of the Scientific Director, NIMHD. The successful candidate will oversee a combination of studies, including outpatient, inpatient, epidemiological, clinical protocols, and laboratory studies. Emphasis will be placed upon investigators with a primary research interest in clinical research; however, the selected candidate must adopt the NIMHD strategies in utilizing an interdisciplinary approach toward the science of prevention, diagnosis and treatment of chronic diseases that disproportionately affect the underserved populations in the U.S.

QUALIFICATIONS: Candidates must have an established and nationally or internationally recognized record in the conduct and supervision of clinical research in a discipline relevant to the field of minority health and health disparities research. Candidates should also have an established record of experience with clinical training, institutional review boards, and compliance with current clinical safety and regulatory issues. Candidates must have a Doctor of Medicine degree from a school in the United States or Canada accredited by the Liaison Committee on Medical Education (LCME) in the year of the applicant's graduation, or a Doctor of Medicine or equivalent degree from a non-LCME accredited medical school that is certified by the Educational Commission for Foreign Medical Graduates (ECFMG) or hold a Fifth Pathway certificate issued prior to December 31, 2009. Candidates must be board certified or board-eligible in a medical specialty approved by the American Board of Medical Specialties (ABMS), and have the ability to obtain medical licensure in the U.S.

SALARY/BENEFITS: The Clinical Director, NIMHD, will be appointed at a salary commensurate with his/her qualifications and experience. Full Federal benefits, including leave, health and life insurance, retirement and savings plan (401K equivalent) will be provided. This position is subject to public financial disclosure requirements.

HOW TO APPLY: Interested candidates should send a letter of interest, including a brief description of research and administrative experience; curriculum vitae and bibliography; and full contact information for three to five individuals who may be contacted to provide letters of reference. Application packages should be sent to the **National Institutes of Health (NIH), National Institute on Minority Health and Health Disparities, c/o Dr. Richard Cannon, Chair, Search Committee, 6707 Democracy Blvd., Suite 800, Bethesda, Maryland 20892,** or electronically: keta.lawson@nih.gov; **Subject Line: NIMHD Clinical Director Search.** For further information about the position, please contact Ms. Keta Lawson at 301-594-3986 or keta.lawson@nih.gov. ALL information provided by the candidates will remain confidential and will not be released outside the NIMHD search process without a signed release from candidate. The NIH encourages the application and nomination of qualified women, minorities, and individuals with disabilities.

APPLICATIONS MUST BE RECEIVED BY MONDAY, MARCH 19, 2012

DHHS and NIH
are Equal Opportunity Employers

NW220687R

Neurobiology of Disease Faculty Position

Gladstone Institutes and
the University of California, San Francisco

The Gladstone Institute of Neurological Disease and the University of California, San Francisco (UCSF) invite applications for a faculty position at the level of Associate or Full Professor. Of particular interest are neuroscientists and neurologists with broad expertise in chemistry, computational neuroscience, systems biology or neuroimmunology, who are interested in investigating molecular or cellular mechanisms and novel therapeutic strategies relevant to Alzheimer's disease, other neurodegenerative disorders, schizophrenia, autism or related disorders. Primary criteria for appointment will be outstanding records of innovative research and academic performance, including landmark papers in leading journals, as well as proven abilities or high potential to establish a rigorous and substantial independent research program, provide exemplary mentorship, and engage in fruitful collaborations.

The successful candidate will join an interactive group of investigators in Gladstone's state-of-the-art research facility at UCSF's Mission Bay campus. S/he will have joint appointments in the Gladstone Institute of Neurological Disease, the Department of Neurology, the Neuroscience Graduate Program and the Biomedical Sciences Graduate Program at UCSF. Excellent salary support is provided. Women and underrepresented minorities are especially encouraged to apply. The search will continue until the position is filled. However, to ensure full consideration, applications should be received by February 29, 2012.

Please send curriculum vitae, description of achievements and research interests, and the names of three references to:

GIND/UCSF Search Committee
Gladstone Institute of Neurological Disease
1650 Owens Street, San Francisco, CA 94158
gindsearch@gladstone.ucsf.edu

GLADSTONE

The J. David Gladstone Institutes and UCSF are Affirmative Action/Equal Opportunity Employers. They undertake affirmative action to assure equal employment opportunity for underutilized minorities and women, for persons with disabilities, and for Vietnam-era veterans and special disabled veterans.

Research Position at ICYS, NIMS, Japan

The International Center for Young Scientists (ICYS) of the National Institute for Materials Science (NIMS) is now seeking a few researchers. Successful applicants are expected to pursue innovative research on broad aspects of materials science using most advanced facilities in NIMS **(http://www.nims.go.jp/eng/index.html)**.

In the ICYS, we offer a special environment that enables young scientists to work independently based on their own idea and initiatives. All management and scientific discussions will be conducted in English. An annual salary between 5.03 and 5.35 million yen (level of 2011) will be offered depending on qualification and experience. The basic contract term is two years and may be renewed to one additional year depending on the person's performance. A research grant of 2 million yen per year will be supplied to the ICYS researcher.

All applicants must have obtained a PhD degree within the last ten years. Applicants should submit an application form, which can be downloaded from our web site, together with a resume (CV) and a list of publications. A research proposal on an interdisciplinary or integrated area related to the materials science should also be submitted. The application letter should reach the following address via e-mail or air mail by March 30, 2012. Visit our website for more details **(http://www.nims.go.jp/icys/)**.

ICYS Administrative Office,
National Institute for Materials Science
Sengen 1-2-1, Tsukuba, Ibaraki 305-0047, Japan
e-mail: icys-recruit@nims.go.jp

DUKE INSTITUTE FOR GENOME SCIENCES & POLICY

Duke University School of Medicine

Director, 'Omics Data Analysis Core Resource
Duke University

We are seeking a Director who will develop and oversee a full-service core resource to facilitate analysis across the full spectrum of 'omics data (including computational and/or statistical analyses of comprehensive datasets). Services to be provided are expected to vary from project to project but should include the full range of consultation and project planning, fee-for-service data analyses, and long-term collaborations, utilizing a variety of scientific approaches to best meet the goals and expectations of a variety of clients from across the Duke campus. The core resource will be based in the Duke Institute for Genome Sciences & Policy (**www.genome.duke.edu**), in conjunction with the School of Medicine (**www.medschool.duke.edu**).

The Director will have a PhD or equivalent degree in a quantitative field (e.g. computer science, statistics or computational biology) with substantial experience working with a range of large 'omics datasets and an orientation towards the genome sciences and their applications in the life sciences and biomedical research. Depending on qualifications and experience, the successful candidate may qualify for a regular-rank faculty appointment in the IGSP at the rank of Assistant or Associate Research Professor.

The Director will administer the data analysis resource, supervise staff scientists to meet the needs of the core resource, coordinate activities among all components of analysis support, liaise with relevant units on campus, integrate and coordinate activities with other key leadership and/or administrative functions. In addition to developing and directing the core resource, the Director will coordinate educational efforts, ranging from one-on-one training, to hands-on workshops and possibly formal courses.

Interested candidates should submit their electronic applications, including a *curriculum vitae*, a brief statement of research experience and interests, and names and contact information of a least three referees to **julia.s.walker@duke.edu**. Review of applications will begin **April 1, 2012**.

Duke University is an Equal Opportunity/Affirmative Action Employer. Females and minority candidates are especially encouraged to apply.

Faculty Scientists - Pediatrics

The Department of Pediatrics at The University of Texas Medical School at Houston seeks faculty scientists with interests in the following research areas: **complex birth defects, such as craniofacial disorders, intrinsic defects affecting cartilage and bone growth, and neuro- and lung developmental biology.** These research interests will complement those already established in the Department of Pediatrics and allow for collaborations. The University of Texas Medical School at Houston is situated in the Texas Medical Center, the largest medical center in the world composed of 35 medical and research facilities including The University of Texas M.D. Anderson Cancer Center, University of Texas School of Public Health, and Harris County Hospital District. Facilities within the University include state-of-the-art microscopy, genomics, proteomics, histopathology and mouse cores and vivarium. Positions are available at the assistant, associate professor and professor levels commensurate with previous experience. These positions are highly competitive with regard to salary, start-up funds and laboratory space. Applicants should have one of the following degrees: PhD, MD or MD/PhD. Applicants with microscopy experience are encouraged to apply. Successful candidates will be expected to develop and sustain research programs with extramural funding and play an integral role in new program initiatives.

Applicants should send a statement of research interests, curriculum vitae and names and addresses of three references to: **Dr. Jacqueline T. Hecht, PhD, University of Texas Medical School Department of Pediatrics, Rm. 3.316, Houston, TX 77030 Email: Jacqueline.T.Hecht@uth.tmc.edu**

Women and minority candidates are encouraged to apply. UTHealth | The University of Texas Health Science Center at Houston is an EO/AA employer, M/F/D/V. This is a security sensitive position and thereby subject to Texas Education Code §51.215. A background check will be required for the final candidate.

UTHealth™
The University of Texas
Health Science Center at Houston



Two Professor or Associate Professor of Systems Biology Positions

The Department of Systems Biology at Harvard Medical School invites applications for TWO faculty positions, which may be filled either at the tenure-track Associate Professor or Full Professor level. We seek creative thinkers who take risks in defining and addressing important problems in biology and medicine, and who use quantitative experimental, computational and/or theoretical approaches in their work.

The first position is an open position which may be filled in any area of systems biology. The second position is focused on the use of systems biology approaches in the discovery and evaluation of drugs (systems pharmacology).

For the systems pharmacology position, research on any aspect of the intersection between quantitative biology, mathematical modeling and pharmacology in cells, animals and patients is of interest, including (but not limited to): studying the effects of drugs and drug candidates on the behavior of biological systems from a quantitative, modeling-driven perspective; studying the mechanistic basis for individual-to-individual or tissue-to-tissue variation in drug effects using metabolomic, proteomic imaging, computational or other approaches; novel high-content approaches to studying therapeutic and physiological mechanisms using drugs; rational approaches to the design of combination therapy; mechanistic and computational approaches to drug toxicity and off-target activities; and systems approaches to the treatment or prevention of infectious disease.

The Department has a diverse faculty with backgrounds in cell biology, biochemistry, physics, mathematics, chemistry, computer science, engineering and medicine, and offers a lively and supportive environment in which to perform interdisciplinary science. The successful candidate will become a member of Harvard's Ph.D. Program in Systems Biology, a cross-Harvard interdisciplinary program that attracts extraordinary graduate students. A doctoral degree is required.

The deadline for applications is **March 31, 2012**. References will be requested once a short list has been selected.

To apply, please submit a statement of research interests (~ three pages) and a curriculum vitae to:
http://academicpositions.harvard.edu/postings/3770

Applications from, or nominations of, women and minority candidates are encouraged.
Harvard is an Affirmative Action/Equal Opportunity Employer.

FACULTY POSITION - Center for Skeletal Disease Research Program

Van Andel Research Institute (VARI) is creating a preeminent program in Skeletal Disease research, combining the skills and expertise of VARI staff and with those of external community partners. The goal of the Program is to become a Center of Excellence in the field of bone biology, supporting basic, applied, and clinical research for the advancement of knowledge, the improvement of health, and the treatment of bone diseases.

VARI is located in a rapidly growing medical community in Grand Rapids, Michigan, and it currently houses 21 laboratories devoted to basic cancer research, technology development, and translational research. VARI is affiliated with the Translational Genomics Research Institute (TGen) in Phoenix, Arizona.

Applications are invited from candidates who have a Ph.D. or equivalent degree with a background in genetics, endocrinology, biomedical engineering, or cell biology, as related to bone disease. Candidates will be expected to have a demonstrated record of productivity and previous success in obtaining external funding. Salary and start-up funds are competitive and commensurate with academic qualifications and experience. Information about the department can be found at **http://www.vai.org/Research/Labs/CellSignalingandCarcinogenesis.aspx**

Qualified applicants should apply online at **www.vai.org/employment**. Applicants should include their curriculum vitae, a statement of research interests and goals, and the names and contact information for three references. Review of applications will begin **January 23, 2012**, and will continue until the position is filled.

To learn more about VARI/TGen, please visit www.vai.org

Van Andel Research Institute is an Equal Opportunity Employer.

Van Andel Institute®
www.vai.org

Institut Pasteur

Junior Faculty (G5) Recruitment in Immunology
Junior Faculty (G5) Recruitment in Statistical Genetics
Institut Pasteur, Paris

The Institut Pasteur announces an international call for candidates wishing to create independent young researcher groups on its Paris campus in France. The call responds - in the framework of The French Government program entitled "Investments for the Future" - to the recent award to Institut Pasteur of a Laboratory of Excellence (LabEx) named Milieu Intérieur. Outstanding candidates fostering new concepts in immunology and/or genetics are encouraged to apply (**www.pasteur.fr/immuno**).

In the context of this recruitment, the Institut Pasteur wishes to develop new themes of research including (but not limited to): systems and computational analyses of immunity, harnessing innate and adaptive immunity for vaccine development, molecular, environmental and systemic control of inflammation; identification of new mechanisms of immune regulation, and statistical and computational genetics.

Candidates must have defended their PhD thesis on or after February 1, 2004 (women with children are eligible up to 10 yrs after their PhD). Short-listed candidates will be invited for an interview in September 2012. Successful candidates will be appointed as head of a group of up to 6 people for a period of 5 years. The start-up package includes the salary for the group leader (if necessary), a postdoctoral position, a technician, part-time secretarial assistance, basic laboratory equipment and a contribution to running costs. Candidates will also have access to on-campus facilities including state-of-the-art technology platforms.

Candidates should send their formal applications before **May 31st, 2012** by e-mail to the **Director of Scientific Evaluation, Prof. Alain Israël**, at the Institut Pasteur (**g5mi@pasteur.fr**). The application should comprise the following (in order) in a single pdf file: • A brief introductory letter (candidates are encouraged to contact **Matthew Albert**, (**albertm@pasteur.fr**) for further information) • A Curriculum Vitae and a full publication list • A description of past and present research activities (up to 5 pages with 1.5 spacing) • The proposed research project (up to 10 pages with 1.5 spacing) including a title and a summary • The names of 3 scientists from whom letters of recommendation can be sought, together with the names of scientists with a potential conflict of interest from whom evaluations should not be requested.

Institut Pasteur

Young Group Leader Positions

The Institut Pasteur announces an international call for candidates wishing to establish independent research groups on its Paris, France campus. The recruitments are part of the French Government's Laboratory of Excellence (LabEx) programme called Revive, recently awarded to the Institut Pasteur on "Stem Cells and Regenerative Biology and Medicine." Candidates will be integrated into the cutting edge interdisciplinary environment provided by the Department of Developmental Biology. Candidates specializing in the field of stem cells in the context of developmental and cell biology, genetics, epigenetics, regeneration and ageing are encouraged to apply.

To be eligible, candidates must have defended their PhD on or after May 31, 2004 (women with children are eligible up to 10 yrs after their Ph.D). Successful candidates will be appointed as head of a group of up to 6 people for a period of 5 years. The budget (up to 1,500,000€ over 5 years) includes the salary for the group leader, a three-year postdoctoral position, a technician's position, part-time secretarial assistance, a substantial contribution to running costs and equipment, and access to on-campus facilities including state-of-the-art technology core facilities.

Candidates should send their formal applications by e-mail to the **Director of Scientific Evaluation, Prof. Alain Israël**, at the Institut Pasteur (**g5revive@pasteur.fr**). The deadline for applications is **May 31st, 2012**. Short-listed candidates will be contacted for interview in June-August 2012 and recruitment decisions announced by October 2012. Further information on the Revive program can be found at **http://www.pasteur.fr/labex/revive**.

Applicants should provide the following (in order) in a single pdf file:
• A brief introductory letter of motivation, including the name of the proposed group. Candidates are encouraged to contact the coordinator of the Revive programme **Shahragim Tajbakhsh** (**shaht@pasteur.fr**) • A Curriculum Vitae and a full publication list • A description of past and present research activities (up to 5 pages with 1.5 spacing) • The proposed research project (up to 10 pages with 1.5 spacing) • The names of 3 scientists from whom letters of recommendation can be sought, together with the names of scientists with a potential conflict of interest from whom evaluations should not be requested.

Mentored Experiences in Research, Instruction and Teaching Program

MERIT

Postdoctoral Scholars

Postdoctoral Scholars for MERIT Program, a NIH IRACDA program, at the University of Alabama at Birmingham is seeking individuals who are interested in outstanding teaching and research experiences during their postdoctoral training. The MERIT Program will provide opportunities for research experience at UAB and teaching experience at minority serving institutions, including Oakwood and Stillman Colleges.

MERIT Fellows are supported for three years at NRSA rates beginning at $38,496; are provided health insurance at no charge, a yearly travel allowance to professional meetings; and yearly research or training allowance.

Applicants to the MERIT Program must be PhD candidates or recent PhD graduates (within the past year) and a U.S. citizen or non-citizen national; individuals with comparable degrees, including MD and DVM, are also eligible.

Deadline for applications is **April 1, 2012**. Application materials as well as other information are available on the MERIT website: **http://iracda.meritprogram.org**.

Women and persons from diverse backgrounds, including underrepresented racial and ethnic groups, individuals with disabilities, and individuals from disadvantaged backgrounds, are encouraged to apply.

UNIVERSITY OF MICHIGAN

Assistant Professor Position in Pharmaceutical Sciences

The Department of Pharmaceutical Sciences at the University of Michigan College of Pharmacy invites applications for a tenure-track faculty position at the Assistant Professor level. A successful applicant will be expected to develop an independent research program in physical, chemical, biological or computational aspects of drug transport, delivery/targeting or biopharmaceutics. For example:

- Structure-based functional studies of drug transport mechanisms and drug delivery vehicles
- Chemical and genetic dissection of drug transport mechanisms in model organisms
- Noninvasive, bioimaging-based approaches to pharmacokinetic analyses
- Mechanism- and systems-based structure-biodistribution relationship studies
- DNA, RNA, protein or supramolecular engineering of site-directed therapeutic agents
- Nanotechnology, devices or materials for drug delivery and controlled release

We seek applicants with outstanding records of research productivity and growth potential, and a willingness to teach graduate and professional students in pharmaceutical sciences and pharmacy. Applicants should submit a pdf file of their CV and a 3-5 page description of their proposed research program to **Jeanne Getty** (**jgetty@umich.edu**), and have three letters of reference sent separately to the same email address. The University of Michigan is committed to recruiting, supporting and fostering a diverse community.

The University of Michigan is an Equal Opportunity/Affirmative Action Employer.

2050-ONE CHALLENGE:
FEEDING 9 BILLION PEOPLE



THAT IS WHY
WE NEED YOUR SKILLS

INRA IS RECRUITING
51 SCIENTISTS

FIRST AGRICULTURAL INSTITUTE IN EUROPE AND SECOND IN THE WORLD, THE FRENCH NATIONAL INSTITUTE FOR AGRICULTURAL RESEARCH IS RECRUITING IN THE FOLLOWING DOMAINS:

Biochemistry • Molecular Biology • Genomics • Endocrinology • Physiology • Microbiology • Infectious Diseases • Ecology • Environmental Sciences • Quantitative Genetics • Agronomy • Plant Sciences • Animal Production Sciences • Mathematics • Statistics • Sociology • Economics

orc.fr – Crédit photo : GettyImages

www.international.inra.fr

Applications
from 26 January to
28 February 2012

FOOD AND NUTRITION
AGRICULTURE
ENVIRONMENT

INRA
targeted research

THE UNIVERSITY OF TEXAS
Health Science Center at Tyler

The University of Texas Health Science Center at Tyler invites applications from extramurally funded, outstanding scientist/administrators to serve as **Chairman of Cellular and Molecular Biology**. Administrative experience required. Administrative responsibilities include oversight/development of a productive 15 member faculty group and of a biotechnology master's graduate program. Track record of successful research and current extramural funding required. Resources to support this recruitment include ample laboratory space, additional faculty positions to support a laboratory team or recruitment, an endowment and unique UT System resources.

Tyler is located midway between Dallas and Shreveport amidst the picturesque lakes and piney woods of East Texas. The mission of the basic and clinical research at the UT Health Science Center focuses on **lung injury/repair, pulmonary infectious diseases, coagulation and immunology** and a new $40 million academic building that opened November 2011. A complete listing and description of current faculty research interests can be found online via UTHSCT's website **http://www.uthct.edu/Research**.

The successful candidate will bring a dynamic independent research program in a discipline related to the mission of UTHSCT. Preference given to programs in either lung inflammation and repair, aspects of matrix biology or oncology. Associate and Full Professor level candidates will be considered. Applicants should submit their *curriculum vitae*, a statement of future administrative and research plans and the names of three references to: **Dr. Anna Kurdowska, Faculty Search Committee Chair, University of Texas Health Science Center at Tyler, 11937 US Highway 271, Tyler, Texas 75708-3154**, or by email to **anna.kurdowska@uthct.edu**.

UTHSCT *is an EEO/AA Employer M/F/V/D. This position is security sensitive and subject to Texas Education Code 51.215 which authorizes the employer to obtain criminal history information.*

KAUST
Through Inspiration, Discovery
King Abdullah University of Science and Technology

Director, Office for Competitive Research Funds (OCRF)

Department/Division: Research Office
Reports to: Vice President Research

Position Summary:

Responsible for the planning and administration for funding of competitive research programs.

Major Responsibilities:

- Conduct the strategic planning, establishment, and administration of funded competitive research grant programs that meet the overall goals of the institution.
- Assesses and recommends priorities across the research objectives of the institution.
- Provides administrative leadership and vision for the research grant program.
- Prepares, proposes and administers the research budget for competitive funding programs.
- Responsible for implementing and managing the merit review process for proposals submitted.
- Conduct policy setting, and program organization for the funding of competitive research programs.
- Assesses and balances program needs among the different disciplines, recommends priorities and allocation of resources, including preparation of budget estimate.
- Assesses the needs and trends in research, in order to propose timely research programs that provide a competitive advantage to the community.
- Fosters multidisciplinary research projects in line with the objectives.
- Overseas the evaluation of proposals and recommendation for awards as well as declinations.

Competencies:

- Broad understanding of universities where science and engineering research is conducted.
- Excellent knowledge of grant administration, fiscal management and budget preparation.
- Ability to establish an organizational vision and to implement it in a continuously changing environment.
- Ability to utilize community inputs, discipline-specific studies, and advisory committee recommendations to design and implement new programs.
- Skill in recognizing, developing and implementing programs in cross-cutting research.
- Demonstrated ability to implement and manage in timely fashion a merit-based competitive grant program.
- Ability to manage a process that ensures the quality, integrity, and consistency of awards and declinations in the grant programs.

Qualifications:

- Ph.D. in Science or Engineering
- Substantial evidence of scholarship and leadership in disciplines related to science and Engineering and/or strong demonstrated leadership experience in high level grant program management.
- Demonstrated ability to manage human, information, and financial resources.
- Excellent communication and interpersonal skills
- Ability to work collaboratively with faculty and university research administration fostering a cooperative work environment.
- Strong and effective verbal and written communication skills in English

To apply, visit: http://www.kaust.edu.sa



TEXAS TECH UNIVERSITY
HEALTH SCIENCES CENTER
Paul L. Foster School of Medicine

ASSISTANT or ASSOCIATE PROFESSOR
Center of Excellence in Cancer Research

The newly created Center of Excellence in Cancer Research at the Paul L. Foster School of Medicine at El Paso is seeking highly qualified applicants for tenure-track faculty positions at the Assistant or Associate Professor level in the Department of Biomedical Sciences. Successful candidates are expected to develop an independently funded research program in cancer research or a related field. The positions report to the Director of Basic Science Research of the Center of Excellence in Cancer Research.

Minimum qualifications: M.D., Ph.D., or M.D./Ph.D. degree in a field related to cancer, three years of postdoctoral experience, and a strong publication record.

Preferred qualifications: Candidates with experience in cancer research, experience using the latest technologies and funded grant support. (Only candidates with funded grant support will be considered for Associate Professor Rank.) A competitive salary, startup package, and comprehensive benefits are available.

Interested candidates must apply online at website: **http://jobs.texastech.edu**, requisition **#80343- Asst Professor and 81927 Associate Professor**.

For further information applicants may inquire confidentially to: **Rajkumar Lakshmanaswamy Ph.D.**, e-mail: **rajkumar.lakshmanaswamy@ttuhsc.edu**, Director of Basic Science Research of the Center of Excellence in Cancer Research. The position is open until filled. Application review will begin immediately.

Texas Tech University Health Sciences Center is an Equal Opportunity/Affirmative Action Employer.

UAB

Department of Biochemistry and Molecular Genetics
University of Alabama at Birmingham
Schools of Medicine and Dentistry
NMR Faculty Positions

Faculty positions (tenure track junior and senior faculty and/or tenured senior faculty) are available for outstanding investigators with extensive experience in the application of High-Field NMR Spectroscopy to study the structural biology of proteins of significance in human diseases. Structural biology areas of interest include, but not limited to, stem cell biology, virology, glycobiology, cancer cell biology, membrane proteins, immunology, and drug discovery and design. Nationally competitive salaries, start-up packages and space allocations, as well as complete access to the Central Alabama High-Field NMR Facility consisting of a new state-of-the-art Bruker 850 MHz NMR system with a cryoprobe and lower NMR field systems, will be offered to the successful candidates. Preference will be given to NIH funded investigators. UAB is a highly interactive environment with strong basic and clinical science programs and Research Centers. Birmingham is a beautiful and affordable city with many cultural attractions.

Applicants should send a C.V., a summary of research interests and the names of three references before **February 29th, 2012** to:

Dr. Tim Townes
Chairman, Department of Biochemistry and Molecular Genetics
University of Alabama at Birmingham
Kaul Genetics Building, Room 502
720 20th Street South
Birmingham, AL 35294
Email: ttownes@uab.edu

UAB is an Equal Opportunity/Affirmative Action Employer committed to fostering a diverse, equitable and family-friendly environment in which all faculty and staff can excel and achieve work/life balance irrespective of ethnicity, gender, faith and sexual orientation. UAB also encourages applications from individuals with disabilities and veterans.

IIN Postdoctoral Fellowships in Nanotechnology

The International Institute for Nanotechnology (IIN) at Northwestern University is seeking extraordinary, young scientists and engineers who are pursuing leading-edge nanotechnology research for IIN Postdoctoral Fellowships. A global hub of excellence in the field, the IIN unites more than $550 million in nanotechnology research, infrastructure, and education under a single umbrella. Its collaborations with other universities, research institutions, and industry partners span 18 countries—and bridge the boundaries among science, engineering, and medicine.

Two-year IIN Postdoctoral Fellowships include a $65,000 stipend, as well as research and travel funds per annum.

Qualified candidates must be U.S. citizens and expect to earn a doctoral degree within the next year. They must have demonstrated innovation as well as outstanding achievement in their doctoral research and possess independent research abilities and ambitious scientific goals. Applicants must not hold any position, paid or unpaid, with Northwestern University throughout the nomination and award process.

Application Process:
Applicants must secure a postdoctoral appointment with an IIN faculty member (see faculty list at iinano.org)—and be nominated for an IIN Postdoctoral Fellowship by the sponsoring professor. The IIN is not accepting self-nominations and cannot respond to all queries. Please contact professors directly and mention your interest in the IIN Postdoctoral Fellowship. After candidates are nominated by sponsoring faculty, they will be evaluated by the IIN Executive Committee. Select nominees will be invited to apply.
www.iinano.org
nanotechnology@northwestern.edu

Deadline:
IIN Postdoctoral Fellowships are awarded on a rolling basis, up to six per year.

Northwestern University is an Affirmative Action, Equal Opportunity Employer. Women and minorities are encouraged to apply.

NORTHWESTERN UNIVERSITY

INTERNATIONAL INSTITUTE FOR NANOTECHNOLOGY
Northwestern University

BASIC SCIENTIST - ASSISTANT, ASSOCIATE, or PROFESSOR
DEPARTMENT OF OTOLARYNGOLOGY/HEAD AND NECK SURGERY
STANFORD UNIVERSITY SCHOOL OF MEDICINE

The Department of OHNS (**http://med.stanford.edu/ohns/**) is recruiting for a basic science tenure-track faculty position. The successful candidate will be appointed at the level of assistant, associate, or full professor.

Scientists from a wide variety of disciplines are welcome to apply as long as their research relates to issues relevant to otolaryngology. A few illustrative fields include developmental biology, genetics, molecular and cellular biology, biophysics, cancer, auditory physiology, voice physiology, auditory and vestibular prosthesis development, bioengineering, stem cell and gene therapy. Collaborations with academic clinicians is encouraged. The successful researcher will be part of an interdisciplinary and collaborative team in a lab close to Stanford campus with ample opportunity for interaction with a broad spectrum of scientists including world-class programs in neuroscience, genetics, biomedical engineering, and bioinformatics, to name a few.

Resources available include substantial funds for equipment acquisition and program initiation, as well as appropriate laboratory facilities.

The predominant criterion for appointment in the University Tenure Line is a major commitment to research and teaching.

Letters of inquiry and curriculum vitae as well as the names and addresses of five references should be sent to: **Stefan Heller, PhD - Chair of Basic Science Search Committee, Department of Otolaryngology – Head & Neck Surgery, 801 Welch Road, Stanford, CA 94305-5739; sheller@ohns.stanford.edu**.

Stanford University is an Equal Opportunity Employer and is committed to increasing the diversity of its faculty. It welcomes nominations of and applications from women and members of minority groups, as well as others who would bring additional dimensions to the university's research, teaching and clinical missions.

Programm zur Förderung der Rückkehr des wissenschaftlichen Spitzennachwuchses aus dem Ausland

Ministerium für Innovation, Wissenschaft und Forschung des Landes Nordrhein-Westfalen

Sie forschen an vorderster Front im Bereich Lebenswissenschaften und möchten mit ihren herausragenden Ideen zur Bewältigung der großen gesellschaftlichen Herausforderungen auf den Feldern Gesundheit, Ernährung, Energie oder Klimawandel beitragen. Der Forschungsstandort Nordrhein-Westfalen bietet Ihnen die Chance zum Aufbau und zur Leitung einer selbstständigen Nachwuchsgruppe an einer Hochschule Ihrer Wahl in Nordrhein-Westfalen.

Im Falle einer erfolgreichen Bewerbung sind dafür über einen Zeitraum von fünf Jahren bis zu 1,25 Mio. EUR vorgesehen. Die Leitungsposition ist mit Entgeltgruppe 15 TVL – vergleichbar W2 – dotiert. Sie erhalten eine personengebundene Finanzierungszusage und etablieren Ihr Labor an einer Hochschule Ihrer Wahl in Nordrhein-Westfalen, welche Ihnen die beste Zukunftsperspektive und eventuell auch Tenure-Track bietet.

Der Beginn dieser Förderung ist für das vierte Quartal 2012 vorgesehen und steht unter dem Vorbehalt der Freigabe durch den Haushaltsgesetzgeber des Landes Nordrhein-Westfalen.

Sie forschen derzeit außerhalb Deutschlands und verfügen über eine Promotion, die nicht länger als sechs Jahre zurückliegt (bei Medizinern nicht länger als neun Jahre). Ihr Lebensmittelpunkt lag vor dem Auslandsaufenthalt in Deutschland, und Sie können insgesamt mindestens 24 Monate erfolgreicher wissenschaftlicher Forschung außerhalb Deutschlands vorweisen. Wenn dies alles auf Sie zutrifft, freuen wir uns auf Ihre Bewerbung unter

www.rueckkehrerprogramm.nrw.de

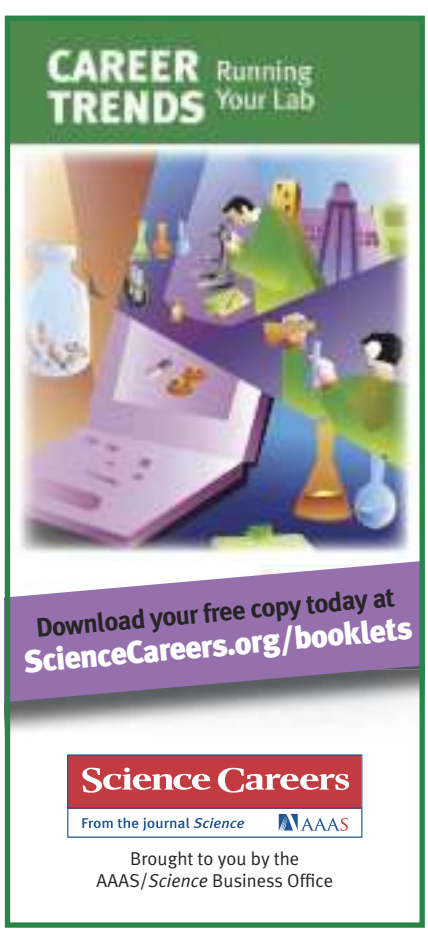
Nähere Informationen zu Bewerbungsunterlagen sowie eine detaillierte Beschreibung des Programms finden Sie auf der angegebenen Internetseite.

Bitte reichen Sie Ihre Bewerbungsunterlagen bis zum **26. März 2012 (Deadline)** online ein.

Das Land Nordrhein-Westfalen fördert die berufliche Entwicklung von Frauen. Bewerbungen von Frauen werden daher besonders begrüßt. Bewerbungen geeigneter schwerbehinderter Menschen sind erwünscht.

WISSEN SCHAFFT CHANCEN.NRW

www.wissenschaft.nrw.de



EXCELLENT JOB OPPORTUNITIES IN QATAR

Qatar Foundation
لإطلاق قدرات الإنسان
Unlocking human potential.
CELEBRATING 15 YEARS

*The **State of Qatar** is an Arab emirate in Southwest Asia, occupying the small Qatar Peninsula on the northeasterly coast of the larger Arabian Peninsula. It is bordered by Saudi Arabia to the south; otherwise the Arabian Gulf surrounds the state. An oil rich nation, Qatar has the highest GDP per capita in the world where Qatar's wealth and standard of living compare well with those of Western European States. More than 100 nationalities live and work in harmony in the country of 1.5 million people.*

Qatar Foundation for Education, Science and Community Development is a private, chartered, nonprofit organization, founded in 1995 by His Highness Sheikh Hamad Bin Khalifa Al-Thani, Emir of Qatar. Guided by the principle that a nation's greatest resource is the potential of its people, Qatar Foundation aims to develop that potential through a network of centers devoted to progressive education, research and community welfare.

Qatar Biomedical Research Institute would like to invite applications from qualified candidates for the following positions *(For more details about each position please visit www.qf.org.qa):*

Code	Vacancy Title
IRC20035	Principal Investigator Stem Cells
IRC20036	Senior Scientist Stem Cells
IRC20037	Scientist Stem Cells

The minimum requirements for these positions are a PhD in Biomedical Sciences, hands-on laboratory experience; and a demonstrated strong record of publications, conference papers, reports and/or professional and/or technical contributions in the relevant Stem Cell areas of research.

The compensation will include attractive tax free salary and additional benefits such as furnished accommodation, annual paid leave, medical insurance, etc.

For more details about Qatar Foundation and to apply please visit our website **www.qf.org.qa**, or send your resume including the code of the position applied for in the subject of the email to **recruitment@qf.org.qa**. The closing date to receive applications is **20th** of **February 2012.** Only shortlisted applicants will be notified.



Nontraditional Careers: Opportunities Away From the Bench

Webinar

Want to learn more about exciting and rewarding careers outside of academic/industrial research? View a roundtable discussion that looks at the various career options open to scientists and strategies you can use to pursue a nonresearch career.

Now Available On Demand
www.sciencecareers.org/webinar

Produced by the *Science*/AAAS Business Office.

Science Careers
From the journal *Science* AAAS

POSITIONS OPEN

FACULTY POSITION

The Department of Molecular & Cellular Physiology invites applications for a tenure-track position at the level of **ASSISTANT/ASSOCIATE PROFESSOR.** Successful applicants will be expected to develop an independent, nationally funded research program. Preference will be given to individuals with an interest and record of achievement in cardiovascular research. Information about the departmental research focus is available at **website: http://www.shreveportphysiology.com.** A generous startup package and appropriate space will be offered. Applicants should have a Doctoral degree and relevant postdoctoral experience. Applications will be reviewed as they are received until the position is filled. Send curriculum vitae and names of three references to: **D. Neil Granger, Ph.D., Boyd Professor & Head, Department of Molecular & Cellular Physiology, LSU Health Sciences Center, 1501 Kings Highway, Shreveport, Louisiana, 71130-3932, fax: 318-675-6005, e-mail: dgrang@lsuhsc.edu.** *Louisiana State University Health Sciences Center is an Affirmative Action/Equal Opportunity Employer.*

ASSISTANT PROFESSOR
Wildlife Ecology and Management

Purdue University invites outstanding candidates to apply for an academic-year, tenure-track faculty position at the rank of assistant professor in wildlife ecology and management. Visit **website: http://www.ag.purdue.edu/fnr/** for details. Ph.D. in wildlife, ecology, zoology, or related discipline and demonstrated expertise in the field of natural resources is required. The position includes research and teaching responsibilities. Submit a cover letter, curriculum vitae, summary of research interests, statement of teaching philosophy and interests, and arrange for three letters of reference to be sent to: **Search Chair, Purdue University, Department of Forestry and Natural Resources, 715 W. State Street, West Lafayette, IN 47907-2061; telephone: 765-496-9495, e-mail: pzollner@purdue.edu.** Review of applications begins 29 February 2012 and continues until the position is filled. *A background check will be required for employment in this position. Purdue University is an Equal Opportunity/Equal Access/Affirmative Action Employer fully committed to achieving a diverse workforce.*

POSTDOCTORAL POSITION
Herman B Wells Center for Pediatric Research
Indiana University School of Medicine

A postdoctoral position is available at Indiana University School of Medicine. The project is on understanding the role of marrow niche in hematopoietic malignancies with specific focus of the dysregulation of hematopoietic and mesenchymal stem cells in gene-modified animal models (**Yang et al.** *Cell* PMCID:PMC2788814, 2008; **Li et al.** *Blood* PMCID:PMC2742339, 2009, and **Li et al.** *Blood* PMID:21803851, 2011). Qualified applicants should have a Ph.D. or M.D. in the biological sciences with solid experience in protein-protein interactions, chromatin IP, flow cytometry, and gene targeting. Highly motivated candidates can electronically send cover letter, curriculum vitae, and three references to **Feng-Chun Yang,** M.D.-Ph.D., **e-mail: fyang@iupui.edu** and **Lisa Harris, e-mail: litully@iupui.edu.**

Indiana University is an Equal Employment Opportunity/Affirmative Action Employer, (Minorities/Females/Persons with Disabilities).

CAREER OPPORTUNITY—Doctor of Optometry (O.D.) degree in 27 months for Ph.D.s in science and M.D.s. Excellent career opportunities for O.D./Ph.D.s and O.D./M.D.s in research, education, industry, and clinical practice. This unique program starts in March of each year, features small classes, and 12 months devoted to clinical care.

Contact the Admissions Office, **telephone: 800-824-5526** at **the New England College of Optometry, 424 Beacon Street, Boston, MA 02115.** Additional information at **website: http://www.neco.edu, e-mail: admissions@neco.edu.**

POSITIONS OPEN

BIOLOGY

The Department of Biology at the College of Wooster invites applications for a one-year visiting position as **VERTEBRATE PHYSIOLOGIST** to teach introductory biology and upper level courses in Comparative Animal Physiology, Natural History of the Vertebrates, and to direct undergraduate research in the College's required Independent Study Program beginning Fall 2012. Applicants should have a Ph.D.; postdoctoral research and/or teaching experience preferred.

Send curriculum vitae, statements of research and teaching philosophy, transcripts, and three letters of recommendation to **Dr. Dean Fraga,** Chair of Biology, the College of Wooster, Wooster, Ohio (**e-mail: biology@wooster.edu**). Electronic applications preferred and should be received by March 7, 2012, for full consideration.

DIRECTOR

U.S. Geological Survey Western Fisheries Research Center, Seattle. Molecular to ecosystem scale fisheries research throughout the Western U.S.; six laboratory locations support genetic, conservation, habitat, climate change, and other investigations. Competitive salary and federal benefits. Apply at **website: http://www.usajobs.gov.** Title: Western Fisheries Research Center Director, GS-0401/0482-15. *The federal government is an Equal Opportunity Employer.*

Your career is our cause.

Get help from the experts.

www.sciencecareers.org

- Job Postings
- Job Alerts
- Resume/CV Database
- Career Advice
- Career Forum

Science Careers
From the journal *Science* AAAS

MARKETPLACE

Widely Recognized Original & Guaranteed

KlenTaq 1

8¢/u Truncated Taq DNA Polymerase Withstand 99°C

US Pat #5,436,149
Call: **Ab Peptides**
Fax: 314•968•8988

e-mail: abpeps@msn.com
1•800•383•3362
www.abpeps.com